DUDLEY KNOX LIBRARY
NA
MC
DUATE SCHOOL
93943-5101

# REPORT DOCUMENTATION PAGE

Form Approved
OMB No. 0704-0188

Public reporting burden for this collection of information is estimated to average 1 hour per response, including the time for reviewing instruction, searching existing data sources gathering and maintaining the data needed, and completing and reviewing the collection of information. Send comments regarding this burden estimate or any other aspect of this collection of information, including suggestions for reducing this burden, to Washington headquarters Services, Directorate for Information Operations and Reports, 1215 Jefferson Davis Highway, Suite 1204, Arlington, VA 22202-4302, and to the Office of Management and Budget, Paperwork Reduction Project (0704-0188) Washington DC 20503

| | | |
|---|---|---|
| 1.AGENCY USE ONLY *(Leave blank)* | 2.REPORT DATE<br>December 1994 | 3.REPORT TYPE AND DATES COVERED<br>Doctoral Dissertation (Dec 1982 - Dec 1994) |

**4.TITLE AND SUBTITLE** Vortex Element Analysis of Selected Time-Dependent Flows

**5.FUNDING NUMBERS**

**6.AUTHOR(S)**
Michael Rex Maixner

**7.PERFORMING ORGANIZATION NAME(S) AND ADDRESS(ES)**
Naval Postgraduate School
Monterey CA 93943-5000

**8.PERFORMING ORGANIZATION REPORT NUMBER**

**9.SPONSORING/MONITORING AGENCY NAME(S) AND ADDRESS(ES)**

**10.SPONSORING/MONITORING AGENCY REPORT NUMBER**

**11.SUPPLEMENTARY NOTES** The views expressed in this thesis are those of the author and do not reflect the official policy or position of the Department of Defense or the U.S. Government.

**12a.DISTRIBUTION/AVAILABILITY STATEMENT**
Approved for public release; distribution is unlimited.

**12b.DISTRIBUTION CODE**

**13.ABSTRACT***(maximum 200 words)* Previous investigations of oscillating (harmonic) flow past circular cylinders via the discrete vortex method have met with limited success due to a variety of reasons. These assumptions have proven to be too severe, and cannot allow the prediction of the kinematics and dynamics of the oscillating flow about bluff bodies in general and about a circular cylinder in particular.

In the current analysis, the ambient velocity was given by $U = U_m \sin \omega t$, and the velocity distribution and the boundary layer were calculated about the cylinder at suitable time intervals. Several methods were implemented to predict separation, all of which required a minimum of arbitrary assumptions. Nascent vortices were placed at the separation points in such a manner that the Kutta condition was satisfied. Several functional forms of dissipation were investigated, but it was found not to be of overriding influence in the flow kinematics. Counter vortices were found to be a necessary aspect of the analysis, providing continuity from one half cycle to the next. Flow visualization experiments were conducted for a Keulegan-Carpenter number of 10 as a basis for comparison. The kinematics obtained from the numerical model produced a vortex shedding pattern which was typical of those observed experimentally for higher Keulegan-Carpenter numbers. Significant problems were encountered in the prediction of boundary layer separation.

At this point, it was obvious that the interaction of a vortex with a boundary layer warranted analysis in a much simpler flow situation; the blade-vortex interaction (BVI) problem proved to be ideal. A boundary layer code which predicted separation on an infinite flat plate under the influence of a line vortex was adapted to the BVI problem, so that it could be used with a semi-infinite plate in a flow field comprised of a free stream and numerous discrete vortices. Although data are not readily available for the comparison of force and moment data on a semi-infinite flat plate, the kinematics resulting from the interaction of the primary vortex and the shed vorticity are most encouraging. The kinematics and approximate relative strengths of the shed vortices are in agreement with the observations of several researchers.

**14. SUBJECT TERMS** Unsteady flow, vortex element, discrete vortex, harmonic flow, oscillaing flow,circular cylinder, flat plate, boundary layer

**15.NUMBER OF PAGES**
293

**16.PRICE CODE**

| 17. SECURITY CLASSIFICATION OF REPORT | 18. SECURITY CLASSIFICATION OF THIS PAGE | 19.SECURITY CLASSIFICATION OF ABSTRACT | 20.LIMITATION OF ABSTRACT |
|---|---|---|---|
| Unclassified | Unclassified | Unclassified | UL |

NSN 7540-01-280-5500

Standard Form 298 (Rev. 2-89)
Prescribed by ANSI Std 239-18
298-102

Approved for public release; distribution is unlimited

# VORTEX ELEMENT ANALYSIS OF SELECTED TIME-DEPENDENT FLOWS

Michael R. Maixner
Captain, United States Navy
B.S., United States Naval Academy, 1972
S.M.M.E., Massachusetts Institute of Technology, 1977
O.E., Massachusetts Institute of Technology, 1977

**DOCTOR OF PHILOSOPHY IN MECHANICAL ENGINEERING**

from the

**NAVAL POSTGRADUATE SCHOOL**
**December 1994**

Richard S. Elster, Dean of Instruction

Thesis
M27772
c.1

# ABSTRACT

Previous investigations of oscillating (harmonic) flow past circular cylinders via the discrete vortex method have met with limited success due to a variety of reasons. These assumptions have proven to be too severe, and cannot allow the prediction of the kinematics and dynamics of the oscillating flow about bluff bodies in general and about a circular cylinder in particular.

In the current analysis, the ambient velocity was given by $U = U_m \sin \omega t$, and the velocity distribution and the boundary layer were calculated about the cylinder at suitable time intervals. Several methods were implemented to predict separation, all of which required a minimum of arbitrary assumptions. Nascent vortices were placed at the separation points in such a manner that the Kutta condition was satisfied. Several functional forms of dissipation were investigated, but it was found not to be of overriding influence in the flow kinematics. Counter vortices were found to be a necessary aspect of the analysis, providing continuity from one half cycle to the next. Flow visualization experiments were conducted for a Keulegan-Carpenter number of 10 as a basis for comparison. The kinematics obtained from the numerical model produced a vortex shedding pattern which was typical of those observed experimentally for higher Keulegan-Carpenter numbers. Significant problems were encountered in the prediction of boundary layer separation.

At this point, it was obvious that the interaction of a vortex with a boundary layer warranted analysis in a much simpler flow situation; the blade-vortex interaction (BVI) problem proved to be ideal. A boundary layer code which predicted separation on an infinite flat plate under the influence of a line vortex was adapted to the BVI problem, so that it could be used with a semi-infinite plate in a flow field comprised of a free stream and numerous discrete vortices. Although data are not readily available for the comparison of force and moment data on a semi-infinite flat plate, the kinematics resulting from the interaction of the primary vortex and the shed vorticity are most encouraging. The kinematics and approximate relative strengths of the shed vortices are in agreement with the observations of several researchers.

DUDLEY KNOX LIBRARY
NAVAL POSTGRADUATE SCHOOL
MONTEREY CA 93943-5101

# TABLE OF CONTENTS

I. INTRODUCTION ..... 1

II. DISCRETE VORTEX MODELS APPLIED TO SINUSOIDALLY OSCILLATING FLOW ..... 10

A. INTRODUCTION ..... 10

B. FLOW KINEMATICS ..... 10

C. FORMULATION OF THE PRESSURE EQUATION ..... 13

D ALTERNATIVE METHODS OF EVALUATING THE RESISTANCE ..... 17

E. PREVIOUS INVESTIGATIONS ..... 21

F. SYNOPSIS OF THE PREVIOUS INVESTIGATIONS ..... 25

III. ELEMENTS OF THE DISCRETE VORTEX MODEL ..... 27

A. INTRODUCTION ..... 27

B. SEPARATION POINT PREDICTION ..... 27

C. INTRODUCTION OF VORTICITY ..... 34

D. ASYMMETRY INITIATION ..... 36

E. CONVECTION SCHEME ..... 38

F. CIRCULATION REDUCTION ..... 39

G. COUNTERVORTICITY ..... 46

H. VORTEX CLUSTER AMALGAMATION ..... 48

I. REDISCRETIZATION ..... 49

IV. A NEW DISCRETE VORTEX MODEL FOR OSCILLATING FLOWS ..... 51

A. INTRODUCTION ..... 51

B. DETAILS OF THE NUMERICAL MODEL ..... 51

C. VERIFICATION OF THE MODEL ..... 54

D. FLOW VISUALIZATION ..... 63

E. FIXED SEPARATION POINTS ..... 64

F. USE OF AN INTEGRAL MOMENTUM BOUNDARY LAYER SEPARATION CRITERION....88

G. TURBULENT BOUNDARY LAYER....109

H. USE OF CEBECI-CARR PROGRAM TO PREDICT SEPARATION....110

I CONCLUDING REMARKS....110

V. PARALLEL BLADE-VORTEX INTERACTIONS....129

A. INTRODUCTION....129

B. PREVIOUS INVESTIGATIONS....129

C. PROBLEM FORMULATION....136

D. BOUNDARY LAYER SEPARATION....139

E. NASCENT VORTEX PLACEMENT....141

F. TIMESTEP SIZE....141

G. CORE GEOMETRY....141

H. DISSIPATION....143

I. INDUCED VELOCITY CALCULATIONS....145

J. WALL ANNIHILATION....145

K. VORTEX COMBINATION....145

L. POTENTIAL FLOW BASELINE RUNS....145

M. $U_\infty = \beta = 0$: VISCOUS EFFECTS INCORPORATED....146

N. $0 < U_\infty \leq 1$ ($0 < \beta \leq ½$): VISCOUS EFFECTS INCORPORATED....148

O. $U_\infty > 1$ ($\beta > ½$): VISCOUS EFFECTS INCORPORATED....149

P. CONCLUDING REMARKS....149

VI. CONCLUSIONS....189

APPENDIX A. VORTEX-DRIVEN BOUNDARY LAYERS....191

APPENDIX B. PROGRAM PLATE.FOR....211

APPENDIX C. PROGRAM PLTPLT.FOR....239

LIST OF REFERENCES.....263

INITIAL DISTRIBUTION LIST.....277

# NOMENCLATURE

| | |
|---|---|
| A | Amplitude of flow oscillation |
| a | Downstream offset distance of primary vortex above plate |
| B | Maximum value of asymmetry (Chapters II - IV)<br>Also, dissipation parameter (Chapter V) |
| c | Cylinder radius |
| C(t) | Time-dependent Bernoulli constant |
| $C_a$ | Added mass coefficient |
| $C_m$ | Inertia coefficient, $C_m = 1 + C_a$ (Chapters II - IV)<br>Also, moment coefficient (Chapter V) |
| $C_d$ | Drag coefficient, $C_d = F_d / \rho c U_m^2$ |
| $C_{ilf}$ | In-line force coefficient, $C_{ilf} = F_{ilf} / \rho c U_m^2$ |
| $C_l$ | Lift coefficient, $C_l = F_l / \rho c U_m^2$ |
| D | Cylinder diameter, $D = 2c$ |
| F | Force |
| H | Thwaites' boundary layer shape factor |
| $i$ | $\sqrt{-1}$ |
| I | Impulse of a vortex pair |
| Im{ } | Imaginary part of a complex quantity |
| **K** | Keulegan-Carpenter number, $\mathbf{K} = 2\pi A/D = U_m T/D$ |
| L | Length of cylinder |
| p | Pressure |
| Q | Streamwise flow in boundary layer |
| q | Complex velocity, $q = u + iv$ |
| r | Radial distance |

| | |
|---|---|
| $r*$ | Core radius, $r* = 1.24\sqrt{\nu t}$ |
| $\mathbf{R}$ | Reynolds number, $\mathbf{R} = U_m D/\nu$ |
| $\mathbf{R}_v$ | Vortex Reynolds Number, $\mathbf{R}_v = \Gamma/2\pi\nu$ |
| Re{ } | Real part of an imaginary quantity |
| s | Linear coordinate along cylinder surface, $s = c\theta$ |
| t | Time |
| T | Period of flow oscillation (Chapters II - IV)<br>Also, Thwaites' boundary layer shape factor (Appendix A) |
| u | x-component of velocity |
| U | Ambient flow speed |
| $U_m$ | Maximum ambient velocity |
| $U_o$ | Velocity on inner side of the shear layer at separation (Chapters II - IV)<br>Also, plate reference velocity, $U_o = \Gamma_{primary} / \pi a$ (Appendix A) |
| $U_{plate}$ | Maximum velocity induced on plate, $U_{plate} = U_\infty + \Gamma_{primary} / \pi a$ |
| $U_s$ | Outer boundary layer flow speed at separation point |
| v | y-component of velocity |
| v (r, t) | Radial velocity due to a vortex |
| w | Complex potential function, $w = \phi + i\psi$ |
| x | Longitudinal coordinate |
| y | Transverse coordinate |
| z | Complex variable, $z = x + iy$ |
| $\bar{z}$ | Complex conjugate, $\bar{z} = x - iy$ |
| $\lvert z \rvert$ | Modulus of z |

*Greek symbols*

| | |
|---|---|
| $\beta$ | Frequency parameter, $\beta = \mathbf{R/K} = D^2/\nu t$ (Chapters II - IV)<br>Also, nondimensional velocity ratio, $\beta = U_\infty / U_{plate}$ (Chapter V) |
| $\Gamma$ | Total circulation of a vortex |
| $\delta$ | Boundary layer thickness (Chapters II - IV)<br>Also, nondimensional boundary layer calculation coefficient,<br>$\delta = g^2 U(\ln U)' / \nu$ (Appendix A) |
| $\delta^*$ | Boundary layer displacement thickness |
| $\Delta$ | Difference operator |
| $\Delta t$ | Time step |
| $\theta$ | Angle, measured counter-clockwise from positive x-axis (Chapters II - IV)<br>Also, boundary layer momentum thickness (Appendix A) |
| $\theta_{stag}$ | Stagnation angle |
| $\nu$ | Kinematic viscosity of the fluid |
| $\nu_t$ | Eddy viscosity |
| $\rho$ | Density of the fluid |
| $\tau$ | Nondimensional cycle time in radians, $\tau = 2\pi t / T$ |
| $\tau_w$ | Wall shear |
| $\lambda$ | Thwaites' dimensionless boundary layer parameter |
| $\xi$ | Dimensionless distance along plate, $\xi = x/a$ |
| $\eta$ | Dimensionless distance in boundary layer normal to plate, $\eta = y/g$ |
| $\phi$ | Potential function |
| $X^2$ | Nondimensional vortex dissipation parameter, $X^2 = r^2 / \Gamma_o t$ |
| $\Psi$ | Stream function (Appendix A) |
| $\psi$ | Stream function (Chapters II - V)<br>Also, nondimensional boundary layer calculation coefficient, $\psi = g^2 U \xi' / \upsilon$ (Appendix A) |
| $\omega$ | Vorticity, $\omega = \partial v/\partial x - \partial u/\partial y$ |

*Subscripts*

| | |
|---|---|
| amalg | Amalgamated |
| cop | Center of pressure |
| cov | Center of vorticity |
| iv | Due to imaginary vortices |
| L.E. | Plate leading edge |
| n | n-th vortex |
| nv | Nascent vortex |
| o | Initial or original |
| rv | Due to real vortices |
| uf + d | Due to uniform flow plus doublet |
| $v^2$ | Due to velocity squared |
| vort | Due to real and imaginary vortices |
| $\infty$ | Condition at infinity |
| ,x | Partial derivative with respect to x |

*Superscripts*

| | |
|---|---|
| i | Image vortex |
| ′ | Nondimensionalized quantity (Chapters II - IV)<br>Also, derivative with respect to distance along the plate (Chapter V, Appendix A) |
| * | Physical velocity component |
| ^ | Vector quantity |

# ACKNOWLEDGEMENTS

In the course of this investigation, numerous people have rendered significant assistance in a variety of ways. Distinguished Professor T. Sarpkaya initially suggested the problem and spent incalculable hours in discussing the project, making suggestions, and guiding me throughout. Indeed, he has done his utmost to provide me with his keen insight into the discrete vortex model and in the underlying fundamentals of the fluid mechanics. I cannot thank him enough.

Doctoral committee members, both past and present, warrant a special note of thanks for their assistance. I am particularly indebted to the Chairman of the Department of Mechanical Engineering, Professor Matt Kelleher, and to the twice Naval Engineering Curricular Officer, Captain Walt Ericson, for their friendship and understanding during the course of this investigation. To the U.S. Navy I am most grateful for the opportunity to undertake research at the doctoral level, first under the Burke Program while in residence at the Naval Postgraduate School (1981-1985), and more recently for funding my travel and per diem while completing the degree from a distance. Computer time for the harmonic flow analysis was donated by the Naval Postgraduate School, as was programming and debugging assistance; most notably assisting with the latter were Messrs. Rich Donat, Stephan Lamont, Larry Frazier, and Ed Donnellan (W.R. Church Computer Center). For the more recent work on blade-vortex interactions, the Naval Sea Systems Command was most helpful in loaning a laptop computer on which the calculations were performed.

Significant assistance was provided by the following individuals in obtaining reference materials at the institutions indicated: Roger Martin, Ron Rodriguez , and Ken Lauderdale (Dudley Knox Library at the Naval Postgraduate School); Professor Howard Hufford (University of Bath, England); Professor John Rose and Ms. Kathy Abbott (Queen Mary and Westfield College of the University of London); and Mr. John Parrent of the technical library at the Ministry of Defence, Foxhill, Bath. In the course of the harmonic flow visualization photography, skillful assistance was provided in the fabrication and operation of the test facility by Messrs. Jack McKay, Charles Crow, and Tom McCord, all of the machine shop in

the Department of Mechanical Engineering; Ms. Dale Ward was also instrumental in the photographic aspects of the experiments. Recently, Professor Frederick Sherman was most gracious in clarifying various portions of his text, and in providing updated errata.

Finally, I thank my family for their support and understanding during my entire doctoral program. During the most trying of times, Gretchen and her parents were always there, urging me on. This work is dedicated to the memory of Anna, and to Bethany Ann and Michael Patrick; for Bethany and Michael I wish the satisfaction and understanding which come from putting forth their best effort in any academic endeavor.

# I. INTRODUCTION

The interaction of vorticity with a bluff body constitutes one of the most complex problems in fluid mechanics. Even without the influence of vorticity on the body, many aspects of the problem are already exceedingly difficult, and render accurate numerical simulation of the phenomenon almost impossible. For example, the seemingly simple case of a circular cylinder in impulsively-started flow is an unsteady kaleidoscope of fluid mechanics phenomena where the shed vorticity does not return to the body. With the addition of approaching vorticity, whether shed from the same body or another, the degree of difficulty of the problem increases by a least an order of magnitude, as exemplified by an oscillating cylinder or by a helicopter blade seeing its own vortex.

Perhaps the most challenging of all these approaching vorticity problems is that of harmonic flow, wherein the vorticity shed by the body in previous cycles returns to the body. In analyzing a sinusoidally oscillating flow, the most serious difficulty is the description of the time-dependent forces acting on a body. Stokes [1851] arbitrarily decomposed the time-dependent force into an inertial force and a drag force, which were linearly dependent on acceleration and velocity, respectively. Whereas Stokes' analysis was based on unseparated flow, the case of separated flow still poses significant difficulties for theoretical analysis. Nearly a century after Stokes' paper, Morison et al [1950] conducted experimental studies on the forces on piles. In the analysis of their data, they divided the force into a component due to drag (as obtained in the case of constant velocity) and a component due to the fluid acceleration. Accordingly, a drag coefficient $C_d$ and an inertia coefficient $C_m$ were introduced into the expression for force per unit length:

$$F(t) = \frac{1}{2}\rho U|U|DC_d + \rho\pi\frac{D^2}{4}\frac{dU}{dt}C_m, \tag{1.1}$$

where U and dU/dt represent the ambient flow velocity and acceleration, respectively. As contrasted with Stokes' results, the drag force in the Morison equation is proportional to the square of the velocity, reflecting the fact that the drag is predominantly pressure drag (rather than skin friction) since the flow is

now separating from the cylinder. The assumptions and limitations associated with the use of the Morison equation are manifold, but it has still proven to be of significant worth in many engineering applications.

In the case of ideal flow, $C_m$ should be equal to 2 for a circular cylinder; it would also appear reasonable that $C_d$ would assume a value close to its steady state value for a viscous flow (about 1.2 at moderate Reynolds numbers). In practice, both $C_d$ and $C_m$ have shown significant deviations from the above-mentioned values. The question which arises is: which values of $C_d$ and $C_m$ are most appropriate for use in the Morison equation?

Keulegan and Carpenter [1956] performed the first systematic evaluation of Fourier-averaged inertia and drag coefficients, working at relatively low Reynolds numbers with horizontal plates and cylinders placed in the node of a standing wave. They employed a Fourier series representation of the force, assuming it to be an odd-harmonic function of $\tau = 2\pi t/T$, so that $F(\tau) = -F(\tau + \pi)$, and have shown that

$$C_d = -\frac{3}{4}\int_0^{2\pi} \frac{F\cos\tau}{\rho D U_m^2}\, d\tau \tag{1.2}$$

and

$$C_m = \frac{2}{\pi^3}\frac{U_m T}{D}\int_0^{2\pi} \frac{F\sin\tau}{\rho D U_m^2}\, d\tau. \tag{1.3}$$

Alternatively, $C_d$ and $C_m$ may be determined through the use of the method of least squares (Sarpkaya and Isaacson [1981] ), which seeks to minimize the errors between experimentally measured and calculated forces. This procedure yields

$$C_d = -\frac{8}{3\pi}\int_0^{2\pi} \frac{F|\cos\tau|\cos\tau}{\rho D U_m^2}\, d\tau \tag{1.4}$$

and

$$C_m = \frac{2}{\pi^3}\frac{U_m T}{D}\int_0^{2\pi}\frac{F\sin\tau}{\rho D U_m^2}d\tau. \tag{1.5}$$

It should be noted that Equations (1.3) and (1.5) are identical; although Equation (1.4) is not identical to the value obtained through a Fourier analysis (Equation (1.2)), the use of both equations in practice shows no significant difference between these alternative formulations.

Sarpkaya [1976, 1978, 1981a, 1981b] has shown that:

- Not only do $C_d$ and $C_m$ depend on **K** and **R**, but also on the relative roughness of the cylinder.
- The Morison equation represents the measured force with reasonable accuracy in the inertia-dominated (**K** < 10) and drag-dominated (**K** > 20) regimes.
- In the drag-inertia dominated region (10 < **K** < 20), the Morison equation is incapable of accurately representing the measured force with sufficient accuracy. This was first pointed out by Keulegan and Carpenter [1956]; the large difference between measured and calculated forces (termed "residues" by Sarpkaya) are due to the occurrence of relatively large lift forces, fractional shedding of a few vortices, and asymmetries in the in-line force.

In the drag-inertia dominated regime, the flow patterns associated with relatively few vortices become exceedingly complex; the Morison equation utilizes constant, averaged, force-transfer coefficients which do not incorporate the complex history of the flow. Sarpkaya [1981a] has performed a detailed residue analysis wherein higher odd harmonics were incorporated, thereby significantly reducing the magnitude of the residues.

The foregoing discussion has pointed out how controlled laboratory experiments have aided in the understanding of the many and interrelated facets of an extremely complex and highly nonlinear problem. Mathematical or numerical methods have been utilized to obtain nearly exact solutions of some loading situations; this class of problem pertains to the flow about large bodies in the diffraction regime where the

ratio of the characteristic body dimension relative to the wave length is greater than about 0.2, and viscous and separation effects are considered to be of minimal impact. The hydrodynamic loading situations wherein the effects of diffraction and separation are of equal significance are those with which the current work is concerned, and are also those which are the most practically significant fluid-structure interaction problems. Theoretical solutions are non-existent for separated bluff-body flows, even for the relatively simple case of steady unidirectional ambient flow, wherein the vortices are allowed to interact with one another and the base of the body, but are continuously convected downstream, never to return to the generating surface.

Aside from the first studies into the gross aspects of wake formation by von Kármán [1911] and Bènard [1908], some of the most meaningful investigations into the details of the bluff-body vortex shedding process were performed by Fage and Johansen [1928], Gerrard [1966, 1967], Bloor and Gerrard [1966], von Schmidt and Tilmann [1972], Roshko [1954], and others. As pointed out by Cisotti (see Birkhoff [1950]), it soon became evident that an ambient two-dimensional flow about a two-dimensional bluff-body did not result in a two-dimensional wake. Prandtl (see Sarpkaya and Isaacson [1981] ) noted that only a portion (roughly 60% for a cylinder in unidirectional flow) of the original circulation survives beyond the wake formation region. The Navier-Stokes equations, when used in conjunction with some suitable spatial and temporal differencing technique (finite difference, finite element, etc.) to numerically simulate separated bluff-body flows, are limited to low-Reynolds number flows (about $\mathbf{R} < 5000$); in order to faithfully reproduce the velocity gradient across a vanishingly thin shear layer, an extremely fine mesh must be employed, resulting in excessive computation time and exorbitant storage requirements. High Reynolds number flows, on the other hand, require methods such as the discrete vortex models (hereafter referred to as the DVM's), which utilize a finite number of point vortices to represent the shear layers; appropriate modifications are usually made to the vortex cores to account for viscous effects and to alleviate many of the problems associated with vortex-to-vortex proximity. There is not one DVM—there

is a DVM for every application, changes being made to suit the situation. DVM's have been employed with reasonable results in many different flows:

- Unidirectional flow past bluff bodies
  - Flat plates at a variety of angles of attack: Belotserkovskii and Nisht [1973], Kuwahara [1973], Sarpkaya [1975], Kiya and Arie [1977a, 1977b, 1980]
  - Circular cylinders: Bellamy-Knights [1967], Gerrard [1967], Sarpkaya [1968], Davis [1969], Laird [1971], Chaplin [1973], Chorin [1973], Clements [1977], Kuwahara [1978], Sarpkaya and Shoaff [1979], Van der Vegt and Huijsmans [1984], Van der Vegt and de Boom [1985], Smith [1986], Tiemroth [1986a, 1986b], Smith and Stansby [1987, 1988], Van der Vegt [1988]
  - Elliptical cylinders: Izumi et al [1982]
  - Rectangular cylinders: Nagano et al [1981, 1982], Inamuro et al [1983, 1984], Sarpkaya and Ihrig [1986]
  - Airfoils: Ham [1968], Katz [1981], Basuki and Graham [1987], and Shigemi [1987]
  - Finned circular cylinders: Nielsen [1960], Telste and Lugt [1980]
  - Non-circular Cylinder: Shoaff and Franks [1981]
- Harmonic flow past bluff bodies
  - Flat plates: Kudo [1979, 1981]
  - Circular cylinders: Ward and Dalton [1969], Stansby [1977, 1979, 1981], Sawaragi and Nakamura [1979], Ikeda and Himeno [1981], Stansby and Dixon [1983], Ikeda [1984a, 1984b], Mostafa [1987]

- The DVM's have been used in many other applications:
    - Flow across sand ripples: Longuet-Higgens [1981]
    - Simulation of a Savonius rotor: Ogawa [1984]
    - Cascade flow: Shirahata et al [1982]
    - Rotating cylinders (Magnus effect): Kimura and Tsutahara [1987]
    - Cambered plates: Mostafa [1987], Munz [1987], Sarpkaya et al [1987]

The above list is far from complete and is presented only to give a sampling of the many applications of the DVM's. For a more complete and critical analysis of the DVM and its many applications, see the excellent reviews by Sarpkaya [1989, 1994]. In the case of unidirectional flow, the vortices are convected away from the generating surface, so that the inability of the DVM's to deal with both small and large structures in the wake has less and less influence on the body as time progresses; in fact, interference between the body and the vortices is confined mostly to the vortex formation region. The shed vortices in a harmonically oscillating ambient flow have, however, a dual effect. First, the boundary layer, pressure distribution, outer flow, and the generation and survival rate of new vorticity are signficantly affected by the returning vortices. Second, the returning vortices exhibit a strong influence on the motion of the primary separation points. As an example, the primary separation points on a circular cylinder undergo excursions of $\pm 3^{\circ}$ in unidirectional flow (Sarpkaya and Shoaff [1979] ), whereas in harmonically oscillating flow, experiments (Grass and Kemp [1979] and Sarpkaya and Butterworth [1992] ) have shown that the mobile separation points can experience relatively large excursions (on the order of $120^{\circ}$) in the course of a single cycle. These effects are further exacerbated by a host of additional items, which include, but are not limited to, vortex diffusion/decay and the fact that vorticity is, in reality, three-dimensional due to turbulent mixing, finite spanwise coherence, and finally, to the random nature of the vortices themselves. The net result is that, even for a given Keulegan-Carpenter number, there exist

numerous flow modes and the eventual cycle-to-cycle variations (Sarpkaya and Wilson [1984] ). As noted by Sarpkaya [1985], "the stronger and better correlated the returning vortices, the sharper and more pronounced the changes are in pressure distribution on the body and in the integrated quantities such as the lift, drag, and inertia coefficient." The above applications of the DVM to harmonic flow about bluff-bodies have been plagued by the requirement to incorporate gross simplifications and/or numerous disposable parameters, and all have met with significant difficulties. A universally applicable DVM for harmonic flow about bluff-bodies has yet to be devised.

Applications of the finite element method for steady and oscillating flow past a circular cylinder have been presented by Moorty and Olson [1989], and for steady and oscillating flow past a circular cylinder by Pattani and Olson [1988]. In the former study, the streamlines exhibited considerable irregularity and/or discontinuity, and no comparisons to experimental results were made for model verification. In the latter investigation, good agreement was found with flow visualizations. Excellent success has been achieved in the simulation of harmonic flows about circular cylinders through the use of the finite difference scheme by Wang [1989] and Wang and Dalton [1991], albeit only for small Reynolds numbers ($\mathbf{R} < 3000$). This finite difference scheme has subsequently been used to calculate non-impulsively started flow about a circular cylinder (Frederickson [1990] ) and for impulsive, non-impulsive, oscillatory, and oscillatory plus mean flows (see, e.g., Putzig [1991], Sarpkaya et al [1992] ); again, results were in reasonable agreement with experimental data, but were limited to relatively small Keulegan-Carpenter and Reynolds numbers. In general, the higher-order finite difference form of the Navier-Stokes equations is limited to small **R** and **K** due to numerical stability, computer storage and runtime considerations, and the general difficulty of dealing with turbulent flows. The Reynolds number is effectively reduced when truncation errors result in an artificial viscosity, the magnitude of which is unknown.

A series of much more basic numerical simulations of vorticity approaching bluff bodies has been carried out; the genesis for the investigation of this problem has been myriad, and ranges from the

interaction of turbulence with structures to the interaction of vortices with helicopter blades, submarine and missile control surfaces, and the like. Panaras [1987] investigated the effect of vortical structures as they passed successively closer to an airfoil, eventually impinging thereon and splitting; of specific interest in this study was the method of vortex representation (single point vortex, circular clusters of smaller vortices, or originally parallel sheets of vortices) and the effect of these various vortex configurations on the pressure field around the airfoil. This work was extended by Panaras [1990] to study the impingement and splitting of vortices on a corner and the resultant pressure distributions, as had been done initially by Conlisk and Rockwell [1981]. Since they were intended to provide insight into the overall impact of the vortices on the solid boundaries they were approaching, these potential flow models failed to incorporate the no-slip condition and hence the generation of new vorticity at the solid boundaries. Detailed pressure and force measurements resulting from vortex impingement on a corner were presented by Tang and Rockwell [1983] and Kaykayoglu and Rockwell [1985]; these experimental data revealed the existence and significance of secondary vorticity shed from the solid boundary. The importance of secondary vorticity has been reported by many investigators (Bergeson and Porter [1960], Stansby and Dixon [1982], Sarpkaya [1989] ); indeed, in many numerical analyses, the failure to properly introduce vorticity from the primary separation points and to incorporate the effects of secondary vorticity will most likely preclude faithful prediction of the forces on the body and replication of the flowfield kinematics.

Based upon experience gained from a discrete vortex analysis of harmonic flow about a circular cylinder, the current work will continue with an analysis of the incorporation of viscous effects into the discrete vortex model as a result of the near passage or impingement of vortices on a bluff body. The insight gained from this detailed investigation will allow subsequent more realistic studies of harmonic flows about bluff bodies to be undertaken. In doing so, the ultimate purpose will be the understanding of separated, time-dependent turbulent flows. The question of whether the discrete vortex model represented a laminar or turbulent flow field will have to be addressed in light of more recent developments where the

parcels of vorticity could be treated as deformable so as to satisfy the conditions of solenoidality, rather than merely representing laminar or pre-turbulent flows with non-deformable cores of vorticity.

# II. DISCRETE VORTEX MODELS APPLIED TO SINUSOIDALLY OSCILLATING FLOW

## A. INTRODUCTION

Although DVM's have been widely and successfully applied to separated bluff-body flows, there have been relatively few applications of DVM's to the case of sinusoidally oscillating (hereafter referred to as "harmonic") flow. For a variety of reasons, the return of vorticity to the body makes analysis of this flow an order of magnitude more difficult than for the unidirectional case.

After considering the basic elements which are common to all harmonic flow analyses, the previous investigations will be reviewed and compared with one another.

## B. FLOW KINEMATICS

For a two-dimensional flow, the complex potential is given by

$$w(z,t) = \varphi + i\psi, \tag{2.1}$$

where

$$z = x + iy, \tag{2.2}$$

and where $\varphi$ and $\psi$ are, respectively, the time-dependent velocity potential and the time-dependent stream function . The Cauchy-Riemann conditions dictate that the velocity components be given by

$$u = -\frac{\partial\varphi}{\partial x} = -\frac{\partial\psi}{\partial y} \tag{2.3}$$

and

$$v = -\frac{\partial\varphi}{\partial y} = \frac{\partial\psi}{\partial x} \tag{2.4}$$

Taking the partial derivative of the complex potential with respect to z, one obtains

$$\frac{\partial w}{\partial z} = -u + iv. \tag{2.5}$$

For the flow about a circular cylinder of radius c, a uniform, time-dependent flow is combined with a doublet (whose strength varies in time with the uniform flow) at the cylinder center (see, e.g., Milne-Thomson [1968] ). This gives

$$w(z,t) = -U(t)\left(z + \frac{c^2}{z}\right), \tag{2.6}$$

where $-U(t)z$ is the uniform flow, and $-U(t)c^2/z$ the doublet. Placing a vortex outside the cylinder requires, by virtue of Milne-Thomson's [1968] circle theorem, the introduction of an image vortex of equal magnitude and of opposite sign inside the cylinder. For the general case of a circular cylinder with N (exterior) real vortices, the complex function is obtained by combining the complex functions of all the singularities involved, so that

$$w(z,t) = -U(t)\left(z + \frac{c^2}{z}\right) + \frac{i}{2\pi}\sum_{n=1}^{N}\Gamma_n\left[ln(z - z_n) - ln\left(z - \frac{c^2}{\bar{z}_n}\right)\right]. \tag{2.7}$$

In this analysis, a positive vortex possesses counter-clockwise circulation; additionally, it is assumed that the vortex strengths may be functions of time. The circle theorem dictates that a real vortex at $z = z_n$ has an image at $z = c^2 / \bar{z}_n$ and at $z = 0$. The central image, however, must be excluded because the vortex theorems (Sommerfeld [1950] ) require that vortices shed from the cylinder must leave a circulation opposite to their own on the cylinder. It is easy to see that the removal of this image vortex at the center of the cylinder will not change the Neumann boundary condition of zero normal velocity on the cylinder surface

$$\left[\frac{\partial\varphi}{\partial n}\right]_{r=c} = 0, \tag{2.8}$$

since the streamlines of a vortex are circles. It should be noted that at this point in the analysis no restrictions have been placed on the time-dependent velocity U(t), other than that it be uniform for any instant in time.

Combining Equations (2.5) and (2.7), the velocity at any point z is

$$-u+iv=\frac{\partial w}{\partial z}=-U\left(1-\frac{c^2}{z^2}\right)+\frac{i}{2\pi}\sum_{n=1}^{N}\Gamma_n\left[\frac{1}{z-z_n}-\frac{1}{z-\frac{c^2}{\bar{z}_n}}\right]. \tag{2.9}$$

This equation may also be used in calculating the convective velocity of a vortex at $z=z_n$, provided that the singularity due to the vortex itself is avoided.

Introducing the following change of variables, nondimensional equations may be formulated:

$$z'=\frac{z}{c} \qquad u'+iv'=\frac{u+iv}{U_m} \qquad \Gamma'=\frac{\Gamma}{U_m c}$$
$$w'(z,t)=\frac{w}{U_m c} \qquad t'=\frac{U_m t}{c}. \tag{2.10}$$

Substituting Equations (2.10) into Equations (2.7) and (2.9), and setting $U_m = 1.0$, $c = 1.0$, $U = U_m \sin\omega t$, $\omega = 2\pi/T$, and eliminating the primes for ease of notation, one obtains

$$w(z,t)=\sin\omega\, t\left(z+\frac{1}{z}\right)+\frac{i}{2\pi}\sum_{n=1}^{N}\Gamma_n\left[ln(z-z_n)-ln(z-\frac{1}{\bar{z}_n})\right] \tag{2.11}$$

and

$$-u+iv=\sin\omega\, t\left(\frac{1}{z^2}-1\right)+\frac{i}{2\pi}\sum_{n=1}^{N}\Gamma_n\left[\frac{1}{z-z_n}-\frac{1}{z-\frac{1}{\bar{z}_n}}\right], \tag{2.12}$$

where all velocity components, vortex strengths, and positions in the complex plane are normalized variables, and the complex potential function is also normalized. The above dimensionless variables will be used throughout the remainder of this work unless otherwise noted.

The last equation accounts for well over 90 per cent of the computation time in the numerical analysis, utilized primarily in the evaluation of vortex velocities during their convection, and also in the

evaluation of pressure on the cylinder surface. It is, therefore, prudent to maintain the number of vortices as small as possible, at the same time utilizing a sufficiently small time step to faithfully replicate the flow.

## C. FORMULATION OF THE PRESSURE EQUATION

For a time-dependent flow, the appropriate form of the Bernoulli equation is (see, e.g., Robertson [1965] )

$$\frac{p}{\rho}+\frac{1}{2}q^2-\frac{\partial\varphi}{\partial t}=C(t), \tag{2.13}$$

where C(t) is an arbitrary function of time, and q is the magnitude of the velocity at the point in question. At any instant, C(t) has the same value at all points of the region, and not merely along a streamline. Ignoring the arbitrary constant, the pressure at any point on the cylinder is

$$p(\theta)=\rho\frac{\partial\varphi}{\partial t}-\frac{1}{2}\rho q^2(\theta), \tag{2.14}$$

where $q^2(\theta)$ is the square of the velocity on the cylinder surface (see Figure 2.1). In the evaluation of the first term on the right hand side of Equation (2.14), it is easier to consider it as consisting of three parts:

### 1. Uniform Flow and Doublet Part

For these two elements we have

$$\begin{aligned} w_{uf+d} &= -U(t)\left(z+\frac{c^2}{z}\right) \\ &= \varphi_{uf+d}+i\psi_{uf+d}, \end{aligned} \tag{2.15}$$

so that

$$\varphi_{uf+d}=-2U(t)c\cos\theta \tag{2.16}$$

and

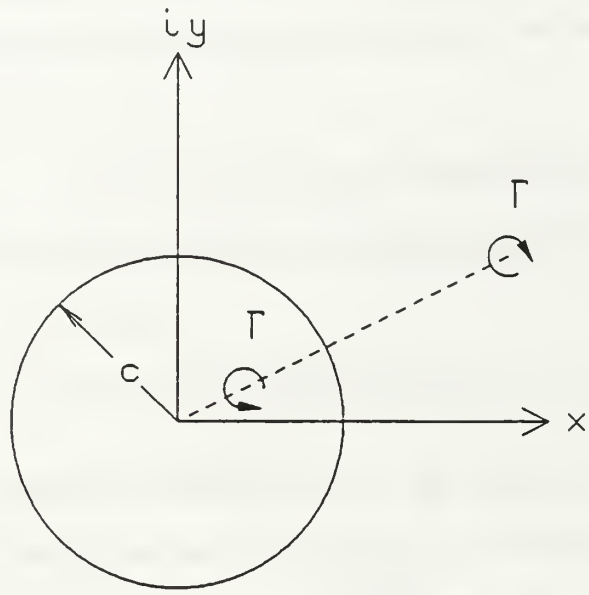


Figure 2.1 Complex coordinate system and cylinder orientation.

$$\left[\rho\frac{\partial\varphi}{\partial t}\right]_{uf+d} = -2\rho c\frac{\partial U}{\partial t}\cos\theta \tag{2.17}$$

$$= -2\rho c\omega U_m \cos\theta\cos\omega t. \tag{2.18}$$

Normalizing this quantity with $\frac{1}{2}\rho U_m^2$ one obtains

$$p_{uf+d} = \frac{\left[\rho\frac{\partial\varphi}{\partial t}\right]_{uf+d}}{\frac{1}{2}\rho U_m^2}$$

$$= -\frac{4\pi}{\mathbf{K}}\cos\theta\cos\omega t. \tag{2.19}$$

## 2. Real and Imaginary Vortices

### *a. Real vortices*

As before, only the real part of the complex potential functions of the real vortices is required for the velocity potential:

$$\left[\rho\frac{\partial\varphi}{\partial t}\right]_{rv} = Re\left\{\frac{i\rho}{2\pi}\sum_{n=1}^{N}\frac{\partial}{\partial t}\left[\Gamma_n ln(z-z_n)\right]\right\}_{r=c} . \tag{2.20}$$

Noting that

$$\frac{\partial z_n}{\partial t} = u_n + iv_n , \tag{2.21}$$

where $u_n$ and $v_n$ are, respectively, the x- and y-components of velocity at the vortex position, one obtains:

$$\left[\rho\frac{\partial\varphi}{\partial t}\right]_{rv} = Re\left\{-\frac{i\rho}{2\pi}\sum_{n=1}^{N}\Gamma_n\frac{u_n+iv_n}{z-z_n}\right\}_{r=c} + Re\left\{\frac{i\rho}{2\pi}\sum_{n=1}^{N}\frac{\partial\Gamma_n}{\partial t}ln(z-z_n)\right\}_{r=c} . \tag{2.22}$$

Again, normalizing with $\frac{1}{2}\rho U_m^2$ , utilizing the nondimensional variables introduced in Equations (2.10), and dropping primes, one has

$$p_{rv} = \frac{\left[\rho\frac{\partial\varphi}{\partial t}\right]_{rv}}{\frac{1}{2}\rho U_m^2}$$

$$= Re\left\{\frac{i}{\pi}\sum_{n=1}^{N}\left[-\Gamma_n\frac{u_n+iv_n}{z-z_n}+\frac{\partial\Gamma_n}{\partial t}ln\left(z-z_n\right)\right]\right\}_{r=1} . \tag{2.23}$$

### *b. Image vortices*

In an analogous fashion, the nondimensional pressure due to the time rate of change of potential functions of the image vortices is

$$p_{iv} = Re\left\{-\frac{i}{\pi}\sum_{n=1}^{N}\left[\Gamma_n \frac{u_n - iv_n}{\bar{z}_n\left(z\bar{z}_n - 1\right)} + \frac{\partial \Gamma_n}{\partial t} ln\left(z - \frac{1}{\bar{z}_n}\right)\right]\right\}_{r=1} . \tag{2.24}$$

*c. Total pressure due to vortices*

Combining the two preceding pressure components, one obtains the nondimensional pressure due to the vortices:

$$p_{vort} = p_{rv} + p_{iv}$$

$$= \frac{1}{\pi} Re\left\{ i\sum_{n=1}^{N}\frac{\partial \Gamma_n}{\partial t} ln\left(\frac{z - z_n}{z - \frac{1}{\bar{z}_n}}\right) - i\sum_{n=1}^{N}\Gamma_n\left[\frac{u_n + iv_n}{z - z_n} + \frac{u_n - iv_n}{(z\bar{z}_n - 1)\bar{z}_n}\right]\right\}_{r=1} . \tag{2.25}$$

### 3. Velocity-Squared Term

On the cylinder surface,

$$q^2(\theta) = \left(\frac{\partial w}{\partial z}\right)\overline{\left(\frac{\partial w}{\partial z}\right)}_{r=c} \tag{2.26}$$

so that, upon normalizing with $\frac{1}{2}\rho U_m^2$, one obtains

$$p_{v^2} = -\frac{\frac{1}{2}\rho q^2(\theta)}{\frac{1}{2}\rho U_m^2} . \tag{2.27}$$

Introducing the normalized cylinder surface velocity

$$q'(\theta) = \frac{q(\theta)}{U_m} \tag{2.28}$$

and dropping the prime for simplicity, one has

$$p_{v^2} = -q^2(\theta). \tag{2.29}$$

### 4. Final Expression for Pressure

Now, combining all of the pressure terms, the following expression for nondimensional pressure on the cylinder surface results:

$$p(\theta) = p_{uf+d} + p_{vort} + p_{v^2} \tag{2.30}$$

$$= -\frac{4\pi}{\mathbf{K}}\cos(\theta)\cos(\omega t)$$

$$+\frac{1}{\pi}Re\left\{ i\sum_{n=1}^{N}\frac{\partial\Gamma_n}{\partial t}ln\left(\frac{z-z_n}{z-\frac{1}{\bar{z}_n}}\right) - i\sum_{n=1}^{N}\Gamma_n\left[\frac{u_n+iv_n}{z-z_n}+\frac{u_n-iv_n}{(z\bar{z}_n-1)\bar{z}_n}\right]\right\}_{r=1} \tag{2.31}$$

$$-q^2(\theta).$$

## D. ALTERNATIVE METHODS OF EVALUATING THE RESISTANCE

There are several methods to evaluate the forces acting on a stationary circular cylinder of unit length immersed in a time-dependent flow containing N vortices of strengths $\Gamma_n$ and locations $z_n$. The various methods will be presented and contrasted.

### 1. Generalized Blasius Theorem

This method (see, e.g., Milne-Thomson [1968] ) actually begins with a pressure integration about the cylinder, and appears in its final form as

$$C_{ilf} + iC_1 = \overline{\frac{i}{2}\int\left(\frac{\partial w}{\partial z}\right)^2 dz} + i\frac{\partial}{\partial t}\int w dz. \tag{2.32}$$

Sarpkaya [1963, 1981a] has applied this method to the problem at hand, and has arrived at the following results:

$$C_{ilf} = -\sum_{n=1}^{N}\Gamma_n(v_n - v_n^1) + \sum_{n=1}^{N}q_n^1\frac{\partial\Gamma_n}{\partial t} + 2\pi\frac{\partial U}{\partial t} \tag{2.33}$$

and

$$C_l = \sum_{n=1}^{N} \Gamma_n (u_n - u_n^i) - \sum_{n-1}^{N} p_n^i \frac{\partial \Gamma_n}{\partial t}, \tag{2.34}$$

where p and q are, respectively, the x- and y-coordinates of a vortex, and the superscript refers to the image vortices. It should be noticed that, since the complex integration in Equation (2.32) is around the cylinder circumference, the singularities associated with the real vortices produced no residues. Accordingly, Equations (2.33) and (2.34) lack terms

$$-\sum_{n=1}^{N} q_n \frac{\partial \Gamma_n}{\partial t} \tag{2.35}$$

and

$$\sum_{n=1}^{N} p_n \frac{\partial \Gamma_n}{\partial t}, \tag{2.36}$$

respectively. Additionally, Sarpkaya [1981a] has pointed out the unacceptability of having $d\Gamma_n/dt = 0$ - since, by referring to Equation (2.33), one may observe that this leads to $C_m = 2$ at all times, which is clearly a deviation from experimental results. Although there have not yet been any accurate measurements made concerning the rate of decay of shed vortices, the arguments presented by Sarpkaya would indicate that a DVM should incorporate some form of vortex strength dissipation or vorticity annihilation through the interaction of oppositely-signed vorticity.

### 2. Time Rate of Change of Impulse of a Vortex Pair

Considering every real vortex to form a pair with its own image (Milne-Thomson [1966] ), the impulse imparted by that pair to the cylinder is

$$\begin{aligned} I_n &= i\rho\Gamma_n \Delta z_n \\ &= i\rho\Gamma_n \left[ z_n - \frac{c^2}{\bar{z}_n} \right] \end{aligned} \tag{2.37}$$

The total impulse acting on the cylinder is the sum of the effect of all of the vortex pairs

$$I = i\rho \sum_{n=1}^{N} \Gamma_n \left[ z_n - \frac{c^2}{\bar{z}_n} \right], \tag{2.38}$$

and the force per unit length acting on the cylinder is the time rate of change of the impulse, plus the appropriate inertial force:

$$D + iL = \frac{dI}{dt} + 2\pi\rho c^2 \frac{\partial U}{\partial t}$$

$$= i\rho \frac{\partial}{\partial t} \sum_{n=1}^{N} \Gamma_n \left[ z_n - \frac{c^2}{\bar{z}_n} \right] + 2\pi\rho c^2 \frac{\partial U}{\partial t}. \tag{2.39}$$

Contrasting this result with that obtained via the generalized Blasius equation, it is seen that Equation (2.39) includes the terms (Equations (2.35) and (2.36)) which were not present in Equations (2.33) and (2.34), respectively.

### 3. Direct Integration of Pressure Around the Cylinder

Both of the preceding methods incorporate differential quantities, and, as such, are extremely sensitive to any vortex strength dissipation, annihilation at the boundary, or amalgamation scheme (these will be discussed in detail in the next chapter). Integration of the pressure around the cylinder (see Figure 2.2), however, gives results which are not only close to either of the above methods, but which are also significantly smoother and more well-behaved. This is true, in general, when comparing numerical integration methods to numerical differentiation (see, e.g., Gerald [1978] ). Accordingly, the following equation was utilized in the current analysis to evaluate the in-line force on the cylinder:

$$C_{ilf} = -\frac{\int_0^{2\pi} p(\theta) c \cos\theta \, d\theta}{\frac{1}{2}\rho U_m^2 D} \tag{2.40}$$

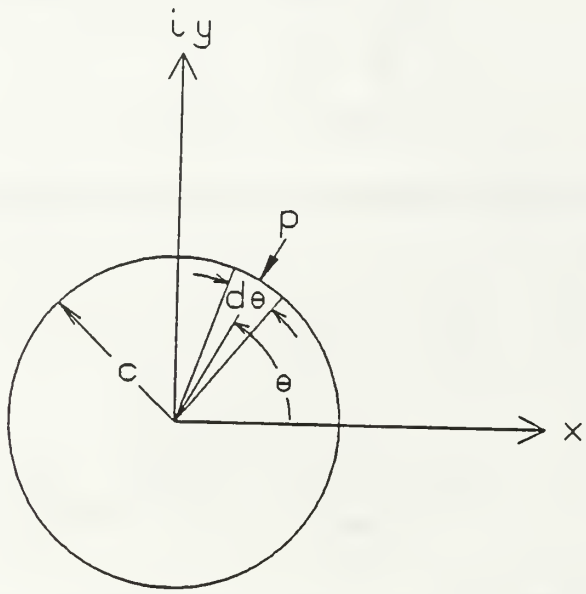


Figure 2.2 Pressure integration.

$$= \frac{c}{D} \int_0^{2\pi} p'(\theta) \cos\theta d\theta \tag{2.41}$$

The prime denoting normalized pressure is dropped for simplicity, and noting that D=2c, one obtains

$$C_{ilf} = -\frac{1}{2} \int_0^{2\pi} p(\theta) \cos\theta d\theta. \tag{2.42}$$

Similarly, to obtain the lift force,

$$C_l = -\frac{\int_0^{2\pi} p(\theta) c \sin\theta d\theta}{\frac{1}{2}\rho U_m^2 D} \tag{2.43}$$

$$= -\frac{1}{2}\int_{0}^{2\pi} p(\theta)\sin\theta d\theta. \tag{2.44}$$

## E. PREVIOUS INVESTIGATIONS

Although some of the DVM's proposed to simulate harmonic flow about cylinders have many realistic features, there are still a whole host of problems which remain to be overcome, each of which is, in itself, a fundamental research problem. These include separation point prediction, creation and destruction of vorticity, asymmetry initiation, the existence of secondary vorticity and its point of introduction, wall-vortex and vortex-vortex interactions, mixing of oppositely-signed vorticity, and the need, in many instances, to know in advance (via flow visualization experiments) the physics of the flow. Moreover, in all of these DVM's it is difficult to specify a particular Reynolds number which describes the flow—instead, only a particular flow regime may normally be specified, depending on the criterion utilized to predict separation. After reviewing various approaches to solving the case of harmonic flow, the next chapter will consider many of the elements of the DVM in more detail.

### 1. Ward and Dalton [1969]

This investigation considered only the case of symmetric vortex shedding over the range $2.5 < \mathbf{K} < 30$, even though most of this range is characterized by asymmetric vortex shedding. The reason for maintaining symmetry was a series of limited flow visualization experiments, wherein it was noted "that, for certain amplitudes and frequencies of motion, the symmetry of the vortex pairs is retained for several oscillations, even through the shedding process." This experimental observation is correct, but what is most important is the quasi-steady flow which follows the transient state. Attempting to base any conclusions on only one cycle of symmetrical, transient flow is inappropriate. More will be said about this later. Additionally, Ward and Dalton employed constant, average locations for the separation points which were based on experimental data. Although it is stated that the numerical experiments were

conducted over a wide range of Keulegan-Carpenter numbers, results are shown only for $\mathbf{K} = 4\pi$, and are not in agreement with the data of Sarpkaya [1976].

### 2. Sarpkaya [1976]

A time-sequence of discrete vortex flow about a circular cylinder for $\mathbf{K} = 9.2$ was included as an appendix to the report, although no details of the analysis were given.

### 3. Stansby [1977, 1979, 1981], Stansby and Dixon [1982, 1983]

Utilizing separation points fixed at $\pm 90°$ on the cylinder, Stansby [1977] sidestepped the issue of separation point prediction. In his next paper [1979], he cited the limited flow visualization of Grass and Kemp [1979] as justification for fixing the separation points at $\pm 90°$; Grass and Kemp presented data for only $\mathbf{K} = 38$, from which it is possible to ascertain a general idea of where the separation zone is located. In fact, the only place where separation "points" exists, per se, is in numerical analyses. The data of Grass and Kemp (Figure 2.3) show separation occurring around the top and bottom of the cylinder for times when the ambient flow is close to its maximum value; one of the essential ingredients of an accurate DVM of harmonic flow, however, is the ability of the returning wake to freely interact with the boundary layer in the creation of new vorticity. By arbitrarily positioning the separation points, the resulting flow pattern is being biased.

When calculating nascent vortex strengths, Stansby utilized not the velocity at the separation point, but rather the velocity of the nascent vortex itself. The result is significantly less vorticity input; compared with most other DVM's, this model would appear to dissipate a significant portion (on the order of 40 per cent) of the nascent vortex strength at the instant of the nascent vortex shedding.

Also noteworthy is that, in his two later papers, Stansby [1979, 1981] has employed a cloud-in-cell technique to calculate the velocities (see, e.g., Baker [1979] and Stansby and Dixon [1982, 1983] ); this is done in lieu of a straightforward induced velocity summation to save computer execution time. Stansby and Dixon [1983] later employed a Lagrangian scheme, and utilized a series of polygonal line

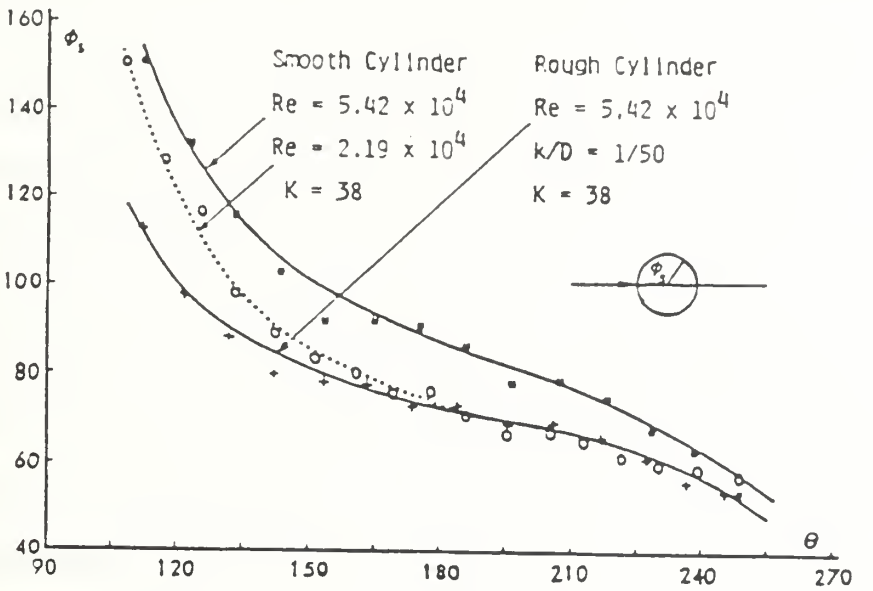


Figure 2.3 Variation of the separation angle over a half cycle (from Sarpkaya and Isaacson [1981] ).

segments to represent the body. Vortex sheet segment strengths were calculated at each time step to satisfy the no-slip condition on the body surface; these were derived from the inversion of an influence matrix which, in turn, utilized tangential velocities calculated immediately inside the body surface. The line segments were then replaced by a series of point vortices. The calculations for **K** = 10 failed to produce the experimentally-observed transverse vortex street.

### 4. Sawaragi and Nakamura [1979]

Although this work was the first in which a dedicated series of flow visualization experiments was conducted in support of numerical work in harmonic flow, only sketches of the various flow patterns were presented. Based on their flow visualization results, the authors did not introduce any artificial asymmetry for **K** < 8; Sarpkaya [1981a] notes, however, that asymmetries in the flow develop in the 4 < **K** < 5 regime. For **K** > 8, Sawaragi and Nakamura halved the strength of the nascent vortices on one

side of the cylinder for an arbitrary length of time following the onset of separation, thereby triggering asymmetry.

The locations of the separation points were calculated using Schlichting's [1932] periodic boundary layer theory; more will be said in the next chapter concerning the propriety of this separation point prediction scheme. Nascent vortices were placed in the flow at the edge of the boundary layer and midway between the current and previous angular location of the separation point; thus, a Kutta condition, as is normally employed in the literature, was not utilized. The image vortices which were not included in Equation (2.7) above, were retained by Sawaragi and Nakamura; therefore, although the zero normal velocity criterion is satisfied on the cylinder, the tangential velocity on the cylinder is incorrect since the Helmholtz circulation conservation theorem has been violated. Finally, calculations are performed for only three-quarters of a cycle, hardly enough time for the transient flow to develop into a quasi-steady state.

### 5. Kudo [1979, 1981]

This study was the first numerical application of harmonic flow to a flat plate oriented normal to the flow. Although the analysis considered flows in the range $\pi/2 < \mathbf{K} < 5\pi$ and for times as high as almost five complete cycles, the flow was treated as symmetric. Kudo's model also incorporated a Kutta condition combined with a very complicated force- and moment-free nascent vortex placement scheme. In the interest of saving computer time, vortices were removed from the flow fields when they traveled a certain distance from the plate; this distance was based on the distance traveled by the vortices shed in the first half cycle.

### 6. Ikeda and Himeno [1981]

In addition to harmonic flow about circular cylinders, this study also included flow about Lewis form cylinders by using a mapping function; Lewis form cylinders find application in the flow about transverse sections of ships floating in a horizontally oscillating fluid medium. Separation was ascertained with Schlichting's [1932] method, as in Sawaragi and Nakamura [1979] above; an attempt

was made to incorporate an arbitrary phase shift in the separation point scheme to bring the results into closer agreement with experimental observations. Vortices were placed at a distance midway between the cylinder and outer edge of the boundary layer. Calculations continued for as long as 2½ cycles, and were performed for the range $2 < \mathbf{K} < 10.5$. As with Sawaragi and Nakamura, the vortex images were retained at the center of the cylinder in Equation (2.7).

### 7. Ikeda [1984a, 1984b]

The model used here is essentially the same employed by Ikeda and Himeno [1981], except that asymmetry was triggered during the first twentieth of a cycle beyond the inception of separation; during this time, nascent vortex strengths were halved on one side of the cylinder. Calculations continued for as long as 2½ cycles, and were performed for a wide range of Keulegan-Carpenter numbers.

### 8. Mostafa [1987]

Working with Sarpkaya, Mostafa [1987] was able to accurately simulate the transverse vortex street characteristic of the range $10 < \mathbf{K} < 20$. Results were presented only for $\mathbf{K} = 12$, and the calculated forces were somewhat larger than those obtained experimentally. It is to be noted that no circulation reduction scheme was employed, nor were any verification runs presented for the limits $\mathbf{K} \rightarrow \infty$ or $\mathbf{K} << 1$.

## F. SYNOPSIS OF THE PREVIOUS INVESTIGATIONS

Each of the above DVM's of harmonic flow suffers from several major arbitrary assumptions, but perhaps the most critical of these concerns the positioning of the nascent vortices. In most of the models the wake is not permitted to interact with the boundary layer and thus affect the angular location of the next nascent vortex. Perhaps the second most significant assumption in some of the above models is that of symmetric flow. In reality, most Keulegan-Carpenter number flows do not develop asymmetries until the flow has executed many cycles; the constraints of most computer systems (execution times and storage limitations) dictate that some artificial method of asymmetry introduction be utilized to shorten the amount of time spent in the transient flow state.

Several of the models were run for less than one cycle. Even if an asymmetry mechanism could be developed to accelerate the transition to the quasi-steady state, most models would require at least 2½ to 3 complete cycles for meaningful results.

Finally, none of the models incorporated any type of dissipation scheme, although Ikeda [1984] did acknowledge the need for one. Several of the applications utilized Lamb vortex velocity models which diffuse with time; note, though, that the strength of a viscous vortex does not change with time. It is felt, however, that the effect of dissipation on flow kinematics is minimal; it will, rather, be of use in bringing the gross aspects of the flow into agreement with experimental results once the kinematics are correct. These and many other elements of the DVM's will be analyzed in an attempt to determine the most phenomenologically correct combination of assumptions to obtain the kinematics of harmonic flow about circular cylinders.

# III. ELEMENTS OF THE DISCRETE VORTEX MODEL

## A. INTRODUCTION

The simulation of harmonic flow about bluff bodies challenges all elements of the DVM. For unidirectional separated flows, the wake remains on the downstream side of the body; although the attached and shed vortices play a role in the separation process, their influence is felt primarily on the base of the body. This influence diminishes rapidly as the vortices continue to move downstream, so that the representation of vortex sheets by an array of discrete vortices is a reasonable approximation. For reversing flows, however, the interaction between the vortices and the generating surface (and among the vortices themselves) is an order of magnitude more complex than in unidirectional flows. As a brief review of the previous investigations has shown, many ad hoc assumptions have been required to overcome these difficulties; the propriety of these assumptions will now be examined in detail, and the most promising solutions will be identified.

## B. SEPARATION POINT PREDICTION

It is possible to accurately predict separation only for bodies with sharp edges. For the relatively simple case of steady, unidirectional ambient flow past bluff bodies without sharp edges, separation points can only be predicted approximately for laminar flows; the situation becomes almost intractable for turbulent flows. Experiments (see, e.g., Sarpkaya and Butterworth [1992] ) have shown that for unsteady flows, mobile separation points may experience large excursions, thereby making the numerical simulation of these flows extremely difficult. Indeed, it has been pointed out by Sarpkaya [1989] that a universally applicable definition of separation for all classes of unsteady flows has yet to be defined. A more extensive discussion on this issue is given by Sarpkaya [1989].

Although flow visualization experiments have verified that several separation points may exist at any instant on a body in harmonic flow, the two most prominent ("primary") vortices are normally shed from shear layers which originate on the forebody, and separate when unable to sustain an adverse

pressure gradient. Numerical techniques can be used for predicting the approximate positions of the separation points, although an arbitrary decision must be made whether to use a laminar (Pohlhausen [1921], Loitsianski [1941], Thwaites [1949], Stratford [1954], etc.) or a turbulent (Stratford [1959], Takada [1975] ) scheme. These methods allow mobile separation points (see, e.g., Sarpkaya and Shoaff [1979], Deffenbaugh and Marshall [1976], or Mostafa [1987] ) and give results superior to those obtained with fixed separation points (Davis [1969], Stansby [1977] ). As the primary vortices grow, the velocities they induce on the base of the body produce additional boundary layers and secondary separation points. The resulting secondary vortices eventually mix with the primary vortices, and are an important aspect of the flow since they reduce the magnitude of the primary vortices. More will be said about countervortices later.

In reversing flows, however, primary and secondary vortices are convected back across the body; this poses significant difficulties in the prediction of separation from bodies which lack sharp edges. If it is assumed that the flow is quasi-steady from one time step to the next, then one of the above-mentioned separation prediction methods for steady ambient flow may be used; each of these methods, however, requires a smooth velocity or pressure distribution for meaningful results, and this proves to be a significant source of difficulty. Consequently, most investigators who have used the DVM for the analysis of the harmonic flow problem have employed either fixed separation points or have predicted separation based on Schlichting's [1932] solution. Ward and Dalton's [1969] use of fixed separation points was based solely on average values determined from flow visualization experiments; during the first half-cycle, separation was assumed to occur at ±60° from the rear stagnation point, and during the second half-cycle, at ±40° from the rear stagnation point. Stansby [1977, 1979, 1981] chose to fix separation at ±90°, arguing that this was close to the separation regions observed by Grass and Kemp [1979]. The use of separation points based on Schlichting's [1932] analysis (Ikeda and Himeno [1981], Ikeda [1984], and Sawaragi and Nakamura [1979] ) is also very arbitrary; Schlichting [1979] has noted that his method is acceptable only if

$$\frac{U_m T}{D} = \mathbf{K} << 1, \tag{3.1}$$

so that it is not a valid method in predicting separation for the higher Keulegan-Carpenter numbers considered in this study. In either case, the wake is not allowed to interact with the boundary layers and to freely influence the location of the separation points. Although the returning vortices affect the magnitude of the shed vorticity, the separation points are slaved to either a fixed location or to a predetermined route with respect to time.

The experimental results of Grass and Kemp [1979] (for **K** = 38) and Sarpkaya and Butterworth [1992] have shown that the separation points on a circular cylinder may experience excursions of 120° during a single half-cycle. The returning wake very strongly affects the positions of the separation points; any DVM of harmonic flow must also have a means whereby the nascent vortices are allowed to vary in *both* magnitude and location in response to the surrounding flow. No satisfactory unsteady separation point prediction technique currently exists for circular cylinders in harmonic flow; even for the case of unidirectional steady flow about circular cylinders, all of the aforementioned methods provide only approximate locations for the separation points.

Mostafa [1987] calculated primary shear layer separation points using the Pohlhausen method (see Sarpkaya and Shoaff [1979] ). When the forebody velocity profile became distorted by returning vortices, separation was said to occur at a point slightly downstream of the maximum velocity or absolute maximum pressure; should the separation angle jump more than 8° from one timestep to the next, the local velocity maximum closest to the maximum absolute pressure was used to determine the separation point. Even with this somewhat time consuming calculation, the plot of stagnation point versus time was very jagged and sporadic, and showed movement of the primary separation point on the order of 120°.

To ascertain the nature of some of the problems associated with the use of a boundary layer method in harmonic flow, the same Pohlhausen technique employed by Sarpkaya and Shoaff [1979] and Mostafa [1987] was utilized in connection with harmonic flow about a circular cylinder. As anticipated,

returning vorticity resulted in forebody velocity distributions with which the Pohlhausen technique could not realistically cope. This occurred in two different ways.

### 1. Discrete Vortex Returning to Forebody

Due to the singular nature of the velocity induced by a point vortex, velocity distributions may be far from smooth. Figure 3.1 shows a cylinder velocity distribution which has been perturbed by two returning discrete vortices, A and B. The solid line in the plot of velocity depicts what the cylinder velocity distribution would have been without the influence of the two point vortices. When entire clusters were "crushed" against the cylinder, the velocity distributions were significantly more irregular. Since the Pohlhausen calculation must proceed from the forward stagnation point, C, downstream, several consequences are possible:

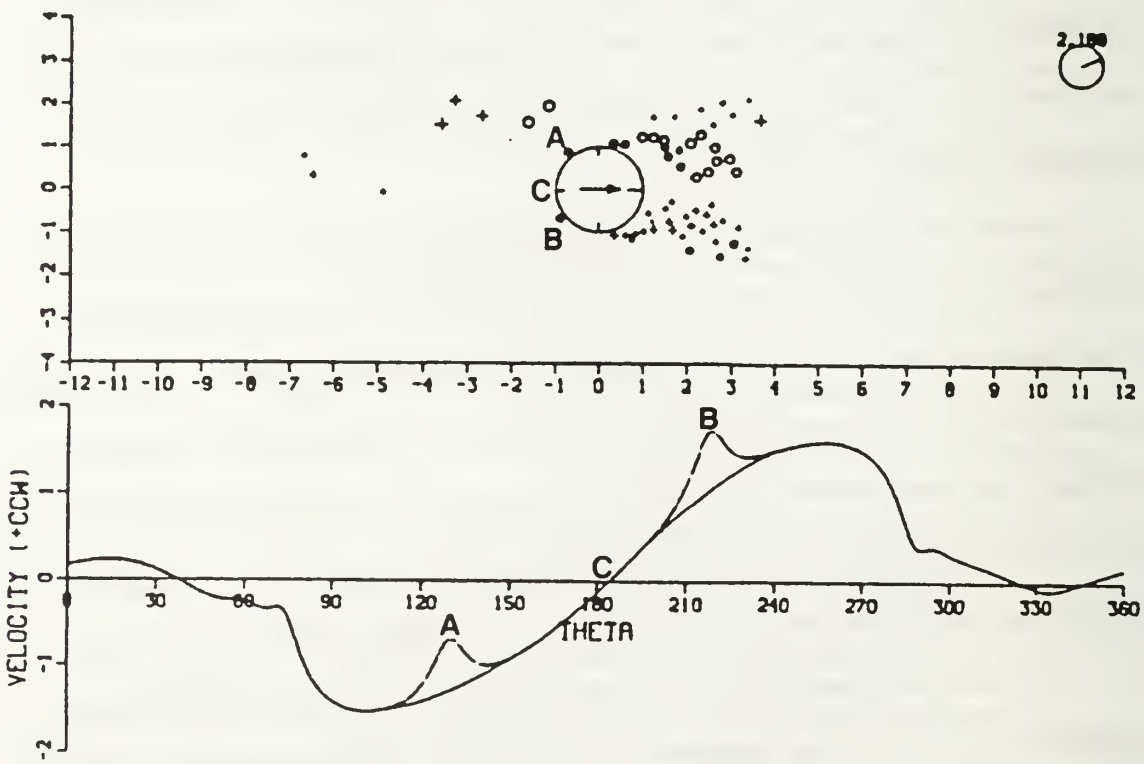


Figure 3.1 Cylinder velocity distribution perturbed by individual discrete vortices.

- The upper separation point could move to the vicinity of point A
- Calculation could fail between points B and C.

Similar problems were reported by Shoaff and Franks [1981] in applying the Pohlhausen method to predict separation on bodies which required numerical transformation, and by Mostafa [1987]. DVM's usually provide for the annihilation of discrete vortices when they approach to within a small distance of a flow boundary; the phenomenological basis for this mechanism is that the core of a real vortex "touches" the core of its image, so that the two cancel each other. Even with this annihilation region extending into the flow for ten per cent of a cylinder radius, problems are still encountered in the velocity distribution on the cylinder. Most of these problems can be alleviated by utilizing a viscous (sometimes referred to as a "finite") vortex velocity calculation, so that the infinite velocity at the vortex center is reduced to zero. The distribution of vorticity is

$$\omega(r,t) = \frac{\Gamma}{4\pi\nu t} e^{\frac{-r^2}{4\nu t}}, \tag{3.2}$$

which results in a velocity distribution of

$$v(r,t) = \frac{\Gamma}{2\pi r}\left(1 - e^{\frac{-r^2}{4\nu t}}\right), \tag{3.3}$$

where r is the radial distance from the vortex center, t is the vortex age, and $\nu$ is a suitably chosen value for viscosity. The core radius may be obtained from $\partial v / \partial r = 0$ (see, e.g., Lamb [1932] ):

$$r^* = 2.24\sqrt{\nu t}. \tag{3.4}$$

There are still, however, occasional instances when use of a finite vortex will be unable to overcome this problem.

### 2. Vortex Cluster Within Approximately One Cylinder Diameter

This is a more realistic effect than is the close approach of a few discrete vortices to the cylinder, since the close passage of a cluster induces a velocity field not significantly different from that produced by a real vortex. A typical velocity distribution is shown in Figure 3.2, where point A denotes the position at which the Pohlhausen technique fails in its march from the forward stagnation point, and the cluster of vortices producing this failure is circled.

In order to overcome the difficulties associated with either the close approach of a few discrete vortices or the relatively distant passage of a vortex cluster, several methods were attempted. Firstly, the Pohlhausen technique utilized by Sarpkaya and Shoaff [1979] for unidirectional flow was analyzed, and it was ascertained that separation occurred when the velocity had dropped to 97 per cent of the maximum velocity on the forebody velocity distribution; this was then employed as a criterion for separation, as had

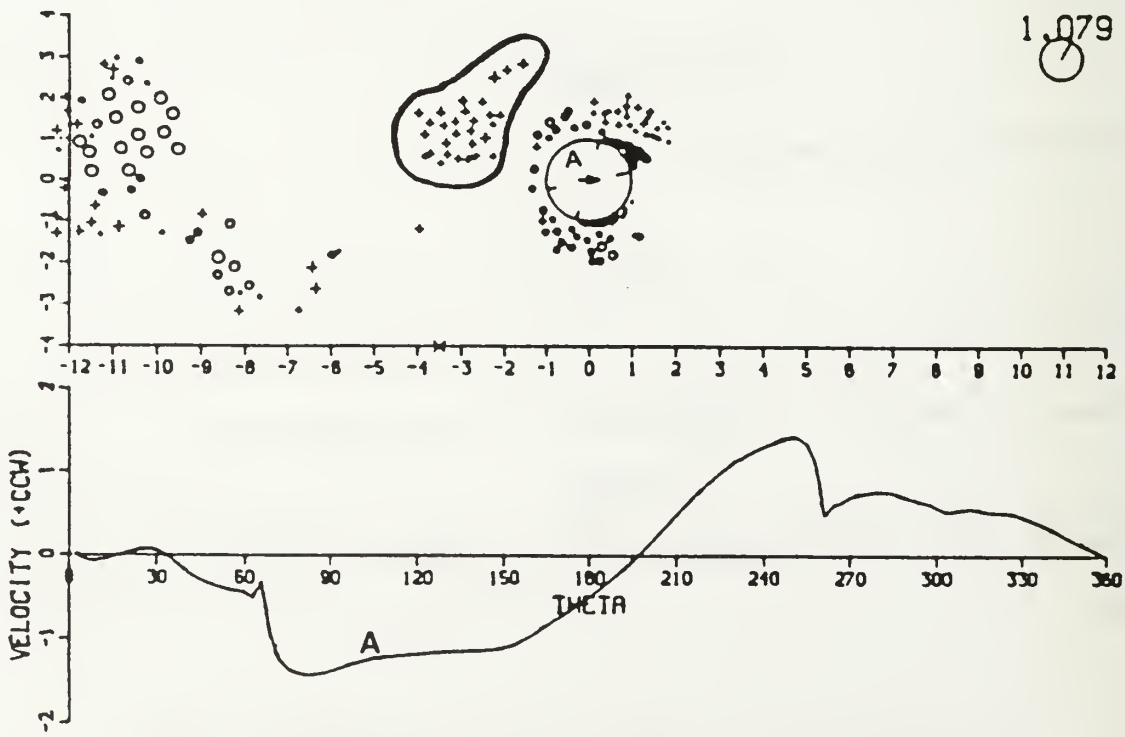


Figure 3.2 Cylinder velocity distribution perturbed by a returning vortex cluster.

been done by Shoaff and Franks [1981], Franks [1983], Stansby and Dixon [1982], and Mostafa [1987]. This achieved only limited success in the case of velocity distributions of the type depicted in Figure 3.3, since large jumps in the separation point were possible whenever the position of maximum velocity changed (see, for example, point A). The kinematics were still significantly different from those observed experimentally, as will be seen in the next chapter.

The use of a laminar boundary layer technique may, in itself, be inappropriate because the boundary layers are turbulent. A series of flow visualization experiments and force measurements on smooth and rough cylinders at very low Keulegan-Carpenter numbers ($0.5 < K < 10$) have shown (Yuen [1985] ) that only for extremely low values of K do the in-line forces agree with the laminar theory of Schlichting [1932]; the flow on the cylinder is turbulent for all other Keulegan-Carpenter numbers, even though the Reynolds number may be small enough to be considered laminar by conventional standards.

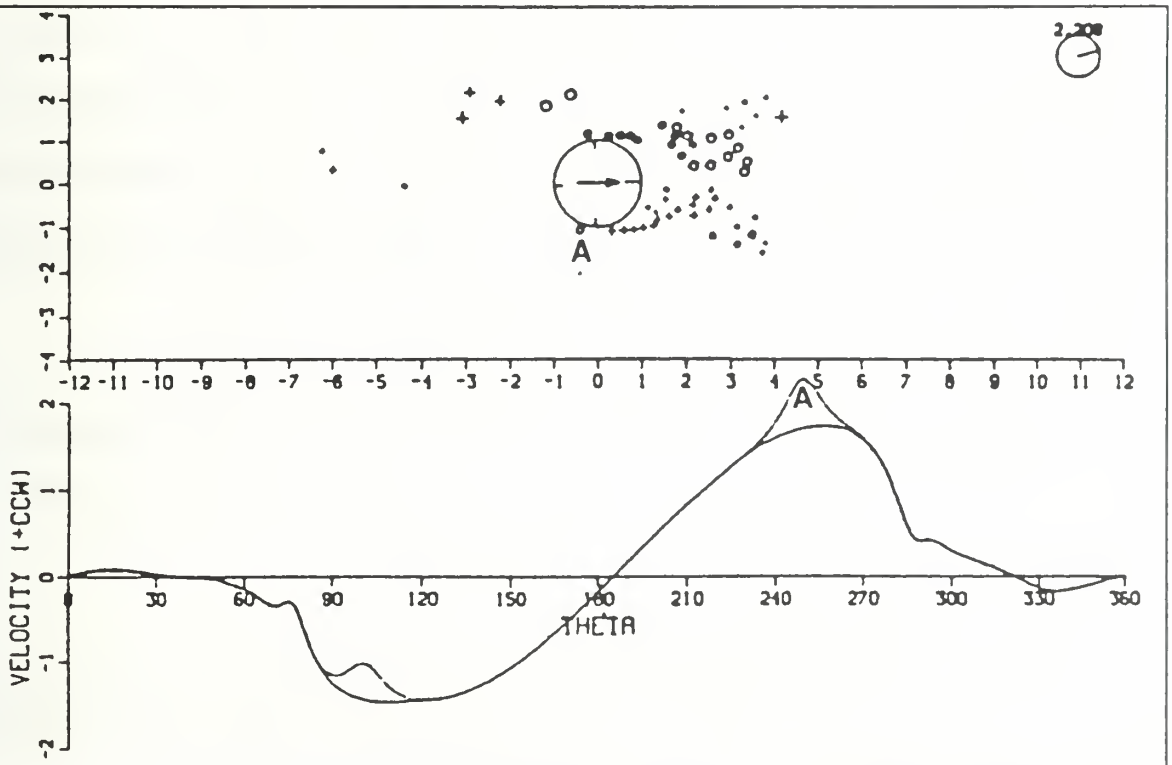


Figure 3.3 Illustration of how rapidly the position of maximum velocity may change due to the close approach of a discrete vortex.

For flows of significance in most ocean engineering applications (i.e., $\mathbf{K} > 4$), a turbulent boundary layer analysis is appropriate. In steady turbulent flows, the boundary layer is capable of withstanding an adverse pressure gradient longer, so that separation occurs on the order of 30° further downstream from the pressure minimum than in a laminar flow. There are several turbulent boundary layer separation techniques available for steady flow (see, e.g., Stratford [1959] or Takada [1975] ); even if it were assumed that a harmonic flow were sufficiently quasi steady for these methods to be applied for the prediction of separation, they would still be susceptible to the same difficulties encountered with the Pohlhausen technique. The change of pressure coefficient along the cylinder surface was utilized as a criterion to predict separation by both Stratford [1959] and Takada [1975]; just as the velocity distribution is perturbed by returning vorticity, so too is the pressure distribution.

In validating his technique for turbulent flow separation prediction, Takada [1975] applied it to several experimental pressure distributions, most of which showed that experimentally determined separation points occur roughly 30° downstream of the pressure minimum. Since the pressure minimum normally occurs very near the velocity maximum, several runs were made in the current research where the nascent vortex was placed at a position 30° downstream of the velocity maximum. Limited success was achieved with this method since the separation point could change radically as the velocity maximum changed during the convection of a cluster back across the cylinder.

Although other procedures were implemented in an attempt to simulate separation from a turbulent boundary layer, no satisfactory method was found. It is still felt that a turbulent boundary layer technique will be the most appropriate separation prediction method for harmonic flow about circular cylinders.

## C. INTRODUCTION OF VORTICITY

In many DVM's, the time rate of introduction of vorticity from the boundary layer per unit length along the cylinder is calculated as

$$\frac{d\Gamma}{dt} = \int_0^{\delta} \omega u dy, \tag{3.5}$$

where $\delta$ is the boundary layer thickness, $\omega$ is the vorticity

$$\omega = \frac{\partial v}{\partial x} - \frac{\partial u}{\partial y}, \tag{3.6}$$

x and y are the coordinates parallel to and orthogonal to the surface, respectively; u and v are the velocity components parallel to and orthogonal to the surface, respectively. Invoking the normal boundary layer assumptions, one obtains the following for the magnitude of the generation rate of vorticity:

$$\frac{d\Gamma}{dt} = \int_0^{\delta} \frac{\partial u}{\partial y} u dy \tag{3.7}$$

$$= \frac{1}{2}\left(U_s^2 - U_o^2\right), \tag{3.8}$$

where $U_s$ is the tangential velocity at the outer edge of the shear layer at the predicted separation point and $U_o$ is the velocity on the inner side of the shear layer. Fage and Johansen's [1928] extensive experiments have shown that one may write

$$\frac{d\Gamma}{dt} = \frac{1}{2} U_s^2. \tag{3.9}$$

In numerical calculations, $d\Gamma/dt$ is replaced by $\Delta\Gamma/\Delta t$ so that the strength of a nascent vortex may be calculated by

$$\Gamma_{nv} = \frac{U_s^2 \Delta t}{2}. \tag{3.10}$$

In the most general case, though, the nascent vortex must be assumed to be a function not only of position, but also of time (see, e.g., Ikeda and Himeno [1981] ), so that

$$\Gamma = \Gamma(s, t), \tag{3.11}$$

where s is arc length along the cylinder surface, $s = c\,\theta$. A differential change in $\Gamma$ is then calculated as

$$d\Gamma = \frac{\partial \Gamma}{\partial t} dt + \frac{\partial \Gamma}{\partial s} ds. \tag{3.12}$$

But

$$\frac{\partial \Gamma}{\partial s} = U_s \qquad\qquad ds = c d\theta \tag{3.13}$$

and $d\Gamma/dt$ may be obtained from Equation (3.9) above. Equation (3.12) then simplifies to

$$d\Gamma = \frac{1}{2} U_s^2 dt + U_s c d\theta \tag{3.14}$$

or, for numerical calculations,

$$\Gamma_{nv} = \frac{1}{2} U_s^2 \Delta t + U_s c \Delta \theta. \tag{3.15}$$

Note that for the case of steady, unidirectional flow, $\Delta\theta$ is approximately equal to zero, and Equation (3.10) results.

The same result may be obtained (Sarpkaya [1985] ) by replacing u in Equation (3.7) by the relative velocity at the separation point:

$$\frac{d\Gamma}{dt} = \int_0^{\delta} \frac{\partial u}{\partial y} (u - U_s) dy \cdot \tag{3.16}$$

Although it is not yet possible to account for all of the unsteady aspects of the harmonic flow problem, Equation (3.15) does bring some of the unsteady effects into play.

## D. ASYMMETRY INITIATION

Without any form of artificial asymmetry, the numerical simulation would produce a flow pattern which retains perfect symmetry about the x-axis, at least until round-off error or some form of numerical instability occurs. In nature, even for the case of unidirectional flow about circular cylinders, the symmetric ambient flow results in the non-symmetric effect of alternate vortex shedding.

It is an experimentally established fact that a sinusoidally oscillating flow will normally require many cylces to establish its quasi-steady state. In the numerical simulation of these flows, execution time

and storage requirements of current computer systems dictate that some form of asymmetry introduction be employed to trigger an otherwise symmetric flow into its quasi-steady state before too many cycles have elapsed. This must be accomplished, however, without shocking the flow; the minimum asymmetry possible should be utilized. For the unidirectional flow past normal flat plates, there may be a very small angle of attack assigned to the flow to trigger the alternate vortex shedding (see, e.g., Kuwahara [1973] ). For flow past flat plates oriented perfectly normal to the flow direction or for flow past bluff bodies without well-defined separation points, asymmetry may be triggered in any number of ways: changing the strength of the nascent vortices on one vortex sheet, giving the vortices in one sheet a small downstream displacement, removing or adding a vortex, etc. These triggering methods are normally accomplished over some finite time period relatively early in the flow's development; in many instances, there may be an optimum time when the flow is most susceptible to any asymmetry. If asymmetry is initiated during this time of maximum sensitivity, the duration and intensity of its application may be minimized.

Several different forms of asymmetry were attempted in the current work. One method reduced the strength of each vortex in one sheet by approximately ten per cent as it passed a certain x-coordinate; this was in effect only during the very early part of the first half-cycle. A second method placed the nascent vortices in one sheet at approximately 90 per cent of the distance from the cylinder calculated with the Kutta condition. Both of these forms of asymmetry introduction resulted in a relatively sluggish asymmetrical growth of the vortex pattern.

For impulsive flow about a circular cylinder, Sarpkaya and Shoaff [1979] utilized an asymmetry which added a downstream displacement to the vortices of one sheet; this displacement varied as a function of nondimensional time (Ut/c) as shown in Figure 3.4, and resulted in a total displacement of approximately one third of a cylinder radius. This form of asymmetry, applied during approximately the first quarter-cycle of harmonic flow (i.e., while the ambient flow was accelerating) resulted in the relative vortex positions at the end of the first half-cycle most closely approximating those observed experimentally at much larger times. The functional form employed was:

$$\Delta x = \frac{B}{2}\left[1 - \cos\left(\frac{t - T1}{T2 - T1}\pi\right)\right]. \tag{3.17}$$

$\Delta x$ is the x-displacement applied to all vortices in one sheet at time t, where T1 is the time of initiation of the asymmetry, T2 is the time of termination, and B is the maximum value for the displacement. For impulsive flow, Sarpkaya and Shoaff [1979] used B = 0.04, T1 = 5.0, and T2 = 9.0.

## E. CONVECTION SCHEME

When convecting the discrete vortices at each time step, a first-order (Eulerian) scheme

$$z(t + \Delta t) = z(t) + q(t)\Delta t \tag{3.18}$$

or higher order schemes, such as the following second order methods, may be utilized (see, e.g., Sokolnikoff and Redheffer [1958] ):

$$z(t + \Delta t) = z(t - \Delta t) + 2q(t)\Delta t \tag{3.19}$$

$$z(t + \Delta t) = z(t) + \frac{1}{2}\left[3q(t) - q(t - \Delta t)\right]\Delta t, \tag{3.20}$$

where q and z are the complex vortex velocity and position, respectively.

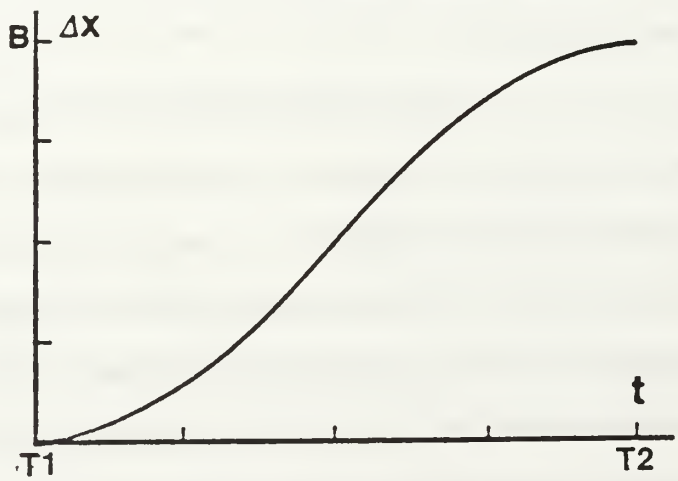


Figure 3.4 Variation of the asymmetry perturbation with time (from Sarpkaya and Shoaff [1979] ).

## F. CIRCULATION REDUCTION

There are three ways in which the circulation of a vortex may be reduced. Although each of these circulation reduction mechanisms is easily implemented in a numerical code, the difficulty lies in the relative and absolute degrees to which each affects the strengths of the vortices in the flow.

### 1. Wall Annihilation

As mentioned previously, the close approach of a vortex to the cylinder can induce very high velocities, with unrealistic effects on the in-line and lift forces, velocity and pressure distributions, etc. In reality, the vortices are not ideal point vortices. As a real vortex approaches a solid boundary, it "sees" its image and, in effect, "rubs" on it; as a consequence, both the real and image vortices are reduced in strength. This physical process may be carried over into the numerical model by specifying an arbitrary annihilation region around the cylinder; should a discrete vortex (i.e., a component of a larger cluster) be convected within this region, it will be assumed to have combined with its image vortex of equal magnitude, but of opposite sign.

The width of this region may be assigned in a variety of ways. If the individual discrete vortices are assumed to have Lamb vortex velocity distributions as in Equation (3.3), real-image combinations may be assumed to occur when their cores touch. Unless unrealistically low Reynolds numbers (i.e., very high numerical viscosity) are assumed, however, the vortices will still be able to approach very close to the cylinder before this annihilation criterion is met, with significant, although not infinite induced velocities. Although this criterion may be viewed as being less arbitrary than others, it is more prudent to assign an arbitrary region surrounding the body, within which vortices are annihilated.

Using such a buffer region of thickness $\Delta r = 0.04$, Sarpkaya and Shoaff [1979] found, just as had previous investigators (Clements [1977], Sarpkaya [1975] ), that this mechanism,

coupled with the combination of oppositely-signed vorticity, resulted in only a 10 to 15 per cent reduction in the strength of a cluster.

When buffer regions of a similar size were utilized in a harmonic flow application, it was found that, even for viscous core vortices, irregular boundary layer velocity distributions resulted on the cylinder; these made boundary layer calculations impossible (see Figure 3.1). As mentioned previously in conjunction with the discussion on separation points, Shoaff and Franks [1981] encountered similar difficulties after performing a mapping, and circumvented the difficulty by smoothing the velocity profile prior to performing a boundary layer analysis. In the present work, this smoothing was not attempted since it could arbitrarily affect the separation point location. Instead, the buffer region was increased to approximately $\Delta r = 0.18$ on the forebody (to allow proper functioning of the boundary layer calculations) and to approximately $\Delta r = 0.10$ on the base of the cylinder; upon flow reversal, these two values were switched. A smaller value for $\Delta r$ on the base of the cylinder was found to "shock" the system upon flow reversal; many vortices close to the cylinder would have been subjected to annihilation immediately upon reversal of the flow. These enlarged buffer regions quite naturally resulted in an increased percentage dissipation for vortex clusters.

### 2. Vortex-to-Vortex Proximity

As two discrete point vortices approach one another, larger and larger convection velocities result until one or both experience(s) an extremely large displacement; orbiting may also result. These motions result from the discrete nature of the individual vortices, and should be avoided. Consequently, when the distance between any two vortices falls below some value, they are combined and the resultant vortex of strength

$$\Gamma_{cov} = \Gamma_1 + \Gamma_2 \tag{3.21}$$

is placed at the "center of vorticity," calculated as

$$z_{cov} = \frac{|\Gamma_1| z_1 + |\Gamma_2| z_2}{|\Gamma_1| + |\Gamma_2|}. \tag{3.22}$$

Had $\Gamma_{cov}$ been very small, and had it been utilized in lieu of the denominator of the last equation, then the center of vorticity would have been at a physically unrealistic position relative to either of the original vortices. Equation (3.22) places the resultant vortex on a line joining the original vortices.

To determine the distance criterion for combination, several methods may be employed. The first specifies that, if the distance between two vortices

$$\Delta r = |\Delta z| = |z_1 - z_2| \tag{3.23}$$

is less than the sum of their core radii (see Equation (3.4)),

$$\begin{aligned} \Delta r^* &= r_1^* + r_2^* \\ &= 2.24\left[\sqrt{\nu t_1} + \sqrt{\nu t_2}\right], \end{aligned} \tag{3.24}$$

then the vortices should be combined. In general, however, the value of viscosity which must be utilized in the simulation of a high Reynolds number flow (a basic premise of the DVM's) is extremely small. Consequently, long before they approach closer than a distance $\Delta r^*$ too many vortices may still induce very large velocities on each other. It seems more prudent, therefore, to specify that two vortices will be combined whenever their separation is less than an arbitrary value; in the present work, the criterion employed is one-tenth of a cylinder radius.

In the current work, this combination is performed only between vortices of opposite sign. Were it allowed to combine discrete vortices of like sign, it would be possible for discrete vortices to grow in magnitude, with consequent unrealistic effects. These include vortex pairing, loss of the general shape of a cluster, and drastic effects on the boundary layer calculations when these large discrete vortices returned to the forebody.

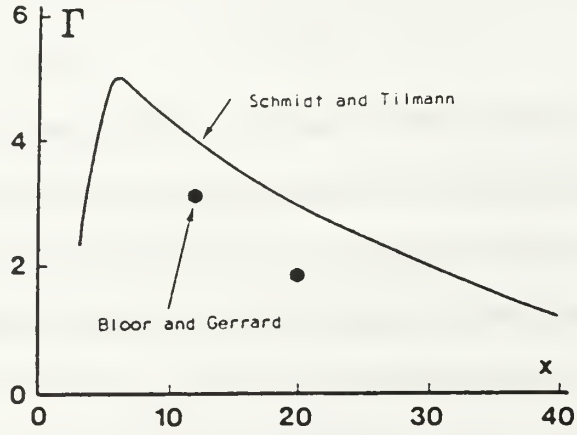


Figure 3.5 Vortex strength versus distance in unidirectional flow (from Sarpkaya and Shoaff [1979] ).

### 3. Artificial Dissipation

Numerical analyses of unidirectional flow (see, e.g., Sarpkaya and Shoaff [1979] ) have shown that the two preceding methods of circulation reduction account for approximately one-fourth to one-third of the total reduction in circulation experienced by a vortex. Experiments by von Schmidt and Tilmann [1972] and by Bloor and Gerrard [1966] (see Figures 3.5 and 3.6) show that while still attached to the cylinder by a feeding shear layer, vortices grow rapidly; simultaneously, however, they lose some of their strength via various circulation reduction mechanisms. The plots of Figures 3.5 and 3.6 should be regarded more as qualitative in nature than quantitative due to Reynolds number and three-dimensional effects and to the methods of evaluation of the values plotted. Sarpkaya [1989] points out that

> In an *inviscid* incompressible fluid of uniform density, subjected to irrotational body forces, the circulation around any closed material curve is invariant (Kelvin's circulation theorem). This is a consequence of the fact that there is no diffusion and vorticity is transported solely by the convection of the fluid. In a *viscous* fluid, however, the circulation about a closed contour moving with the fluid depends on the contour of integration. The rate of change of vorticity in a material volume is due solely to diffusion across the boundary of the volume.

The first two circulation reduction mechanisms mentioned above result from the combination of oppositely-signed vorticity--reduction from these numerical mechanisms, however, does not bring circulation down to levels commensurate with those observed experimentally. The additional reduction

mechanisms may be due to the entrainment of fresh fluid into the shear layers, instabilities in the spiraling vortex sheets, slow viscous reduction, or to some other phenomena. Consequently, any DVM will be unable to faithfully duplicate even the most general features of a real flow (forces, circulation distribution, etc.) unless some additional circulation reduction mechanism is implemented. Sarpkaya and Shoaff [1979] were the first of a relatively few researchers to incorporate a dissipation mechanism in their DVM; they applied a dissipation function which reduced the strength of all vortices (except the nascent vortices) according to

$$\Gamma_n(\text{new}) = \left[1 - \frac{p}{100}\right]\Gamma_n(\text{old}), \tag{3.25}$$

where p was a function of the x-component of vortex location as shown in Figure 3.7.

Kiya and Arie [1980] and Kiya et al. [1982] reduced the strengths of the discrete vortices according to

$$\frac{\Gamma(t)}{\Gamma_o} = 1 - e^{\frac{-a^2R}{4t}}, \tag{3.26}$$

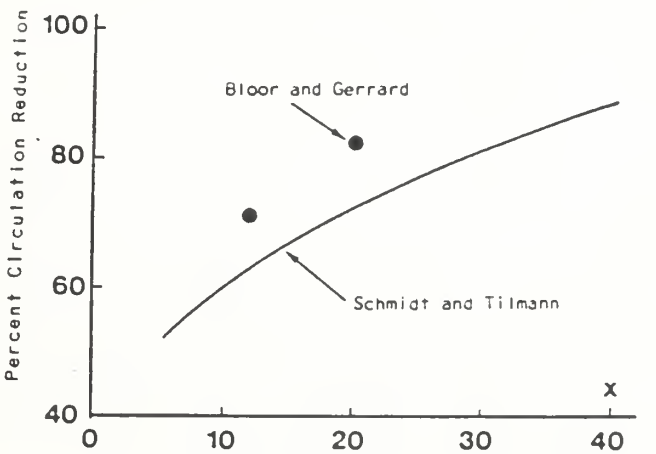


Figure 3.6 Percent of circulation reduction versus distance in unidirectional flow (from Sarpkaya and Shoaff [1979] ).

where $\Gamma_o$ is the initial vortex strength, $\Gamma(t)$ is the strength at time t (the age of the vortex), a is a constant, and **R** is the Reynolds number; this scheme incorporates only a temporal dependence without regard to spatial location.

Nagano et al [1981, 1982] applied an experimentally-based dissipation mechanism to the case of unidirectional flow past rectangular prisms. After performing a vortex strength measurement similar to that used by Fage and Johansen [1928] (Figure 3.8), they claimed that their dissipation mechanism would work in nearly the same fashion as that utilized by Sarpkaya and Shoaff [1979].

In the case of harmonic flow, the three circulation reduction mechanisms mentioned above are all present. Flow visualization experiments have shown that vortices which are convected back across the cylinder can experience significant deformations and consequent reductions in circulation as they are crushed against the cylinder. Quite obviously, there is an additional mechanism, strongly dependent on distance from the cylinder, which exists in addition to all of the reduction mechanisms which exist for unidirectional flow.

Another situation wherein vortex decay must be a function of location as well as of time is the problem of a vortex pair in ground effect; a vortex pair rising towards a free surface may be considered to be the same problem. Squire [1955] proposed the following turbulence model for the reduction in circulation experienced by a vortex pair in ground effect:

$$\frac{\Gamma(t)}{\Gamma_o} = 1 - e^{\frac{-X^2}{4a_o}}, \tag{3.27}$$

where $X^2 = r^2 / \Gamma_o t$, $\Gamma_o$ is the initial vortex strength, t is the vortex age, r is the distance from the vortex center to the ground, and $a_0 = \upsilon_t / \Gamma_o$, where $\nu_t$ is the effective eddy viscosity. This dissipation model has been applied to the case of trailing vortices generated by a submerged lifting surface (Sarpkaya and Henderson [1985] ); although it overpredicts the apparent circulation, it is still felt that the mechanism of circulation reduction is strongly linked to the nondimensional parameter $X^2$.

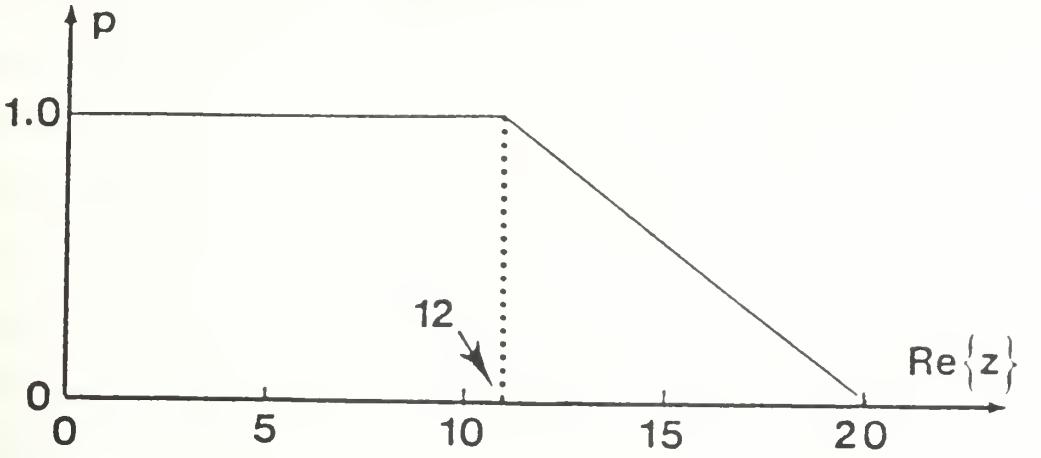


Figure 3.7 Variation of p with distance for t > 5 (from Sarpkaya and Shoaff [1979] ).

A similar decay mechanism may be applied to the case of harmonic flow about cylinders if we write

$$\frac{\Gamma(t)}{\Gamma_o} = \alpha e^{\frac{-\zeta \Gamma_o t}{b^2}}, \tag{3.28}$$

where $\Gamma_o$ is the initial vortex strength, $\alpha$ and $\zeta$ are constants, and b is the distance from the vortex to the body. Note that, with this decay mechanism, vortex strength will decrease with increasing age, or more rapidly, with decreasing distance from a boundary; additionally, stronger vortices will decrease more rapidly than will a weaker vortex, all other things being equal. The $\alpha$-factor acts as a constant turbulent background dissipation, even when the exponential factor approaches unity. Alternatively, the last equation may be recast as

$$\Delta\Gamma \propto \left(\frac{\Gamma}{b}\right)^2 \Delta t, \tag{3.29}$$

where $\Delta\Gamma$ is the reduction in magnitude at each time step, and $\Gamma/b$ varies as the velocity induced on the boundary by the vortex. With this in mind, the vortex which induces a higher velocity on the boundary will experience a higher dissipation, all other things being equal.

Although vortex dissipation is recognized as an important element of the overall problem, many numerical runs have revealed that it is not as significant as originally thought. Having employed all of the various models reviewed above, and others, the proper flow kinematics were still not reproduced. Unless an excessive amount of dissipation was applied, the flow kinematics were not significantly altered.

## G. COUNTERVORTICITY

As the primary vortices grow and roll up behind a cylinder in unidirectional flow, they induce significant velocities on the base of the cylinder. Due to the close proximity of these primary vortices, the velocity and pressure distributions on the base of the cylinder are not nearly as smooth as on the forebody; consequently, several secondary boundary layers and their associated separation points may exist simultaneously on the downstream side of the cylinder (see, e.g., Sarpkaya and Butterworth [1992] ). Due to the highly irregular nature of the velocity and pressure distributions in this region, any of the conventional boundary layer separation techniques would fail. Fortunately, however, there are usually only two secondary separation points which produce vortices of any significant size, so that the numerical analysis is somewhat simplified. Once the secondary separation points are identified and vorticity is generated, the countervorticies are free to combine with other vortices.

Davis [1969], working with Sarpkaya, investigated impulsive flow past a circular cylinder and

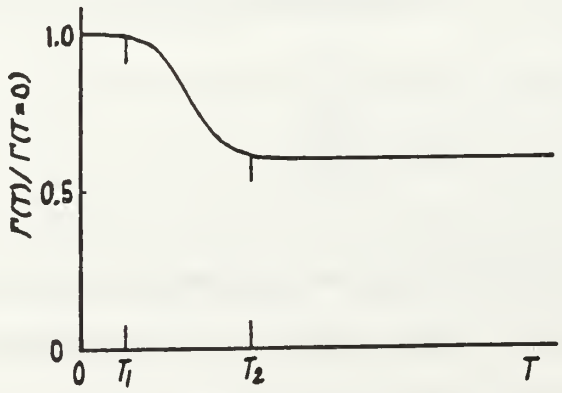


Figure 3.8 Temporal loss of vorticity employed by Nagano et al. [1981, 1982].

extended the idea of countervorticity originally introduced by Bellamy-Knights [1967] (also working with Sarpkaya) and Sarpkaya [1968]. His rear shear layer (countervorticity) separation points were fixed at ±55° from the rear of the cylinder, while the primary separation points were fixed at ±95°. Deffenbaugh and Marshall [1976] also utilized the existence of a rear shear layer; nascent countervorticies were introduced at a distance on the body which was assumed to be proportional to the distance at which primary shear layer separation occurs after the pressure minimum. Neither of these two studies includes any sensitivity analyses to determine system response with and without countervorticies. Stansby and Dixon [1982], however, have investigated the significance of secondary vortex shedding for the case of unidirectional flow, and claimed that countervorticity was able to significantly improve the ability of their model to duplicate experimental results. One might ask why a model such as that employed by Sarpkaya and Shoaff [1979] was able to produce excellent results without using a countervorticity mechanism. A possible reason might be that Sarpkaya and Shoaff had incorporated a turbulent dissipation function, whereas the countervorticity used by Stansby and Dixon may have combined with primary vorticity and effected essentially the same dissipation. Another possible reason is that Stansby and Dixon utilized the velocity of the nascent vortex when calculating the nascent vortex strength with Equation (3.10); this results in vortex strengths of approximately half the magnitude obtained when using the velocity at the separation point in Equation (3.10).

In the current work, countervorticies are introduced at a point at which the rear shear layer velocity decreases to some arbitrary percentage of the maximum velocity in that shear layer. Use of this extremely simple separation criterion overcomes the difficulties posed by the potential existence of a highly irregular velocity distribution on the base of the cylinder; significant difficulty would be encountered if any of the boundary layer methods were utilized in the prediction of separation. The approximate position of introduction is also acceptable since most of the countervorticity tends to congregate in a small triangular area between the primary vortex, the primary feeding sheet, and the cylinder.

It has also been found, however, that for harmonic flow, the countervorticies provide a continuity in the flowfield which allows a smooth and more realistic transition from one half-cycle to the next upon flow reversal (see, e.g., Mostafa [1987] ). The countervorticies from one half-cycle roll back over the cylinder and are the beginnings of the primary vortices for the next half-cycle. If countervorticies are not utilized in the analysis, the system will experience a shock when the new primary shear layers appear at flow reversal. Although countervorticies have a significant impact on the computer run time and storage requirements, they are an essential part of any DVM of harmonic flow about bluff bodies.

## H. VORTEX CLUSTER AMALGAMATION

In the interest of economy of storage space and execution time, many DVM's of unidirectional flow about bluff bodies incorporate some means of cluster combination or amalgamation, whereby all of the N vortices within one cluster are replaced by a single equivalent vortex located at the center of vorticity:

$$\Gamma_{amalg} = \sum_{n=1}^{N} \Gamma_n \tag{3.30}$$

$$z_{amalg} = \frac{\sum_{n=1}^{N} |\Gamma_n| z_n}{\sum_{n=1}^{N} |\Gamma_n|} . \tag{3.31}$$

Note that when all of the amalgamated vortices are of like sign, absolute values are not required in the last equation. When vortices of opposite sign are combined, however, the absolute value signs ensure that a physically realistic position is assigned to the resulting vortex. The first moment of vorticity is not conserved, so that if either the generalized Blasius theorem (Equation (2.32))or the time rate of change of impulse (Equation (2.39)) is used in the calculation of force, discontinuities will occur whenever an amalgamation takes place. Integration of the pressure around the body will usually rèsult in significantly smoother force plots.

The use of amalgamation does not propose to equate the velocity fields before and after the combination; the method finds its applicability in the fact that, if performed sufficiently far away from the body, there will be minimal difference in the flowfield around the body before and after amalgamation. The method has been widely used for unidirectional flow (for a few applications, see Laird [1971], Chaplin [1973], Sarpkaya [1975], and Sarpkaya and Shoaff [1979] ). As pointed out by Sarpkaya [1989], there is no "correct" or "guaranteed" way to perform amalgamation; it is merely an approximation.

In the case of harmonic flow, however, even when amalgamation is performed at a sufficiently distant location, the amalgamated vortices may be convected back across the body. In that case, the induced velocities felt by the body will be vastly different from those which would have been produced by the original cluster. The complex interactions experienced by shed vortices for various Keulegan-Carpenter numbers will be significantly different from those observed experimentally if amalgamation is performed at an inappropriate time or location. Amalgamation should not be performed for at least the first three or four cycles in order to allow the kinematics of the flow to settle into a well-established quasi-steady state pattern; when and if amalgamation is performed, it should only be done to clusters of vorticity which are sufficiently distant from the body, and only on those clusters which have little or no likelihood of returning to the body. It is evident that the incorporation of all of the above logic into a computer code is a formidable task. There are many problems which require consideration, such as the conservation of the first moment of vorticity, conservation of circulation, identification of precisely which discrete vortices are to undergo amalgamation, etc. Consequently, amalgamations are not performed in the current work.

## I. REDISCRETIZATION

The process of rediscretization originally developed by Fink and Soh [1974a] has seen somewhat limited application (see, e.g., Sarpkaya and Shoaff [1979], Fink and Soh [1974b, 1978], Telste and Lugt [1980], Shoaff and Franks [1981], Higdon and Pozrikidis [1985], Hoeijmakers and Vaatstra [1983], and Krasny [1986a] ). Fink and Soh investigated the reasons for the random nature associated with the spiraling of discrete vortex shear layers (originally noted by Rosenhead [1932] ); a reason for this behavior

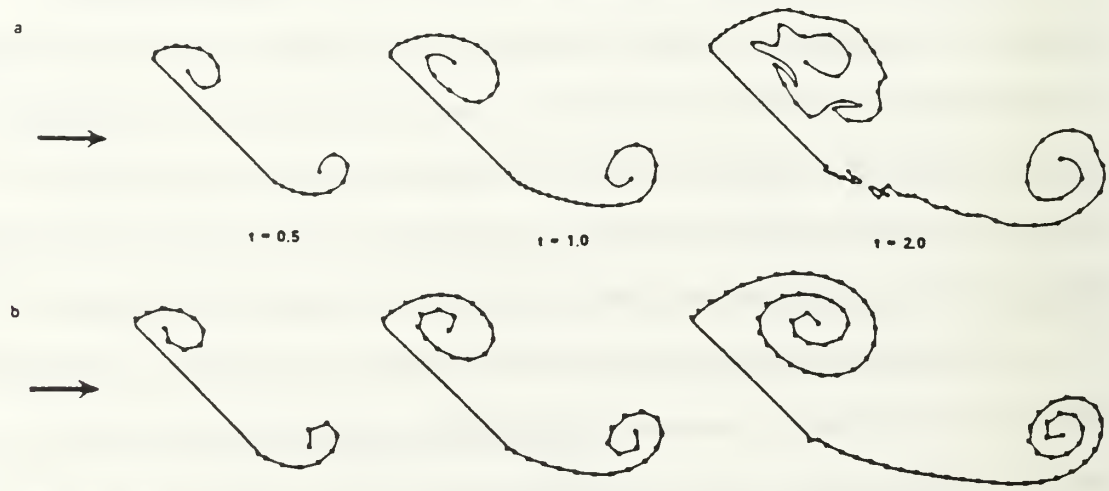


Figure 3.9 Uniform flow past a flat plate at 45° a) without and b) with rediscretization. (From Lugt [1981] )

was found to be a logarithmic error which resulted whenever unequal vortex spacing occurred along a vortex sheet. Their solution to this problem was to redistribute the vorticity along the sheet at every time step to achieve equal vortex spacing. A comparison of results obtained with and without rediscretization is contained in Figure 3.9, taken from Lugt [1981]. It has been shown (Baker [1980] ), however, that curvature effects still produce an error which continues to grow with time; the rediscretization process will delay, but not prevent the inevitable instabilities associated with DVM's. The method is essentially nothing more than an artificial smoothing process, and to include it in an application to the harmonic flow case would not only increase the computer time required, but could also cloud other more important issues.

Having reviewed in greater detail many of the more important aspects of the DVM as applied to unidirectional flow and their extrapolation to the harmonic flow case, the next chapter will show the results of a parametric analysis of these component features.

# IV. A NEW DISCRETE VORTEX MODEL FOR OSCILLATING FLOWS

## A. INTRODUCTION

From the foregoing comparison of previous approaches to the problem of harmonic flow about circular cylinders, the most significant drawback of any of the models is associated with the prediction of flow separation. The use of fixed separation points or of Schlichting's [1932] separation criterion for low **K** are inappropriate since these methods do not allow for the interaction of the returning wake with the primary boundary layers. There are other aspects of the previous methods which require further work (lack of a dissipation scheme, method of asymmetry initiation, etc.), but it is felt that these are secondary issues.

## B. DETAILS OF THE NUMERICAL MODEL

The current model attempts to allow the returning wake to interact with the boundary layers on the forebody, thereby affecting the growth and kinematics of the vortices which are being formed in the current half-cycle. The Pohlhausen method, utilized by Deffenbaugh and Marshall [1976], Sarpkaya and Shoaff [1979], and Mostafa [1987], was used for laminar boundary layers, and other methods were used for turbulent boundary layers; each will be described in detail. Unless otherwise specified, the following items were incorporated in each of the runs:

### 1. Keulegan-Carpenter Number

A Keulegan-Carpenter number of $\mathbf{K} = 10$ was utilized. At very low **K**, the flow maintains a bilateral symmetry and does not allow vortices to move to the side opposite to that on which they were generated. It is precisely this cross-wake motion which is desired in the model, and this begins to manifest itself in the drag-inertia regime ($8 < \mathbf{K} < 15$). On the other hand, the larger the Keulegan-Carpenter number, the larger the number of discrete vortices produced per flow cycle (assuming, of course, that the same timestep size is used throughout the analysis). Consequently, the choice of $\mathbf{K} = 10$ kept the number

of discrete vortices in the flow field to a reasonable level, while allowing computations to run for several cycles in order to reach a quasi-steady state.

### 2. Vortex Proximity-Combination

Vortices were combined only if they were of opposite sign and only when they approached to within a distance of $|\Delta z| < 0.1$. This ensured that a discrete vortex could not grow in magnitude as it returned to the cylinder, thereby hindering any separation point calculations.

### 3. Amalgamation

Amalgamation of a cluster of vortices was not performed. Early attempts at amalgamation in harmonic flow revealed that, as an amalgamated vortex returned to the cylinder, its effect was significantly different from that produced had it not been amalgamated (see, also, Panaras [1987] ).

### 4. Wall Annihilation

The wall annihilation distance was set at 1.18 on the forebody in an attempt to prevent discrete vortices from hindering any separation point calculations; on the base of the cylinder, the annihilation distance was 1.1, so that upon flow reversal, there would not be a significant number of discrete vortices lost when the annihilation distance suddenly increased to 1.18.

### 5. Convection Scheme

A first order convection scheme was used in lieu of a second order scheme, which produced unrealistic flow patterns, due possibly to numerical instabilities associated with the use of a higher order scheme in conjunction with an already very small timestep size.

### 6. Countervorticity

Countervorticity was employed in all runs in order to provide a continuity from one half-cycle to the next. If it were not for the countervorticity, there would be no vorticity introduced into the flow from the time the separation calculations ceased (late in a half-cycle) to the time the separation calculations resumed (upon flow reversal). If these separation calculations commenced without the benefit of any

previous countervorticity calculations, the in-line and lift force plots showed unrealistic and significant discontinuities.

### 7. Asymmetry Initiation

Asymmetry initiation of the type employed by Sarpkaya and Shoaff [1979] was found to be much more suitable than any of the other methods previously discussed. The only difference was that asymmetry was introduced during roughly the first quarter-cycle of flow (T1 = 2.0, T2 = 6.0 in Figure 3.4), or $0.1 < t/T < 0.3$ in order to allow the asymmetry to take effect in a reasonable period of time.

### 8. Dissipation

Several functional forms of dissipation were discussed in Chapter III, and from preliminary investigations, it was ascertained that dissipation itself was probably not the single most important triggering parameter which would produce the proper flow kinematics. As noted by Sarpkaya and Shoaff [1979], the incorporation of dissipation in a DVM of impulsive flow resulted in a reduction of lift and drag force magnitudes, but did not significantly affect the flow kinematics; a similar conclusion was arrived at by Mostafa [1987] for the case of harmonic flow. Dissipation is still, however, an important aspect of the flow, and was incorporated using the same functional form as utilized by Sarpkaya and Shoaff [1979] (see Figure 3.7), but with a value of $p = 0.2$ for the impulsive flow run and $p = 0.5$ for the harmonic flow runs.

### 9. Unsteady Kutta Condition

The unsteady Kutta condition (Equation (3.15)) was employed in all nascent vortex strength calculations.

### 10. Timestep Size

Timestep size was held constant at 0.125.

### 11. Minimum Vortex Strength

Vortices below a certain minimum magnitude (0.005) were removed from the flowfield since their contributions were deemed negligible; this helped to minimize the number of vortices.

### 12. Vortex-Induced Velocity Calculation

The Lamb vortex velocity distribution (Equation (3.3)) was employed throughout.

## C. VERIFICATION OF THE MODEL

The model was run using an impulsive flow in lieu of a harmonic flow, and the resulting kinematics and gross characteristics were found to be in excellent agreement with experimental (Sarpkaya [1978] ) and numerical (Sarpkaya and Shoaff [1979] ) results. The functional forms of asymmetry and dissipation were identical to those used by Sarpkaya and Shoaff [1979], except that p = 0.2 was used instead of the value of p = 1.0 (see Figure 3.7). The annihilation region around the cylinder was 1.06.

Figure 4.1a shows a time sequence through t = 20.0, while Figures 4.1b through 4.1f depict drag and lift forces, separation and stagnation angles, and nascent vortex strengths. The plots of separation angle and nascent vortex strengths refer to two primary (BL1 and BL2) boundary layers and two secondary (BL3 and BL4) boundary layers as indicated in Figure 4.2; for harmonic flows, when the flow is right to left, the primary boundary layers will be BL3 and BL4, and the secondary boundary layers will be BL1 and BL2. It can be seen that the magnitude and location of the secondary nascent vortices vary erratically since the region in which they are formed is highly confused. It is also possible that the secondary separation points may come and go as velocities on the base of the cylinder rise and fall due to the proximity of the primary vortices to the cylinder. (It was found that the inclusion of secondary vorticity in the flow did not significantly improve the results, contrary to the findings of Stansby and Dixon [1982] .) Also shown in Figure 4.2 are the forward stagnation angle and the location of the total force vector acting on the cylinder; the arrow within the cylinder indicates the magnitude and direction of the ambient velocity. Positive (counterclockwise) vortices are indicated by a "+", and negative (clockwise)

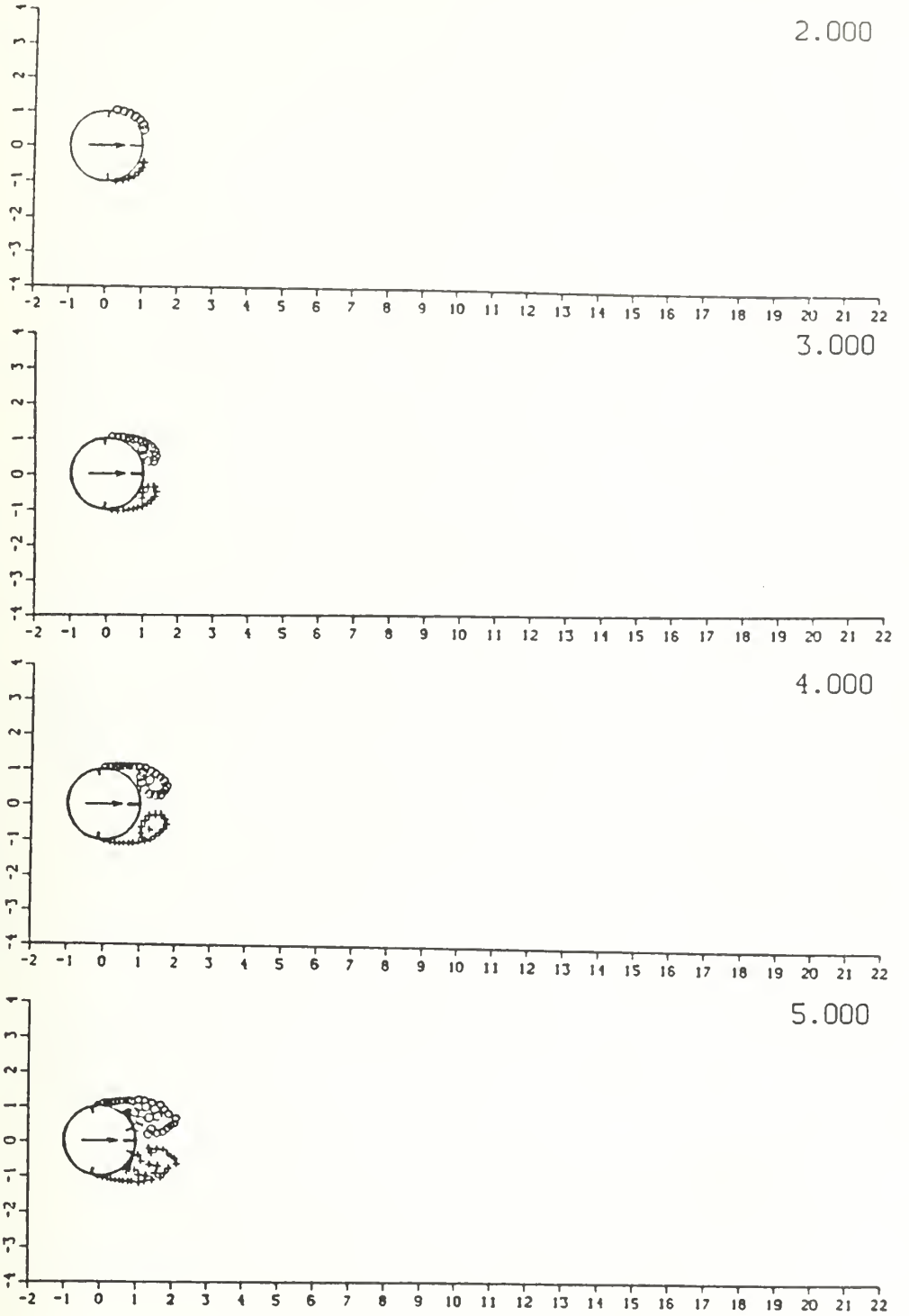


Figure 4.1a Model verification with impulsive flow: Kinematics.

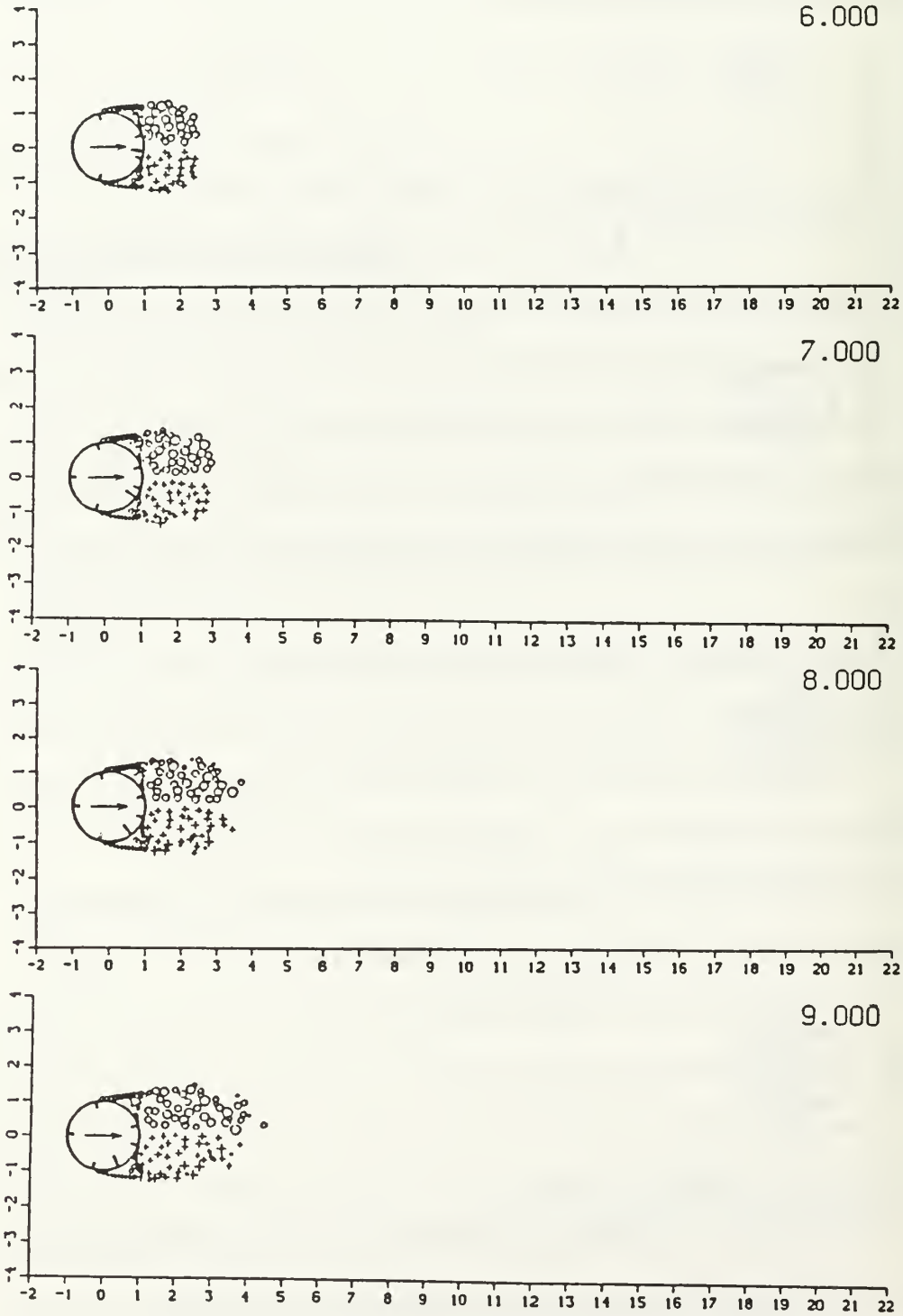


Figure 4.1a (con't.) Model verification with impulsive flow: Kinematics.

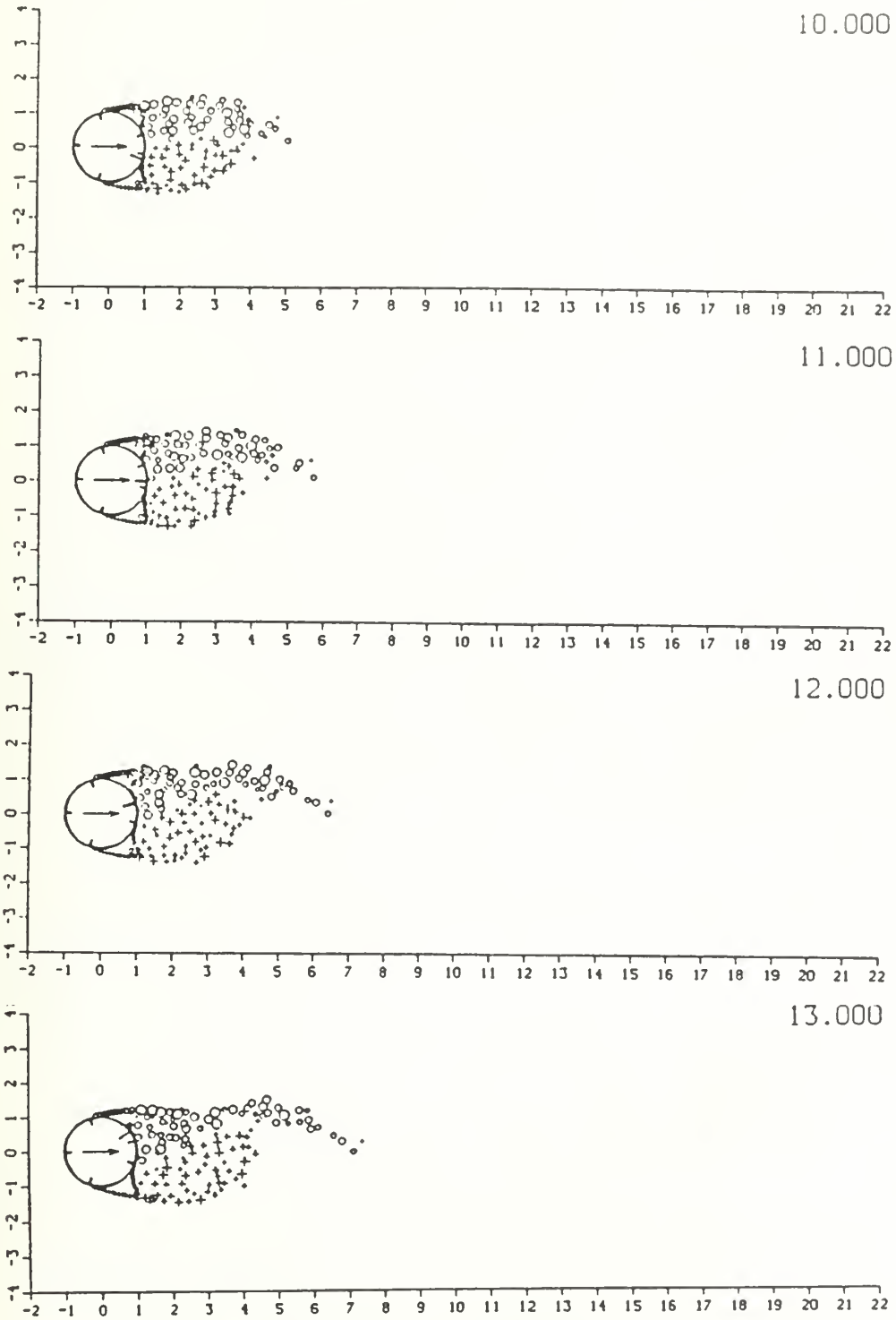


Figure 4.1a (con't.) Model verification with impulsive flow: Kinematics.

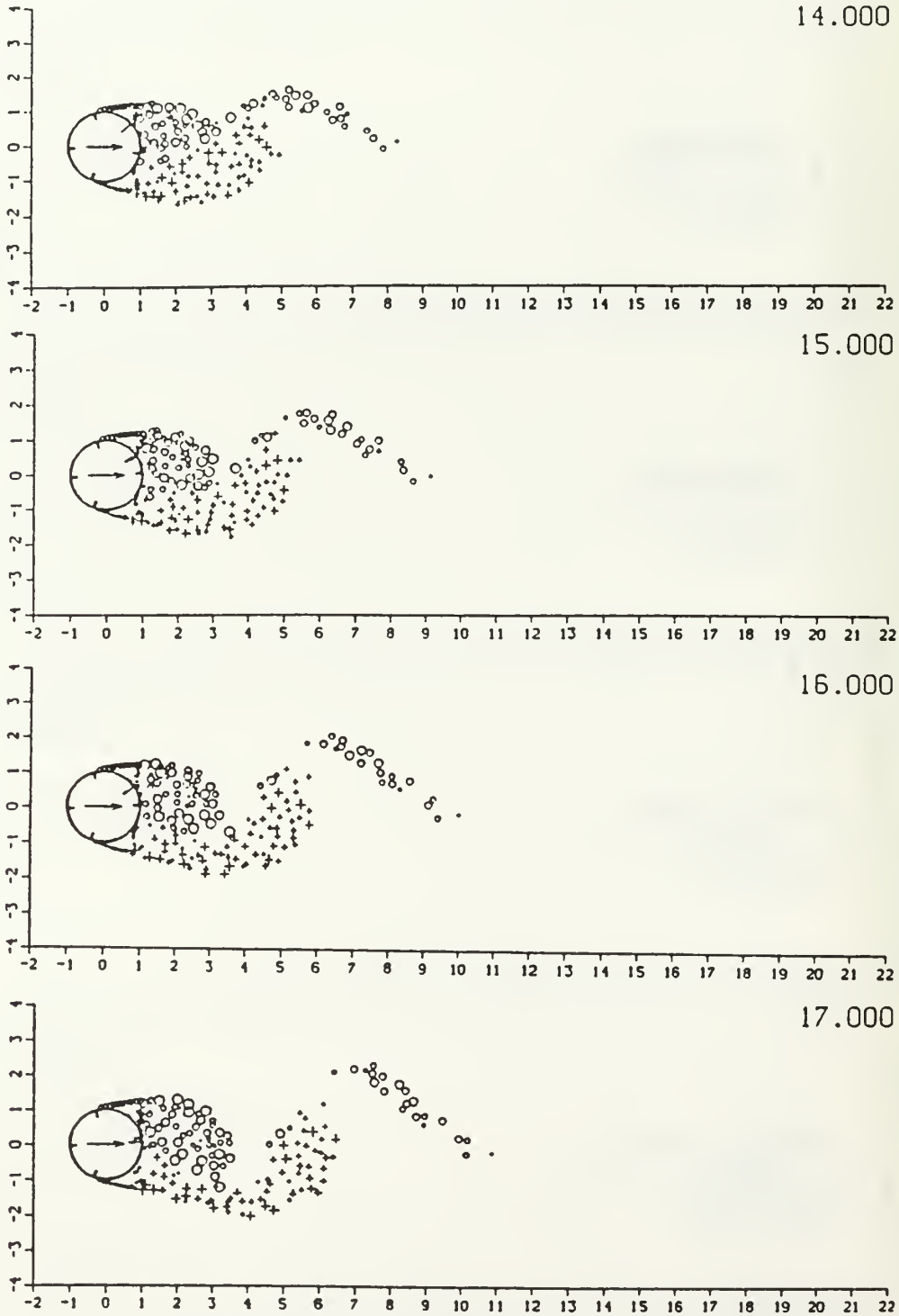


Figure 4.1a (con't.) Model verification with impulsive flow: Kinematics.

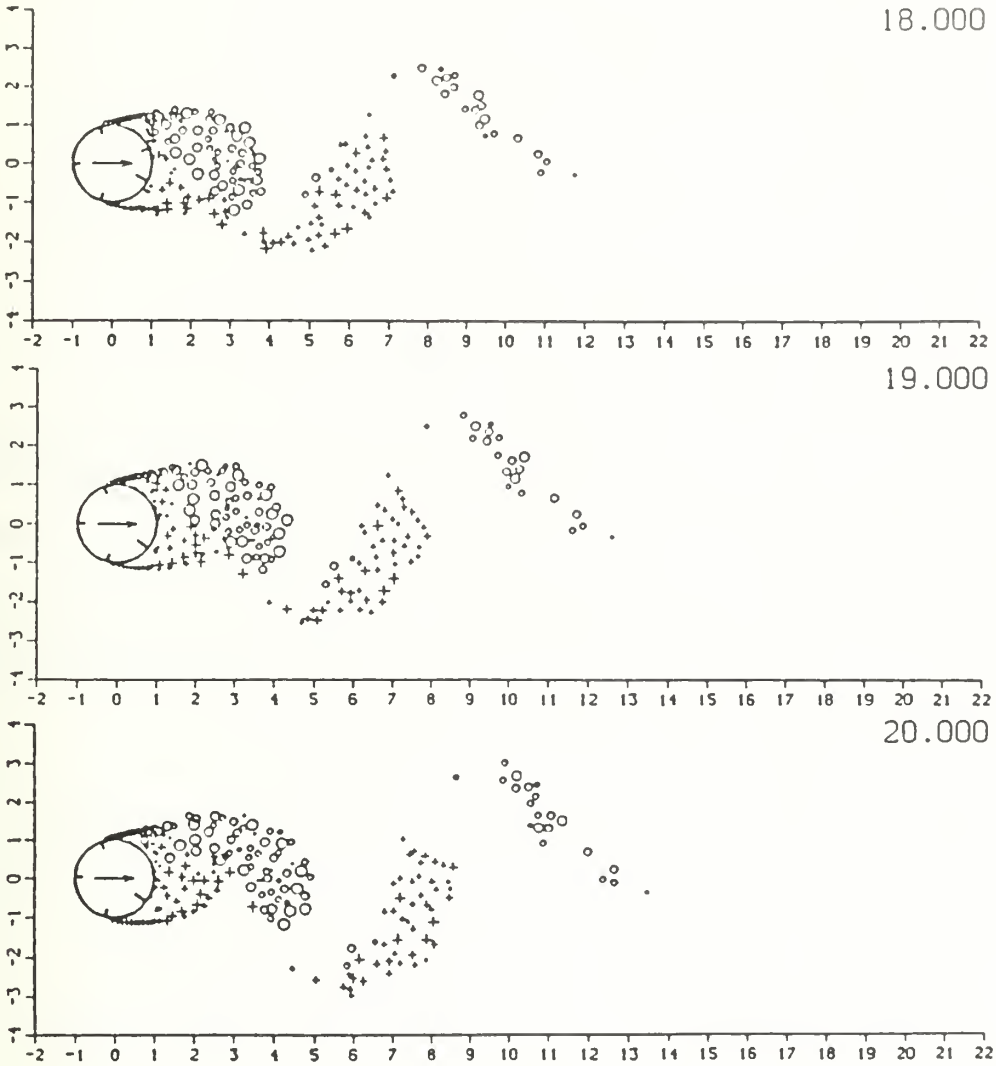


Figure 4.1a (con't.) Model verification with impulsive flow: Kinematics.

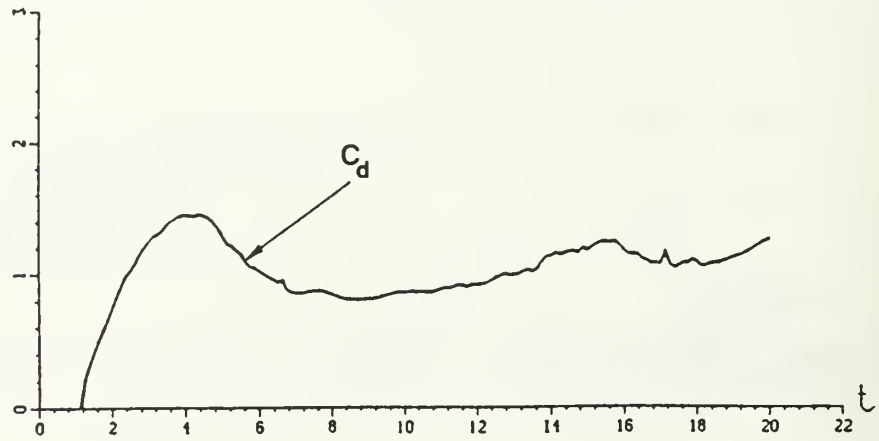


Figure 4.1b Model verification with impulsive flow: Drag.

vortices are indicated by a "0"; the strength of the vortices is proportional to the size of the symbols. In the plots of stagnation and separation angles, angles are measured from the positive x-axis. The plot of lift coefficient is accompanied by a plot of net circulation acting on the cylinder (i.e., the sum of all of the image vortices within the cylinder). The later plots of in-line force coefficients for harmonic flow also include a plot of the ambient flow as a reference.

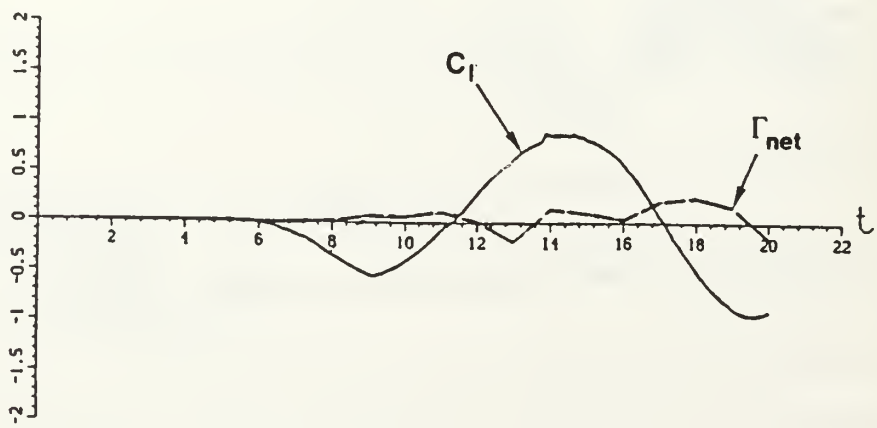


Figure 4.1c Model verification with impulsive flow: Lift.

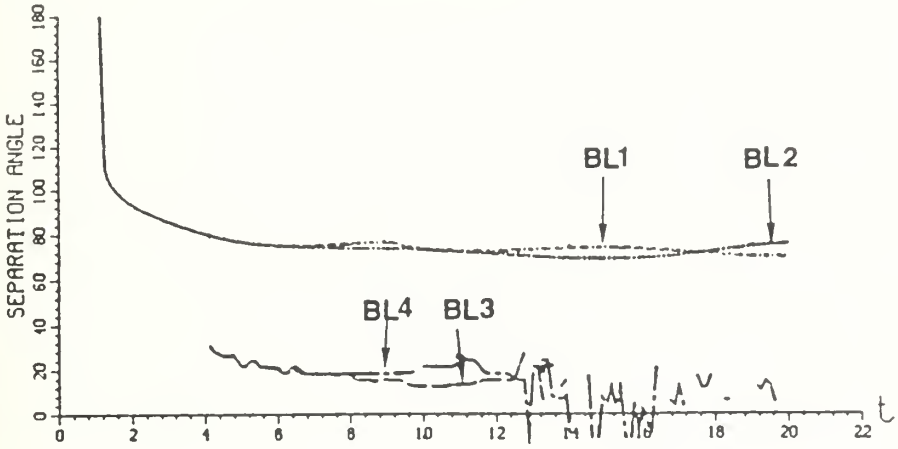


Figure 4.1d Model verification with impulsive flow: Separation points.

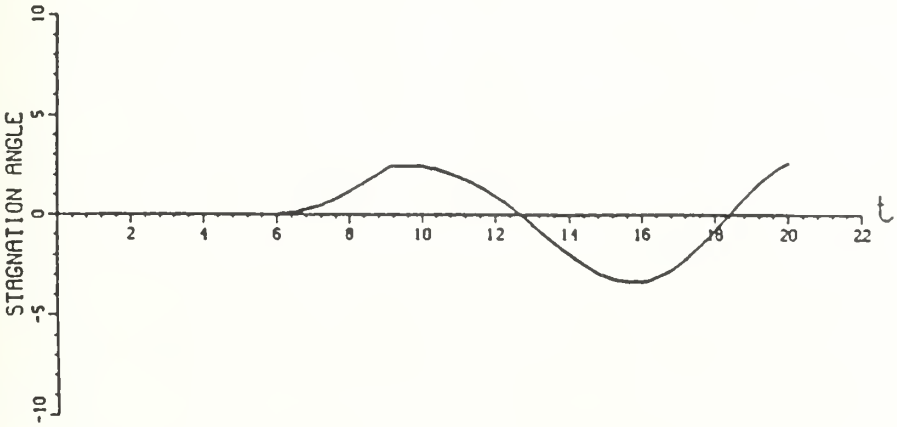


Figure 4.1e Model verification with impulsive flow: Stagnation point.

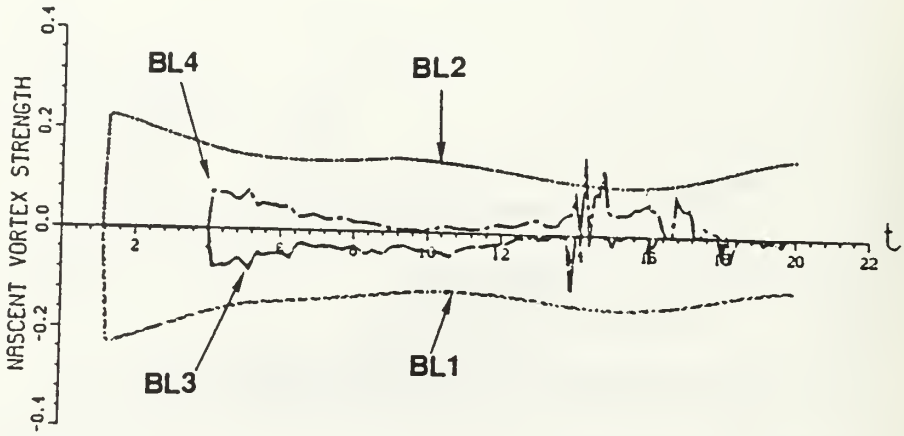


Figure 4.1f Model verification with impulsive flow: Nascent vortex strengths.

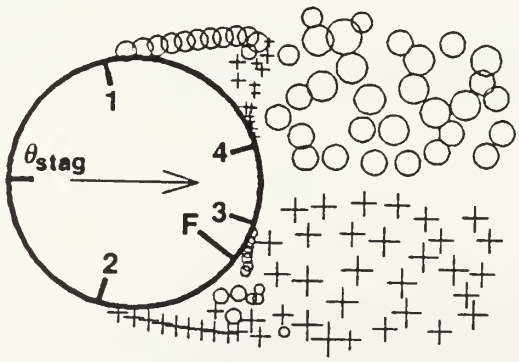


Figure 4.2 Locations of the various vortex sheets (see text for legend).

## D. FLOW VISUALIZATION

Until recently, surprisingly few flow visualization experiments had been performed for harmonic flow about circular cylinders. The data of Grass and Kemp [1979] (see Figure 2.3) for **K** = 38 indicate that the flow begins anew at every flow reversal almost as if it were begun impulsively. Sawaragi and Nakamura [1979] presented sketches of observed flow patterns at various Keulegan-Carpenter numbers, but did not describe in detail what occurred from one half-cycle to the next (see Figure 4.3). Wilson [1983], working with Sarpkaya, obtained detailed pressure measurements about circular cylinders in a U-tube, and was able to predict the vortex shedding patterns depicted in Figure 4.4a for the drag-inertia regime and Figure 4.4b for the drag-dominated regime (see also Sarpkaya and Wilson [1984] ). In the drag-inertia regime, it can be seen that, in each half-cycle, the major or dominant vortex is shed on the same side of the cylinder, so that a "transverse" vortex street results, reminiscent of the Kármán vortex street seen in unidirectional flow. For the drag-dominated regime, however, the vortex shedding pattern is diagonal in nature, with vortex pairing occurring in diagonally opposing quadrants.

A series of flow visualization experiments was conducted by Sarpkaya [1985] in an experimental apparatus at the Naval Postgraduate School in a water table. Figure 4.5 shows a time sequence from a representative run for **K** = 10; in these experiments the cylinder (D = 1.5 inches) was oscillated in a water table of depth 12 inches, using a period of T = 3.0 seconds. The photographs were taken with an automatic Nikon F3 camera. For the photographs shown, **R** = 12,800 and $\beta$ = 1280. The end of the Plexiglas cylinder was within 1/16-inch of the bottom of the water table, so that end effects were minimal. It can be seen that the vortex shedding is indeed on the same side (i.e., left) of the cylinder. By varying the amplitude of oscillation to obtain a Keulegan-Carpenter number of approximately 12, the shedding pattern exhibited an instability, wherein it could shift from the "same side" shedding pattern show in Figures 4.4a and 4.5 to the diagonal pattern shown in Figure 4.4b. These results were in conformance with those presented by Bearman et al [1981] and Wilson [1983]. A detailed and succinct description of

the flow kinematics characteristic of the drag-inertia regime ($8 < \mathbf{K} < 15$) is presented in Sarpkaya and Butterworth [1992] and Sarpkaya [1992].

Williamson [1985] has performed detailed flow visualization experiments with simultaneous force measurements over a wide range of Keulegan-Carpenter numbers; his results agree well with those presented herein. Williamson found that, in the area of interest, there were two broad categories of flow, $7 < \mathbf{K} < 15$ and $15 < \mathbf{K} < 24$, with an intermediate transition over the interval $12 < \mathbf{K} < 15$. In the range of $7 < \mathbf{K} < 13$ (see Figure 4.6a) a transverse street was observed (in Williamson's illustrations, the arrows refer to the cylinder motion, and the vortices are viewed from a reference frame which moves with the cylinder). Over the range $13 < \mathbf{K} < 15$, (Figure 4.6c), the wake is comprised of a series of vortex pairs convecting away each cycle at roughly $45^\circ$ to the flow oscillation direction, and only on one side of the cylinder. Finally, Williamson observed what he refers to as a "double-pair wake" over the interval $15 < \mathbf{K} < 24$ (Figure 4.6c) where two major vortices (i.e., including a minor vortex which never amounts to much, a total of three vortices) are shed per half cycle, so that the fundamental lift force oscillates at three times the cylinder oscillation frequency (Figure 4.6d). Also shown in Figure 4.7 are typical lift and in-line force traces obtained by Williamson in a U-tube for the regime $7 < \mathbf{K} < 15$.

## E. FIXED SEPARATION POINTS

As a first approximation to more sophisticated boundary layer techniques, a computer run was conducted wherein fixed separation points were employed at the top and bottom of the cylinder. In order that results could be compared with those obtained by Stansby [1977], a Keulegan-Carpenter number of $\mathbf{K} = 15$ was utilized, an ambient velocity of $U = U_m \cos \omega t$ was used instead of $U = U_m \sin \omega t$, and neither countervorticity nor dissipation was incorporated in the model. Stansby stated that he initiated asymmetry by moving vortices of the same sign downstream by approximately one-fifth of a radius at approximately $t = 1.0$; accordingly, the current model was modified to produce approximately the same effect by employing $B = 0.0143$ and $T1 = 1.5$ and $T2 = 5.0$ in Figure 3.4. In his calculations, Stansby based the strength of his nascent vortices on the velocity of the nascent vortex itself, and not on the velocity at the

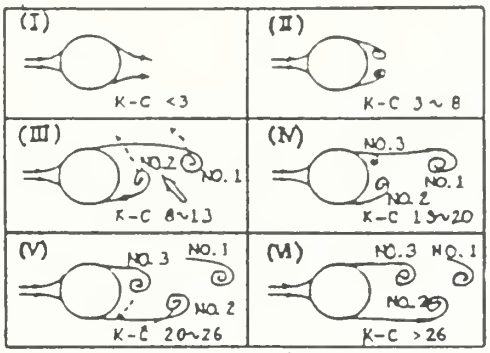


Figure 4.3 Vortex flow patterns as observed by Sawaragi and Nakamura [1979].

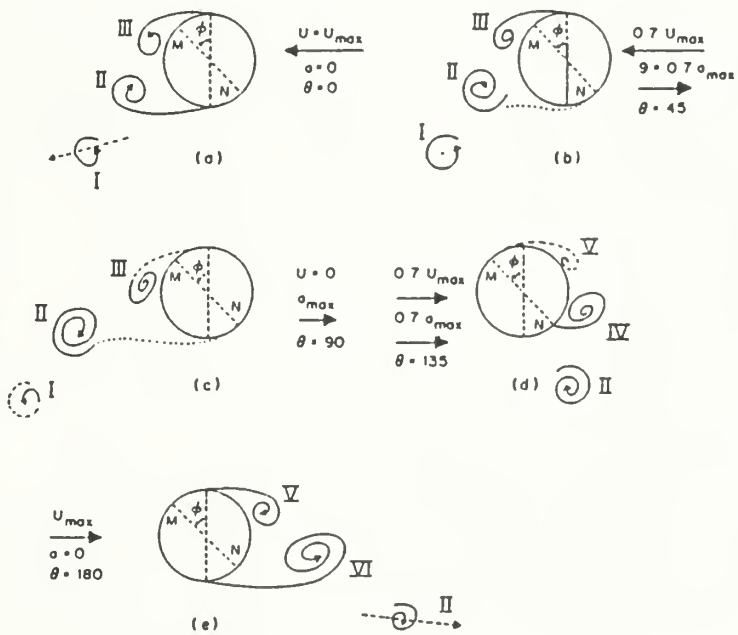


Figure 4.4a Vortex flow patterns as hypothesized by Wilson [1983] for 8 < K < 15.

separation point on the cylinder, as in Equation (3.10). This results in vortices which are approximately 9/16 of the strength calculated via Equation (3.10). By including this factor in the calculation of the strength of nascent vortices, a reasonable approximation of Stansby's calculation should have been achieved.

Stansby's results are shown in Figures 4.8a and 4.8b. In the plot of vortex positions, a "+" denotes a vortex of clockwise circulation, whereas an "X" denotes one of counterclockwise circulation; additionally, those vortices shed during the most recent half-cycle are enclosed by a dashed line. In the

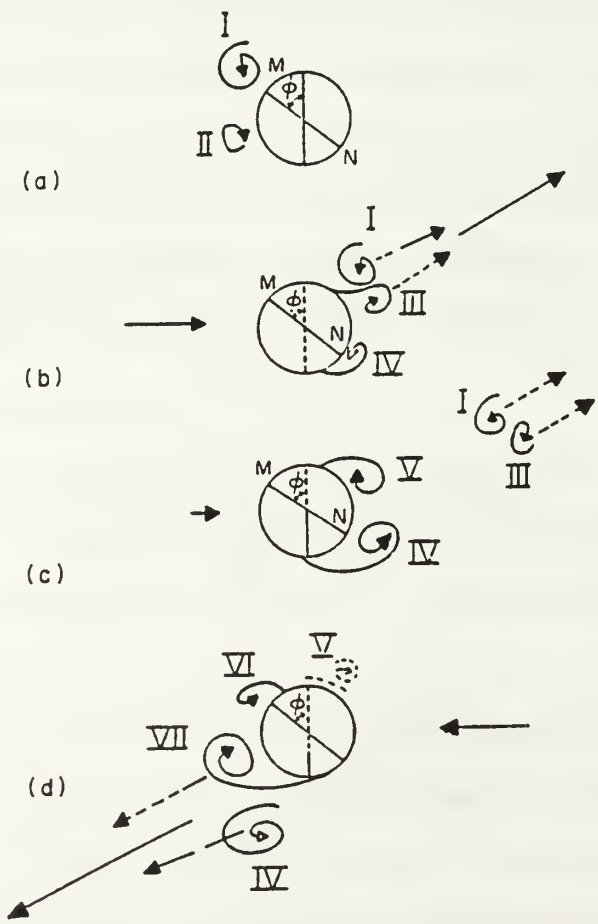


Figure 4.4b Vortex flow patterns as hypothesized by Wilson [1983] for **K** > 20.

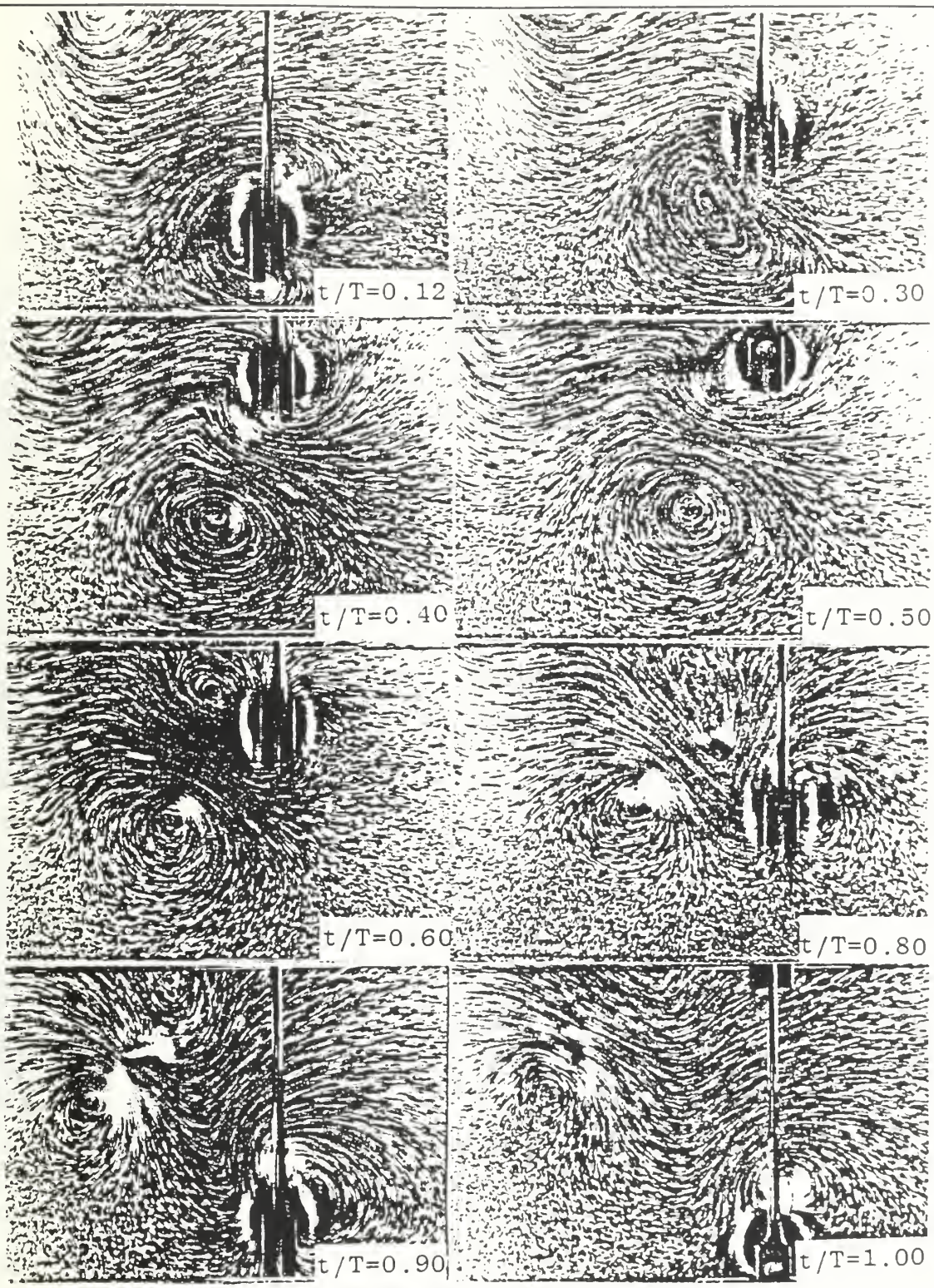


Figure 4.5 Results of flow visualization experiment for K = 10.

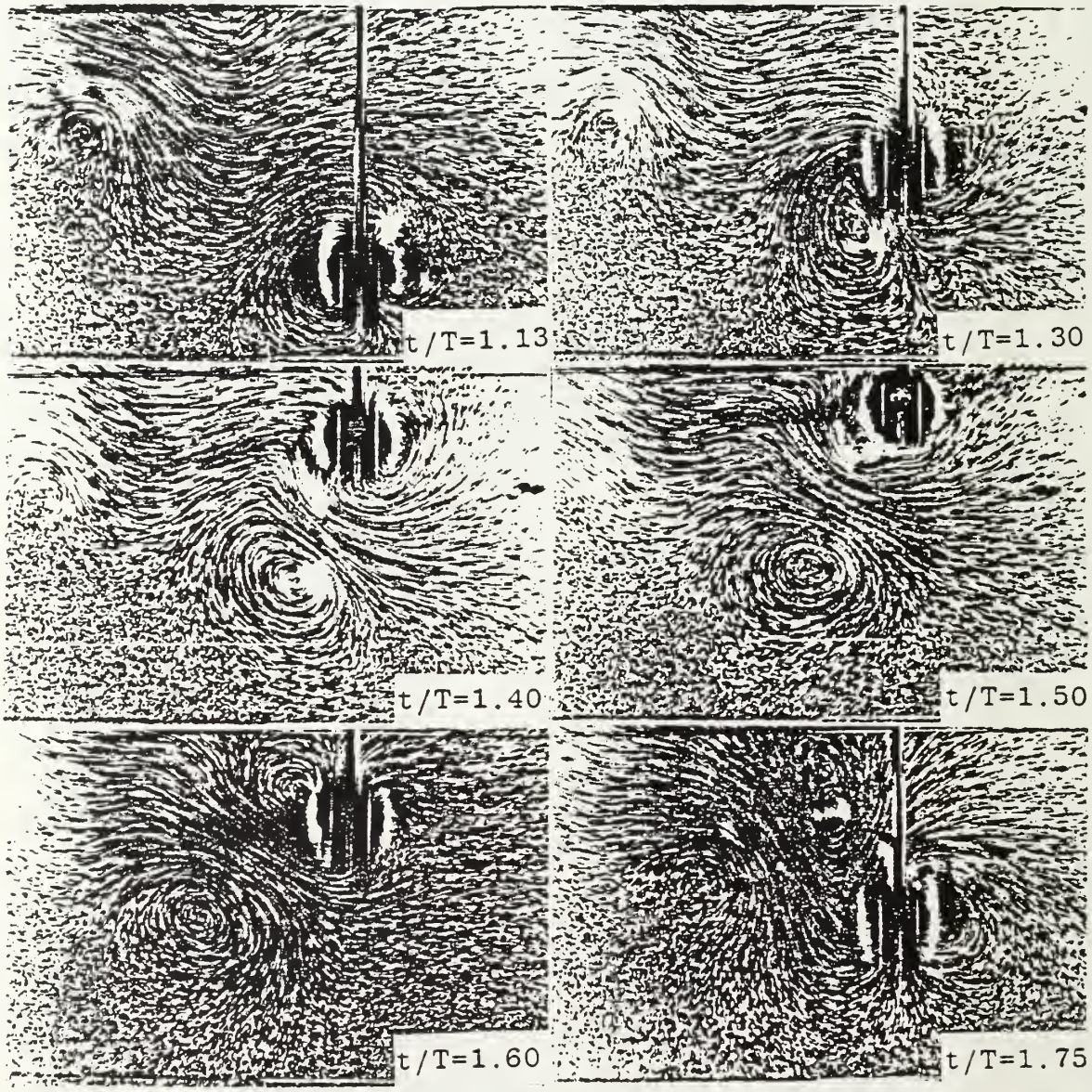


Figure 4.5 (con't.) Results of flow visualization experiment for **K** = 10.

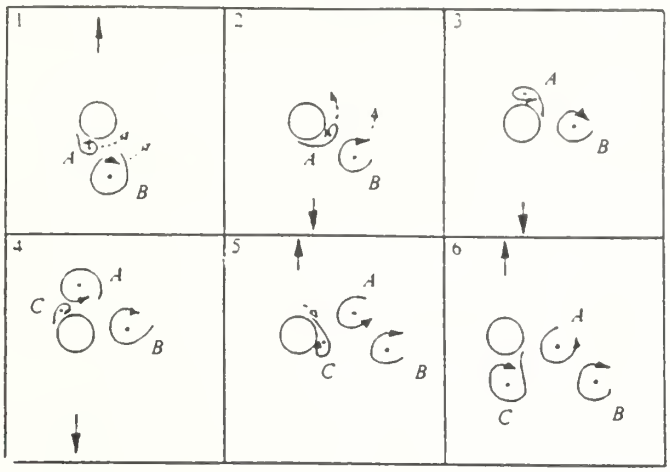


Figure 4.6a Vortex kinematics observed by Williamson [1985] for 7 < **K** < 13.

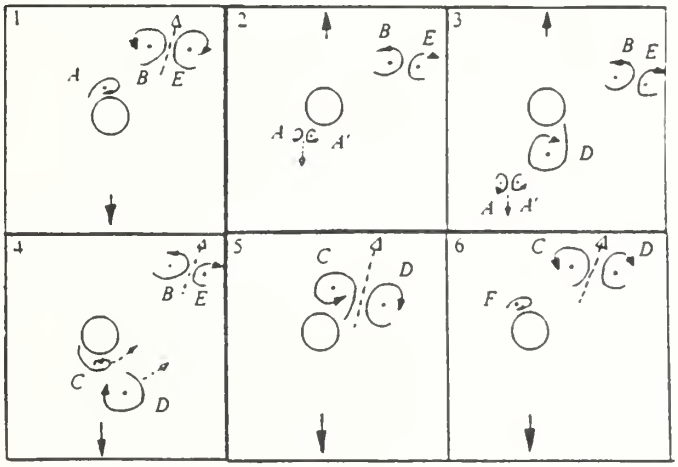


Figure 4.6b Vortex kinematics observed by Williamson [1985] for 13 < **K** < 15.

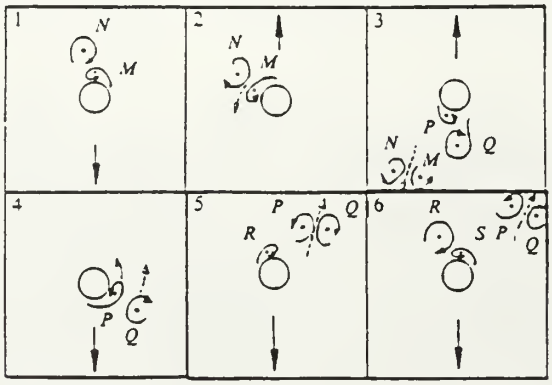


Figure 4.6c Vortex kinematics observed by Williamson [1985] for 15 < **K** < 24.

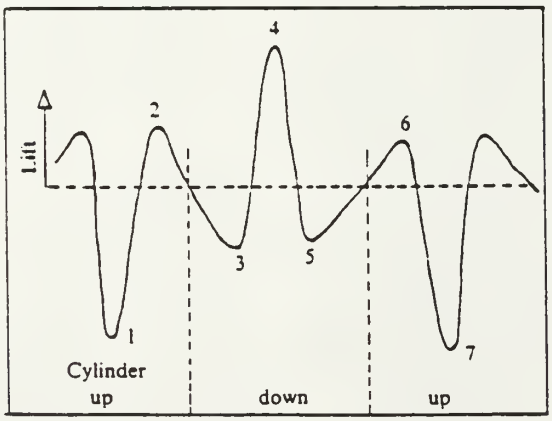


Figure 4.6d Lift force corresponding to 15 < **K** < 24 (from Williamson [1985] ).

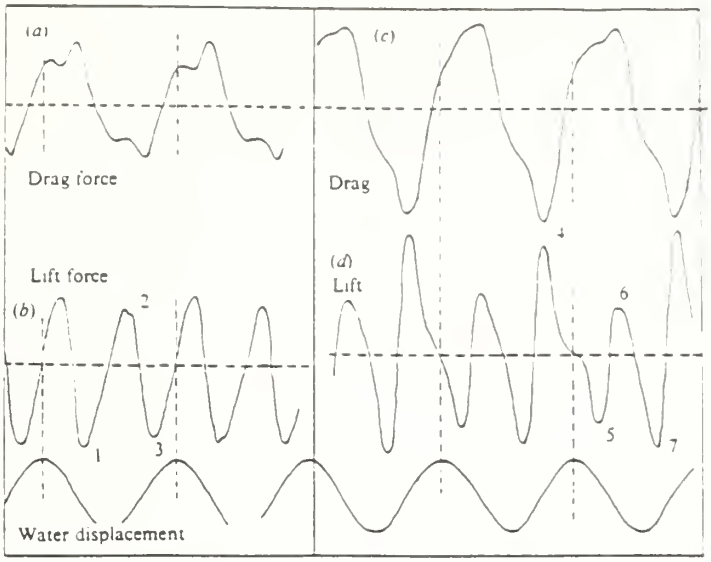


Figure 4.7 Harmonic flow traces: (a), (b) for K = 11 and (c), (d) for K = 13.7 (from Williamson [1985] ).

Figure 4.8a Vortex flow kinematics for K = 15 (from Stansby [1977] ).

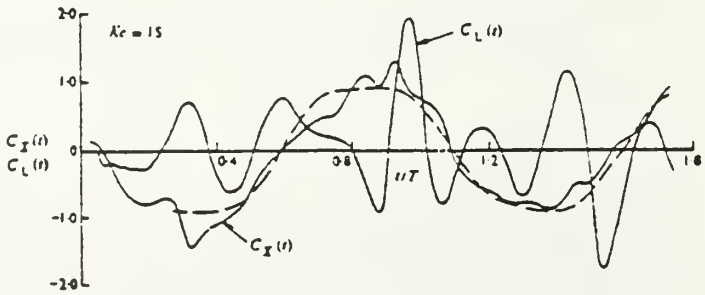


Figure 4.8b Results obtained by Stansby [1977] for **K** = 15.

force plots, $C_x$ denotes in-line force coefficient, $C_l$ the lift coefficient, and the dashed line, the in-line force coefficient predicted by Morison's equation. Results obtained with the current analysis are presented in Figures 4.9a through 4.9d.

In general, the vortex clusters in Stansby's calculations appear to wrap around the cylinder. Also, the shed clusters do not move very far away from the cylinder, which indicates that the vortices are relatively weak and do not, therefore, induce significant velocities upon one another. In the current analysis, as vortex clusters are swept back across the cylinder upon flow reversal, they "strip" or "peel off" several discrete vortices from the attached vortex clusters which are still growing. The flow remains roughly symmetric in the immediate vicinity of the cylinder almost until the end of the first complete cycle, after which the next two major vortices shed from the same (i.e., lower) side of the cylinder, and the third major vortex (at t/T = 2.0 ) appears to be shed from the top of the cylinder.

Aside from a somewhat general agreement in magnitude and shape of the in-line forces, there is no good agreement in the forces predicted by the two models. Despite all attempts to reproduce Stansby's results, this proved to be an unattainable goal. Suffice it to say that neither Stansby's model nor the current simulation of his work was able to faithfully reproduce the experimentally observed flow patterns.

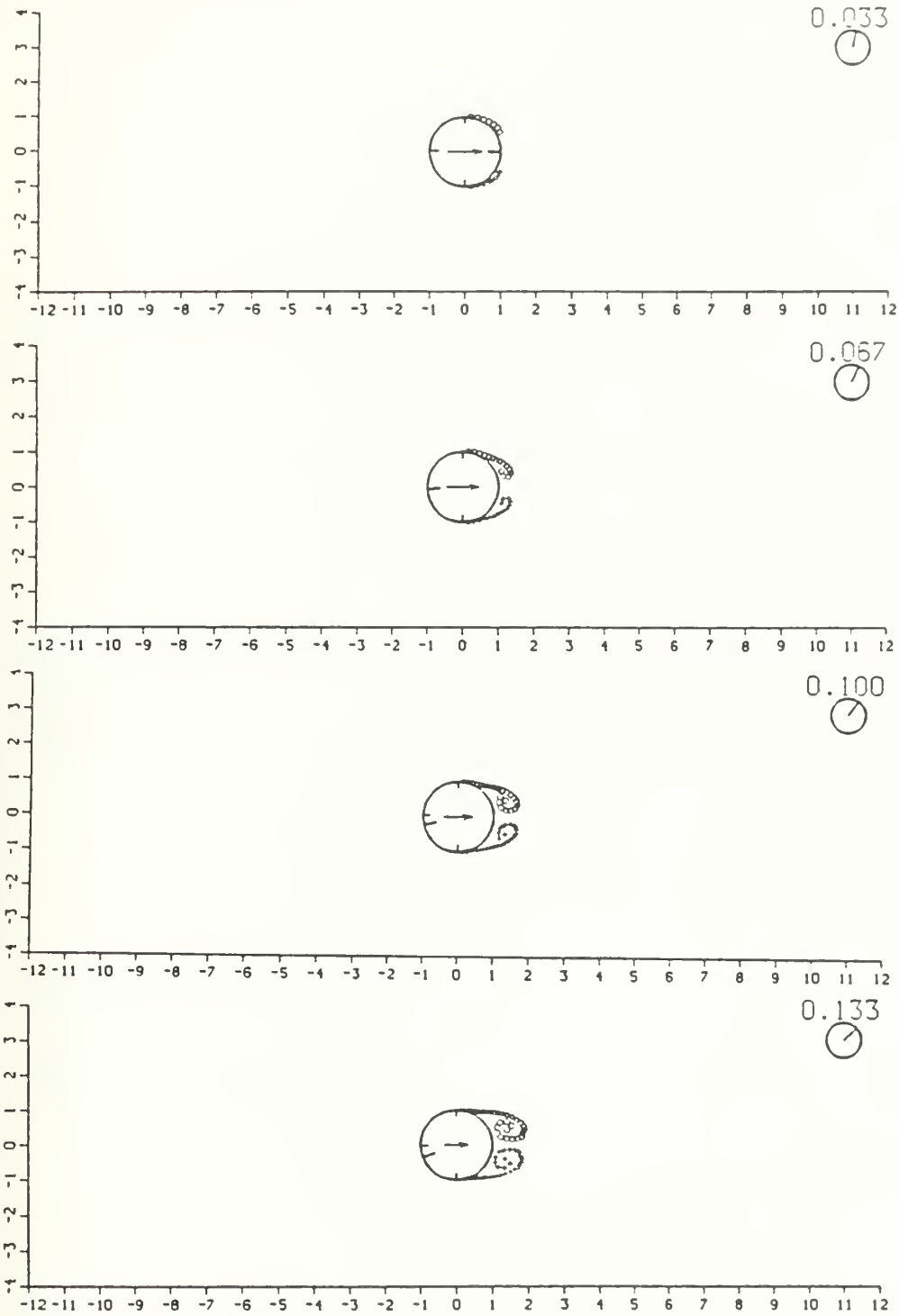


Figure 4.9a Simulation of Stansby's model for **K** = 15: Kinematics.

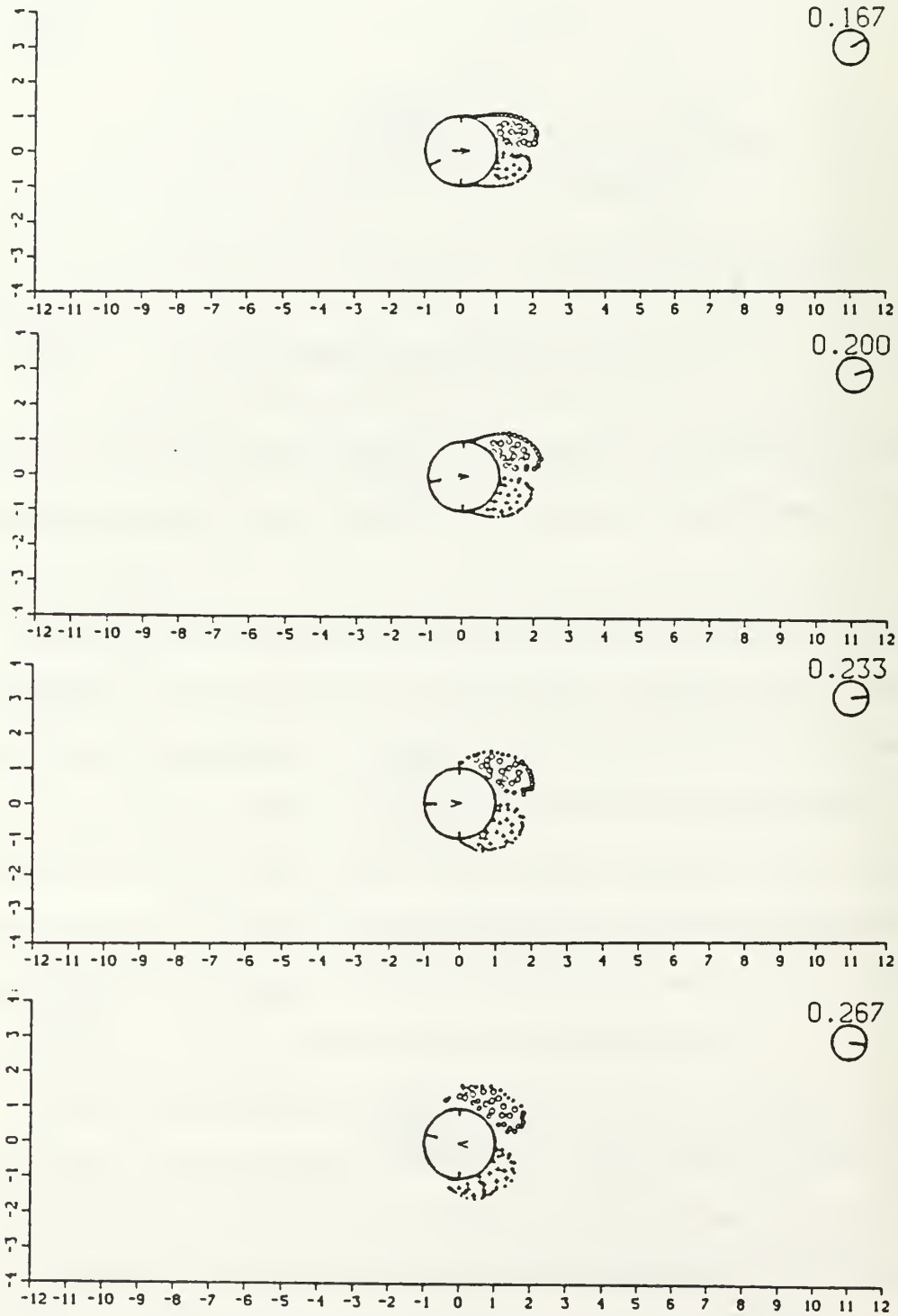


Figure 4.9a (con't.) Simulation of Stansby's model for K = 15: Kinematics.

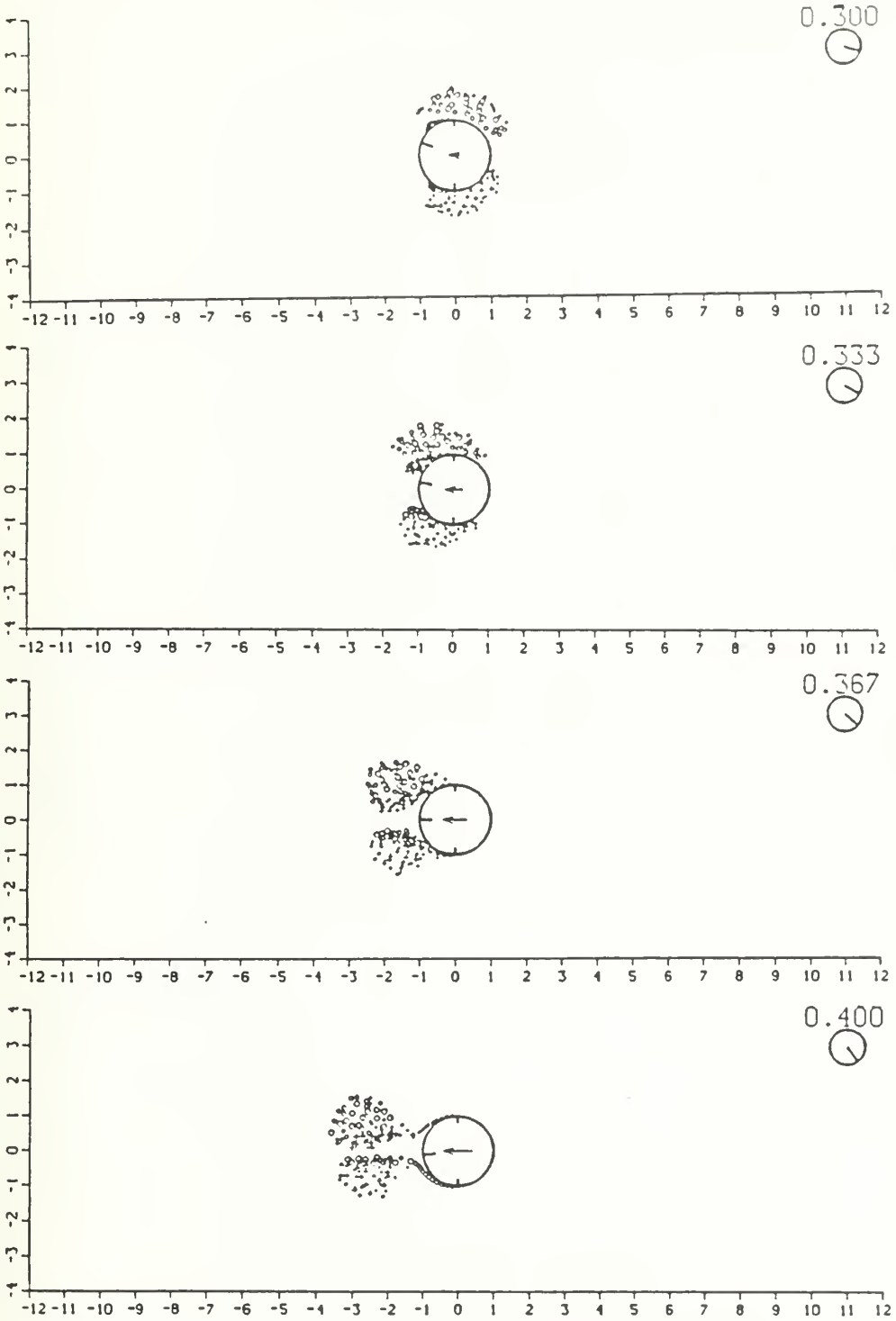


Figure 4.9a (con't.) Simulation of Stansby's model for **K** = 15: Kinematics.

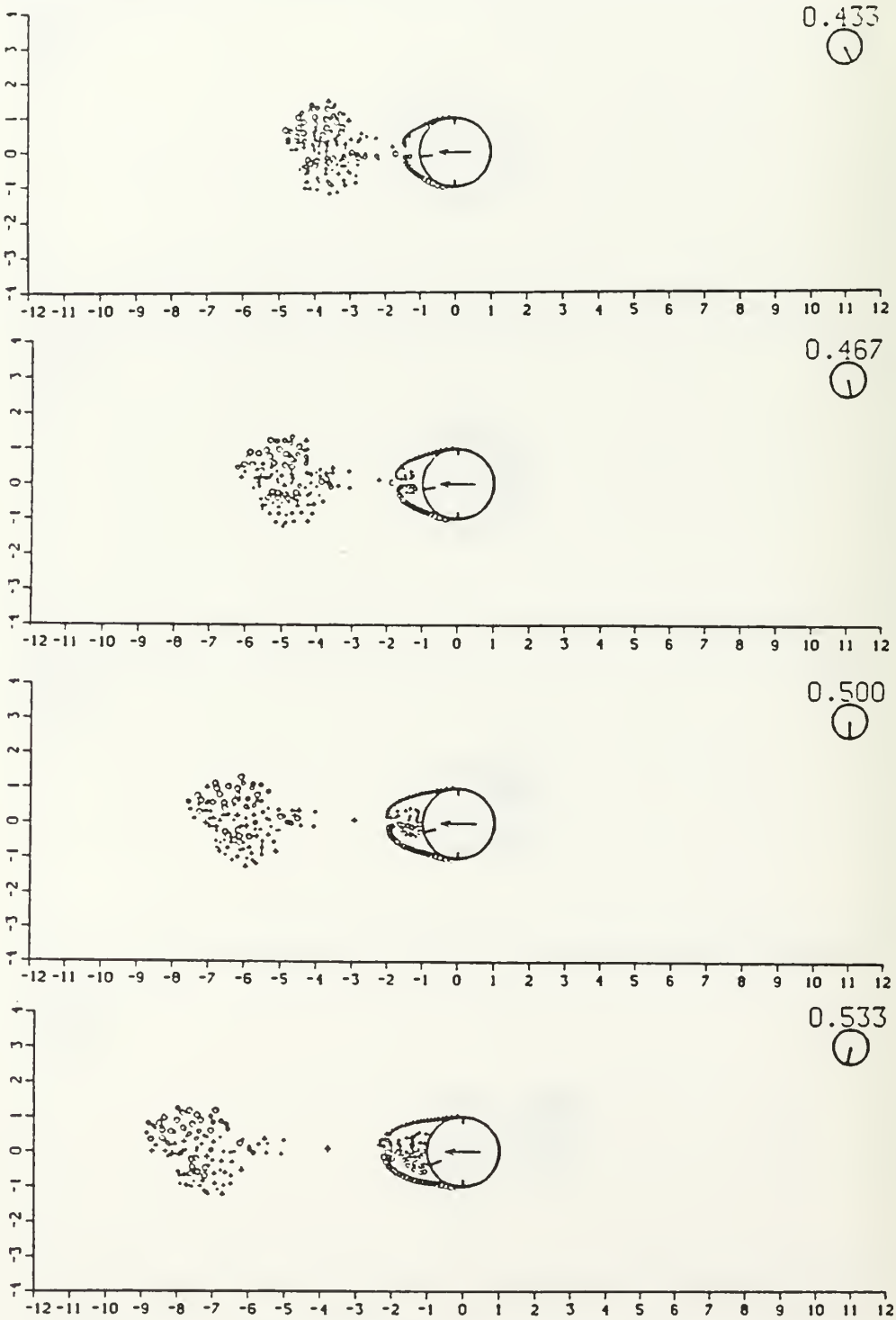


Figure 4.9a (con't.) Simulation of Stansby's model for **K** = 15: Kinematics.

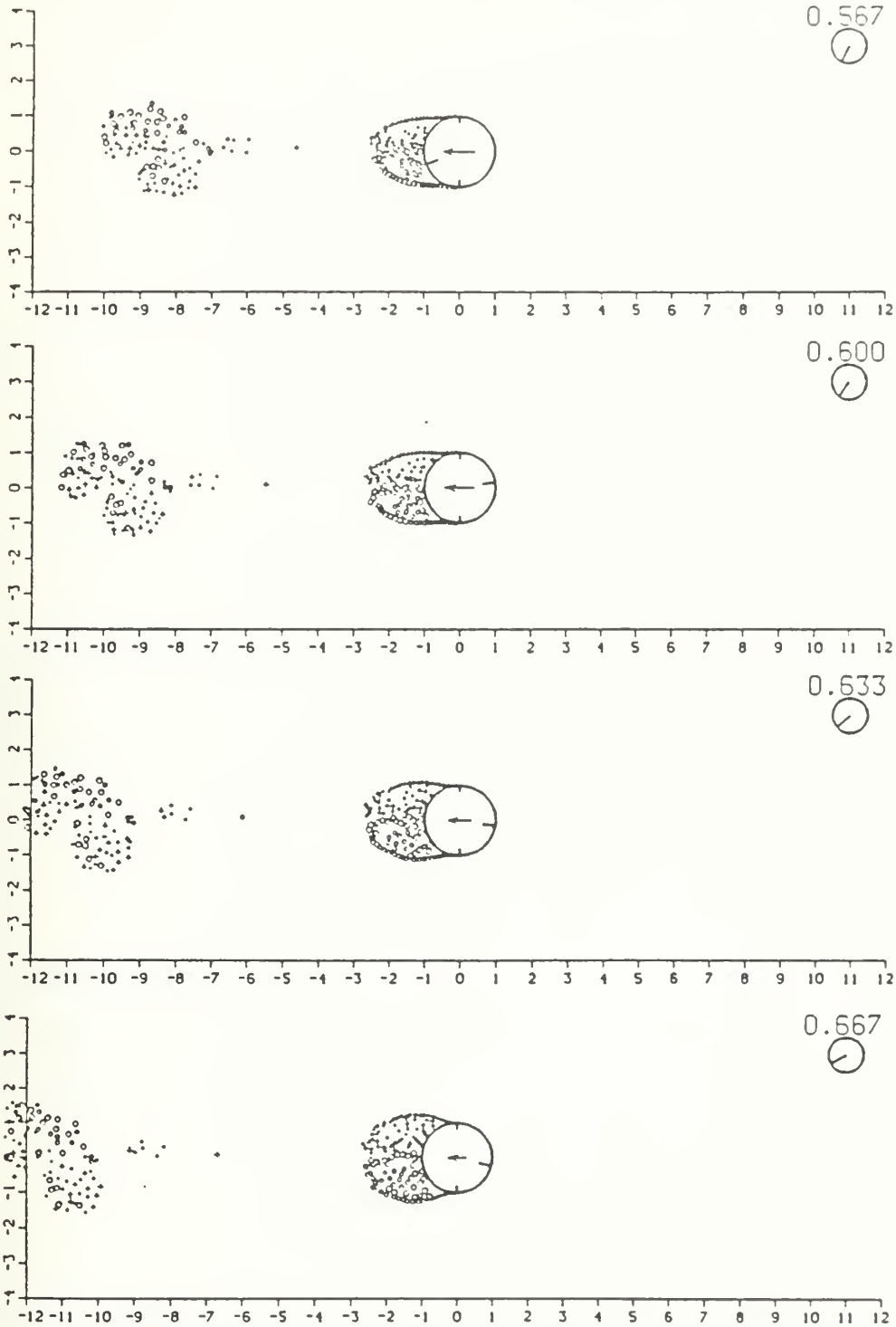


Figure 4.9a (con't.) Simulation of Stansby's model for K = 15: Kinematics.

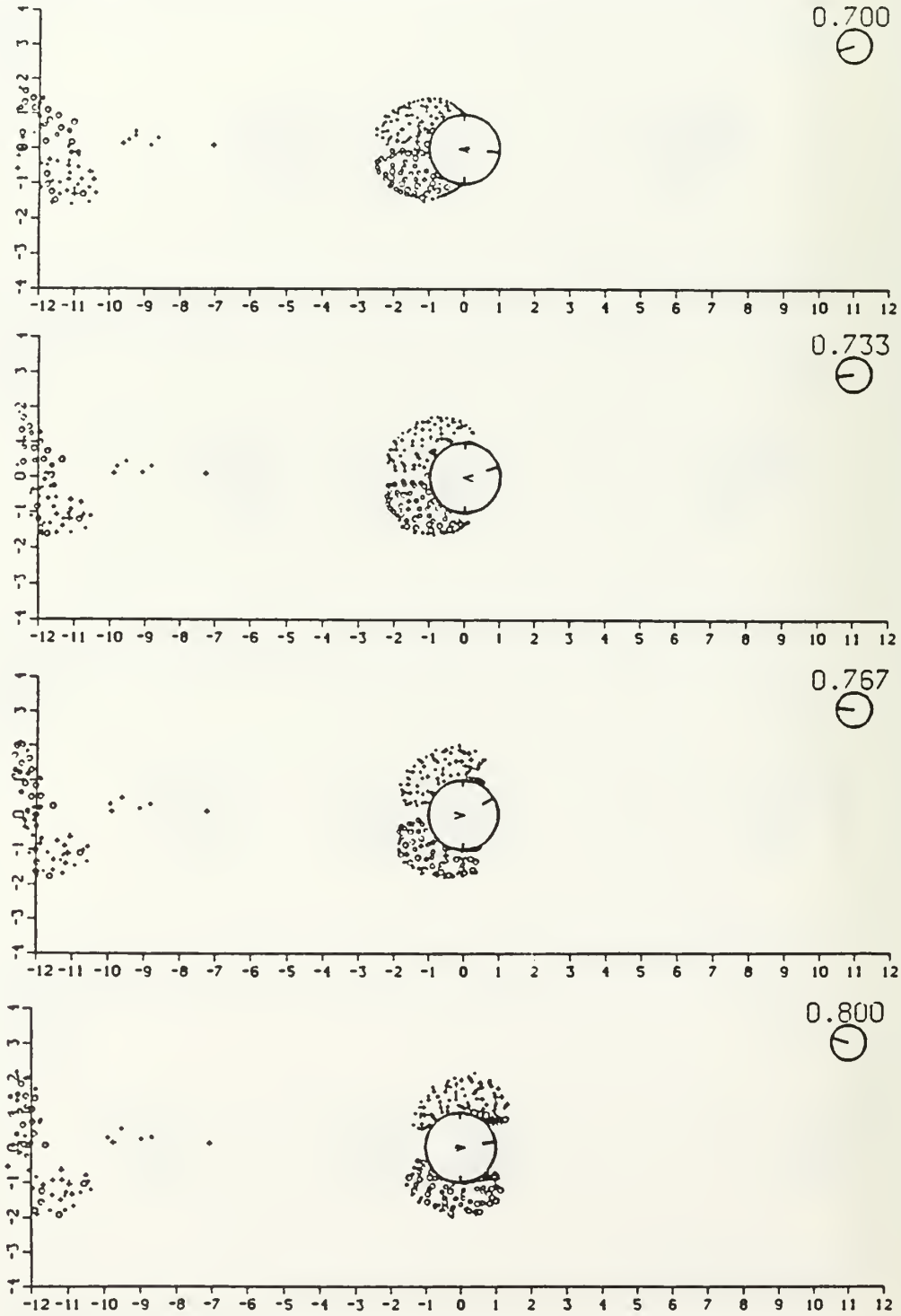


Figure 4.9a (con't.) Simulation of Stansby's model for **K** = 15: Kinematics.

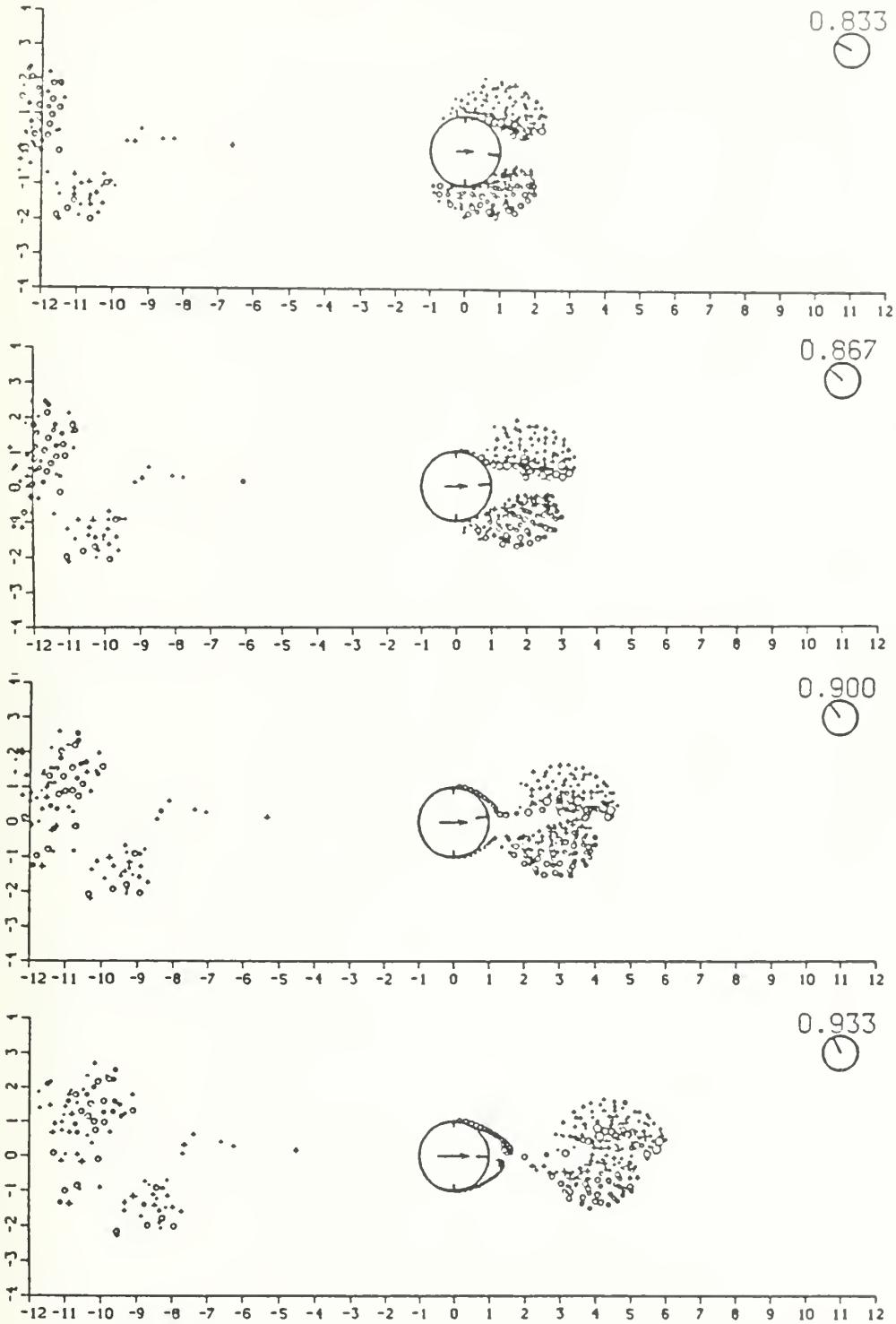


Figure 4.9a (con't.) Simulation of Stansby's model for K = 15: Kinematics.

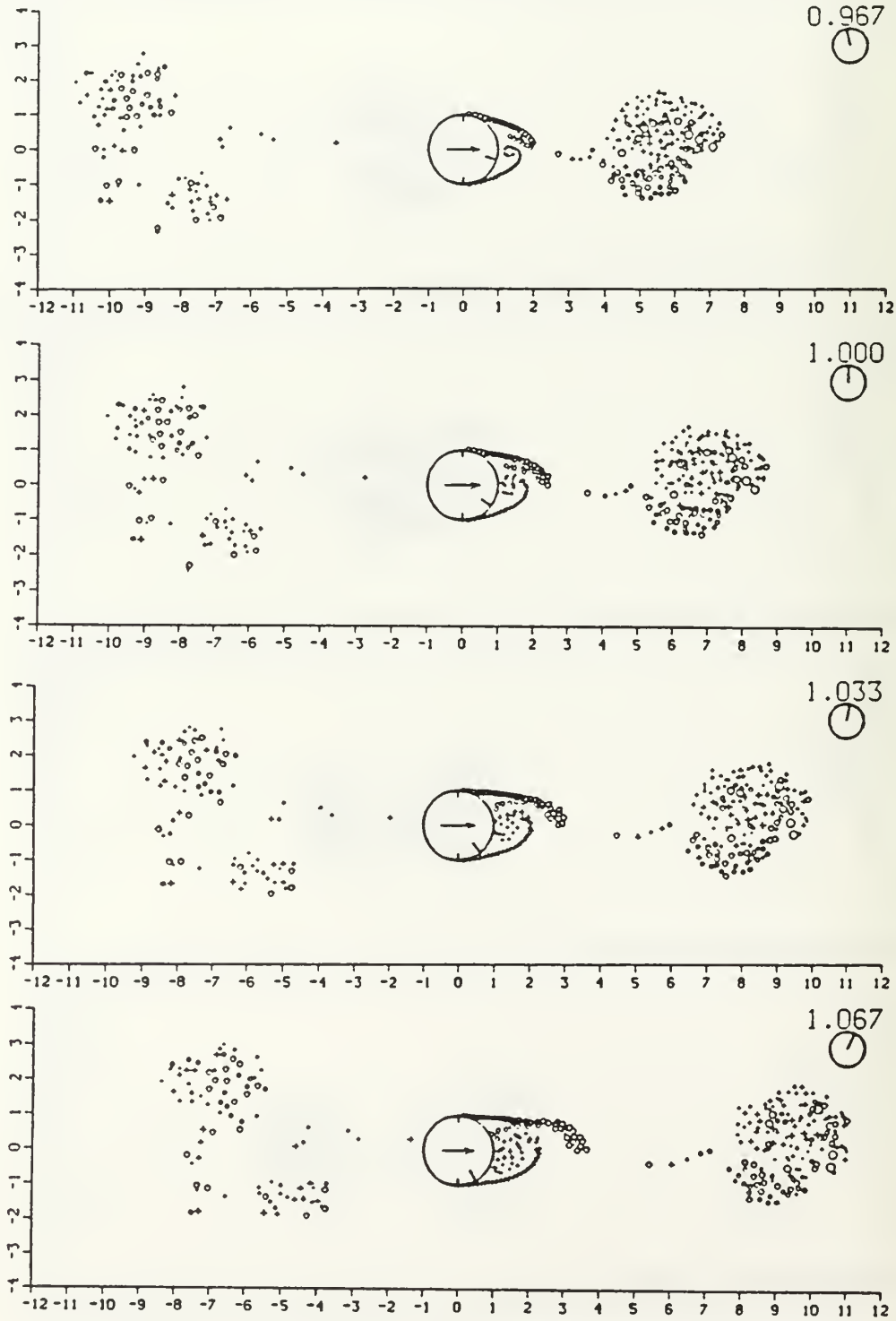


Figure 4.9a (con't.) Simulation of Stansby's model for **K** = 15: Kinematics.

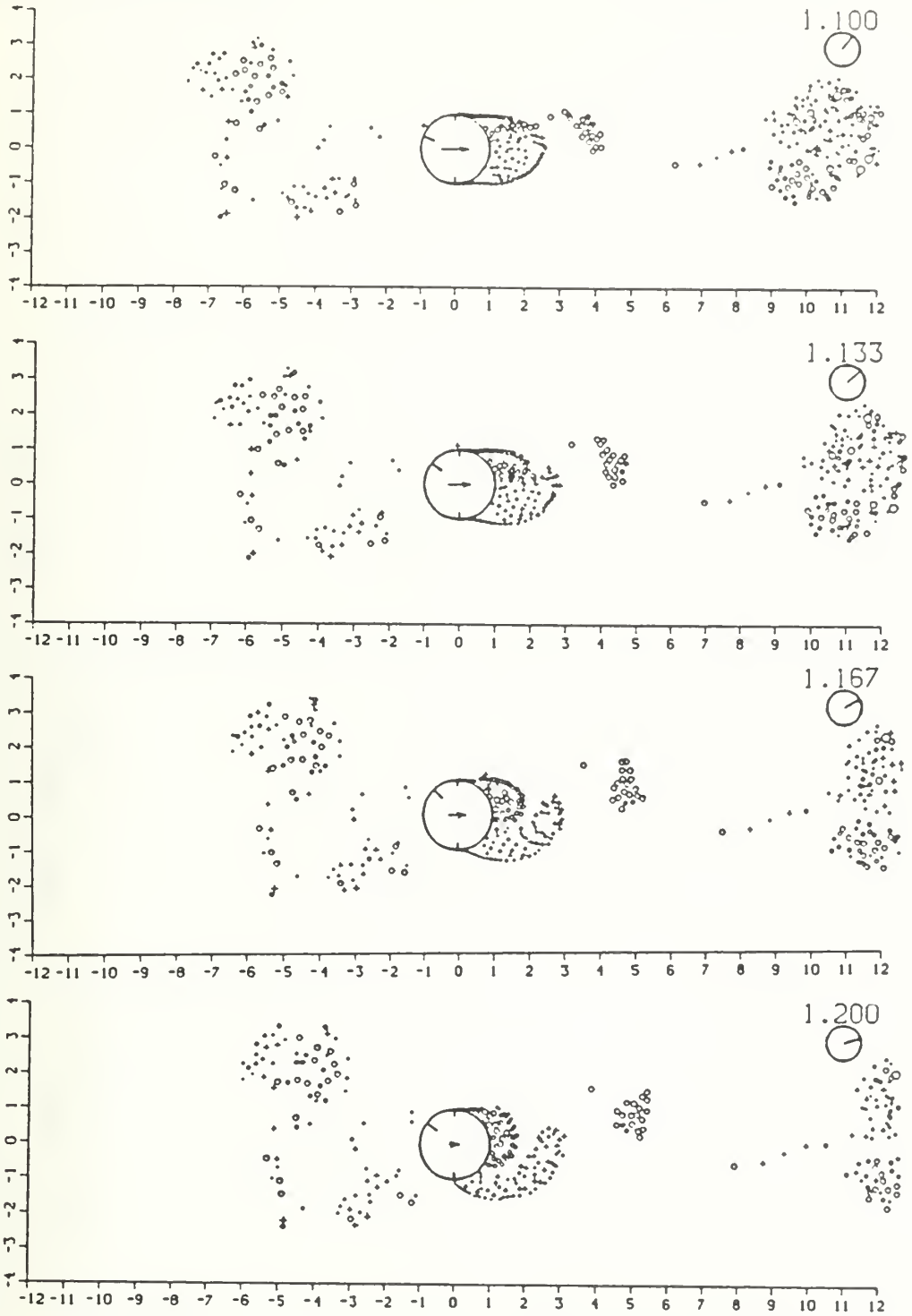


Figure 4.9a (con't.) Simulation of Stansby's model for **K** = 15: Kinematics.

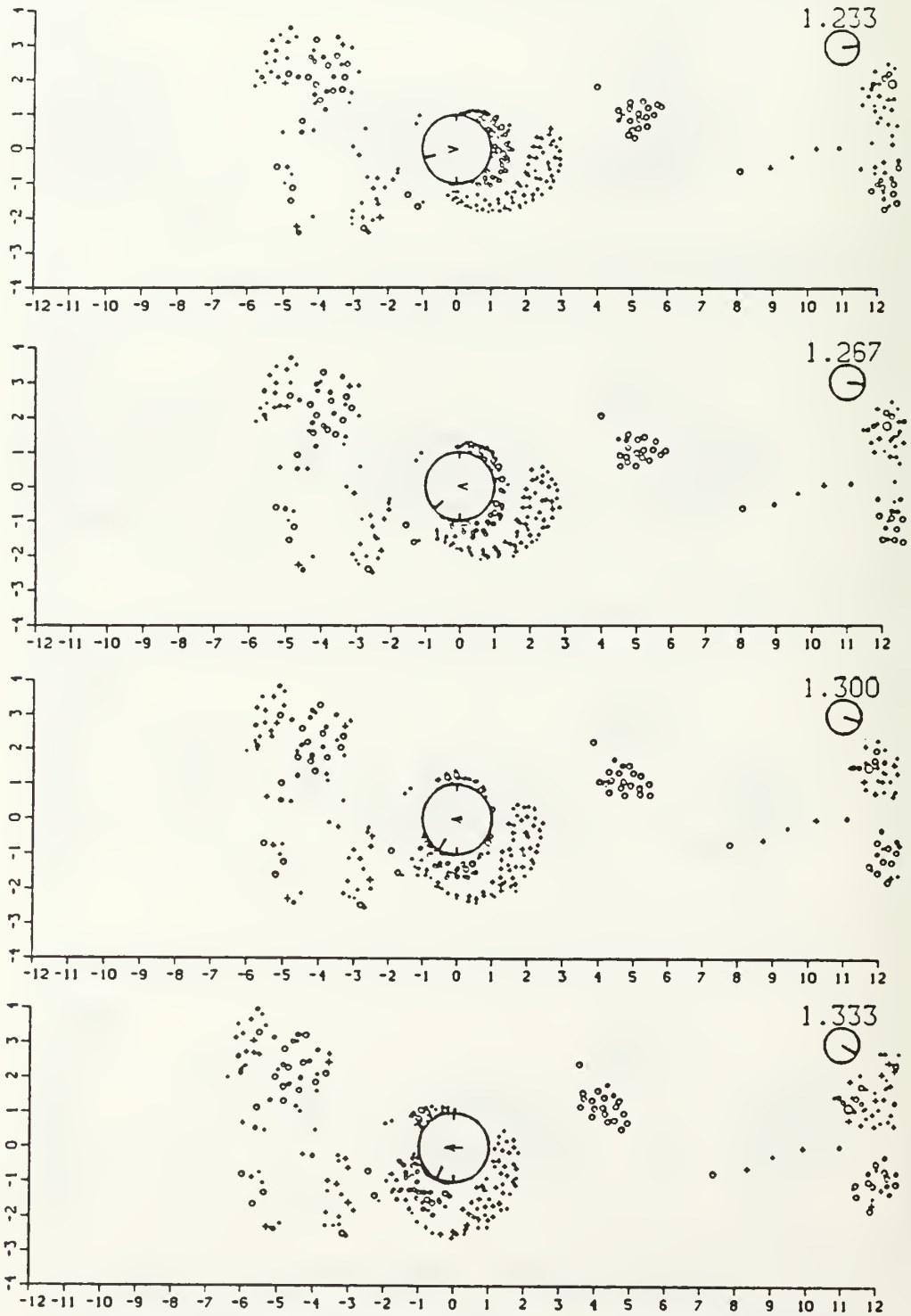


Figure 4.9a (con't.) Simulation of Stansby's model for **K** = 15: Kinematics.

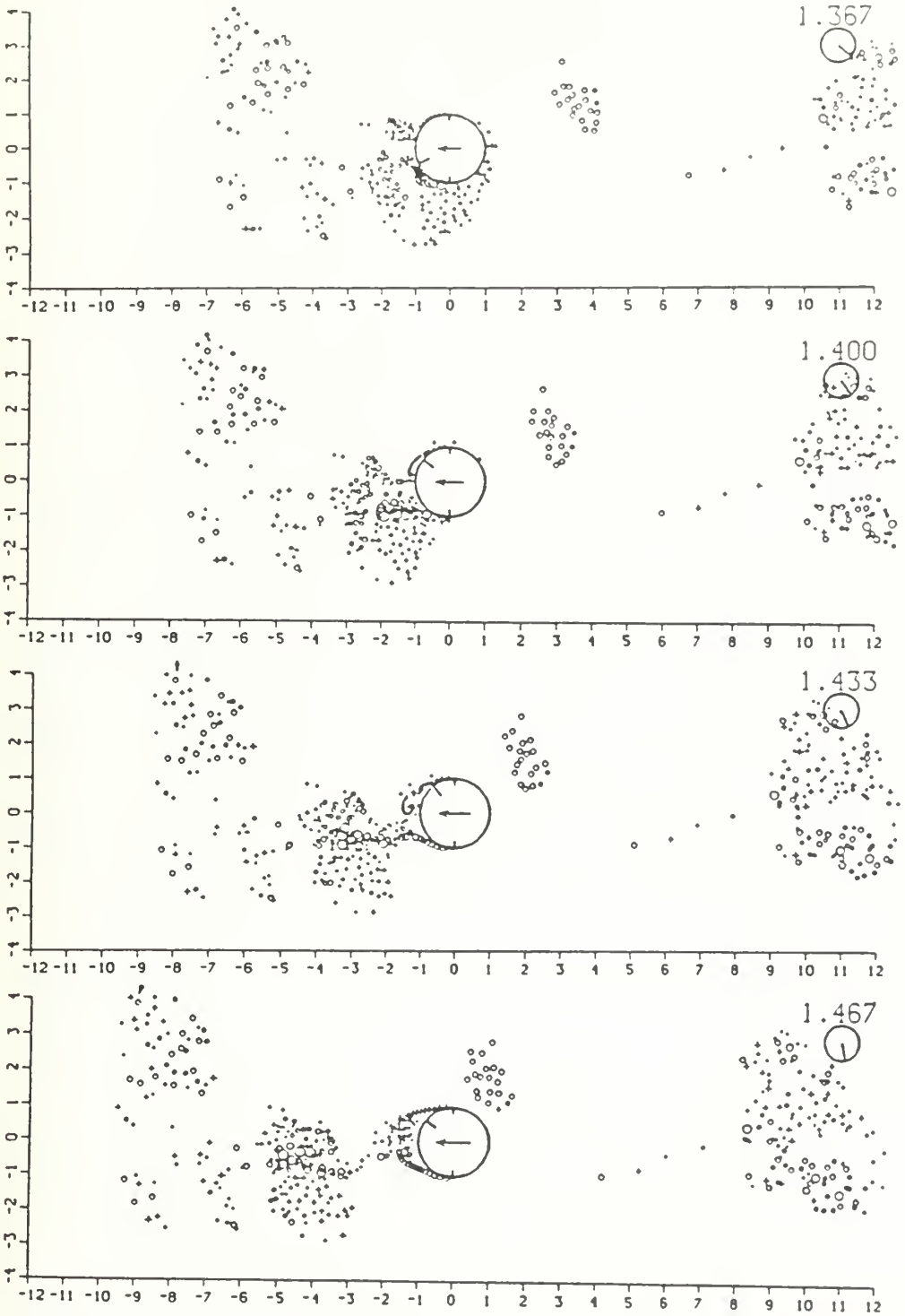


Figure 4.9a (con't.) Simulation of Stansby's model for **K** = 15: Kinematics.

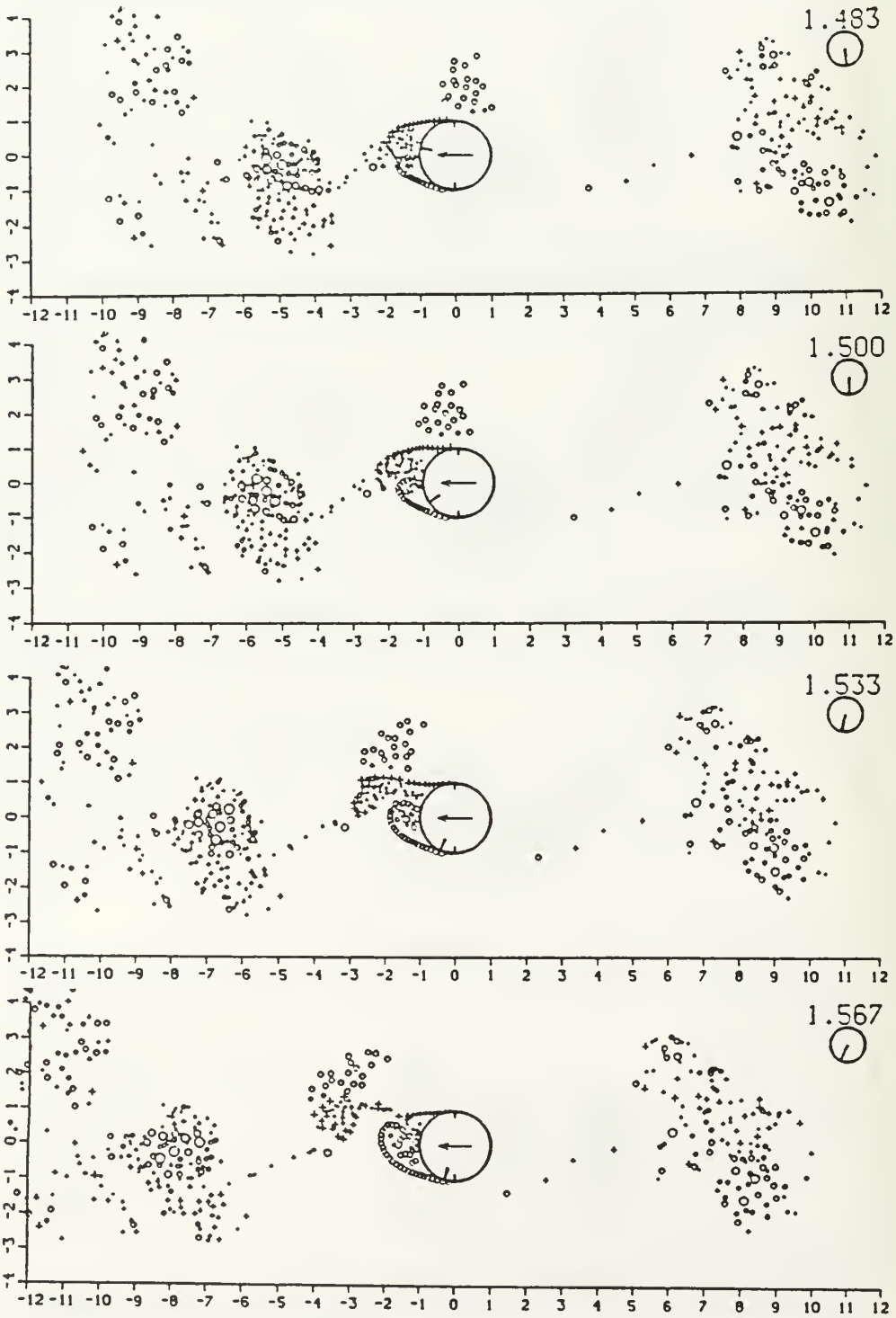


Figure 4.9a (con't.) Simulation of Stansby's model for K = 15: Kinematics.

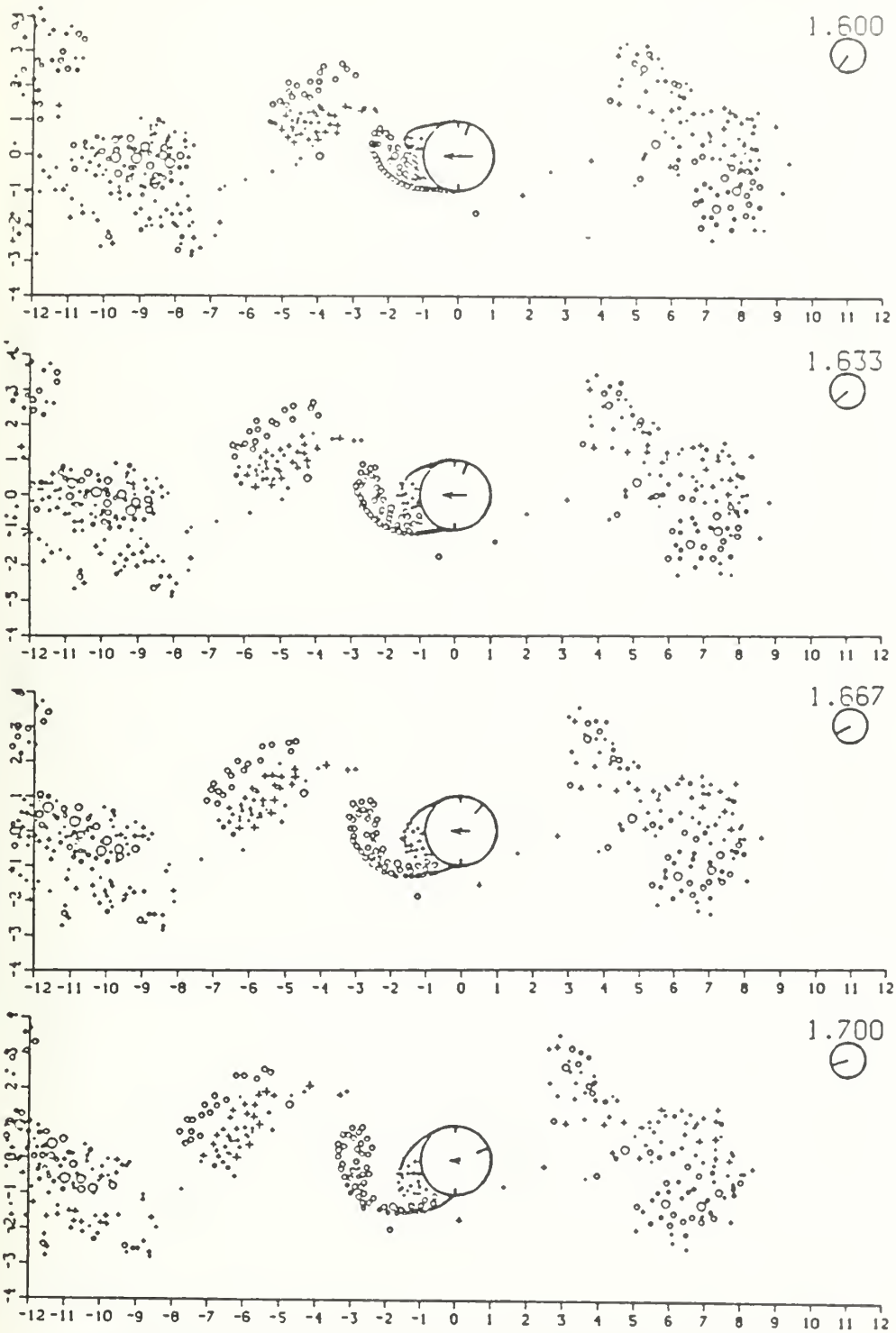


Figure 4.9a (con't.) Simulation of Stansby's model for K = 15: Kinematics.

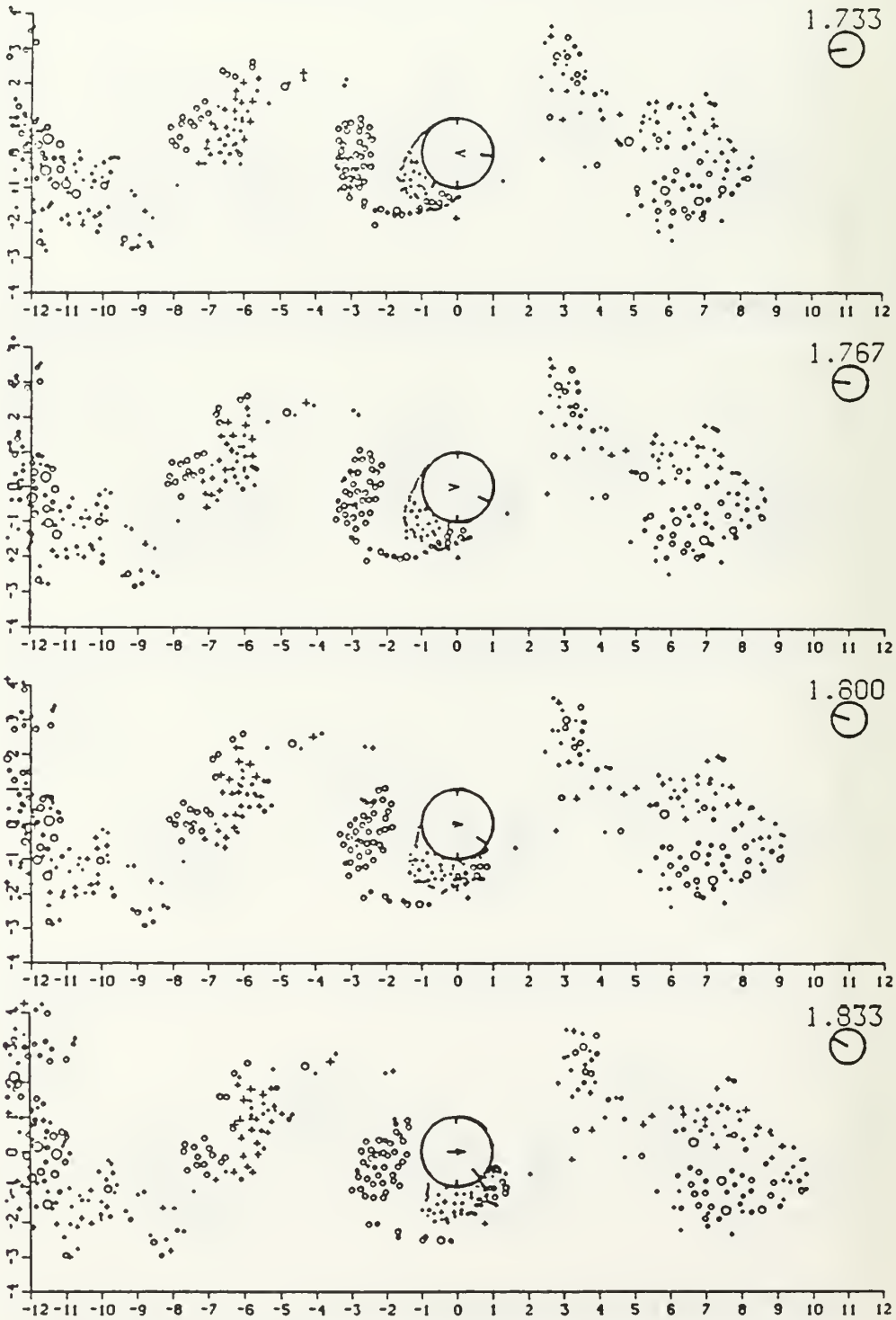


Figure 4.9a (con't.) Simulation of Stansby's model for **K** = 15: Kinematics.

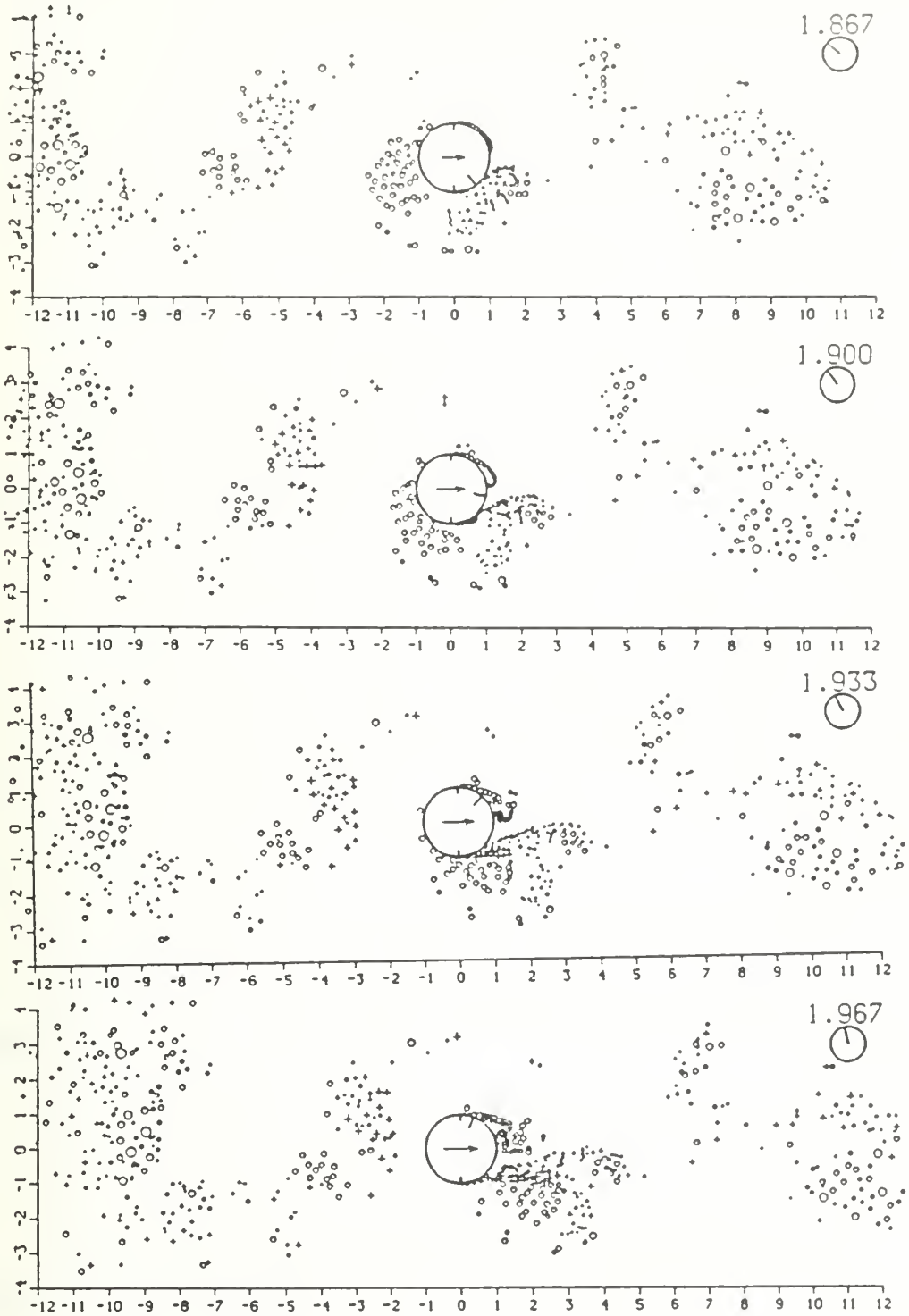


Figure 4.9a (con't.) Simulation of Stansby's model for **K** = 15: Kinematics.

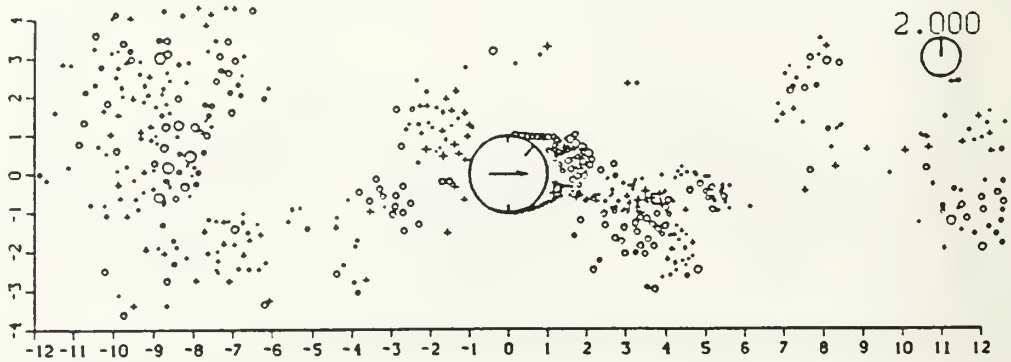


Figure 4.9a (con't.) Simulation of Stansby's model for **K** = 15: Kinematics.

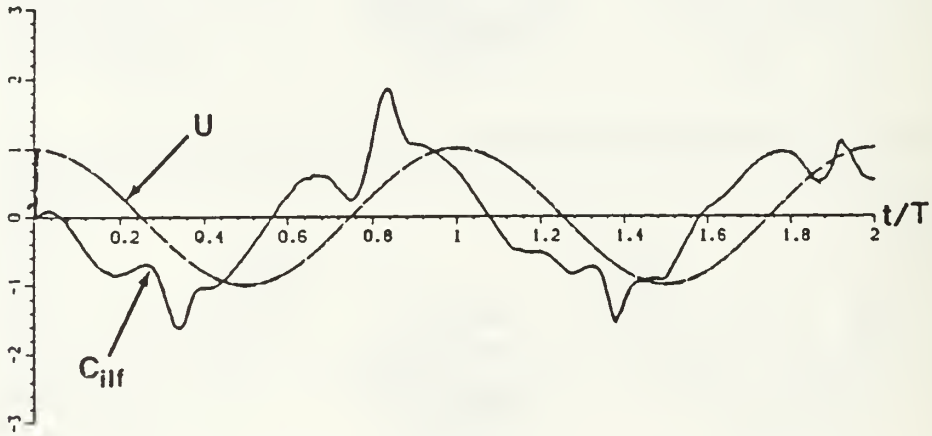


Figure 4.9b Simulation of Stansby's model for **K** = 15: In-line force coefficients.

## F. USE OF AN INTEGRAL MOMENTUM BOUNDARY LAYER SEPARATION CRITERION

Most previous investigations of the problem of harmonic flow about circular cylinders have utilized ad hoc assumptions concerning the location of the separation point. The use of an integral momentum method of predicting boundary layer separation (in this case, the method of Pohlhausen [1921] ) requires none of these assumptions, and allows for the realistic possibility of a mobile separation,

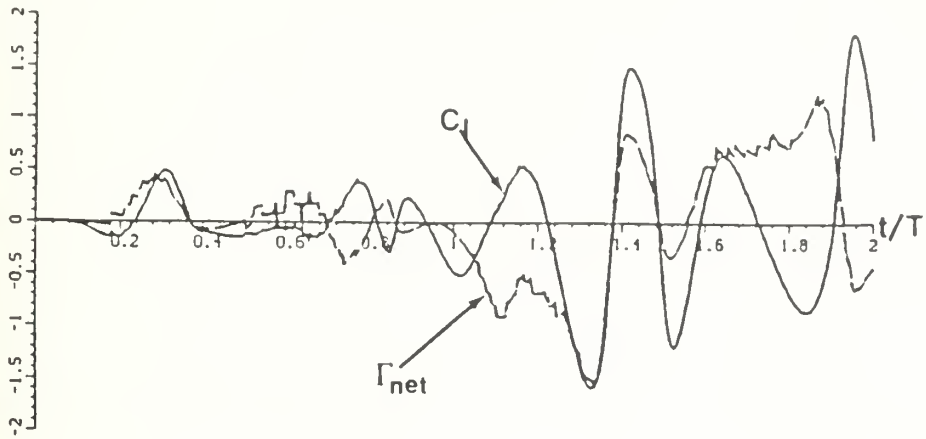


Figure 4.9c Simulation of Stansby's model for **K** = 15: Lift force.

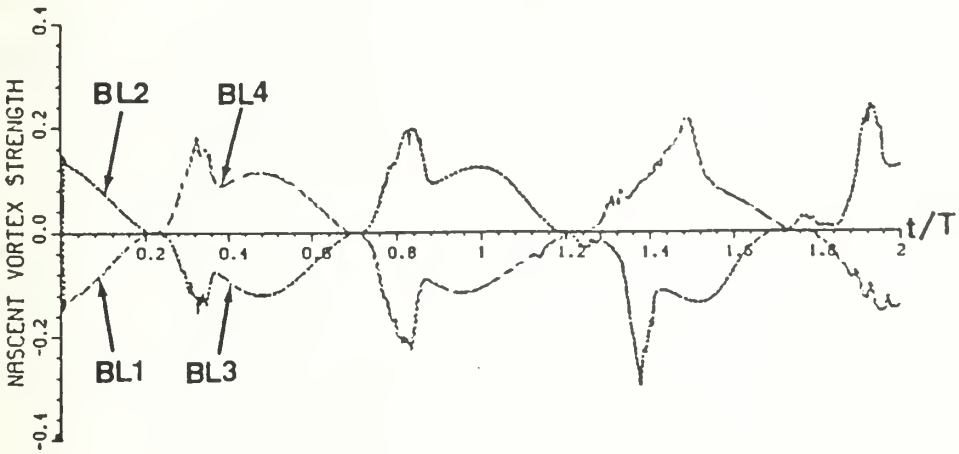


Figure 4.9d Simulation of Stansby's model for **K** = 15: Nascent vortex strength.

point (Deffenbaugh and Marshall [1976], Sarpkaya and Shoaff [1979], Mostafa [1987] ). Most importantly, such a method allows for the free interaction of the returning wake with the boundary layer, although this can produce difficulties as depicted in Figures 3.1 through 3.3. When the velocity distribution is perturbed in such a fashion, any type of an integral momentum calculation cannot predict separation with reasonable accuracy. When such a situation occurred in the present model, separation was said to occur at a position on the cylinder where the velocity had fallen to 97 percent of the maximum velocity. This value was obtained from an analysis of separation data on the impulsive flow run originally utilized in validating the model. A similar method of calculating separation was performed by Franks [1983] and Mostafa [1987].

The results are shown in Figures 4.10a through 4.10f. Again, the proper flow kinematics did not result. Aside from the first cycle of flow which contained transient effects, there is a repeatable diagonal shedding pattern which is characteristic of the shedding observed at higher Keulegan-Carpenter numbers (see, e.g., Figures 4.4b and 4.6c). During this shedding, as a large vortex cluster passes over the shoulder of the cylinder, it "pairs" with a cluster of opposite vorticity which is still growing while attached to a boundary layer. It is, consequently, prematurely "stripped" off of the cylinder, so that there are three vortices shed per half-cycle rather than the two depicted in Figure 4.4b. Although this triple shedding results in the three cycles observed in the lift coefficient, it should be noted that the in-line force coefficient retains reasonable magnitude and qualitative agreement with experimental results.

When the boundary layer calculation failed and the aforementioned velocity ratio method was employed in ascertaining the separation point, the separation angle could still fluctuate as much as 20° with associated fluctuations in nascent vortex strength. Forebody stagnation angles showed variations on the order of 30° from the x-axis. Neither of these two angular fluctuations is physically realistic.

It should be noted that the incorporation of countervorticity in the model adds a significant amount of continuity between successive half-cycles. This is most evident when observing the in-line force trace of a run without countervorticity (Figure 4.11), where it can be seen that the introduction of

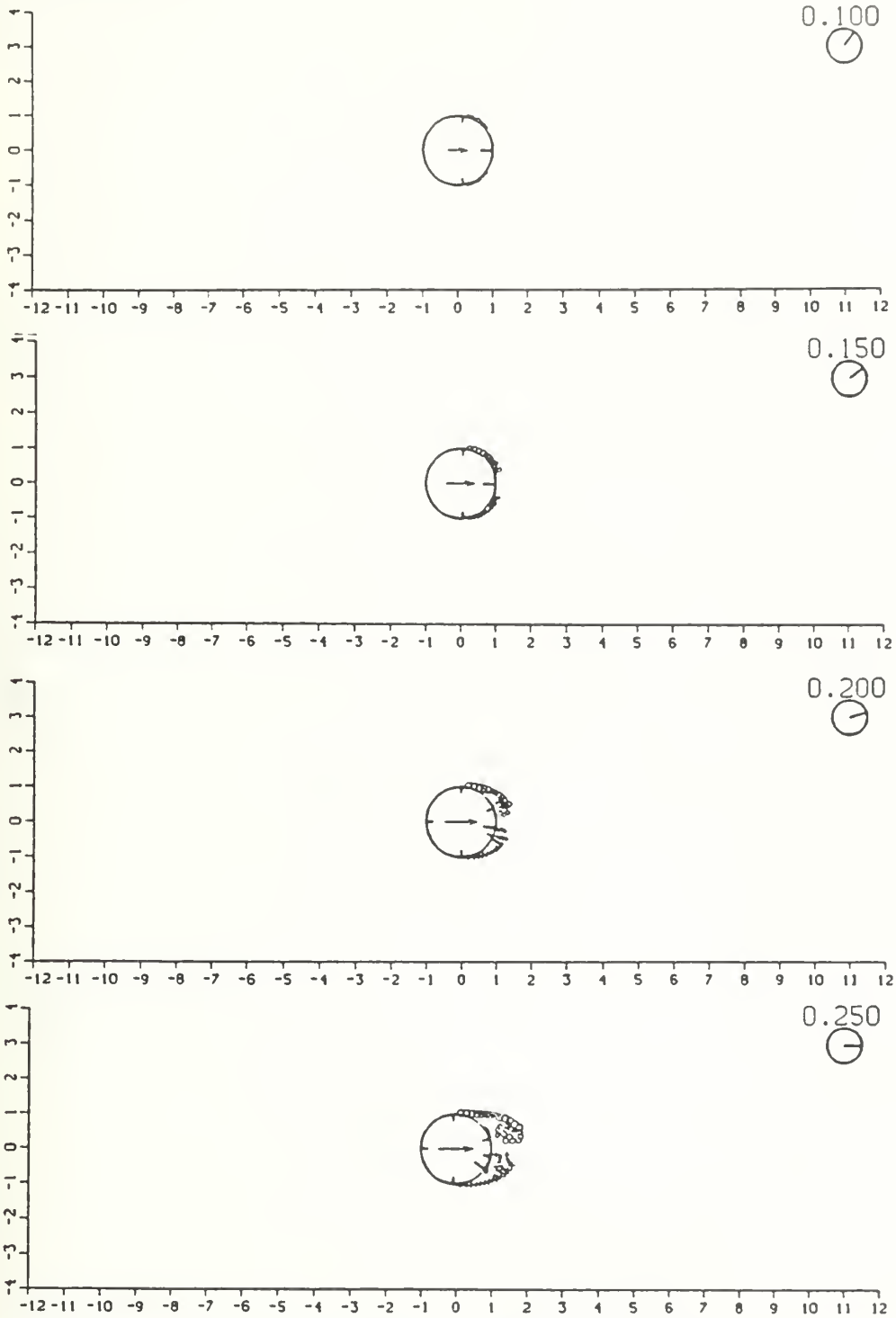


Figure 4.10a Laminar separation criterion for **K** = 10: Kinematics.

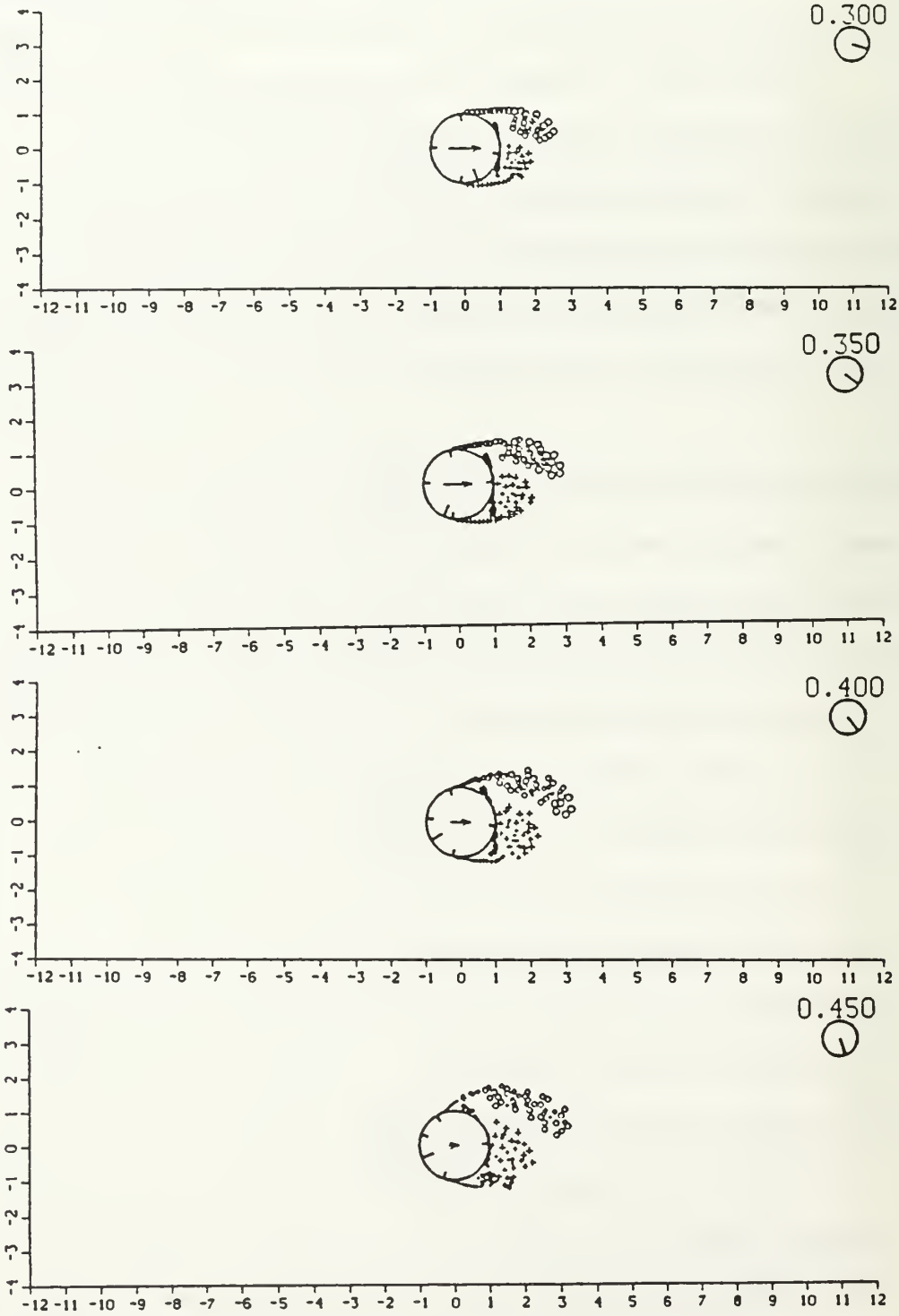


Figure 4.10a (con't.) Laminar separation criterion for **K** = 10: Kinematics.

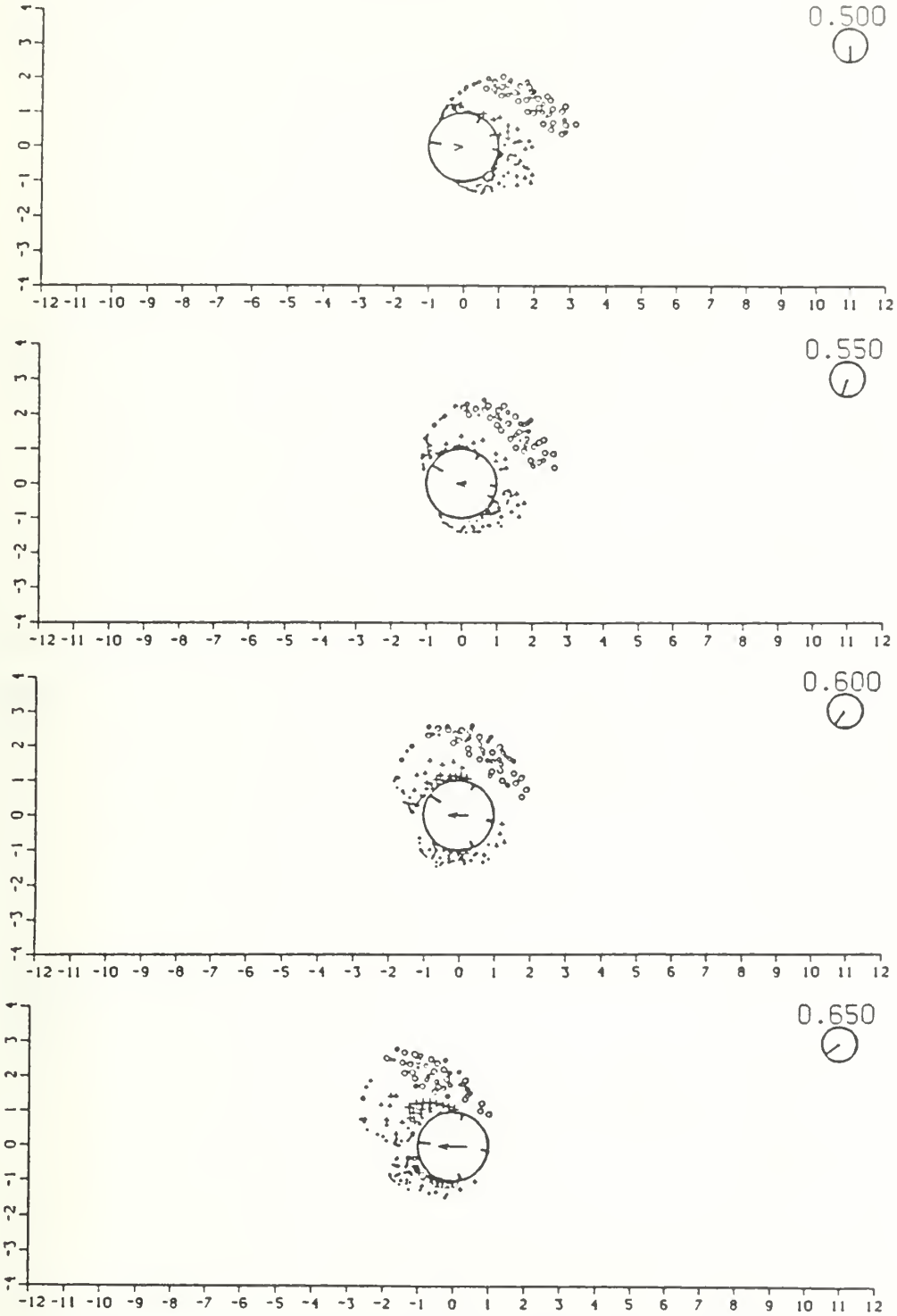


Figure 4.10a (con't.) Laminar separation criterion for **K** = 10: Kinematics.

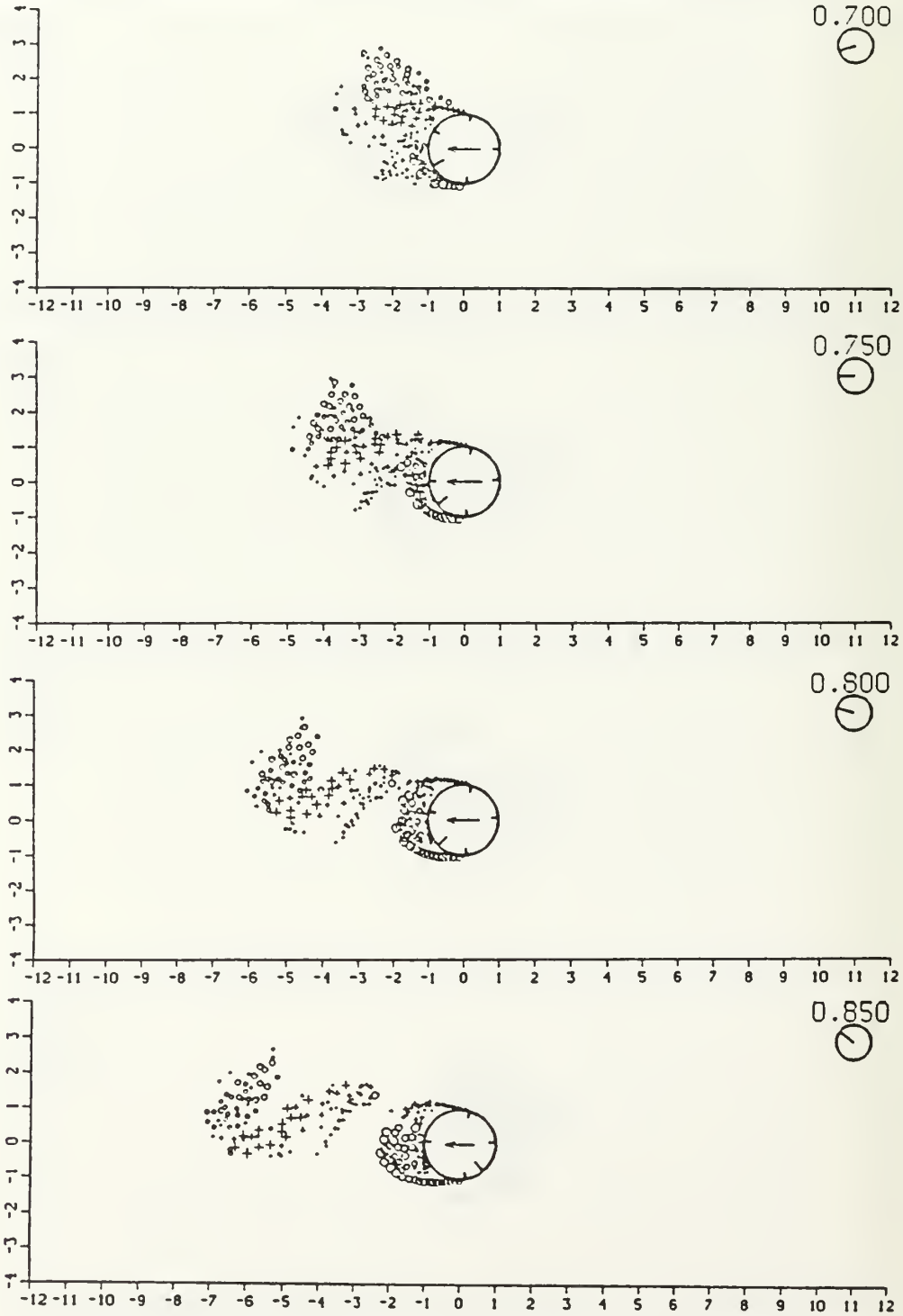


Figure 4.10a (con't.) Laminar separation criterion for **K** = 10: Kinematics.

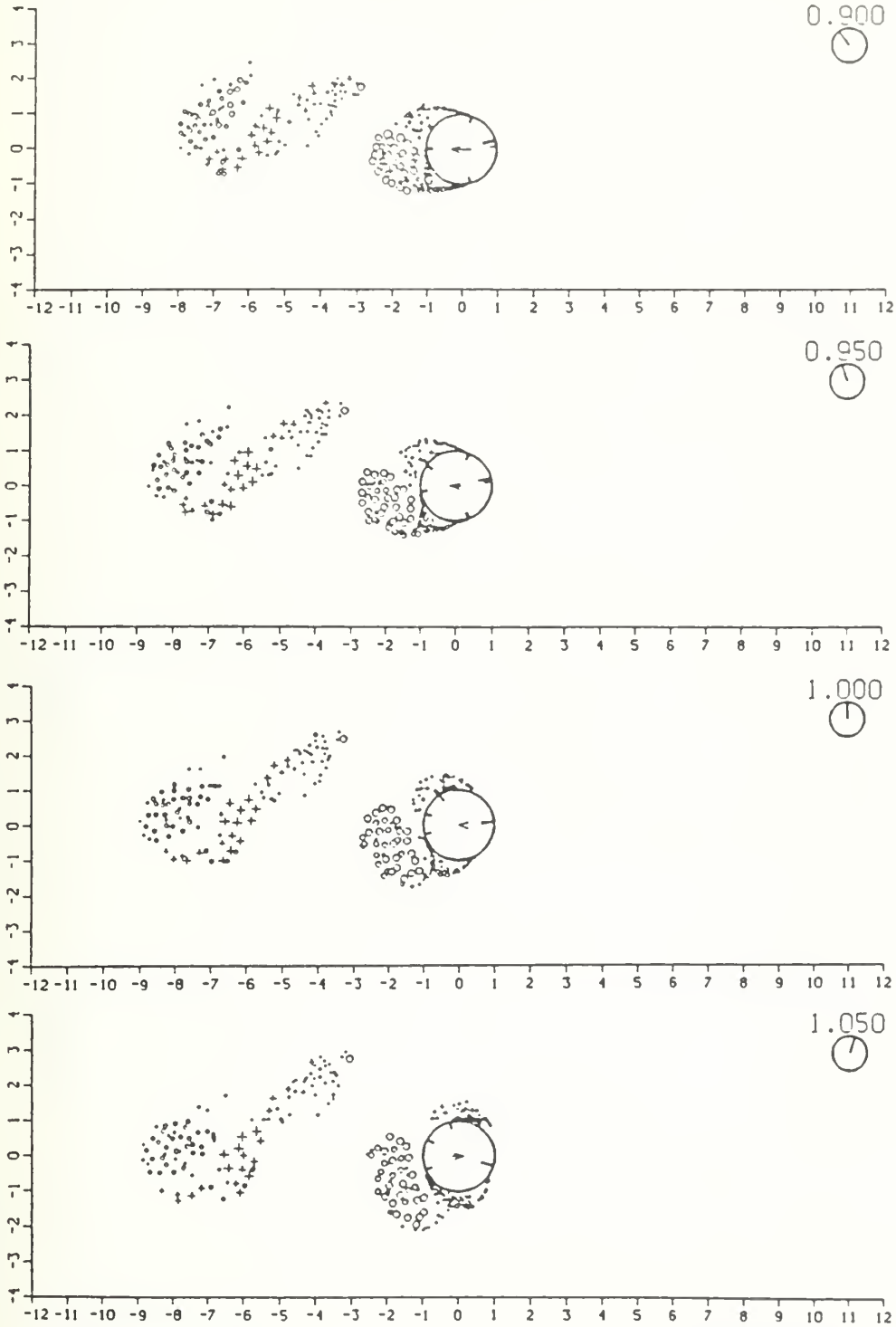


Figure 4.10a (con't.) Laminar separation criterion for **K** = 10: Kinematics.

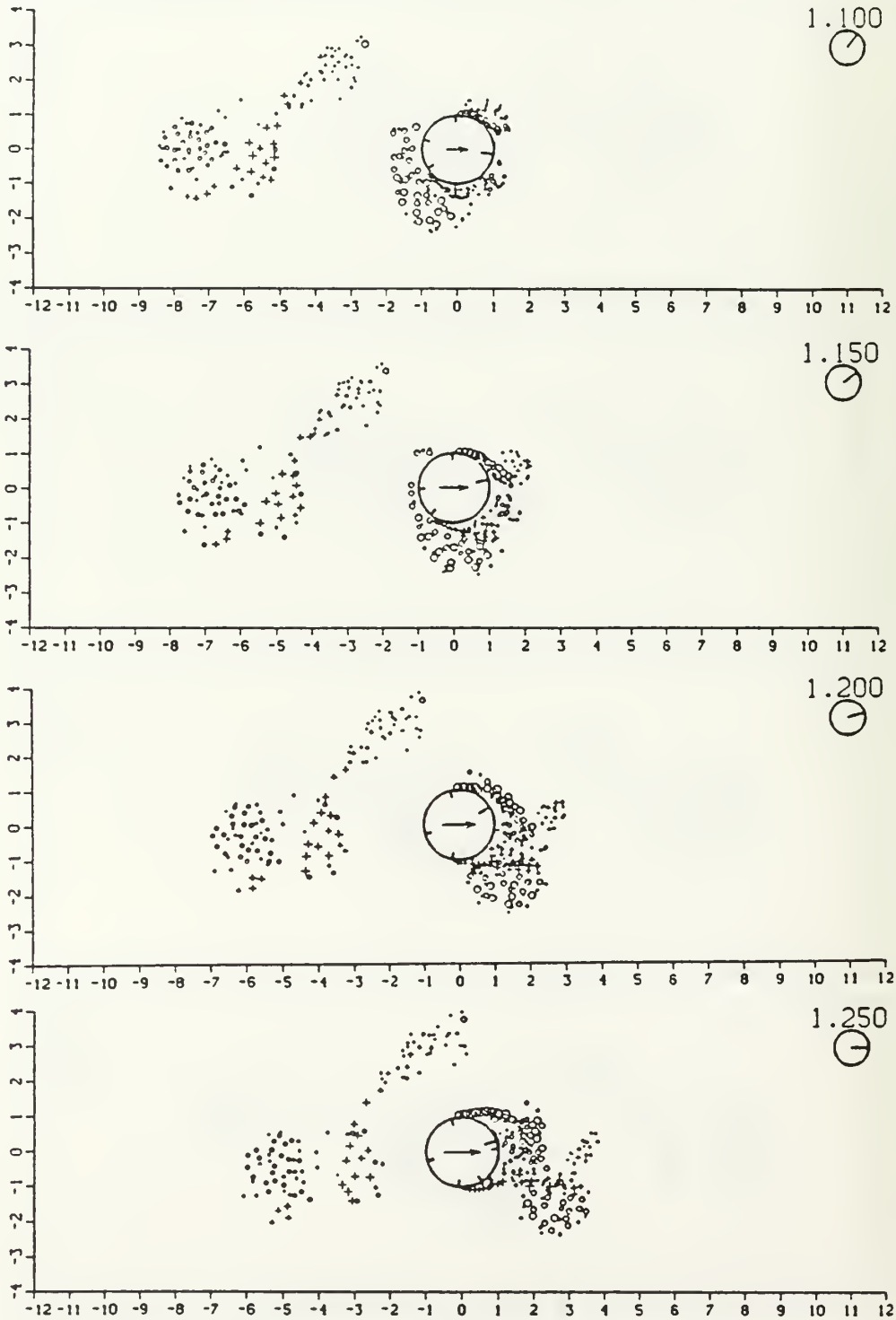


Figure 4.10a (con't.) Laminar separation criterion for **K** = 10: Kinematics.

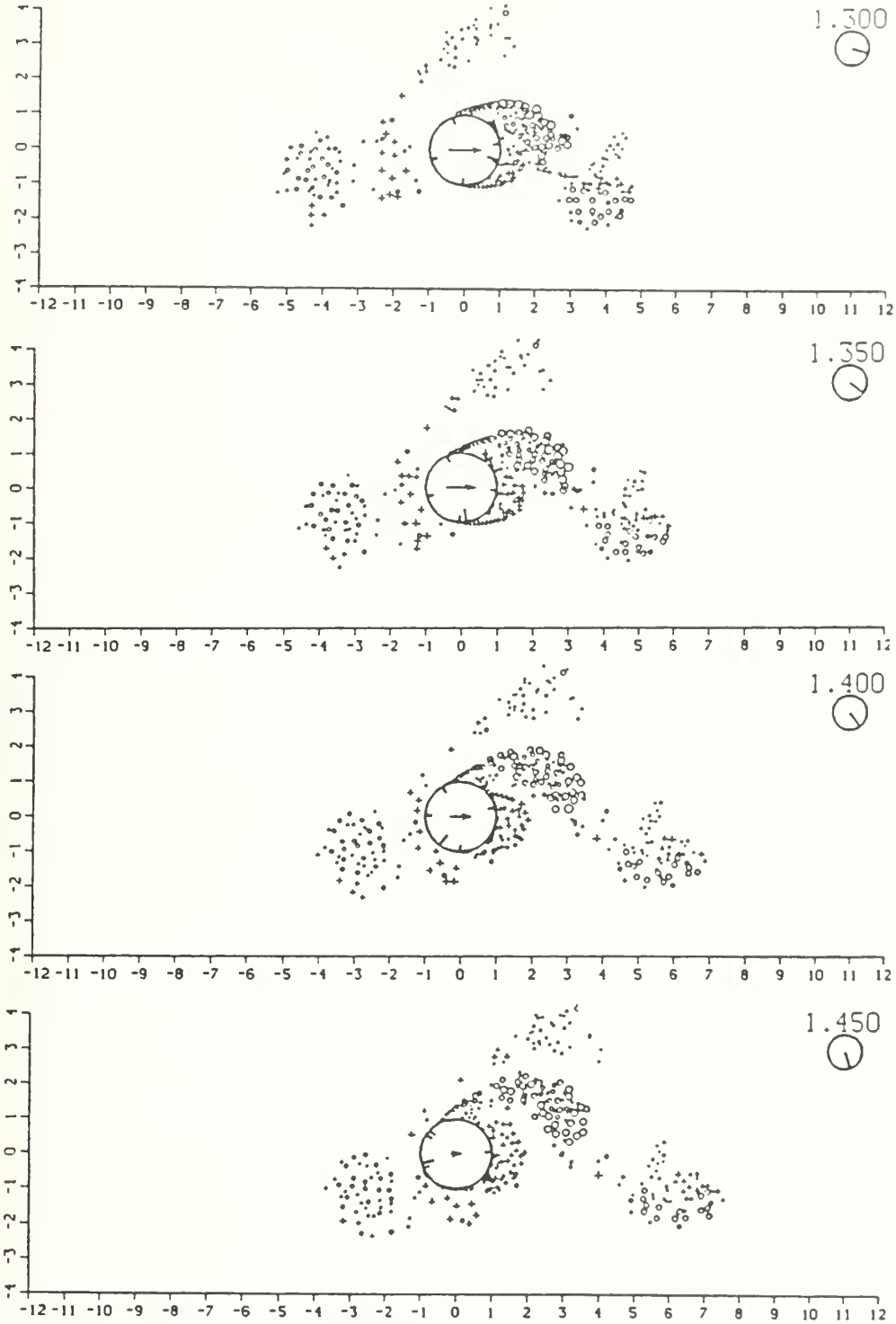


Figure 4.10a (con't.) Laminar separation criterion for **K** = 10: Kinematics.

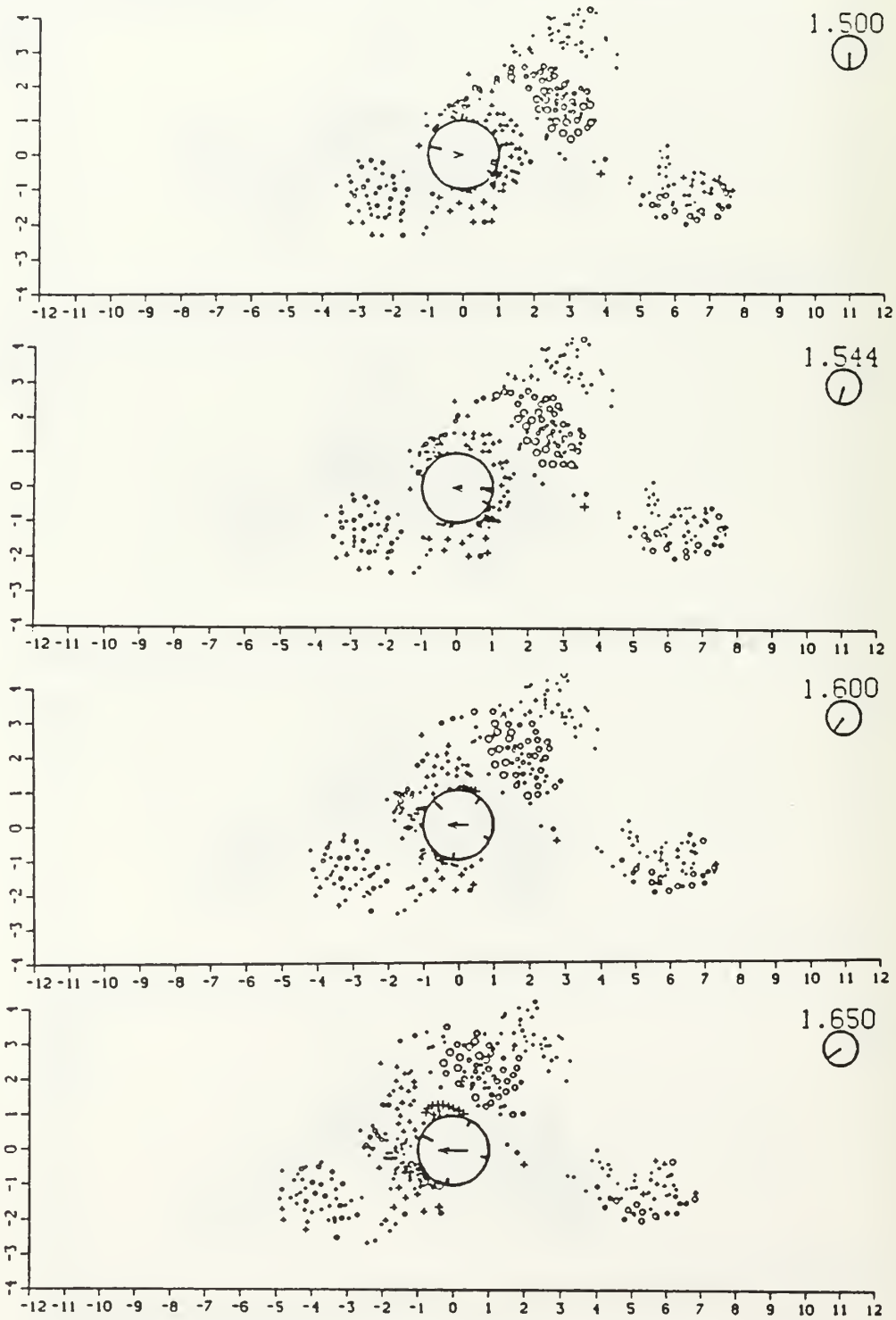


Figure 4.10a (con't.) Laminar separation criterion for K = 10: Kinematics.

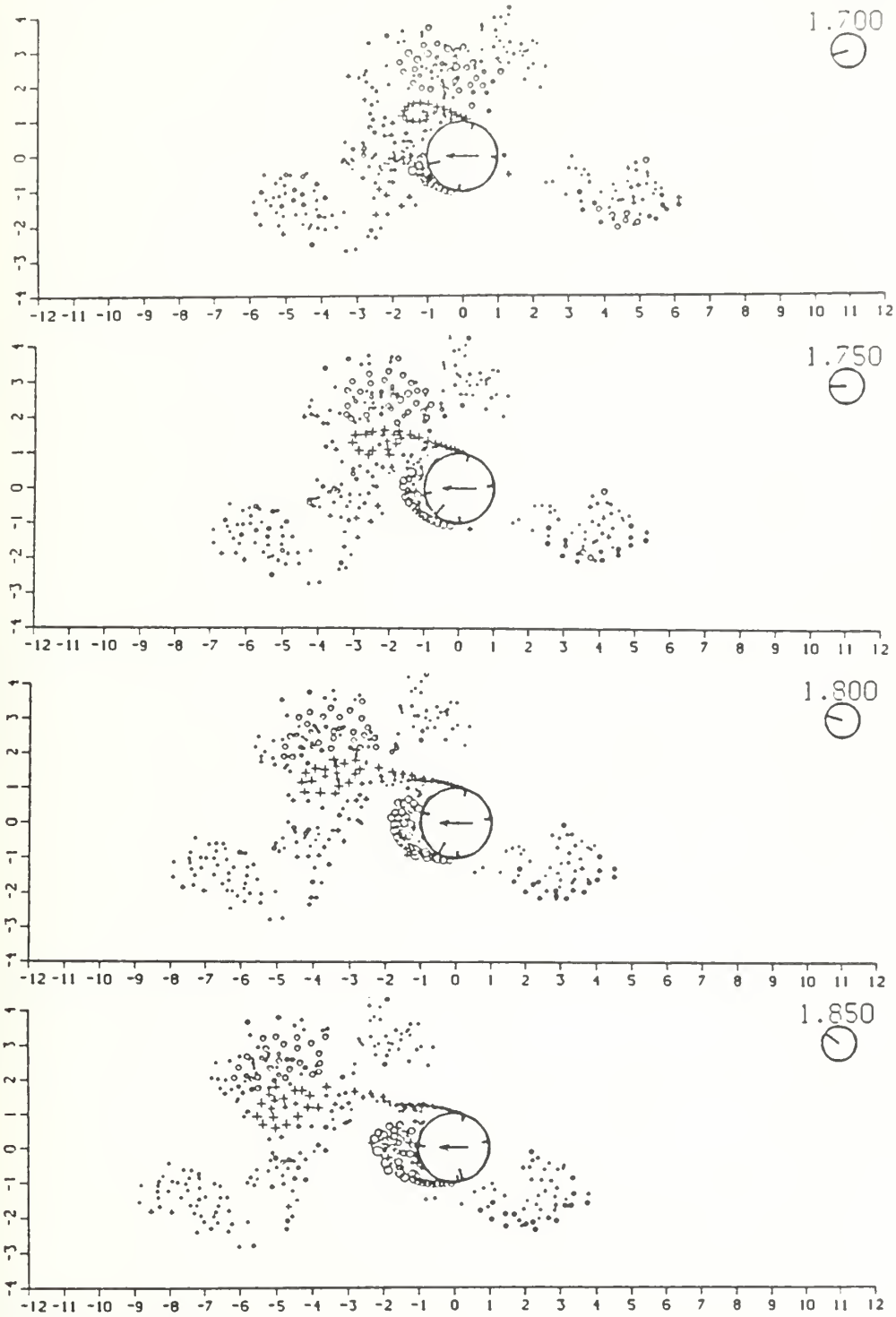


Figure 4.10a (con't.) Laminar separation criterion for **K** = 10: Kinematics.

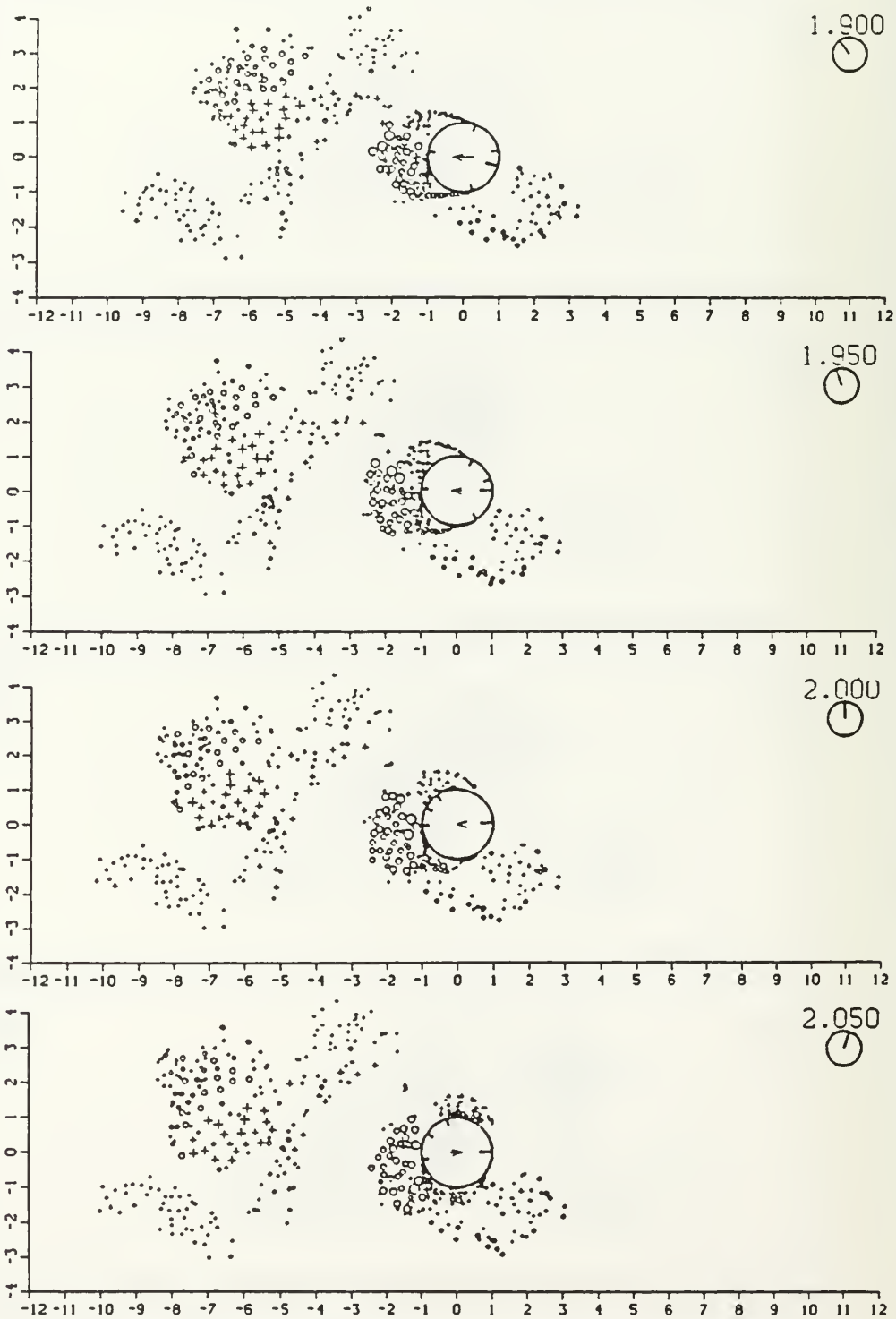


Figure 4.10a (con't.) Laminar separation criterion for K = 10: Kinematics.

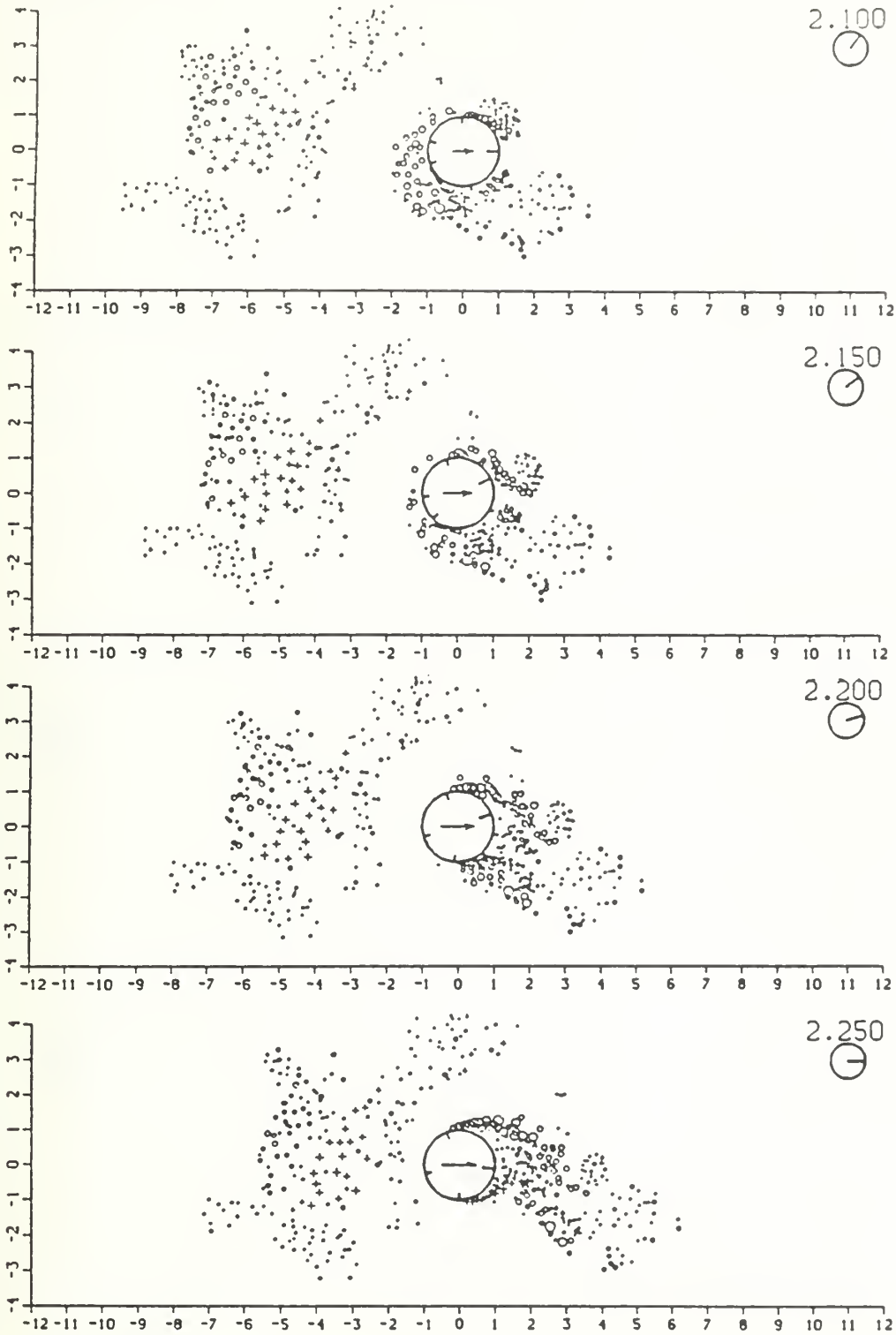


Figure 4.10a (con't.) Laminar separation criterion for K = 10: Kinematics.

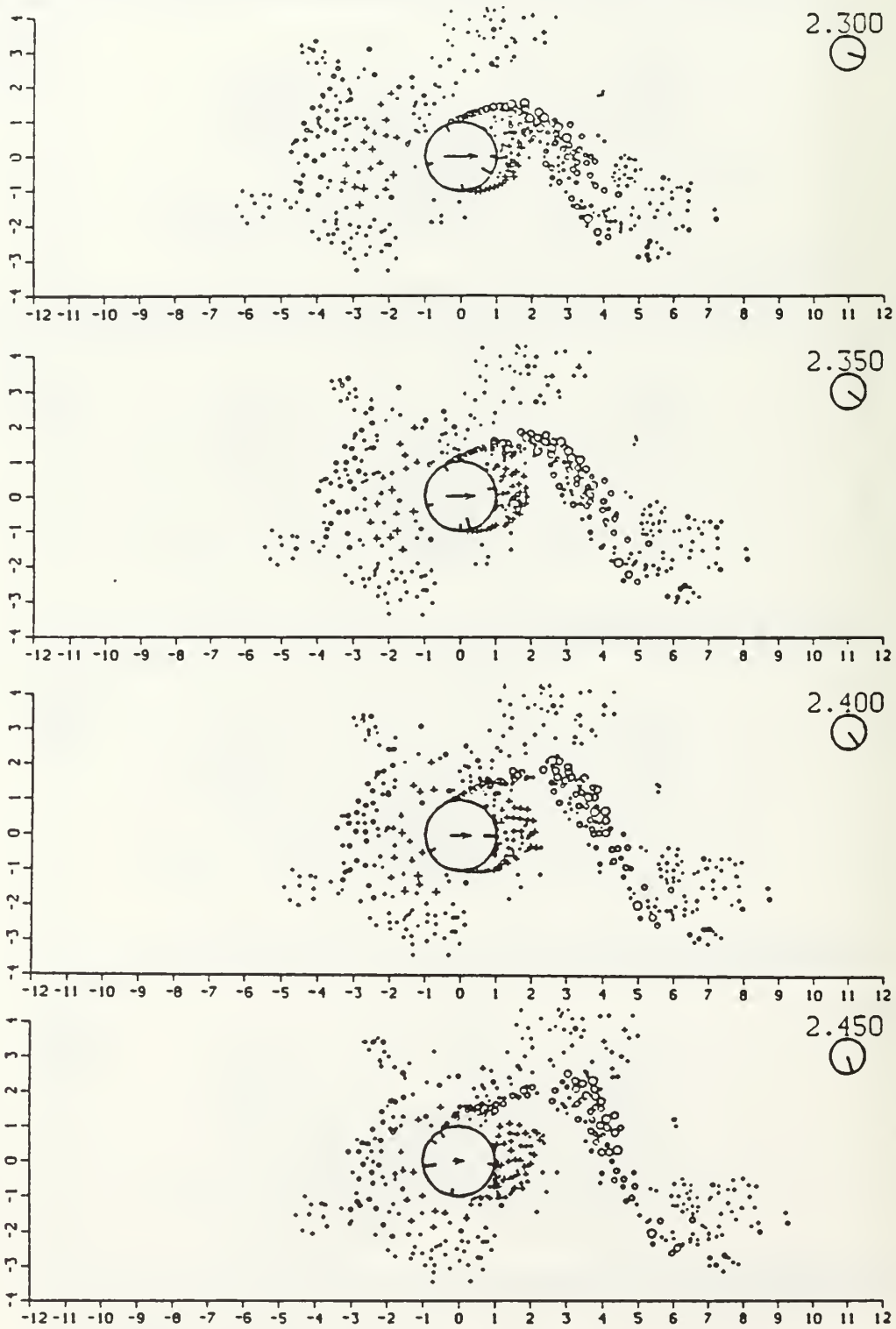


Figure 4.10a (con't.) Laminar separation criterion for **K** = 10: Kinematics.

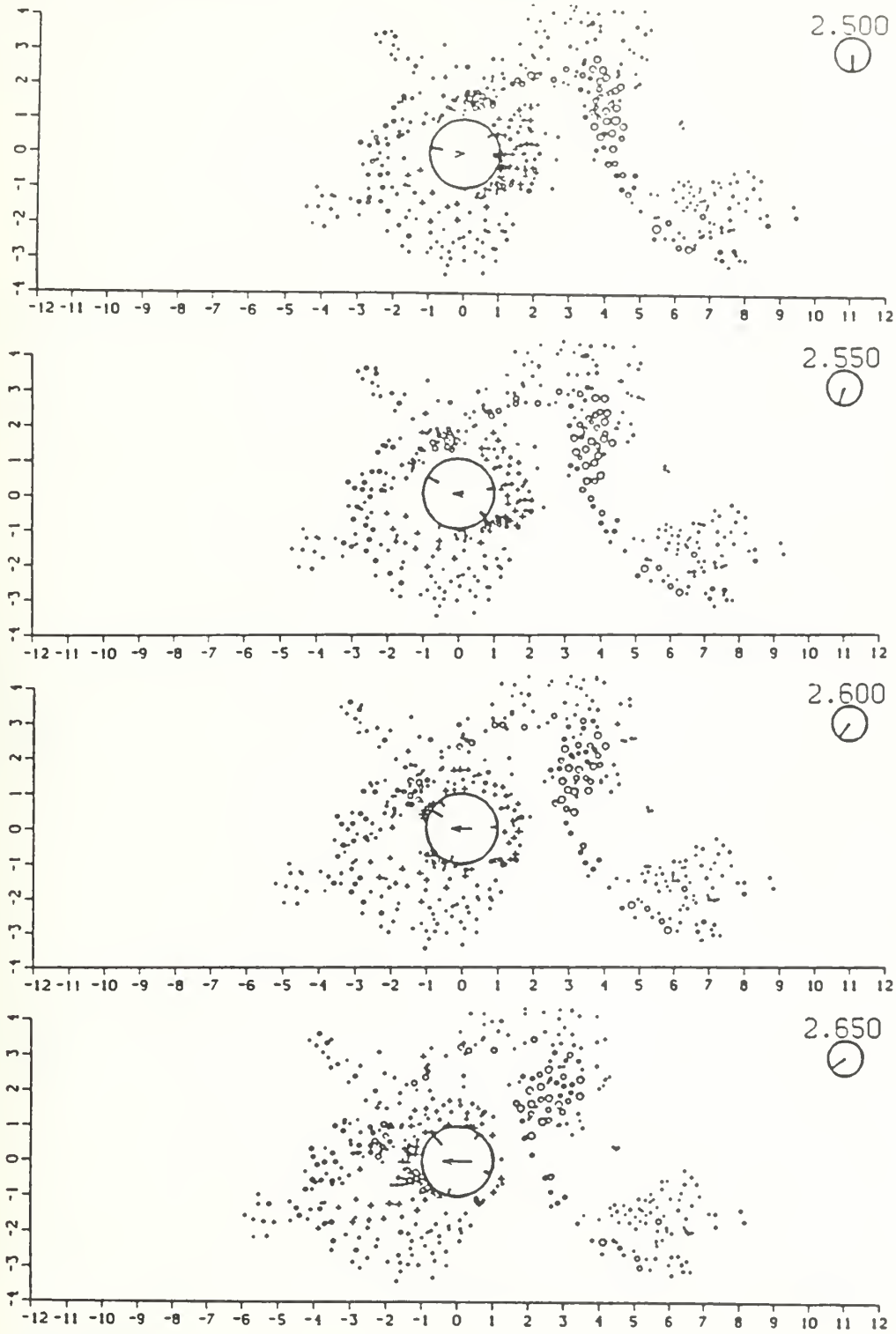


Figure 4.10a (con't.) Laminar separation criterion for K = 10: Kinematics.

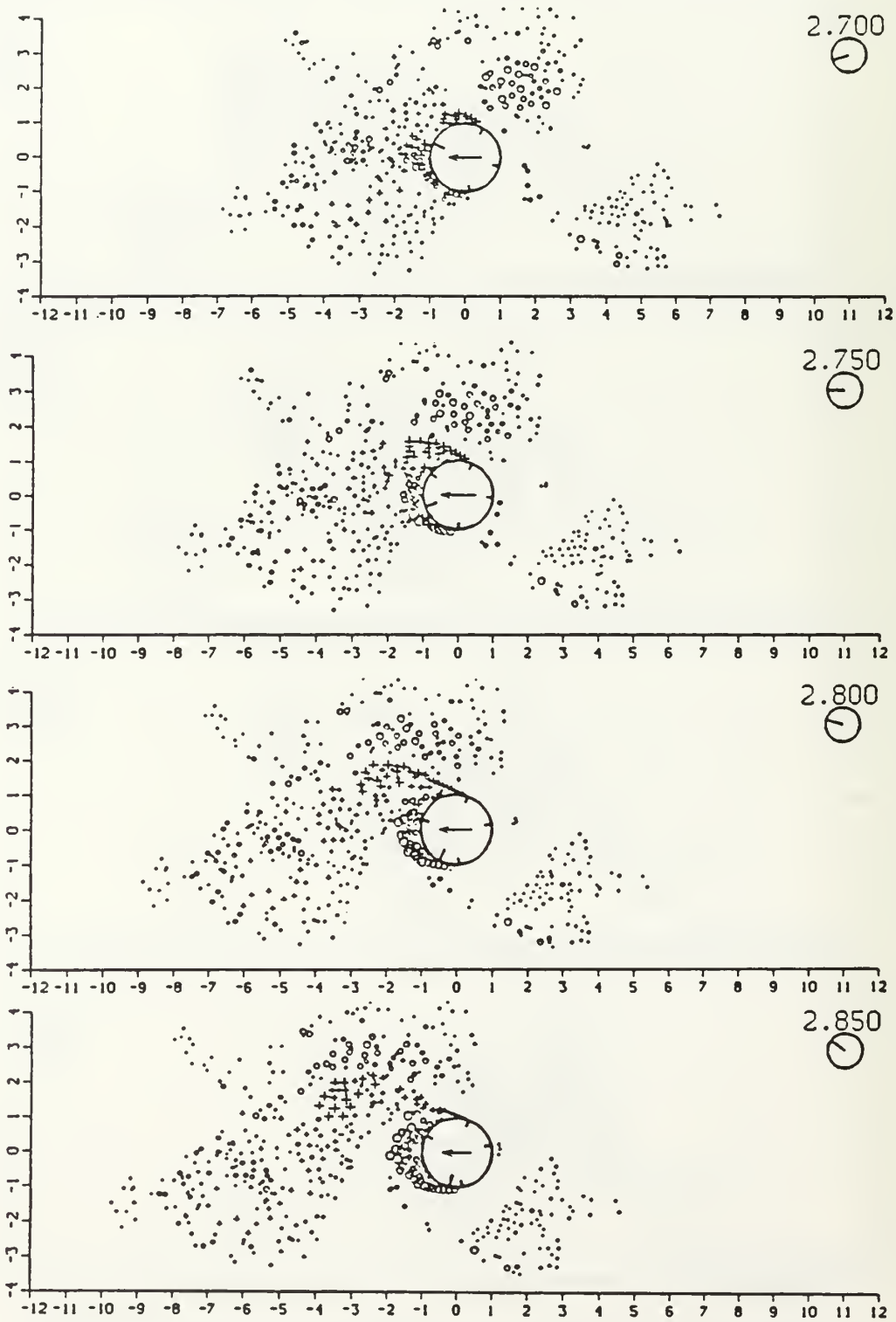


Figure 4.10a (con't.) Laminar separation criterion for **K** = 10: Kinematics.

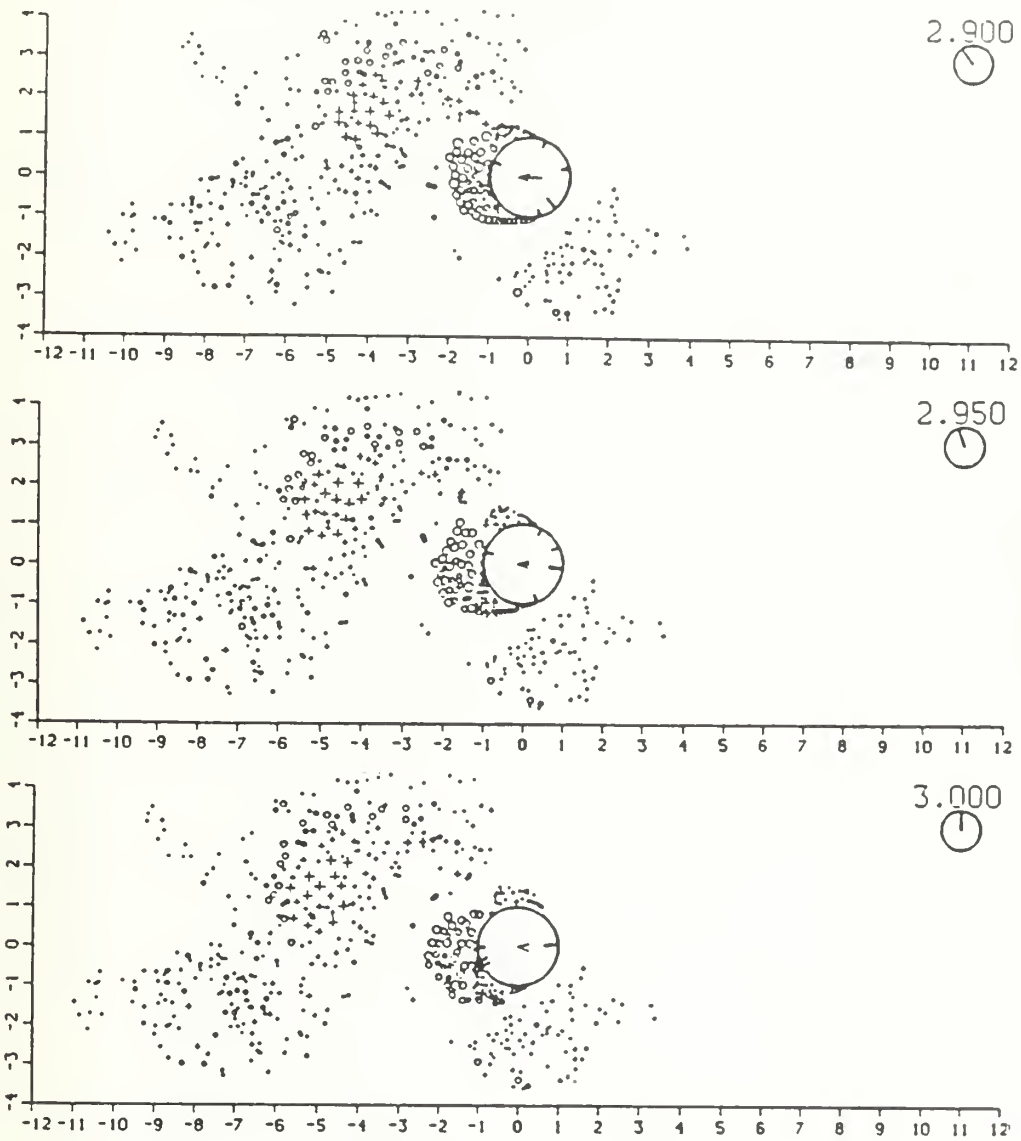


Figure 4.10a (con't.) Laminar separation criterion for **K** = 10: Kinematics.

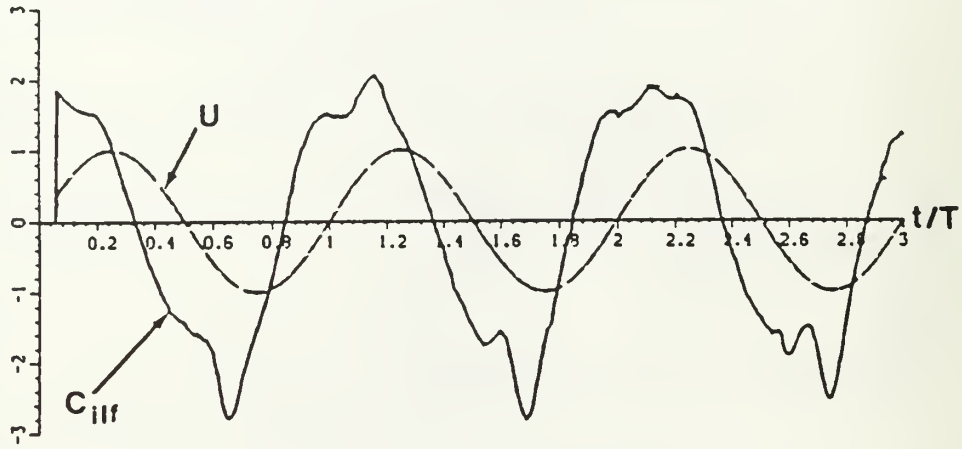


Figure 4.10 b Laminar separation criterion for **K** = 10: In-line force.

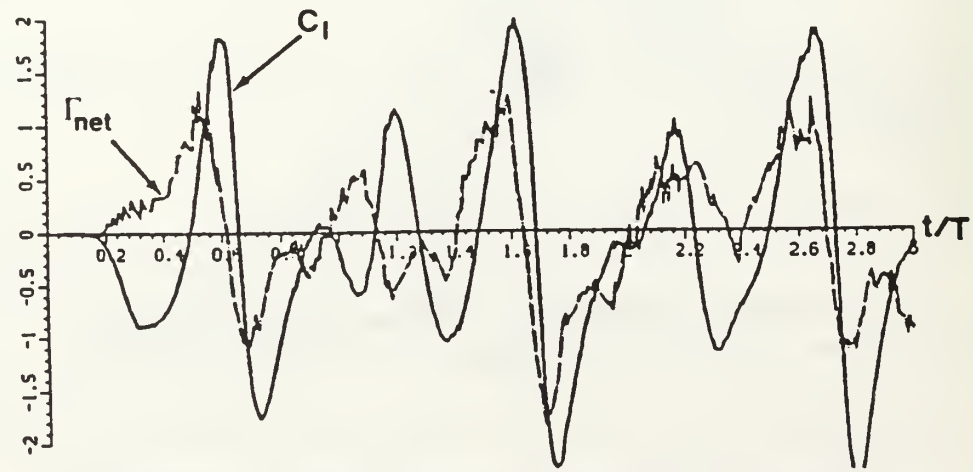


Figure 4.10c Laminar separation criterion for **K** = 10: Lift force.

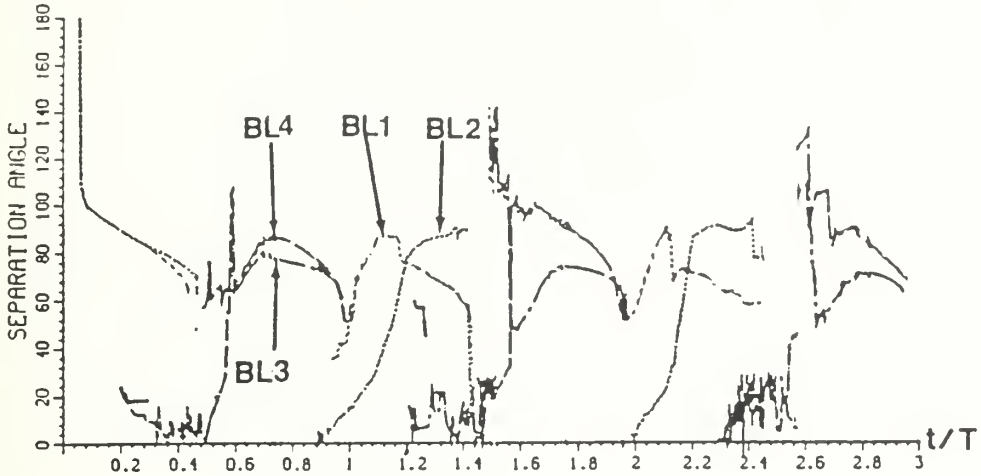


Figure 4.10d Laminar separation criterion for **K** = 10: Separation angle..

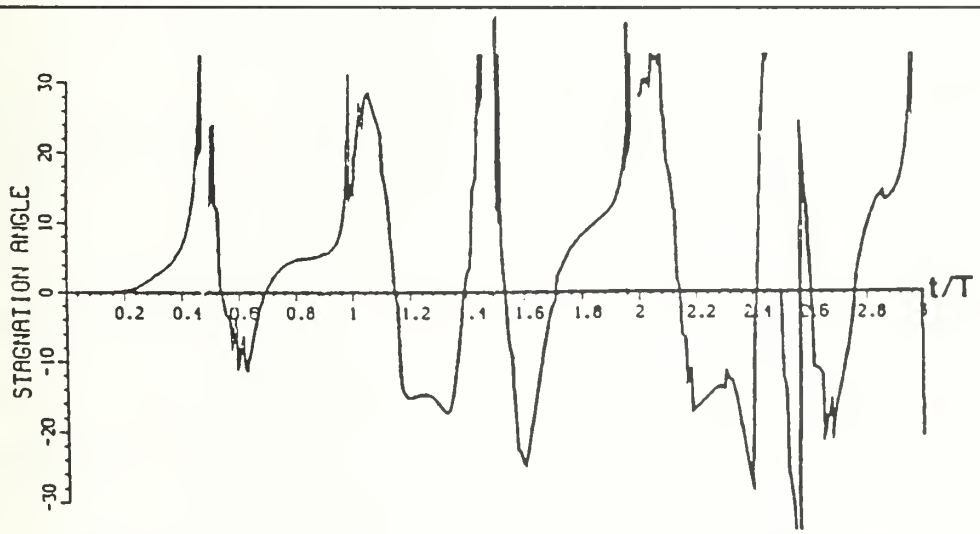


Figure 4.10e Laminar separation criterion for **K** = 10: Stagnation angle.

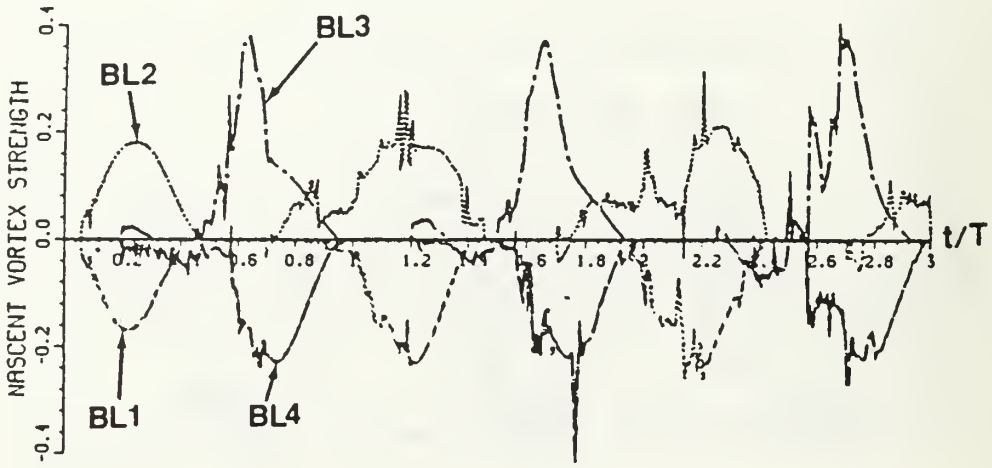


Figure 4.10f Laminar separation criterion for K = 10: Nascent vortex strength.

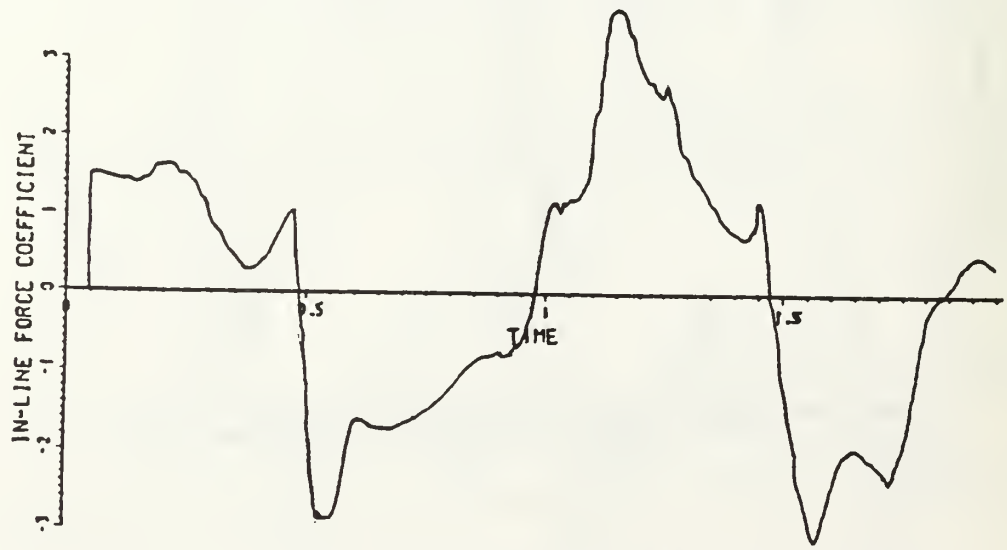


Figure 4.11 In-line force trace for run without counter vorticity incorporated.

nascent vorticity at the beginning of each half-cycle ($t/T = 0.5, 1.0, 1.5$, etc.) radically affects the in-line force. If, however, countervorticity has been incorporated, the model is able to continue from the previous half-cycle without incident (see Figure 4.10b).

Recognizing the sensitivity of the model to conditions in the nascent region, it was thought that it might be appropriate to employ the previously-mentioned velocity ratio method for determining the separation points at all times, and not just when an integral momentum technique failed. It was hoped that this would eliminate, or at least minimize the jumps in both separation position and in nascent vortex strength. Results were not significantly improved, and relatively large excursions still occurred in the separation points due to the close approach of discrete vortices and the subsequent jumps in the location of the velocity maximum.

## G. TURBULENT BOUNDARY LAYER

Yuen [1985], working with Sarpkaya, has found that, at Reynolds numbers heretofore assumed as laminar, even for low Keulegan-Carpenter numbers, the boundary layer is in fact turbulent, rather than laminar. Although several methods of predicting separation of a turbulent boundary layer exist, they are usually either too difficult to implement or very costly in terms of computer time. A simpler solution to test the propriety of implementing a turbulent separation criterion was to use the aforementioned velocity ratio method, but specifying separation to occur at a point at which the tangential velocity has fallen to a value of approximately 86 percent of the maximum tangential velocity. This essentially delayed separation, so that it appeared that the boundary layer was able to sustain an adverse pressure gradient longer than would a laminar boundary layer which separated at approximately 97 percent of the maximum tangential velocity. Plots of vortex positions and other pertinent data are shown in Figures 4.12a through 4.12f. Again, the proper flow kinematics did not result.

The convection of vortex clusters is generally very similar to the run for laminar flow for the first two cycles with the same diagonal shedding pattern and three vortices shed per half-cycle. The magnitudes of discrete vortices are generally 20 percent smaller than in the laminar flow case, due to the

smaller values of separation velocity utilized in Equation (3.15). Because of the smaller magnitude of vortex clusters, smaller mutually-induced velocities result, so that clusters tend to linger longer in the vicinity of the cylinder. Although the separation points are generally 20° to 30° further back than in the laminar case, the positions of the separation points still exhibit significant jumps during the close approach of discrete vortices to the separation region.

## H. USE OF CEBECI-CARR PROGRAM TO PREDICT SEPARATION

Recognizing the susceptibility of all integral momentum boundary methods to perturbations in the boundary layer velocity profile, and also the arbitrariness of specifying a velocity ratio at which separation would be said to occur, a third method was investigated. A computer program for calculating time-dependent laminar or turbulent boundary layers has been developed by Cebeci and Carr [1984]. Preliminary usage of the program on velocity distributions encountered in the current analysis showed that laminar separation occurred within 1° of the Pohlhausen method; turbulent separation was predicted to occur much further downstream, in agreement with the results presented by Takada [1975]. Unfortunately, the program required much too much computer time to be used in conjunction with the discrete vortex method, which by itself, presents significant demands on the computer operating system. Similar demands on system time were encountered by Franks [1983] when implementing an earlier boundary layer program developed by Cebeci [1978]. Cebeci and Carr's program was, therefore, never tested on velocity profiles perturbed as shown in Figures 3.1 through 3.3.

## I. CONCLUDING REMARKS

The present version of the discrete vortex model is incapable of simulating flows wherein shed vortices return to the boundary at which they were generated. Perhaps the two most significant difficulties associated with the model are the accurate determination of primary separation points and the implementation of a realistic vortex decay mechanism. It had been hoped that the use of a separation point scheme which required a minimum of arbitrary assumptions would allow the proper interaction of the shed vortices with the boundary layer, thereby yielding significantly more accurate results than have

any of the previous investigations of the same problem. The only successful duplication of the flow kinematics has been achieved by Mostafa [1987], but the model was not universally applicable to all values of the Keulegan-Carpenter number; neither the current model nor any of the other investigations (save Mostafa's [1987] ) have been able to accurately produce the proper flow kinematics, except in the limit of infinite Keulegan-Carpenter number (i.e., impulsive unidirectional flow).

The in-line force is reasonably well predicted by the current model. It was found that the model required the incorporation of countervorticity in order to provide a smooth transition from one half-cycle to the next. Although recognized to be an important aspect of the problem, vortex dissipation was found not to be of major influence in the flow kinematics. Only when the dissipation was increased to extremely large values were the kinematics significantly affected.

Further research is required in the area of separation point determination, particularly with regard to the difficulties associated with analyzing velocity distributions perturbed as shown in Figures 3.1 through 3.3. It is believed that this is the key to obtaining the proper flow kinematics. Once the problem of flow kinematics has been solved, the important effect of vortex dissipation on force coefficients may be investigated.

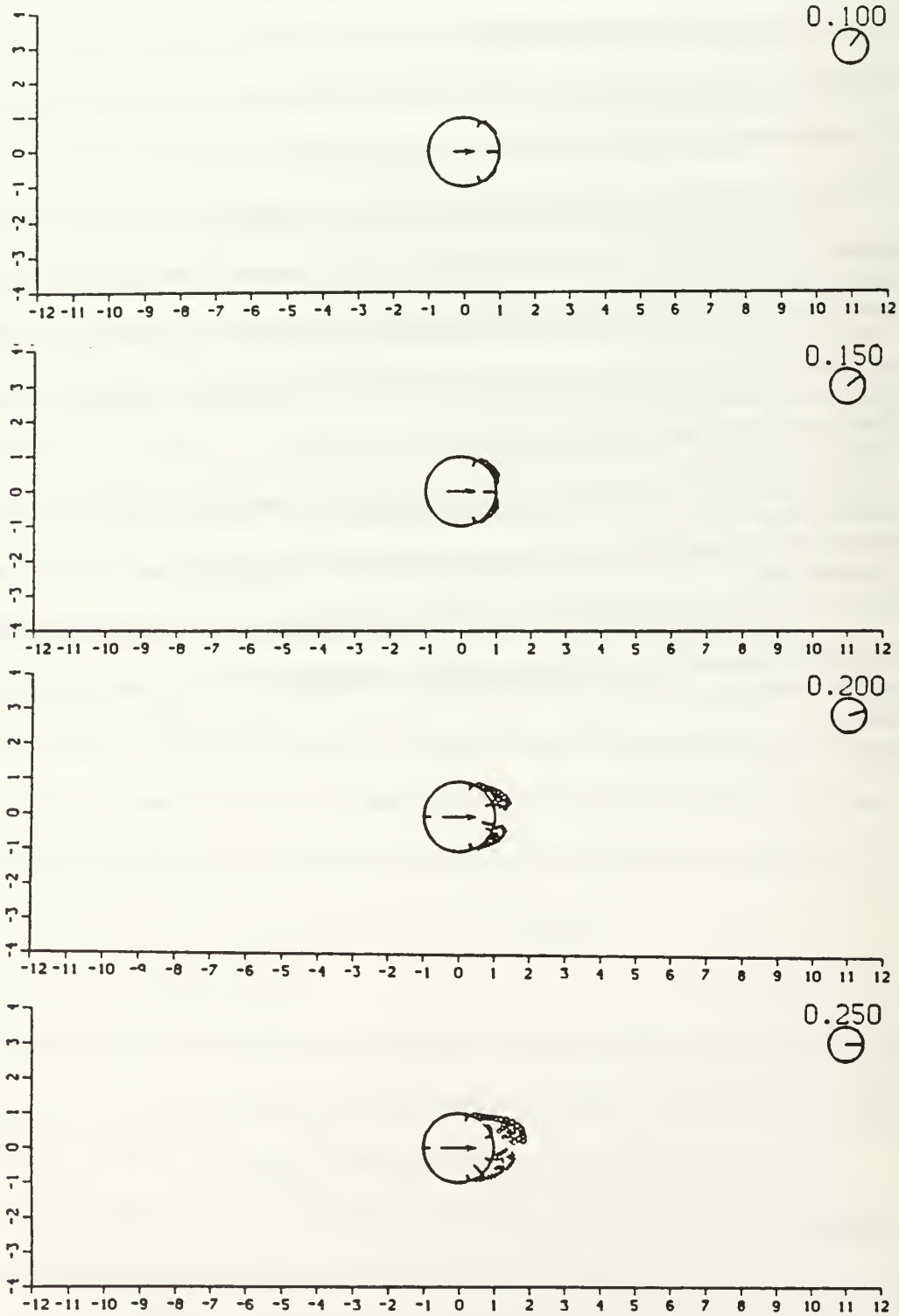


Figure 4.12a Turbulent separation criterion for K = 10: Kinematics.

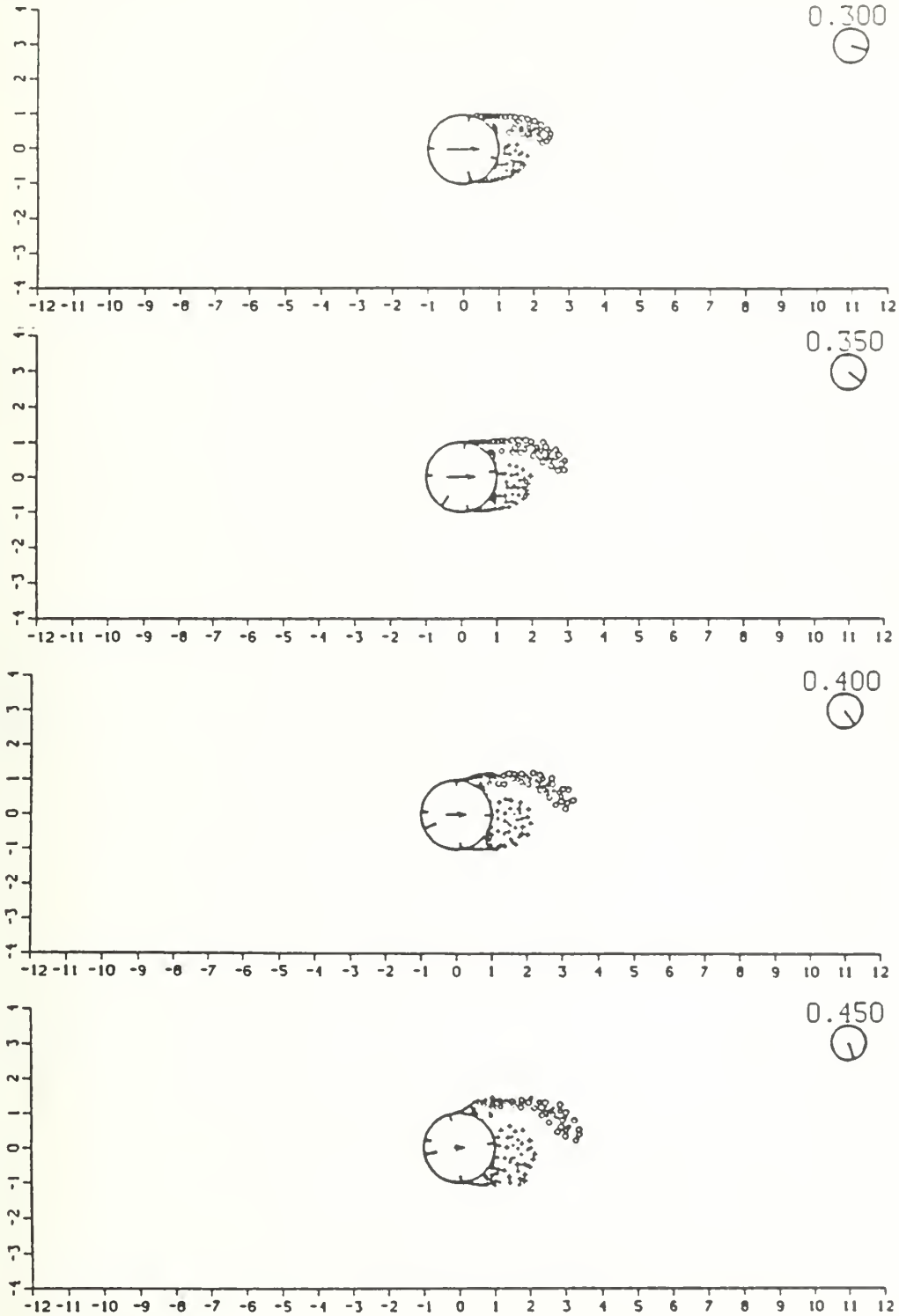


Figure 4.12a (con't.) Turbulent separation criterion for **K** = 10: Kinematics.

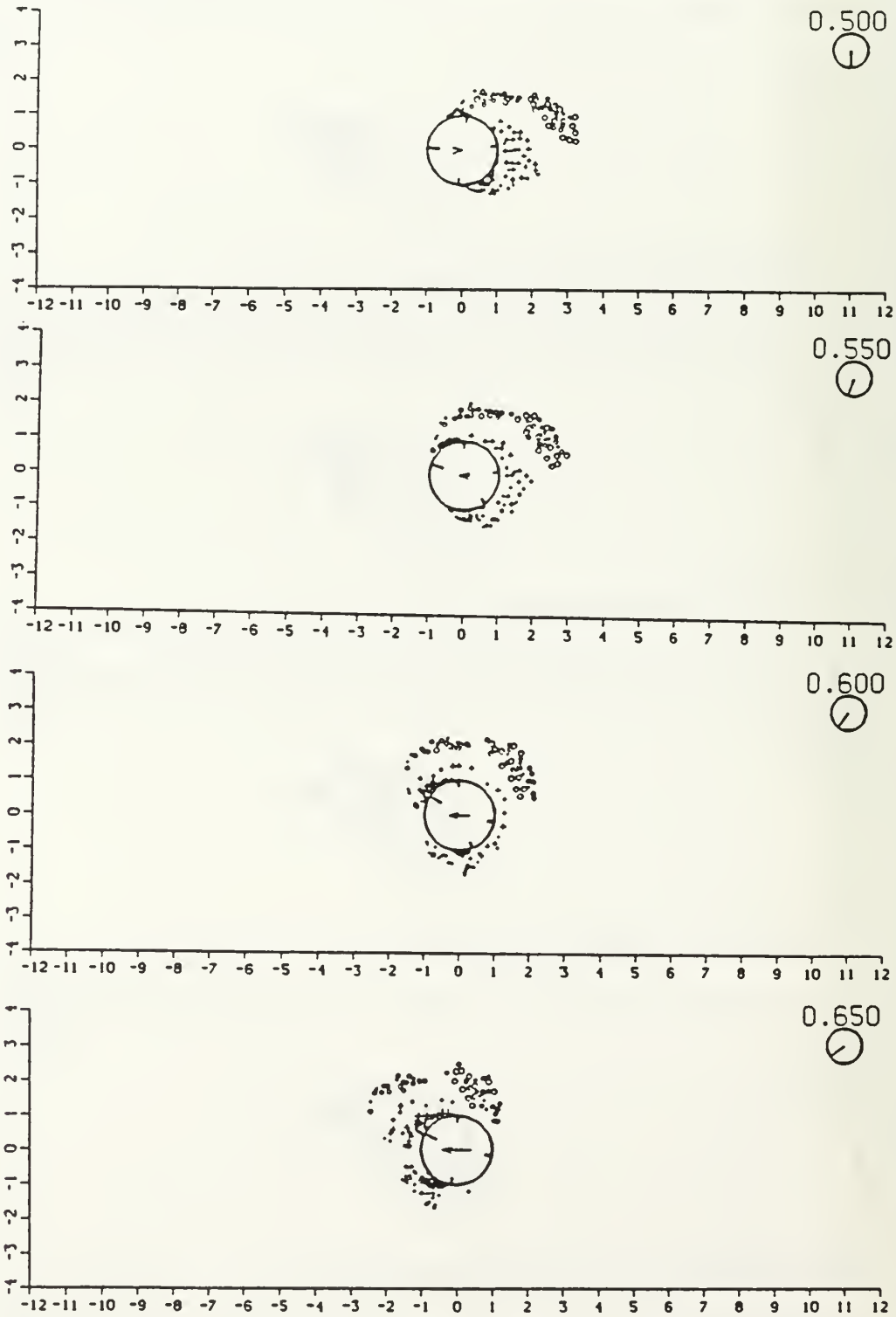


Figure 4.12a (con't.) Turbulent separation criterion for **K** = 10: Kinematics.

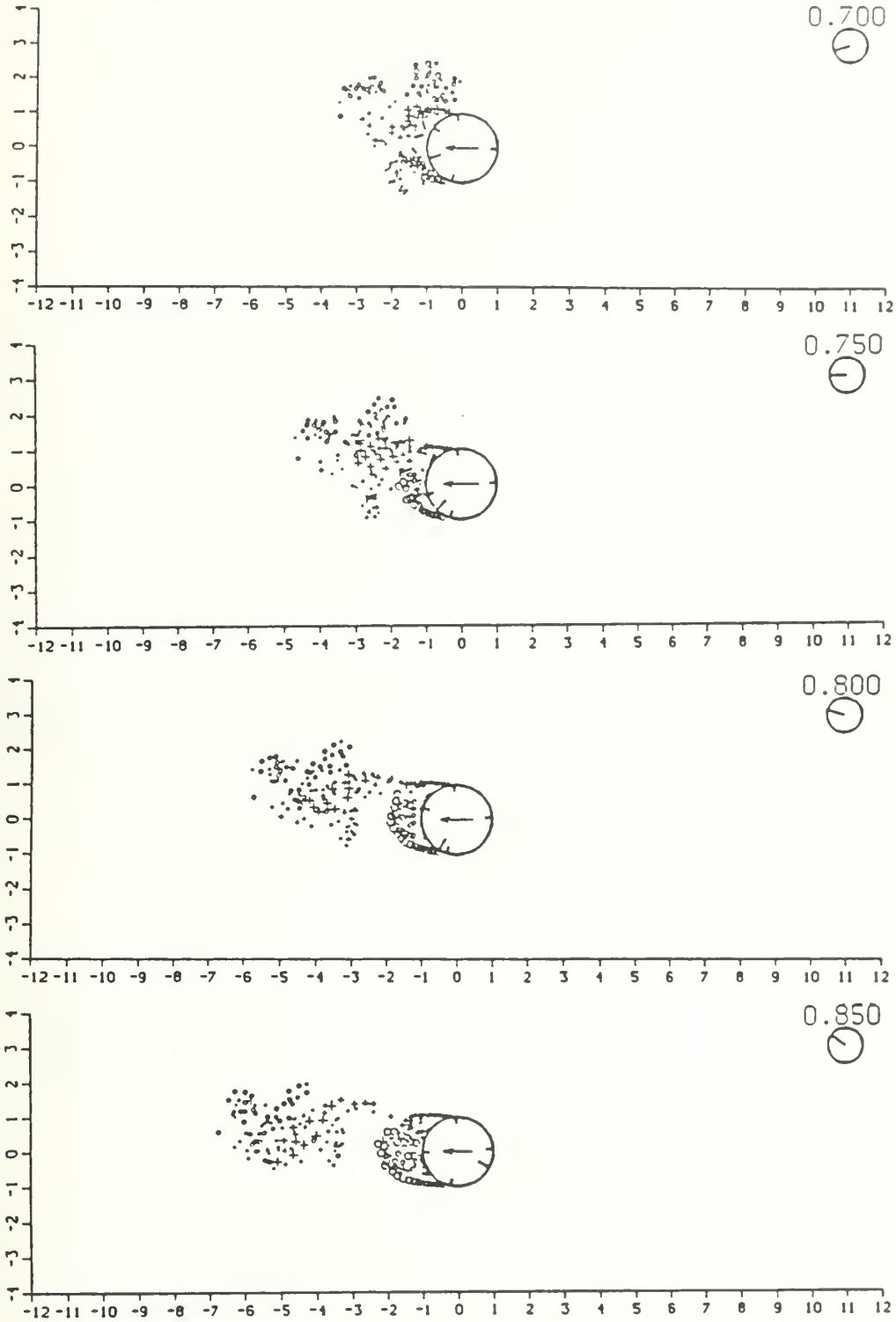


Figure 4.12a (con't.) Turbulent separation criterion for K = 10: Kinematics.

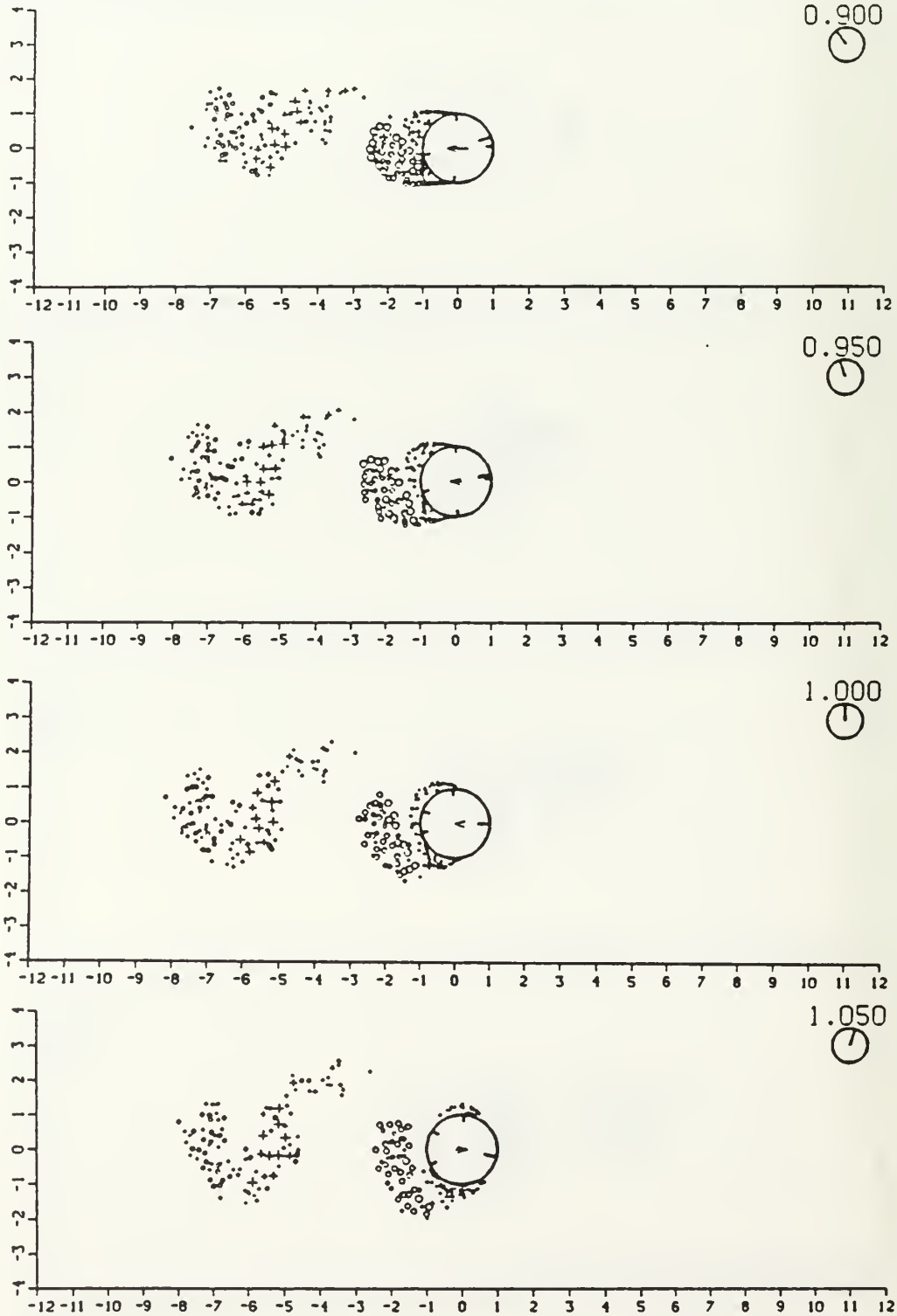


Figure 4.12a (con't.) Turbulent separation criterion for **K** = 10: Kinematics.

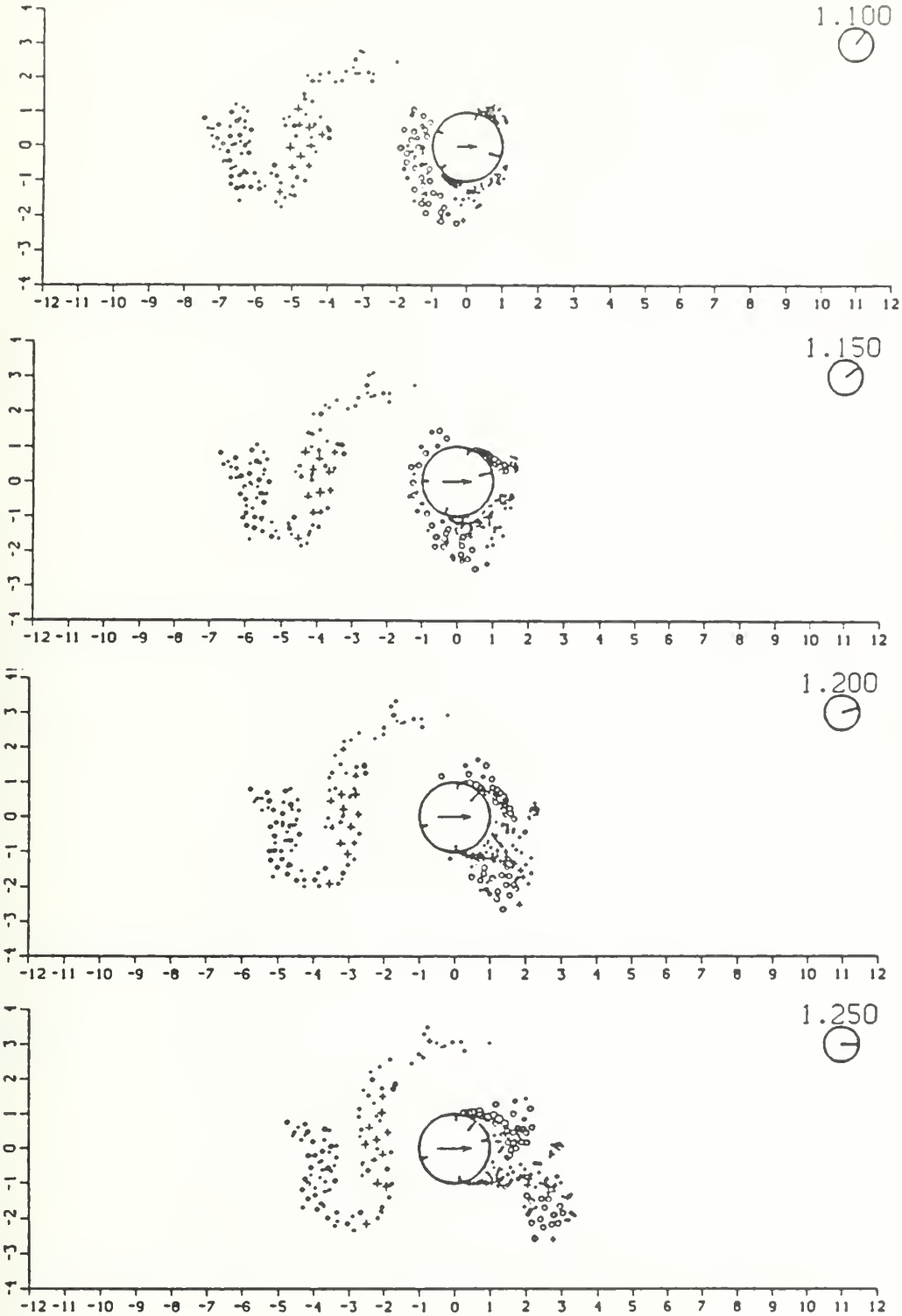


Figure 4.12a (con't.) Turbulent separation criterion for **K** = 10: Kinematics.

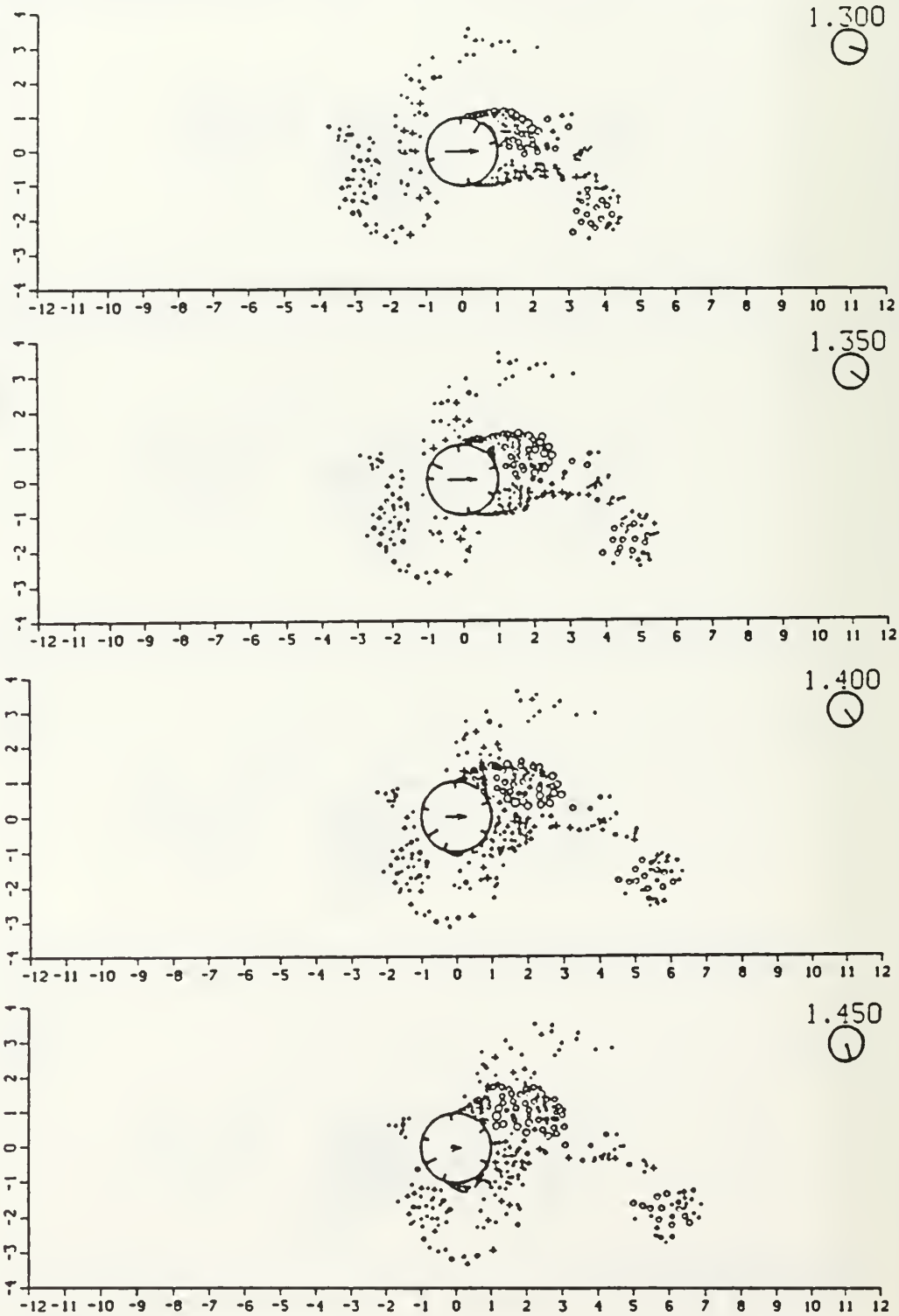


Figure 4.12a (con't.) Turbulent separation criterion for K = 10: Kinematics.

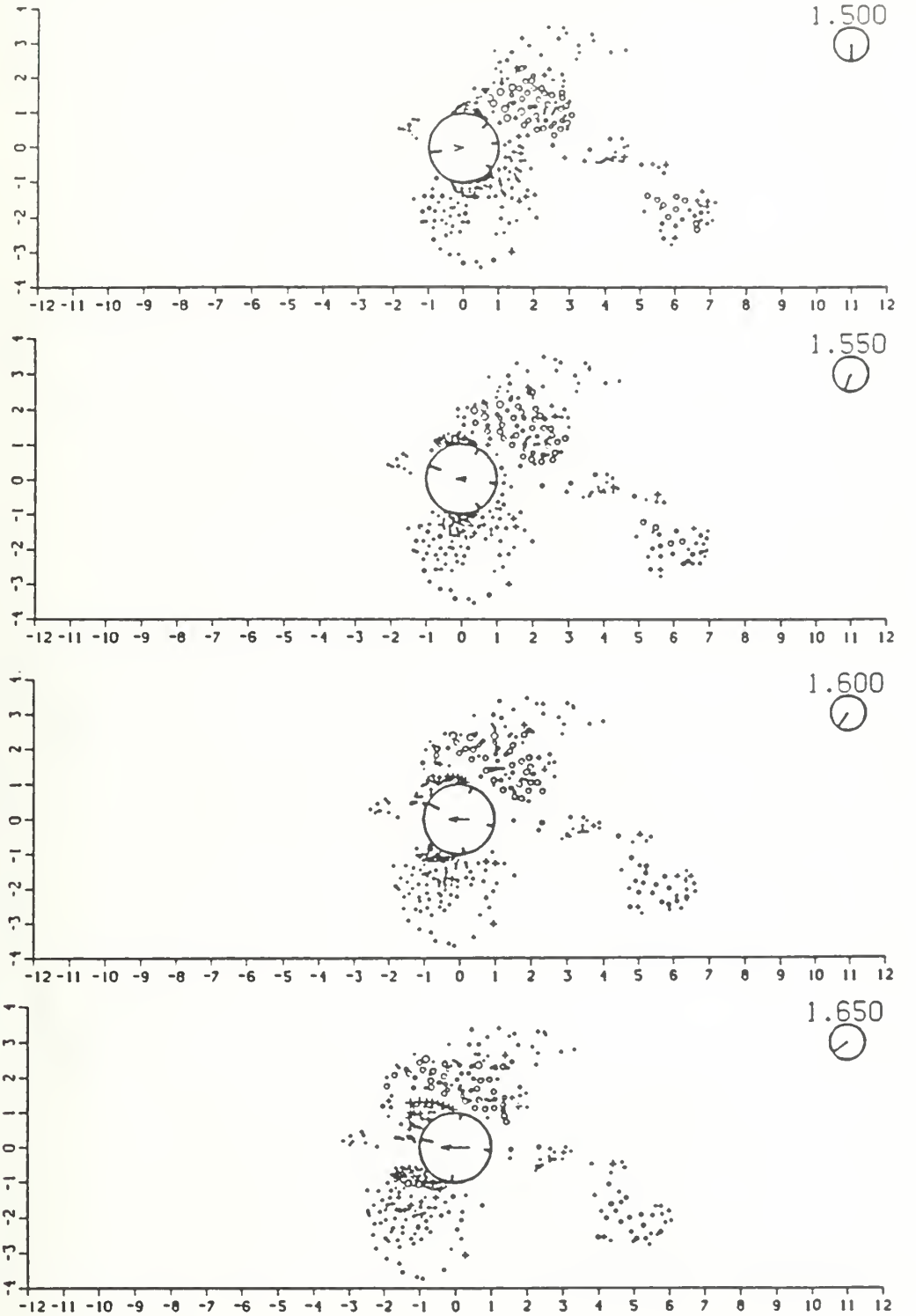


Figure 4.12a (con't.) Turbulent separation criterion for **K** = 10: Kinematics.

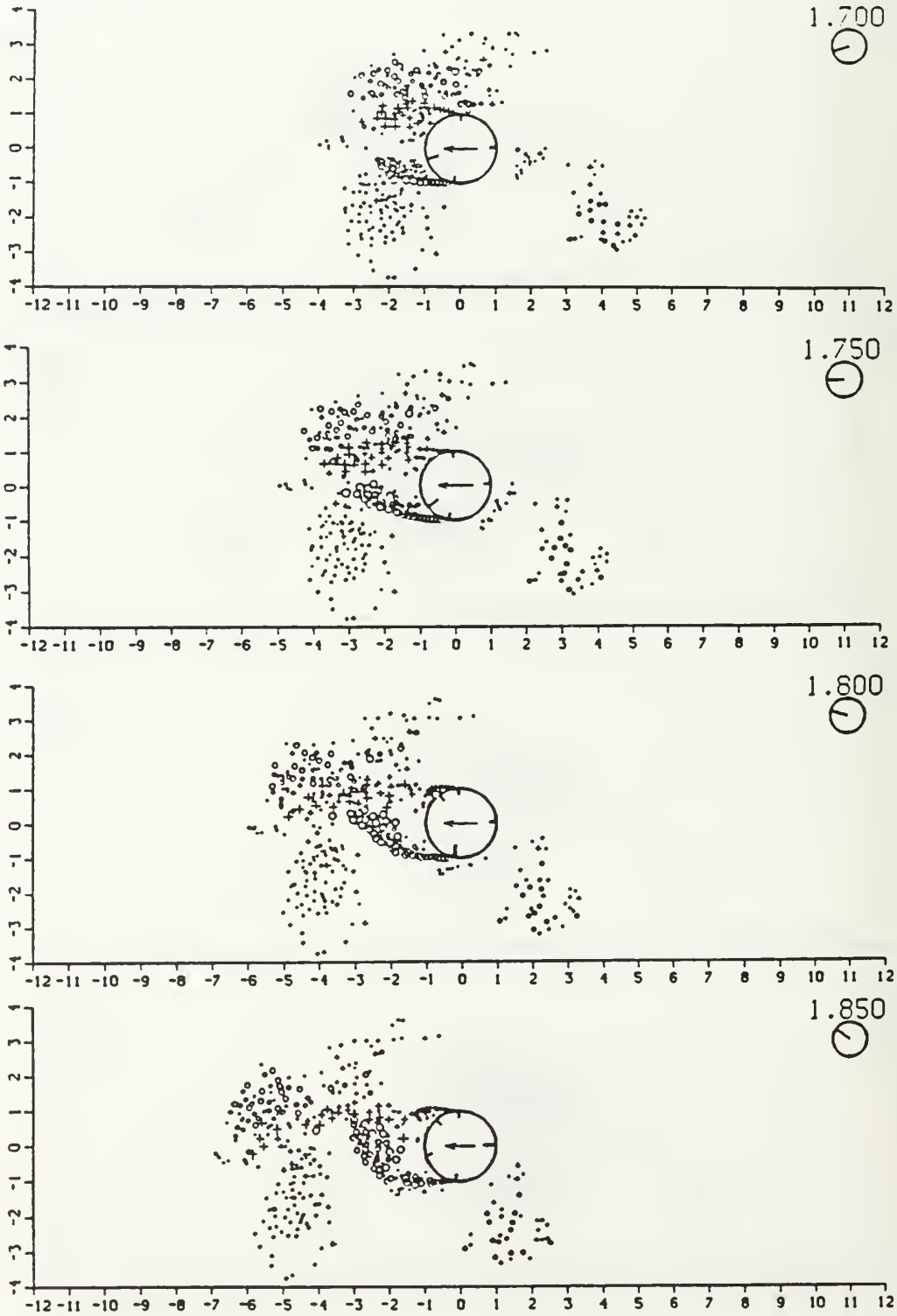


Figure 4.12a (con't.) Turbulent separation criterion for **K** = 10: Kinematics.

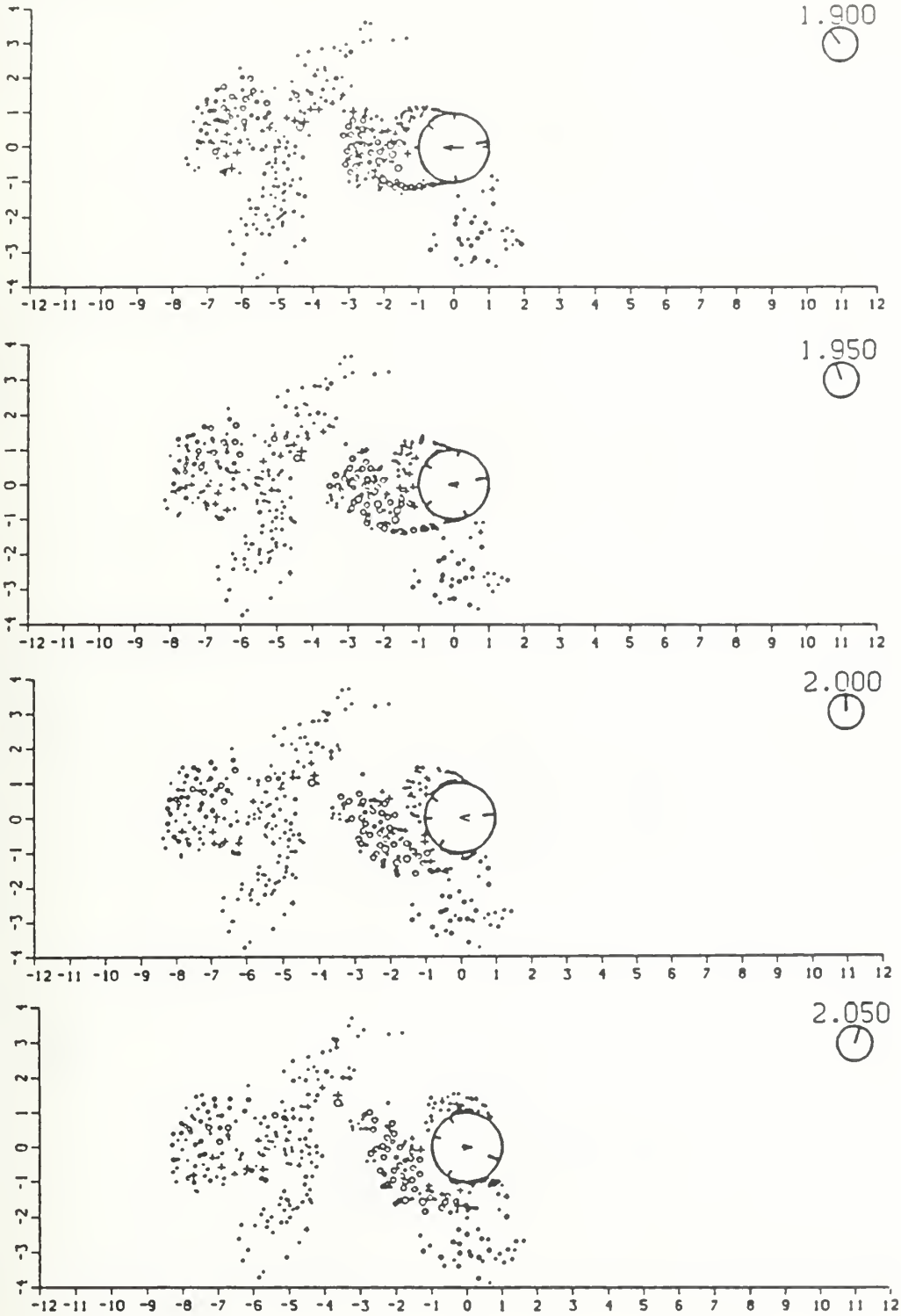


Figure 4.12a (con't.) Turbulent separation criterion for K = 10: Kinematics.

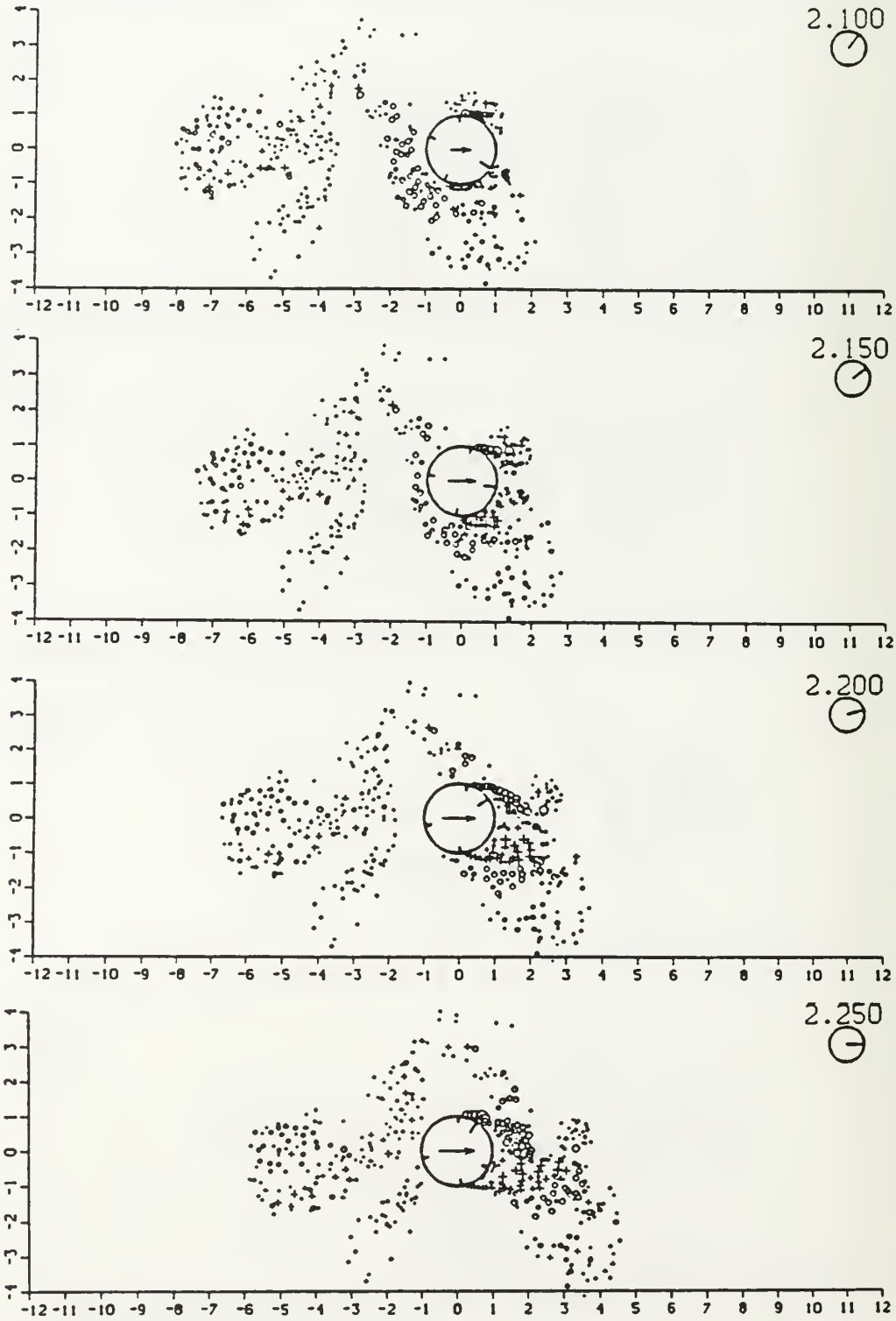


Figure 4.12a (con't.) Turbulent separation criterion for **K** = 10: Kinematics.

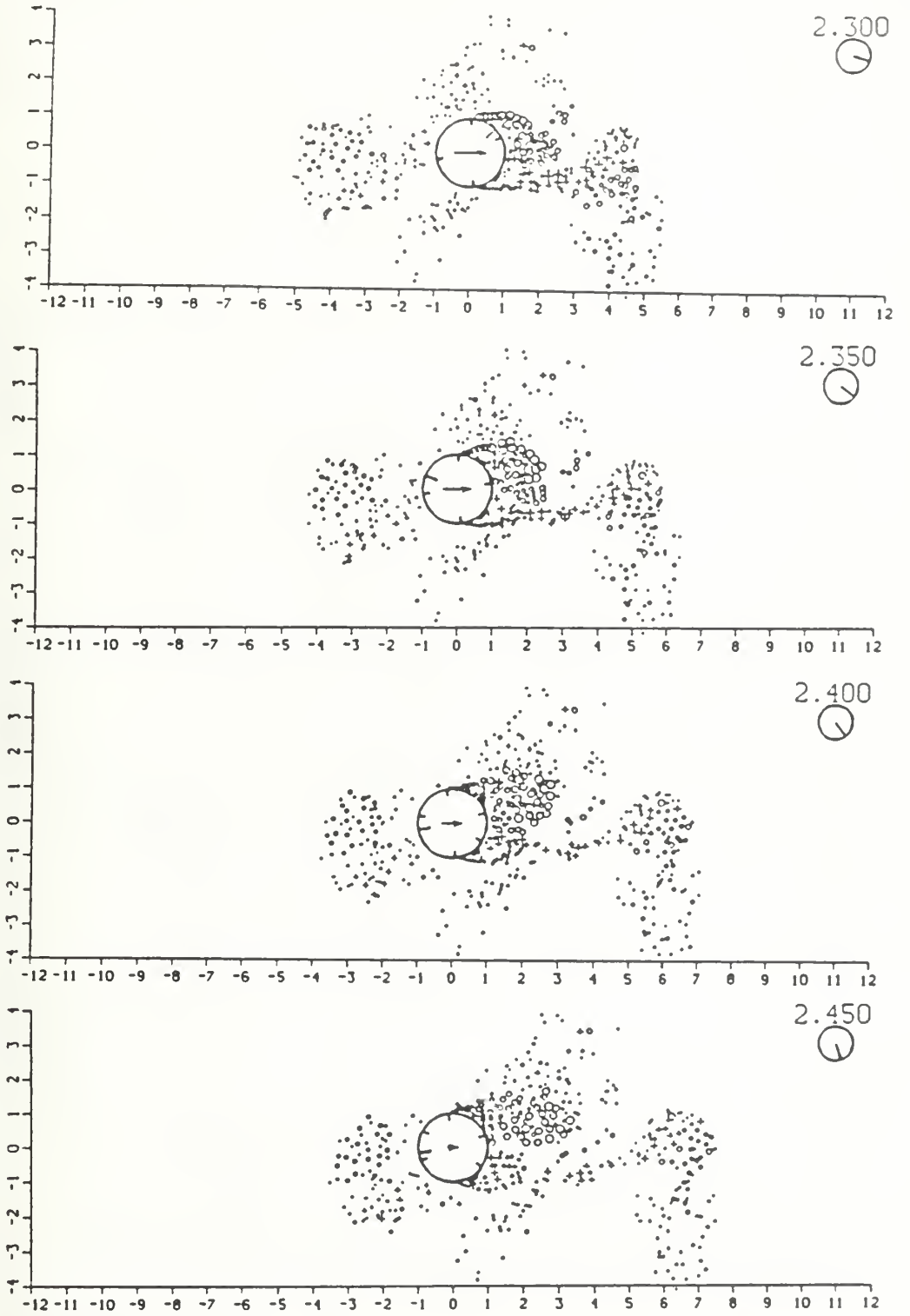


Figure 4.12a (con't.) Turbulent separation criterion for **K** = 10: Kinematics.

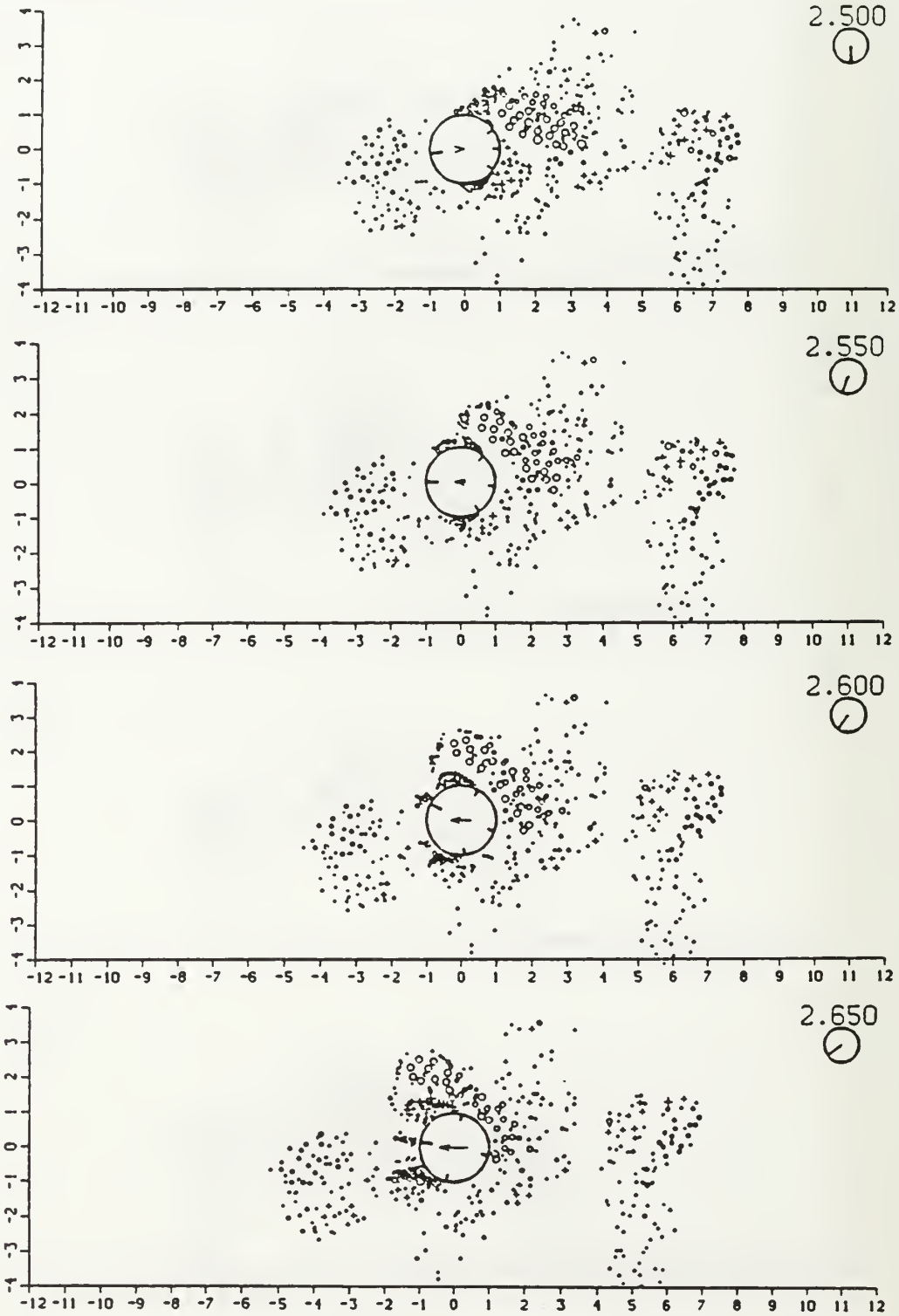


Figure 4.12a (con't.) Turbulent separation criterion for K = 10: Kinematics.

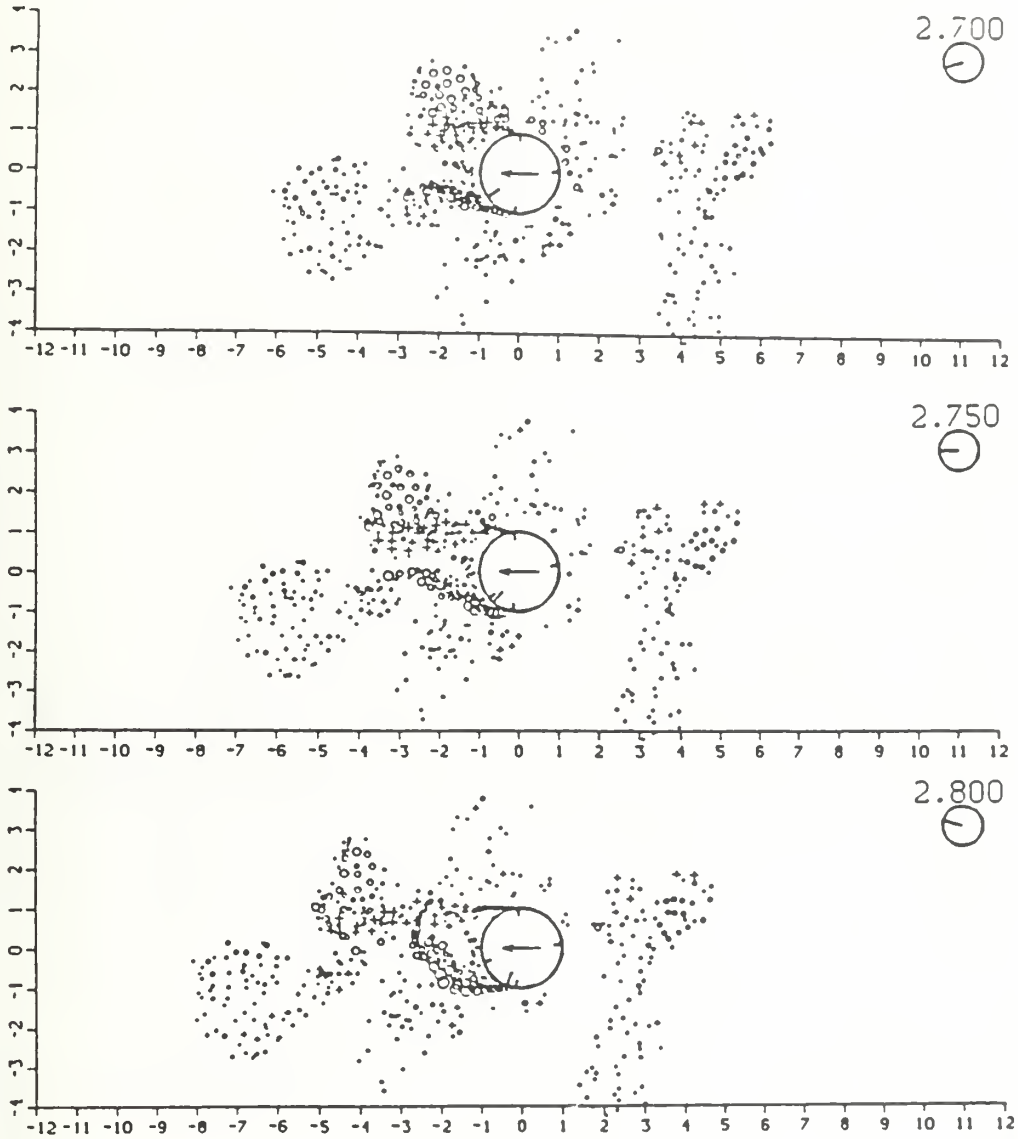


Figure 4.12a (con't.) Turbulent separation criterion for **K** = 10: Kinematics.

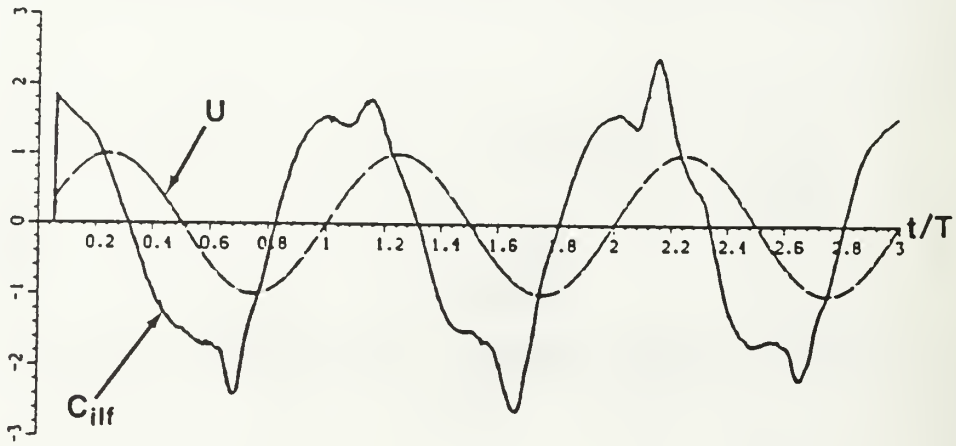


Figure 4.12b Turbulent separation criterion for **K** = 10: In-line force.

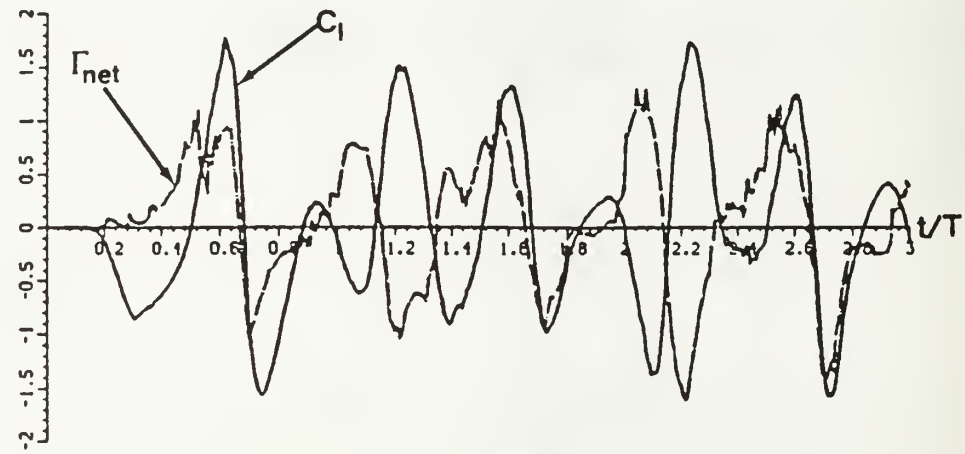


Figure 4.12c Turbulent separation criterion for **K** = 10: Lift force.

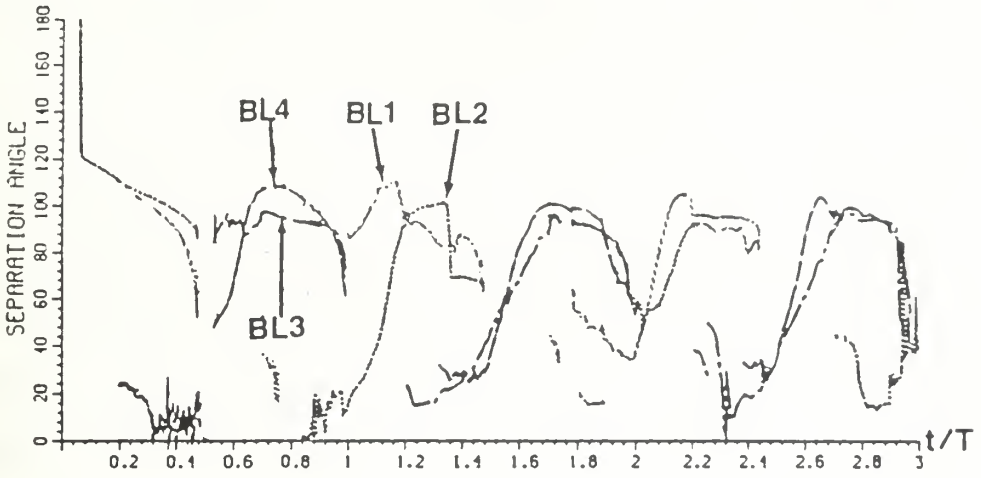


Figure 4.12d Turbulent separation criterion for **K** = 10: Separation angle.

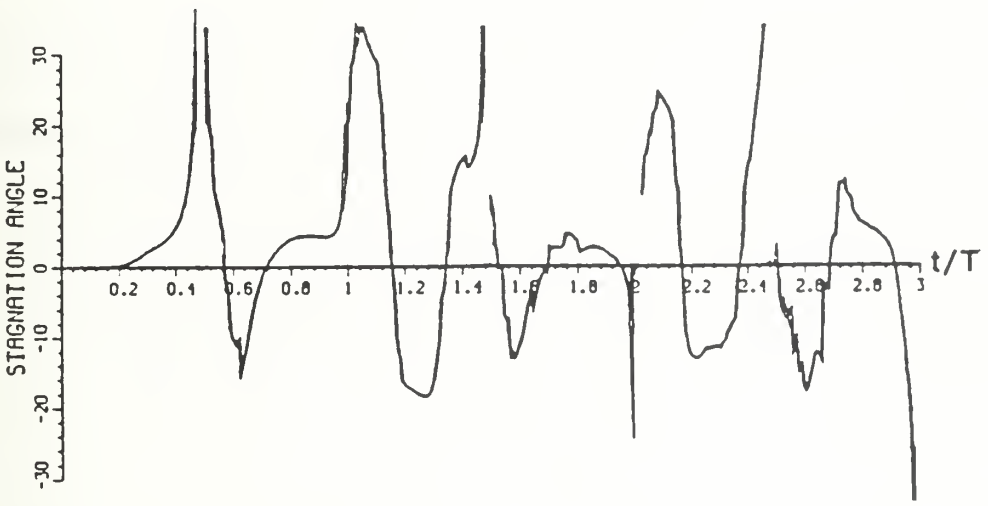


Figure 4.12e Turbulent separation criterion for **K** = 10: Stagnation angle.

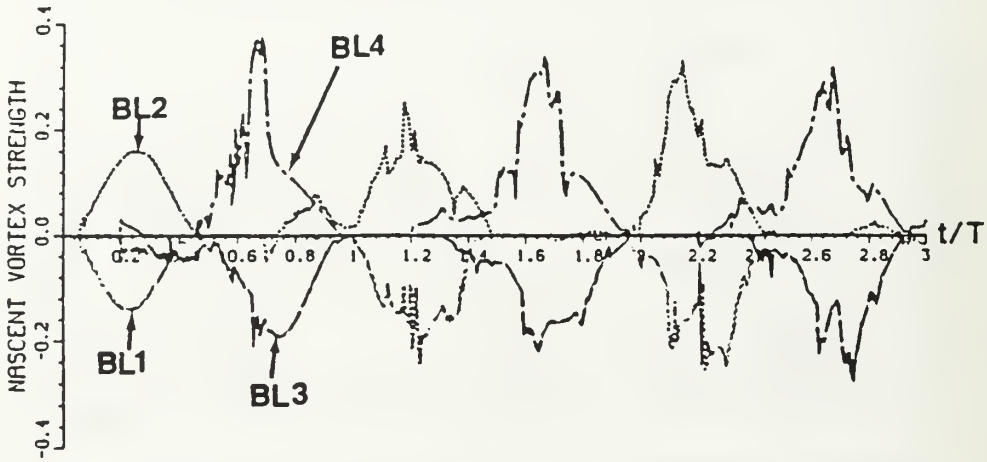


Figure 4.12f Turblent separation criterion for K = 10: Nascent vortex strength.

# V. PARALLEL BLADE-VORTEX INTERACTIONS

## A. INTRODUCTION

In addition to the return of vortices to their generating surface in the case of harmonic flow, there are numerous other engineering applications where regions of concentrated vorticity (in an otherwise irrotational flow) impinge on edges and surfaces: leading tubes in heat exchanger and reactor tube bundles, fluid valve internal surfaces, tall office buildings subjected to wind gusts, supersonic intakes, control surfaces on submarines and surface ships, turbomachinery and helicopter blades passing through shed vortices, flaps on short take-off and vertical landing (STOVL) aircraft, and even computer chips on electrical circuit boards. In many of these situations, not only is the unsteady loading of the impingement edge or surface of importance, but also the radiated noise characteristics. The degree of concentration of the vorticity and the relative orientation of the solid surface on which the vorticity acts will determine the type of the interaction and the nature of the induced pressure field.

## B. PREVIOUS INVESTIGATIONS

As pointed out by Doligalski et al [1994], as a vortex approaches a wall, the viscous response of the near-wall flow is a function of the vortex Reynolds number, $\mathbf{R}_v \equiv \Gamma / (2\pi\nu)$. At higher $\mathbf{R}_v$, the near-wall flow erupts, ejecting a new vortex structure into the outer flow; this phenomenon, first observed by Harvey and Perry [1971] (Figure 5.1 ), results in ejected or erupted (secondary) vortices which are of a strength comparable to the approaching (primary) vortex, and which interact with the primary vortex in an inviscid and most pronounced fashion. Indeed, several researchers have also reported the existence of a smaller tertiary vortex (of the same sign as the primary vortex--see Figures 5.2 and 5.3 ), observed both experimentally and in the course of numerical simulations (Chuang and Conlisk [1989], Walker et al [1987] ). Although concerned with the interaction of coherent vortices with *short* flat plates, the laser-Doppler velocimeter measurements of Swirydczuk et al [1993] showed that strong secondary and tertiary vorticity was produced.

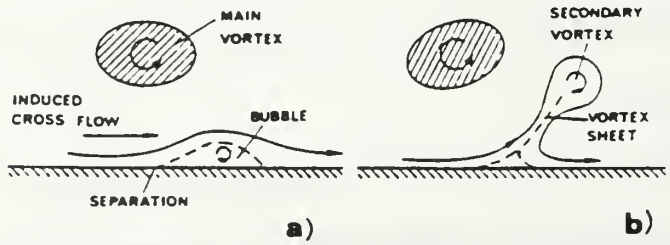


Figure 5.1 Suggested interpretation of total-head surveys: a) section downstream of inital separation, b) subsequent development of secondary vortex. (From Harvey and Perry [1971] )

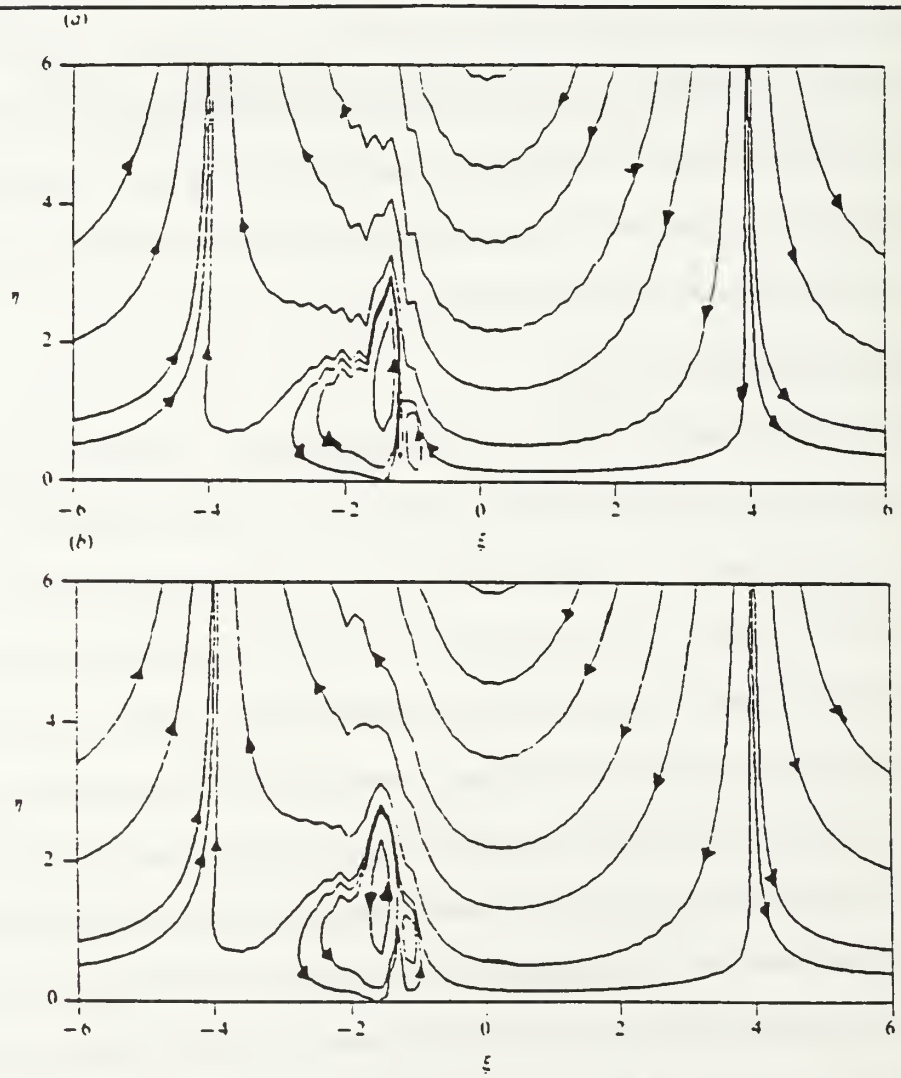


Figure 5.2 Streamline patterns from presence of a vortex above a wall for a) $\mathbf{R} = 4.4 \times 10^4$ and b) $\mathbf{R} = 2.2 \times 10^4$. (From Chuang and Conlisk [1989] )

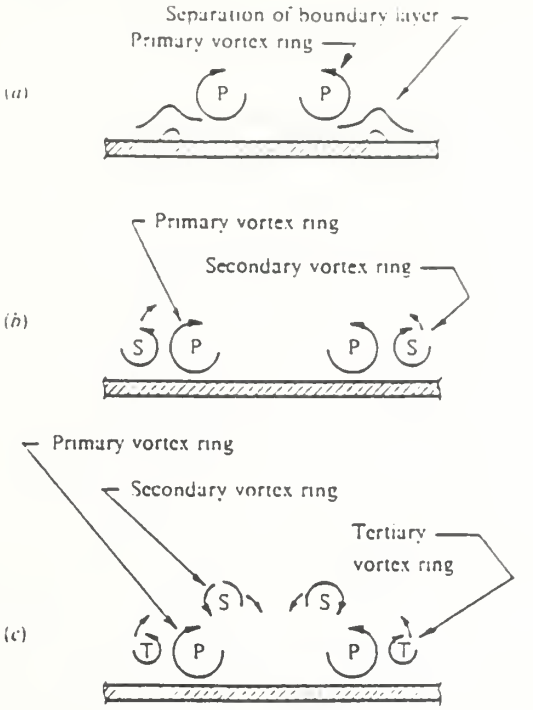


Figure 5.3 Primary, secondary, and tertiary vortex rings: a) primary ring approaching the solid surface and inducing separation in the boundary layer; b) generation of a secondary vortex ring; c) generation of a tertiary vortex ring. (From Walker et al [1987] )

Stremel [1985, 1987, 1990] attempted to model the interaction of a helicopter rotor wake with components of the aircraft other than the rotor. He represented the approaching rotor wake as a series of single, concentrated finite-cored vortices which, as they approached the body (where the flow could no longer be considered inviscid), were "distributed" to a finite difference computational mesh and permitted to convect as part of the viscous solution. Results were presented only for **R** of 40, 100, and 3000 and for body configurations of a circular cylinder and a 4:1 elliptic cylinder at 45° incidence. The interaction of the vortical wake and the body resulted in the generation of vorticity in the form of flow reversal and local separation, and significantly altered loading on the body.

Srinivasan [1985] utilized a perturbation technique in conjunction with Euler and thin-layer Navier-Stokes approaches to investigate two-dimensional (also called parallel) transonic and subsonic blade-vortex interactions (BVI). The close agreement between the thin-layer Navier-Stokes and Euler

solutions led Srinivasan to conclude that viscous effects were negligible, but it must be remembered that this work was concerned with very high speed flows. A similar perturbation technique was also used to further investigate the two- (Srinivasan et al [1986] ) and three-dimensional BVI (Srinivasan et al [1993] ). These researchers recognized the importance of core structure during the close passage of vortices to bodies, and therefore incorporated into their analyses analytically prescribed, finite-cored vortices (Lamb- or Oseen-like); however, these investigations did not account for core distortion, which have been shown to be quite significant by numerous experimental investigations.

Full Navier-Stokes solutions (Tang and Sankar [1987], Kaykayoglu and Graham [1989], and Ohring [1986] ) have also been attempted, but all have been limited to relatively low **R**. Additionally, while numerical solutions of the full Navier-Stokes equations have been successful in predicting many attached flows, such methods suffer from numerical diffusion; it has been found (Tang and Sankar [1987] ) that a vortex released approximately five chordlengths upstream from an airfoil practically disappears by the time it encounters the leading edge.

As mentioned previously, DVM's are most appropriate for situations where the flow of interest contains regions of concentrated vorticity embedded in an otherwise potential flow. Conlisk and Rockwell [1981] were the first to utilize the DVM to study the case of impinging shear layers; their work investigated the movement of single concentrated discrete vortices or clusters of discrete vortices past a sharp corner (Figure 5.4 ). Not surprisingly, they discovered that this simplified approach, although it provided the insight required for further work, failed to model the distortion (and subsequent severing) of the vorticity field near the impingement surface. Panaras [1985] utilized the DVM to investigate the pressure pulses resulting from the interaction between a single concentrated vortex with a ramp and with an ellipse, while Conlisk and Veley [1985] employed it to study the interactions between point vortices and a corner. Poling et al [1987] utilized arrays of single, large vortices approaching an airfoil, and introduced discrete vortices at the trailing edge to satisfy the Kutta condition (Figure 5.5 ).

As noted above, core distortions can be significant when primary vortices come into close proximity to (or even impact) solid boundaries or pass close to another vortex. Hardin and Lamkin [1984] were the first to attempt to incorporate core distortion, employing a finite-difference solution to the Navier-Stokes equations for **R** < 200. Panaras [1985, 1987] and Poling et al [1988, 1991] used various configurations of discrete vortex clusters as they passed close to, and were even split by, an airfoil (Figure 5.6 ); both of these investigations were purely potential, and the latter two introduced discrete vortices at the trailing edge to satisfy the Kutta condition. Panaras [1985, 1987] utilized discrete vortices of equal strength, while Poling et al [1988, 1991] employed a multi-ring distribution of discrete vortices of radially-varying strength to more closely approximate the Gaussian vorticity distribution observed in vortices in nature. More recently, Lee and Smith [1991] discussed vortex instabilities and diffusion which result from the discretization of a vortex into a cluster. Panaras [1990] extended his previous vortex cluster model to investigate vortex impingement on a corner. Kaya [ 1992] and Kaykayoglu and Kaya [1992] investigated the interaction of a Kármán vortex street with elliptical and sharp leading edges; for the case of the sharp leading edge, secondary vorticity was produced to satisfy the Kutta condition as

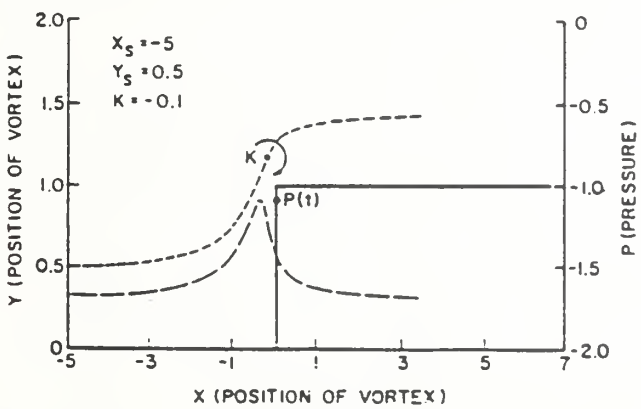


Figure 5.4 Vortex moving past a corner, with path and associated pressure trace; pressure p(t) computed at $z_0 = 0.95i$ in the physical plane. (From Conlisk and Rockwell [1981] )

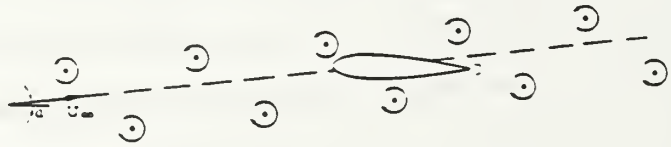

Figure 5.5 Initial configuration of an undisturbed sequence of alternating vortices over an NACA 0012 by Joukowski transformation. (From Poling et al [1987] )

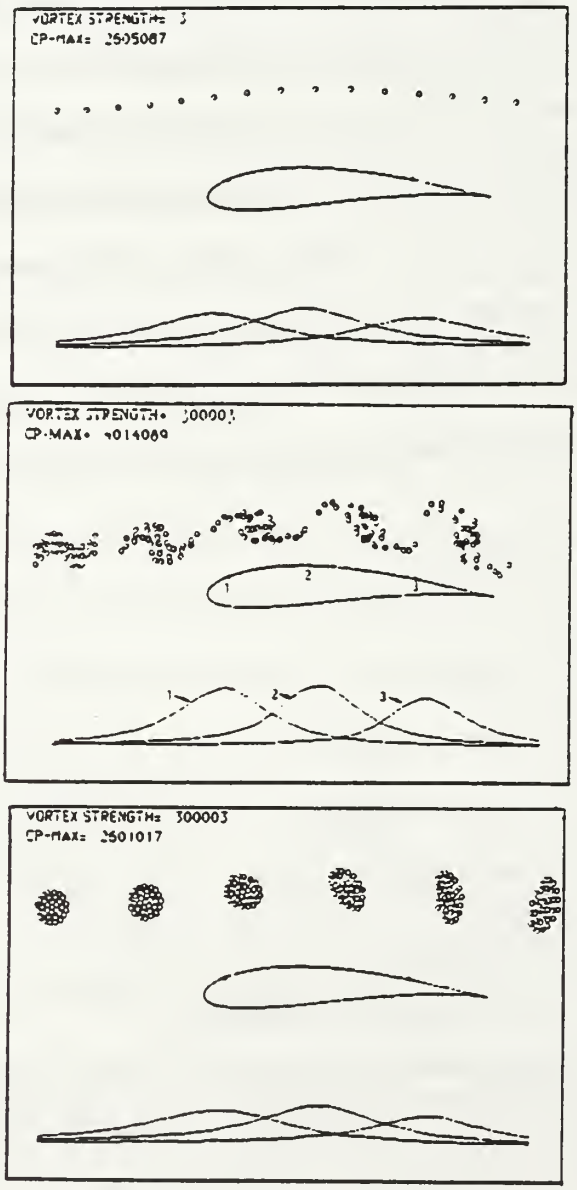


Figure 5.6 Comparison of vortex models, with vortices passing at a large distance from an airfoil. (From Panaras [1987] )

vortices approached the edge and induced high cross flow velocities near the tip. In no other regions was secondary vorticity introduced. More recently, Park and Lee [1994] utilized a hybrid random vortex method (vortex blobs (Chorin [1973] ) and sheets (Chorin [1978] )) to incorporate viscous effects while investigating vortex-wedge interactions.

Various experimental studies of the BVI (Ziada and Rockwell [1982], Rockwell [1983], Kaykayoglu and Rockwell [1985], Rockwell et al [1985], and Wilder et al [1990] ) have provided the basis for the validation of the different numerical simulations. Despite significant progress in these experimental observations, the identification of the separation point or region of vortex eruption remains an unresolved area of fundamental research. The abrupt eruption of secondary vorticity is generic, in that it occurs in conjunction with a wide variety of geometric configurations (vortex rings (Walker et al [1987], Ersoy and Walker [1987], Chu and Falco[1988], and Falco [1991] ), vortex pairs (Ersoy and Walker [1985, 1986] ), stationary rectilinear vortices (Walker [1978] ), and convected rectilinear filaments (Doligalski and Walker [1984], Doligalski et al [1994])), and also for a wide range of $\mathbf{R}_v \equiv \Gamma / (2\pi\nu)$. In all these cases, the vortex induces an adverse pressure gradient on the boundary layer. Whether the existence of a singularity in the boundary layer equations may be considered to be a precursor to separation continues to be a matter of great debate (Elliott et al [1983], Doligalski and Walker [1994], Peridier et al [1991a, 1991b] ). This may in fact not be an appropriate indicator since the solutions for the full Navier-Stokes equations do not exhibit singular behavior at separation. It appears "rather ironic that even though the boundary-layer theory has revolutionized fluid dynamics, the phenomenon which gave impetus to its inception is associated with its failure" (Sarpkaya [1992] ). Whatever the precise mechanism of separation may be, Doligalski and Walker [1984] conclude that the erupted vortical structure resulting from "a convected vortex in a uniform flow will eventually interact strongly with the outer inviscid flow for any convection speed."

Suffice it to say that the eruptive process is a highly unsteady, extremely complex phenomenon which has, to date, defied precise analytical and computational solution. As pointed out by Doligalski et

al [1994], conventional interacting boundary layer methods can only describe this process for a relatively short time. They conclude by stating that what is needed is a scheme which can detect the onset of eruption and react to focus the computational effort on the eruption region; they suggest a hybrid interactive scheme wherein an unsteady boundary layer scheme might be linked to an unsteady Euler solver.

Throughout most of the above-cited works, especially those of an experimental nature, the importance of secondary vorticity is readily evident. It is not enough to invoke the zero normal velocity criterion; the no-slip condition must also be implemented to make the simulation fully realistic; otherwise, the model would be strictly potential in nature. Additionally, all vortices which are introduced (primary, secondary, etc.) must be able to distort and diffuse when encountering either another real vortex or their image vortices at a solid boundary. Aside from the generation of secondary vorticity to satisfy a Kutta condition at a sharp leading edge (Kaya [1992], Kaykayoglu and Kaya [1992] ), the only other treatment of the BVI problem to incorporate a boundary layer-like generation of secondary vorticity was by Park and Lee [1994], but one of its principal drawbacks is the size of the discrete vortex flowfield and the attendant computer run-time. The current work will utilize a more classical boundary layer separation technique in lieu of a random vortex blob method. It is this creation of secondary vorticity and subsequent distortion of vortical structures with which the remainder of this chapter will be concerned.

## C. PROBLEM FORMULATION

The canonical problem of a rectilinear vortex in the vicinity of a semi-infinite flat plate is one which will allow vortex-induced separation to be studied with a minimum of other influences; additionally, a free stream parallel to the plate will be imposed, including the limit of zero free stream velocity. Referring to Figure 5.7, the following are defined:

$U_\infty$ = free stream velocity

$\Gamma_{primary}$ = strength of vortex being convected by free stream.

a = downstream offset distance (height) of primary vortex centroid above plate.

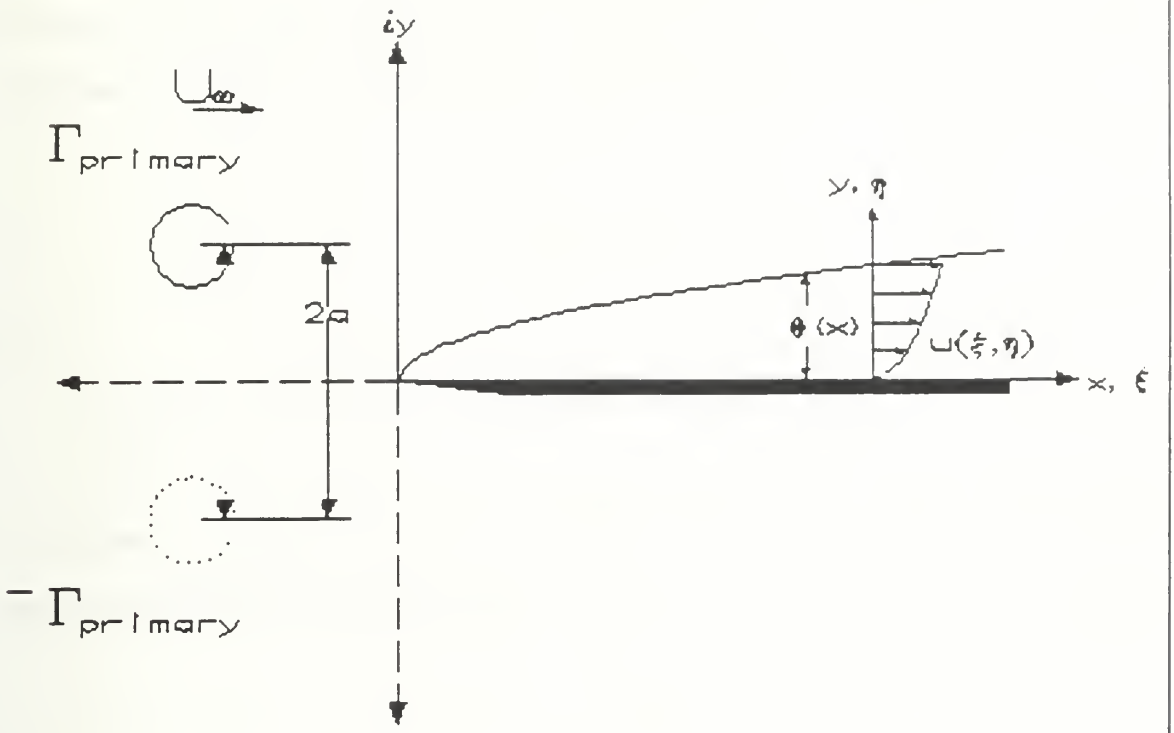


Figure 5.7 Boundary layer on a semi-infinite flat plate due to the presence of a line vortex and a free stream (not to scale).

Due to the simplicity of the problem's geometry, the condition of zero flow normal to the plate can be invoked by situating an imaginary vortex of opposite sign at the complex conjugate of its real counterpart. The origin of the coordinate system is situated with its origin at the plate's leading edge, and aligned so that the uniform flow is in the positive x-direction.

To facilitate presentation of numerical data, nondimensionalization of the relevant equations will be based on the maximum velocity seen by the plate at the edge of the boundary layer (i.e., directly beneath the primary vortex):

$$U_{plate} = U_{\infty} + \frac{\Gamma_{primary}}{\pi a}. \tag{5.1}$$

This accounts for the free stream, the primary vortex, and its image. Using $U_{plate}$ instead of $U_\infty$ circumvents the singularity which would occur when nondimensionalizing in the absence of a free stream. The analysis proceeds in much the same fashion as in Chapter II, with the following nondimensional parameters employed:

$$z' = \frac{z}{a} \qquad u' + iv' = \frac{u + iv}{U_{plate}} \qquad w' = \frac{w}{aU_{plate}}$$

$$t' = \frac{tU_{plate}}{a} \qquad \Gamma' = \frac{\Gamma}{aU_{plate}} \qquad \beta = \frac{U_\infty}{U_{plate}} = \frac{U_\infty}{U_\infty + \frac{\Gamma_{primary}}{\pi a}} \tag{5.2}$$

Additionally, the current analysis will involve approaching vortices of strength $\Gamma_{primary} = \pi$ and initial height above the plate $a = 1.0$; this results in nondimensional equations (primes removed for simplicity) for potential function and velocity of

$$w(z,t) = -\beta z + \frac{i}{2\pi}\sum_{n=1}^{N}\Gamma_n\left[ln(z - z_n) - ln(z - \bar{z}_n)\right] \tag{5.3}$$

$$-u + iv = \frac{\partial w}{\partial z} = -\beta + \frac{i}{2\pi}\sum_{n=1}^{N}\Gamma_n\left[\frac{1}{z - z_n} - \frac{1}{z - \bar{z}_n}\right] \tag{5.4}$$

Following the same procedure utilized in Chapter II, the pressure (nondimensionalized on $\frac{1}{2}\rho U_{plate}^2$) at any point on the plate is calculated as follows:

$$p(z,t) = \frac{1}{\pi} Re\left\{ i\sum_{n=1}^{N}\frac{\partial\Gamma_n}{\partial t} ln\left(\frac{z - z_n}{z - \bar{z}_n}\right) + i\sum_{n=1}^{N}\Gamma_n\left[\frac{-\dot{z}_n}{z - z_n} + \frac{\dot{\bar{z}}_n}{z - \bar{z}_n}\right]\right\} - q^2, \tag{5.5}$$

where q is the velocity at the point in question, z.

Because the geometry involves a semi-infinite plate, forces, moments about the leading edge, and center of pressure calculations must be evaluated as functions of distance along the plate, x:

$$C_l = \frac{\int_0^x p(x,t)dx}{\frac{1}{2}\rho U_{plate}^2 a} x \tag{5.6}$$

$$C_m = \frac{\int_0^x p(x,t)xdx}{\frac{1}{2}\rho U_{plate}^2 a^2} \tag{5.7}$$

$$x_{cop} = \frac{C_m(x)}{C_l(x)} = \frac{\int_0^x p(x,t)xdx}{\int_0^x p(x,t)dx} \tag{5.8}$$

## D. BOUNDARY LAYER SEPARATION

The above discussion has shown that various researchers have expended considerable effort and computational resources in an effort to predict the point (or region) where vortex separation will occur in a boundary layer whose outer velocity profile is due to a primary vortex, either alone or in conjunction with a free stream. It would appear that the various schemes do not lend themselves well to a series of successive separation calculations utilized in conjunction with the introduction of secondary vorticity.

At any point in time, the velocity distribution will be calculated and the corresponding pressure distribution assumed to be impressed on the boundary layer. This fundamental aspect of boundary layer theory, along with von Kármán's integral momentum equation, allows the use of several methods to predict separation, many of which have been discussed in Chapter II. These methods exhibit varying degrees of sensitivity to the external velocity distribution (which will be calculated from potential flow theory), and may not provide either identical or uniformly consistent results. Whichever method is

utilized, it must represent the continuous generation and flux of secondary vorticity into the outer flow by introducing, at each timestep, a discrete vortex whose strength and position depend on the interaction of the unsteady vorticity distributed throughout the wake on the appropriate boundary layer considerations to predict separation.

The type of separation criterion used (i.e., laminar or turbulent) will determine whether the flow is subcritical, critical, or turbulent. In fact, since the DVM becomes more accurate with decreasing shear layer thickness, it is reasonable to assume that the results obtained with a laminar separation criterion would correspond with moderate to high subcritical Reynolds numbers.

Fundamental to any integral-momentum method are that the velocity outside the boundary layer be given, and that the separation points will either remain stationary or fluctuate with small amplitude and velocities about a mean position. Stated differently, it is assumed that the changes in the separation points and the outer flow may permit the flow to be treated as quasi-steady; alternatively, it may be assumed that the contribution of the time-dependent terms in the unsteady velocity distribution are negligible.

In order to attempt a numerical simulation, a new boundary layer separation prediction scheme must be employed, or research must remain restricted to low Reynolds number flows. Consequently, it was decided to use the laminar integral-momentum method proposed by Sherman (1990 ) for boundary layers on solid surfaces beneath a vortex. Another method proposed by Shetz [1993] was considered, but found to rely too strongly on empirical curve fits. A more complete description of Sherman's method is given in Appendix A; briefly described, it employs a coordinate transformation in recasting the boundary layer equations, a power (Blasius) series expansion for the horizontal velocity and stream function to obtain a first guess starting profile, and then Thwaites' approximation to the momentum-integral equation to generate a differential equation for momentum thickness and various shape factors. The Thomas algorithm is used to solve the resulting tridiagonal matrix at each streamwise station for the stream function, boundary layer velocity profile, and velocity derivative with respect to streamwise direction; the results from one station are used as the input to the next station, with calculations continuing until the zero shear stress criterion for separation is achieved.

Sherman (1990 ) provided a FORTRAN program NEWBL which calculated boundary layer separation on an infinite flat plate under a stationary vortex. In the current work, this procedure was first modified to accommodate the separation from a semi-infinite flat plate, utilizing a numerical integration technique (Kuo [1972] ) to estimate Thwaites' integral. Results replicated several data points provided by Sherman; as an additional test, exercising the code to the limit of a zero-strength vortex produced the Blasius boundary layer velocity profile. At this point, the code was modified to accommodate the free stream velocity. A detailed description of the program modifications and the results of a comprehensive parametric analysis are presented in Appendix A.

## E. NASCENT VORTEX PLACEMENT

One of the problems associated with placement of the nascent vortex is that there be no backflow generated by the placement of the nascent vortex itself (for a fuller discussion, see Mostafa [1987] or Sarpkaya [1989, 1994] ). Consequently, once the separation location and velocity had been determined and nascent vortex strength calculated from Equation (3.10 ), the vortex was placed in the flow at an angle of 32° from the normal in the downstream position (see Figure 5.8, from Sarpkaya [1989] ).

## F. TIMESTEP SIZE

A timestep of $\Delta t = 0.125$ was utilized throughout these calculations. A sensitivity study was conducted, and, aside from a significant increase in computation time, revealed no appreciable difference in the locations of discrete vortices, velocity or pressure distributions, or other calculated values.

## G. CORE GEOMETRY

Several different core configurations were evaluated:

- Gaussian vorticity distribution: Poling et al [1988, 1991] utilized a vorticity distribution which was claimed to more closely approximate the Gaussian vorticity distribution found in nature. Strengths of the component vortices were as follows (see Figure 5.9, taken from Polling et al [1991] ):

| | | | |
|---|---|---|---|
| Center Vortex: | $R_a = 0.00$ | $\Gamma_a = \Gamma_{primary}/4$ | $n = 1$ |
| First Ring: | $R_b = 0.10$ | $\Gamma_b = 3\,\Gamma_{primary}/8$ | $n = 2\text{-}9$ |
| Second Ring: | $R_c = 0.15$ | $\Gamma_c = \Gamma_{primary}/4$ | $n = 10\text{-}21$ |
| Third Ring: | $R_d = 0.20$ | $\Gamma_d = \Gamma_{primary}/8$ | $n=22\text{-}45$ |

Within each ring, all vortices were of the same size (i.e., in the second ring, all 12 vortices were of strength $\Gamma_c/12$).

- Random vortex strengths and locations: radial and angular locations made in a purely random fashion; this tends to concentrate vorticity at the center of the core. A maximum strength of $\Gamma = 0.2$ was allowed when assigning vortex strengths in a random fashion. The sum of all vortices in the cluster equals $\Gamma_{primary} = \pi$.

- Random vortex locations, equal strengths: all vortices received a random position, as calculated above. Assigned strengths were all equal, and were as close to $\Gamma = 0.2$ without exceeding that value. The sum of all vortices in the cluster equals $\Gamma_{primary} = \pi$.

- Uniformly random vortex locations, equal strengths: a vortex is assigned a position which is uniformly random within a box within which the core radius is inscribed. If the position falls within the radius, the vortex is assigned that position; if not, another attempt is made until a random position falls within the radius. Strengths assisgned as in the previous instance.

The question then arose as to how to choose the core radius within which the cluster vortices were placed. When set to a value of $r_{core} = 0.2$, regardless of which of the above core distribution schemes was chosen, the component vortices would interact on the next timestep and essentially "explode" into a cluster of roughly 2-3 times the radius initially specified. By gradually increasing the initial core radius, the cluster did not display such radical behavior when a value of $r_{core} = 0.4$ was reached.

The scheme espoused by Poling et al [1988, 1991] resulted in minimal vortex distortion as it was convected with the secondary vortex and its image; this was due principally to the large strength of the

central vortex (one-quarter of the overall strength), about which all vortices in the outer rings would tend to orbit.

The next two vortex core placement schemes resulted in a natural concentration of vortices close to the center; there was no significant difference in vortex movement, induced velocities, or pressure distributions between the two random placement schemes. Random strength assignment may also lead to random straining within the vortex. In general, the random strength scheme resulted in roughly twice as many vortices as did the equal strength methods. Based upon this fact (and the consequent reduction in computation time), the unnatural core structure maintained in the Poling scheme, and the desire to avoid any unnatural concentration of vorticity at the center of the vortical structure, the equal strength/uniformly random distribution method was chosen.

## H. DISSIPATION

From experience gained from working with the DVM in harmonic flow, the most appropriate form of dissipation was deemed to be one which was principally a function of vortex age, (Equation (3.26), reproduced here):

$$\frac{\Gamma(t)}{\Gamma_o} = 1 - e^{\frac{-a^2 R}{4(t-t_o)}} \tag{5.9}$$

$$= 1 - e^{\frac{-B}{(t-t_o)}}, \tag{5.10}$$

where $t_o$ is the time at which a vortex was created. After numerous runs, a value of B = 20 was chosen, which after 92 timesteps, results in an average diffusion of 0.2% per timestep. All vortices, primary and secondary, were subjected to this dissipation.

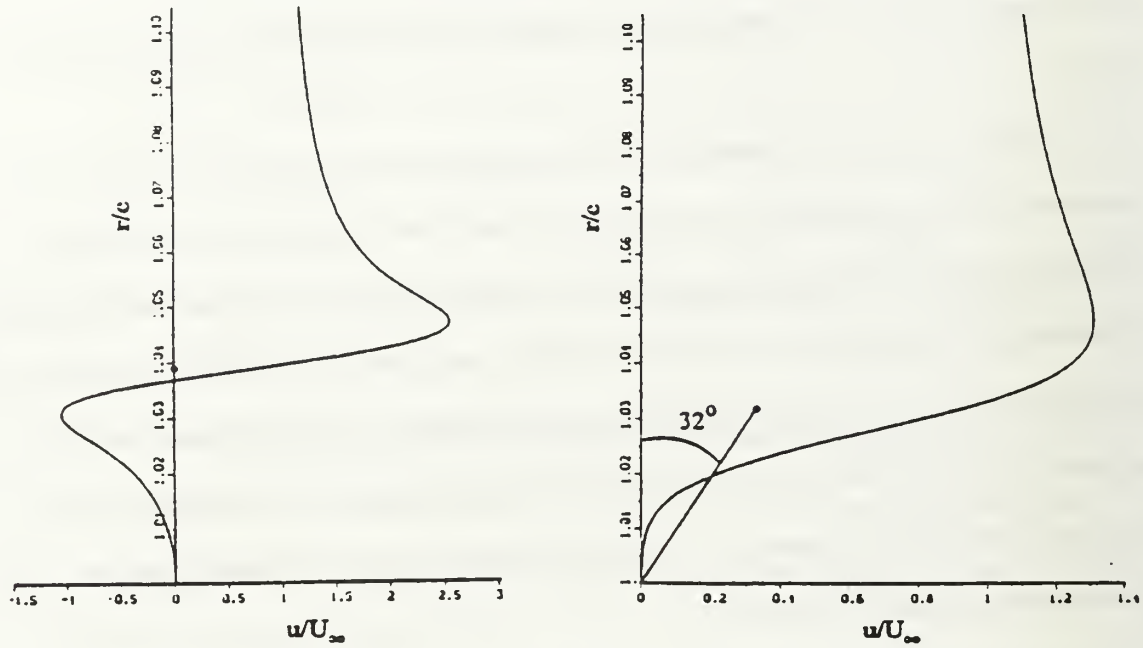


Figure 5.8 Figure on left shows the velocity profile along normal line passing through separation point, with nascent vortex on the normal line; figure to the right shows the velocity profile along the normal with the nascent vortex placed on a 32°-line. (From Sarpkaya [1989] )

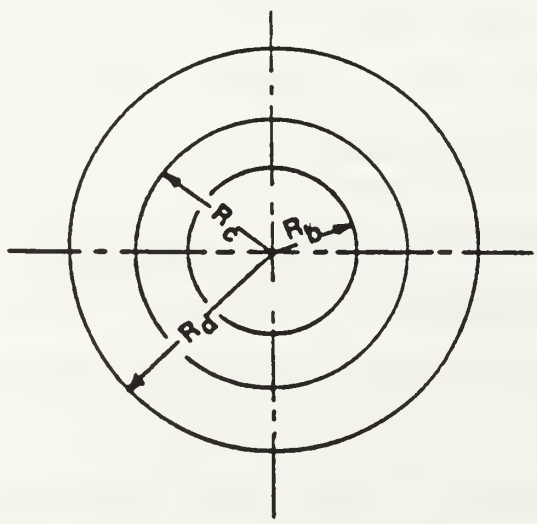


Figure 5.9 Geometry of vortex cluster showing corresponding ring radii around which discrete vortices are placed. (From Poling [1991] )

## I. INDUCED VELOCITY CALCULATIONS

The Rankine vortex scheme was employed throughout with a core or cutoff radius of 0.075 (see Robertson [1965] ), where velocity calculations were conducted according to:

$$r < r_{cutoff}: \qquad -u + iv = \frac{i\Gamma\left|z - z_o\right|^2}{2\pi\ r_{cutoff}^2\left(z - z_o\right)} \tag{5.11}$$

$$r \geq r_{cutoff}: \qquad = \frac{i\Gamma}{2\pi\left(z - z_o\right)} \tag{5.12}$$

## J. WALL ANNIHILATION

Vortices were removed from the flow when their cores touched the wall (i.e., when a vortex made contact with the core of its image); the first 15 vortices were exempted from this criterion to give nascent vortices and other vortices in the separation region the chance to convect away from the wall. At any time, if a vortex is subjected to high induced velocities and convected to a position ahead of the separation point, it is removed from the flow; were this not done, premature boundary layer separation (as noted in Chapter III, Figures 3.1 and 3.2) would result.

## K. VORTEX COMBINATION

Vortices were combined when their cores touched, and only if they were of like sign, using Equations (3.21) and (3.22).

## L. POTENTIAL FLOW BASELINE RUNS

Prior to incorporating viscous effects, a series of purely potential flow baseline runs was conducted. A single rectilinear vortex was introduced at (-2, 1), split into a cluster of equal-strength, randomly-located discrete vortices within a circle of radius 0.4, and allowed to convect under the influence of the real and imaginary vortices and the free stream (when $U_\infty \neq 0$ ). A representative run is shown in Figure 5.10 for $U_\infty = 1$ (i.e., $\beta = ½$ ), and for comparison, the same run without decomposing the vortex (Figure 5.11). In fact, there is no significant difference between the two runs, with the exception that the velocity and pressure curve peaks are slightly more pronounced for the run with only a single

vortex; this is in agreement with the qualitative results of Panaras [1987, 1990]. As anticipated from potential theory, the vortex (single or cluster) proceeds with no change in height above the plate. The plot of induced velocity on the plate shows a value of $\beta$ far upstream and downstream of the current vortex position, where a maximum value of $1+\beta$ is seen at a position immediately beneath the vortex. Qualitatively, the other runs exhibited the same shape pressure and velocity curves, with the only difference being that the curves will be closer to the x-axis for lower values of $\beta$. Additionally, the lift coefficient and center of pressure plot essentially as linear functions of x.

## M. $U_\infty = \beta = 0$: VISCOUS EFFECTS INCORPORATED

In this case, the vortex moves as a consequence only of its image, and lingers over each portion of the plate longer than for situations where a free stream is included; consequently, it is anticipated that viscous effects will be most pronounced for this case. As a further example of the difference between the two methods of representing the primary vortex, examples are shown of a single primary discrete vortex (Figure 5.12 ) and a cluster representation of the primary vortex (Figure 5.13 ). In both cases, since the entire flow field results solely from the primary vortex and its image, boundary layer separation occurs immediately upon starting the calculations, even with the primary vortex at a relatively distant upstream position of (-2, 1)[1] ; a discrete vortex is then introduced at each timestep, and the separation point (marked "s") begins to move towards the leading edge. The array of secondary vortices hugs the wall, and begins to build; maximum discrete vortex size occurs as the primary vortex overtakes the separation point, and the shed vortices begin to roll up into a vortical structure. When the primary vortex has proceeded sufficiently downstream and the separation velocity has fallen below a cutoff value, discrete vortices are no longer produced, the boundary layer calculation is bypassed, and the vortices begin to convect away from the viscous region of the wall in an almost purely potential fashion. From this point on, the only viscous effect is the diffusion associated with vortex age (Equations (5.9) and (5.10)). Continuing to

[1] In fact, by commencing the run at an even more remote upstream position, boundary layer separation did not begin until the primary vortex centroid reached a horizontal position of x = -2.97; then, however, the nascent vortex strength was so small as not to warrant incorporation into the flow.

introduce vorticity beyond a certain point results in numerous recently-shed vortices which, after the passage of the primary vortex, tend to "hug" the plate since they are influenced primarily by their own images (and when $U_\infty \neq 0$, the free stream, as well ). A sensitivity analysis was undertaken to determine the most appropriate cutoff point without affecting the kinematics of the primary and secondary vortices, and was found to be when the separation velocity had fallen to a value of $U_{sep} = 0.4+\beta$. An additional consideration for cutting off discrete vortex production at this point was to minimize computation time; this cutoff criterion was employed for all runs in the current analysis ($0 \leq U_\infty \leq 5$).

Comparing the summary plots (Figures 5.12 and 5.13 ), there is no appreciable difference in vortex strengths. In both instances, the immediate effect is for the primary/secondary vortices to convect away from the plate (and the influence of their images). As can be seen from the sequence of vortex position plots for the single vortex case (Figure 5.12 ), the inability of the primary vortex to distort and strain and the consequent concentration of vorticity at one point eventually results in the secondary vortex orbiting about an essentially stationary primary vortex. Even though the cluster representation allows the primary vortex to deform, this orbiting effect is still prevalent, although to a lesser extent. Harvey and Perry [1971] noted that this spiraling effect was not observed during their experiments, which would confirm their statement (reiterated by Doligalski et al [1994] ) that the primary vortex spawns a secondary vortex of roughly the same magnitude. In fact, the current analysis shows that, for either single or cluster representation of the primary vortes, its magnitude is roughly twice that of the secondary vortex; although a certain amount of vorticity is lost to diffusion, the step reduction in the $\Gamma_{lost}$ curves of Figures 5.12 and 5.13 lead to the conclusion that too much vorticity is lost to boundary annihilation. Were the primary and secondary vortices of similar magnitude, they would convect one another away from the plate at some angle, rather than undergoing the orbiting motion depicted herein. In any event, the motion of the primary vortex is radically altered from the purely potential case where the primary vortex and its image would maintain a constant separation as they moved to the right at constant velocity (see, e.g., Milne-Thomson [1968] ).

Due to the offsetting effect of the primary and secondary vortices, the forces and velocities on the plate are very small, and the center of pressure plots are highly erratic.

## N. $0 < U_\infty \leq 1$ ($0 < \beta \leq ½$): VISCOUS EFFECTS INCORPORATED

For these "intermediate" speeds, the primary vortex begins to experience the effect of a free stream, and is not allowed to remain over any section of the plate for an appreciable time. Although the case of a single discrete vortex representation is not shown here, more severe orbiting was experienced than with a cluster representation due to the higher concentration of vorticity. All cases shown will be for cluster representation of the primary vortex, and include runs for free stream values of $U_\infty = ¼$ (Figure 5.14 ), $U_\infty = ½$ (Figure 5.15 ), and $U_\infty = 1$ (Figure 5.16 ). Here, the free stream is the predominant contribution to the boundary layer outer velocity when the primary vortex is far upstream (in the vicinity of (-2, 1)); consequently, boundary layer separation does not initially occur until the primary vortex is closer to the leading edge ($x = -1.71$ for $U_\infty = ½$, and $x = -1.35$ for $U_\infty = 1$.) For $U_\infty = ¼$ , however, separation begins with the primary vortex centroid at $x = -2$.[2]

Even though the primary vortex was resident in the vicinity of the plate for shorter times (compared to the case of $U_\infty = 0$), secondary vortex strength was still roughly half the magnitude of the primary vortex because the free stream velocity is a major contributor to the separation velocity, used in Equation (3.10) to calculate nascent vortex strength. It is interesting to note that this is the same case for all velocities considered in this intermediate speed range. The net effect of the secondary vortex, in conjunction with the free stream, was to move the primary vortex away from the plate.

Whereas the plots of lift coefficient and center of pressure for the purely potential case were essentially linear functions of x, the effect of secondary vorticity was to negate the effect of the primary vortex in the force and moment integration in the region directly beneath the primary-secondary vortex pair. The effect of these vortices on the velocity and pressure distributions upstream or downstream of the

[2] As was done for the case of $U_\infty = 0$, placement of the primary vortex at an even more remote upstream position resulted in boundary layer separation commencing when the primary vortex centroid reached a horizontal position of $x = -2.17$.

pair was negligible, since to a certain extent, they offset each other, and also since they produce velocities on the plate which had no (or minimal) x-component. This resulted in a flattening of the plot of the location of the center of pressure directly beneath the vortex pair, which would indicate that the center of pressure remained the same when the force and moment integrations ended anywhere beneath the vortex pair. The flat portion of the center of pressure plot was wider and more pronounced at lower values of $U_\infty$.

## O. $U_\infty > 1$ ($\beta > ½$): VISCOUS EFFECTS INCORPORATED

For the sake of categorization, these will be referred to as "high speed" flows, since the predominant effect is that of the free stream; the contribution of the vortices becomes smaller and smaller with increasing $U_\infty$. Two cases are presented: $U_\infty = 2$ ($\beta = 2/3$) (Figure 5.17 ) and $U_\infty = 5$ ($\beta = 5/6$) (Figure 5.18 ).

Boundary layer separation commences with the primary vortex at $x = -1.09$ for $U_\infty = 2$, and at $x = -0.93$ for $U_\infty = 5$. The primary vortex spends substantially less time over each portion of the plate, so that the viscous response of the boundary layer is not given a chance to develop. In essence, the response is the same as if a purely potential calculation were being conducted: very little vorticity is shed, so that the primary vortex is influenced principally by its image and the free stream, and maintains essentially constant vertical position and horizontal convection speed. This is also borne out by the linear relationships of lift coefficient and center of pressure with the x-coordinate. Here, the secondary vortex grows to a magnitude of roughly one-half that of the primary vortex for $U_\infty = 2$ ($\beta = 2/3$), and one-third the primary vortex strength for $U_\infty = 5$ ($\beta = 5/6$); these vortices are not allowed, however, to form a roughly circular cluster before the primary vortex moves downstream. These results agree with those of several researchers working in the subsonic/transonic regime (Srinivasan [1985], Lee and Smith [1991] ), who conclude that viscous effects are negligible.

## P. CONCLUDING REMARKS

Although a steady flow, laminar boundary layer separation criterion has been used in the simulation of a highly unsteady physical process, the qualitative results are most encouraging. The

overall effect of vortex eruption seen in the experiments of Harvey and Perry [1971] are produced, and secondary vortex strengths of the same order as the primary vortex result. For $\beta \leq ½$, the secondary vorticity is formed relatively early in the passage of the primary vortex over the plate, with consequent alteration of the trajectory of the primary vortex up and away from the plate; with higher free stream convection velocities, the amount of orbiting of the secondary vortex about the primary is lessened. Additionally, the secondary vortex appears to be at least half the size of the secondary, and this appears to be the reason for the orbiting of the vortices; although vortex diffusion has been incorporated into the model, the reason for the smaller size of the secondary vortex is attributed to wall annihilation when a vortex core touches that of its image. For $\beta > ½$, secondary vortex effects are minimal, with smaller and smaller secondary vortices convected downstream; in other words, viscous effects become less predominant with higher free stream velocities.

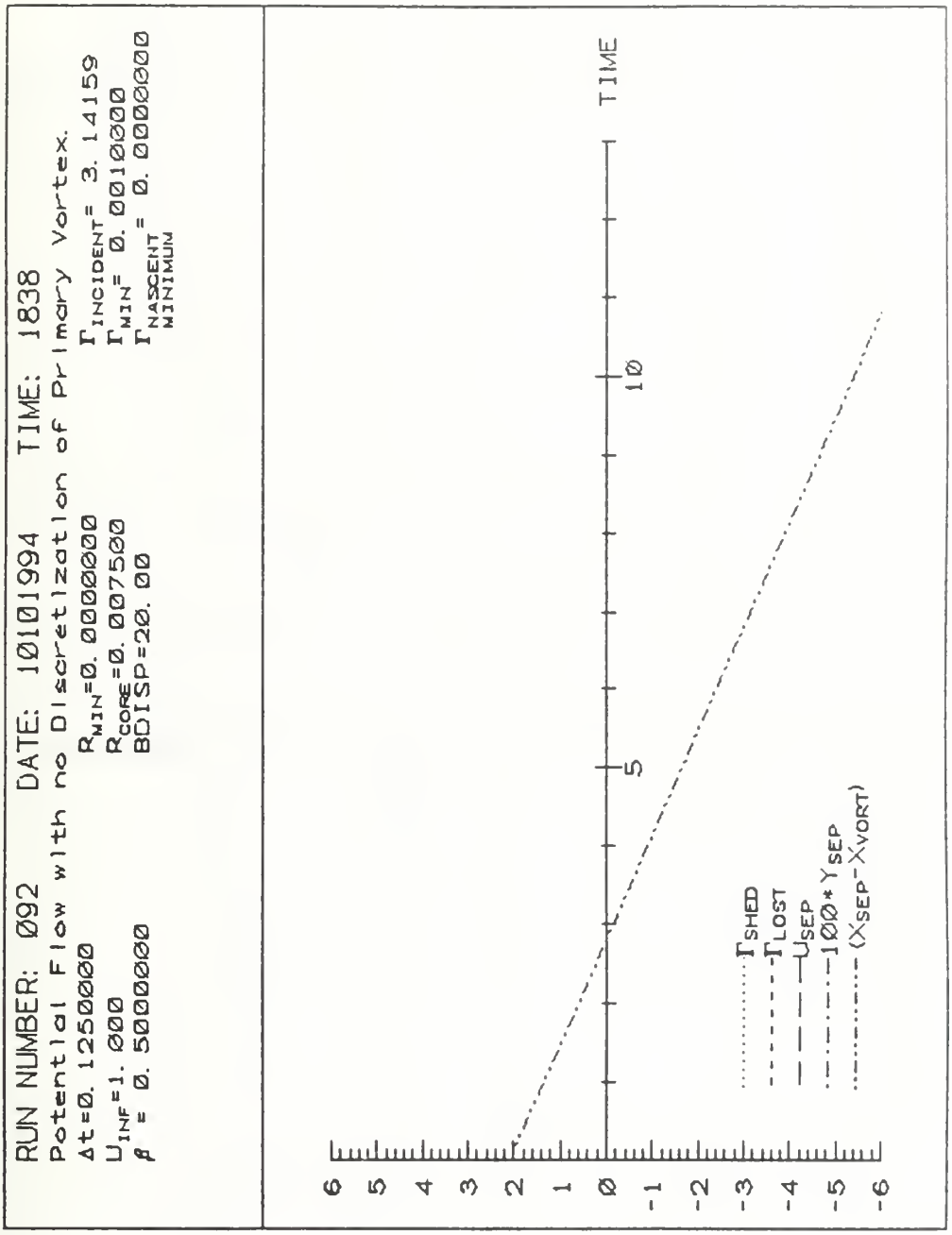


Figure 5.10 Potential flow with no discretization of primary vortex: $U_\infty = 1.0$.

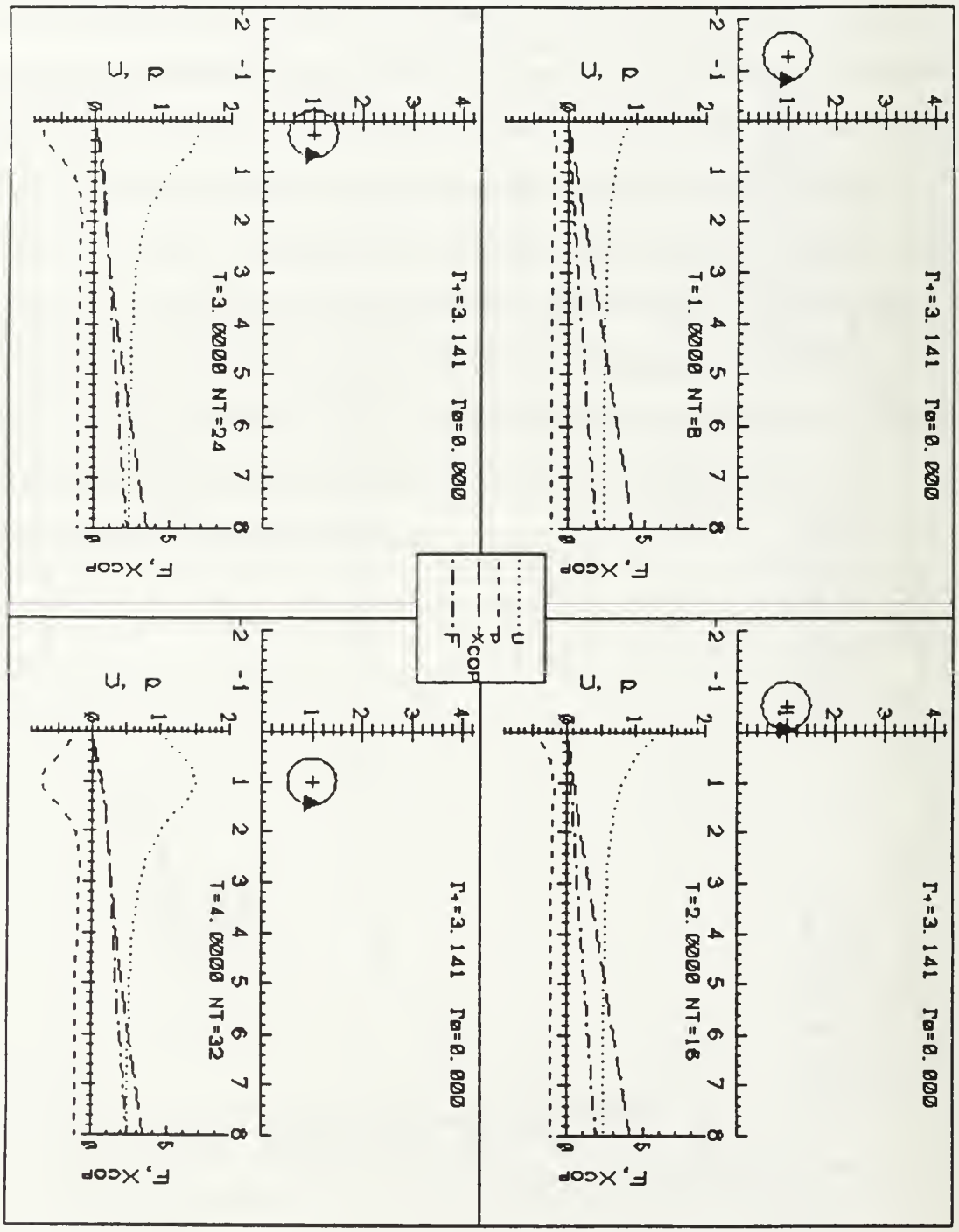


Figure 5.10 (con't) Potential flow with no discretization of primary vortex: $U_\infty = 1.0$.

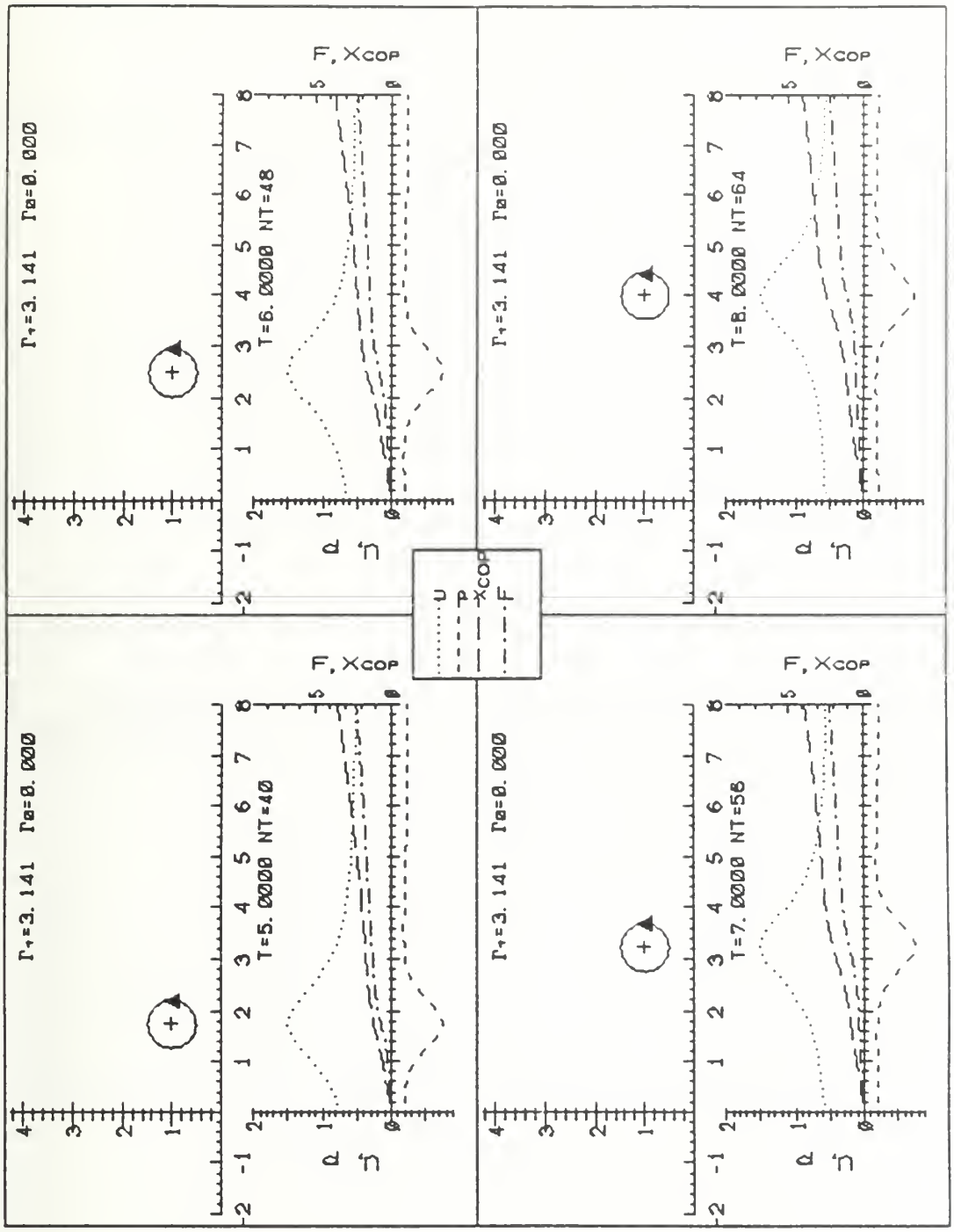


Figure 5.10 (con't.) Potential flow with no discretization of primary vortex: $U_\infty = 1.0$.

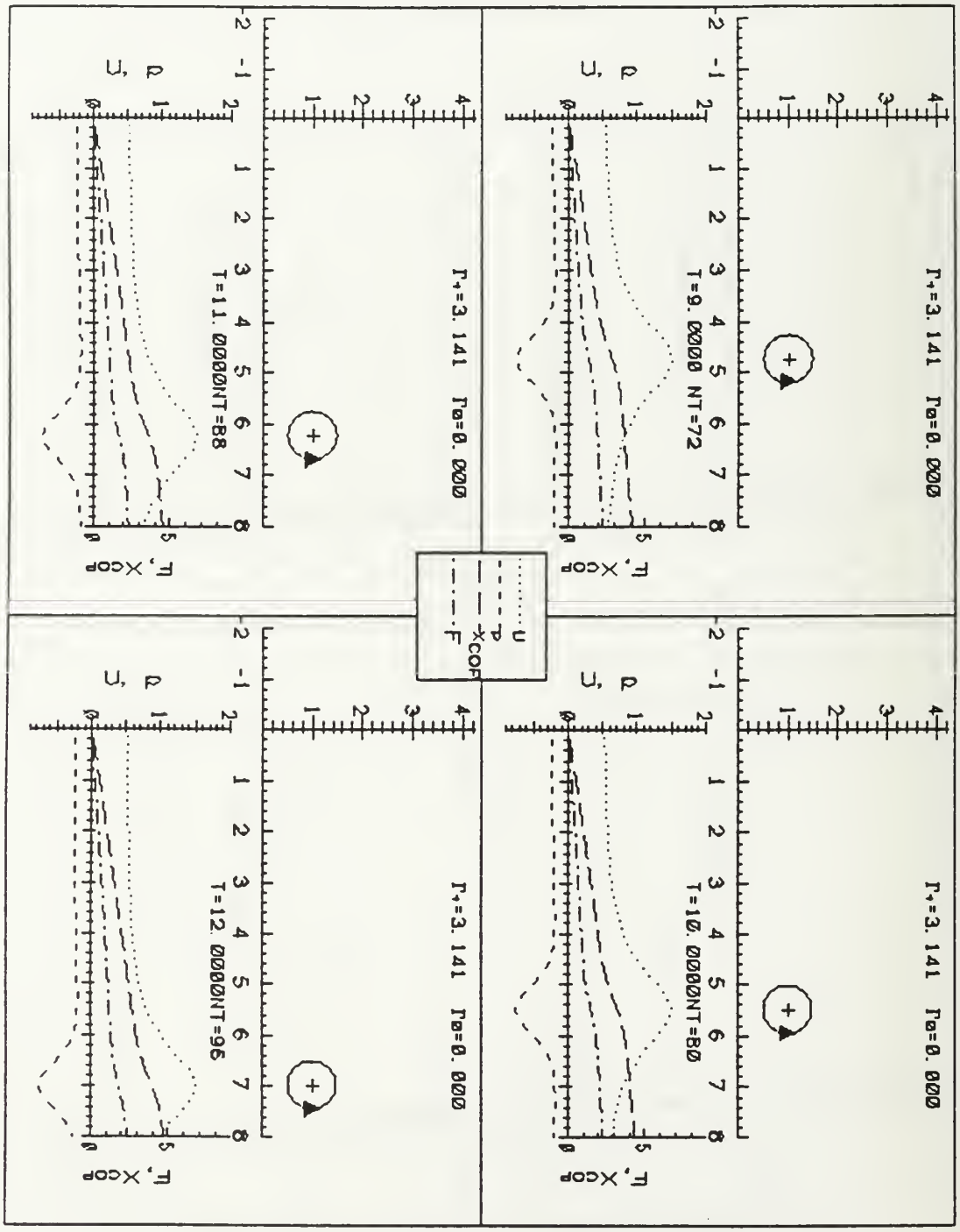


Figure 5.10 (con't.) Potential flow with no discretization of primary vortex: $U_\infty = 1.0$.

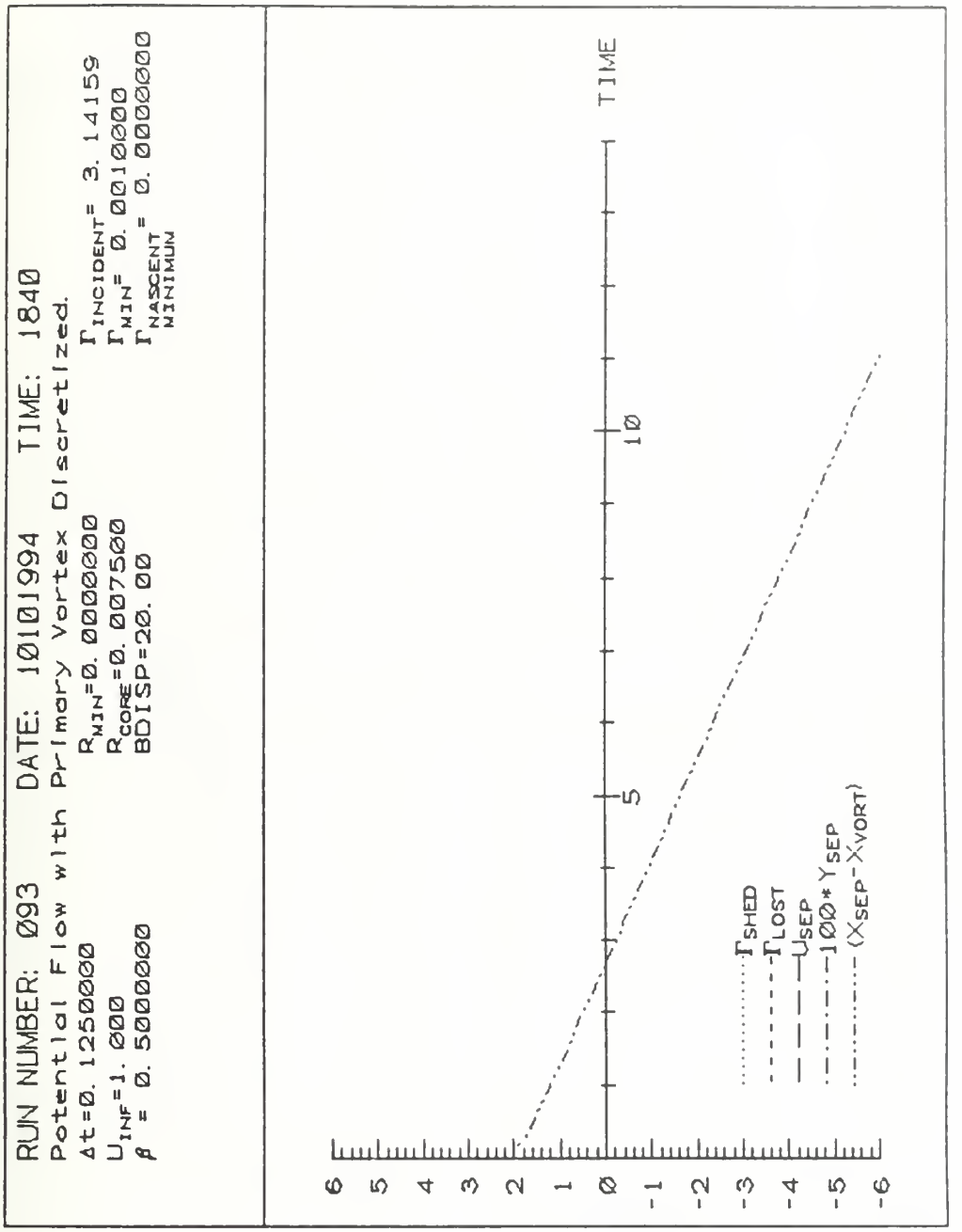


Figure 5.11 Potential flow with primary vortex discretized: $U_\infty = 1.0$.

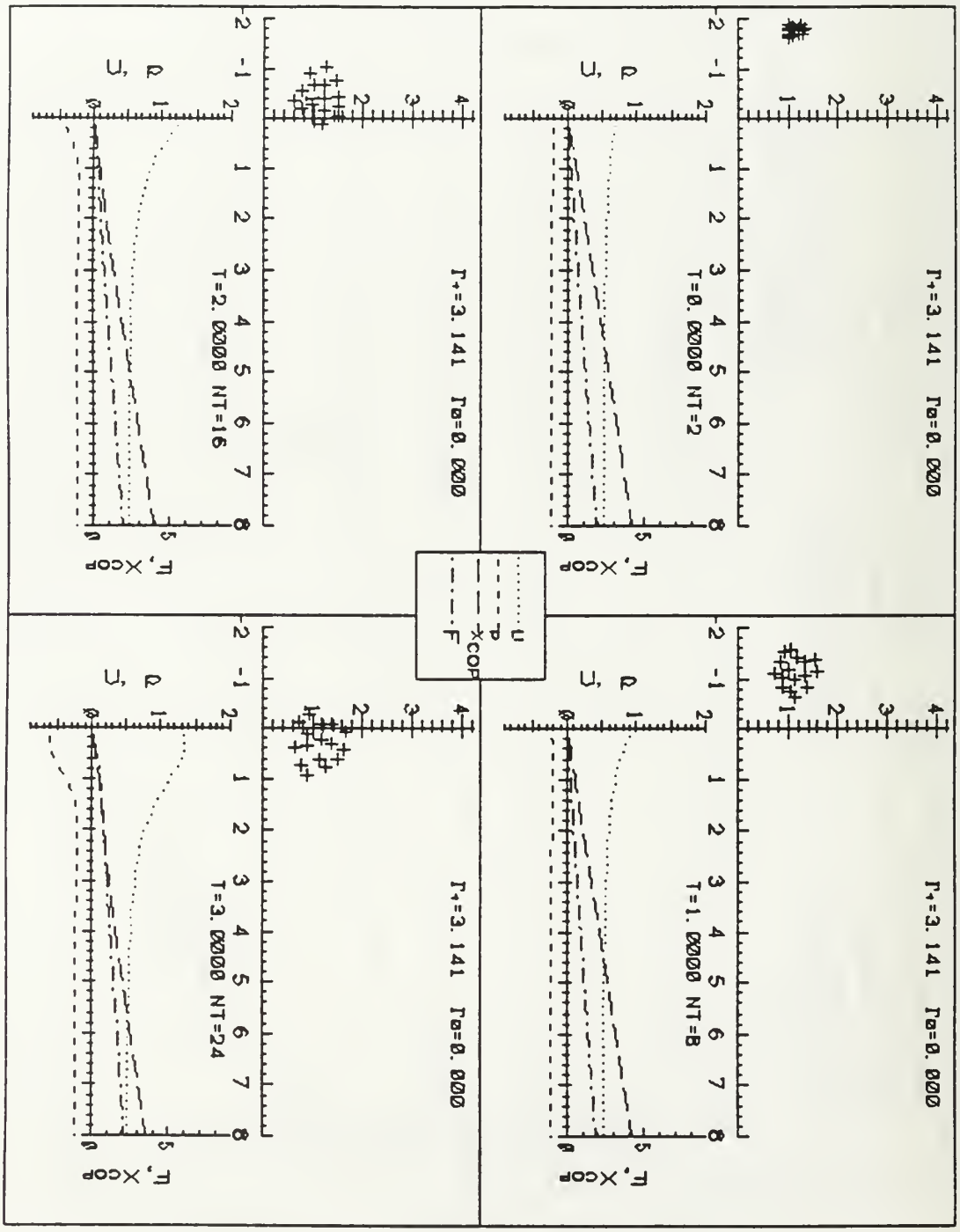


Figure 5.11 (con't.) Potential flow with primary vortex discretized: $U_\infty = 1.0$.

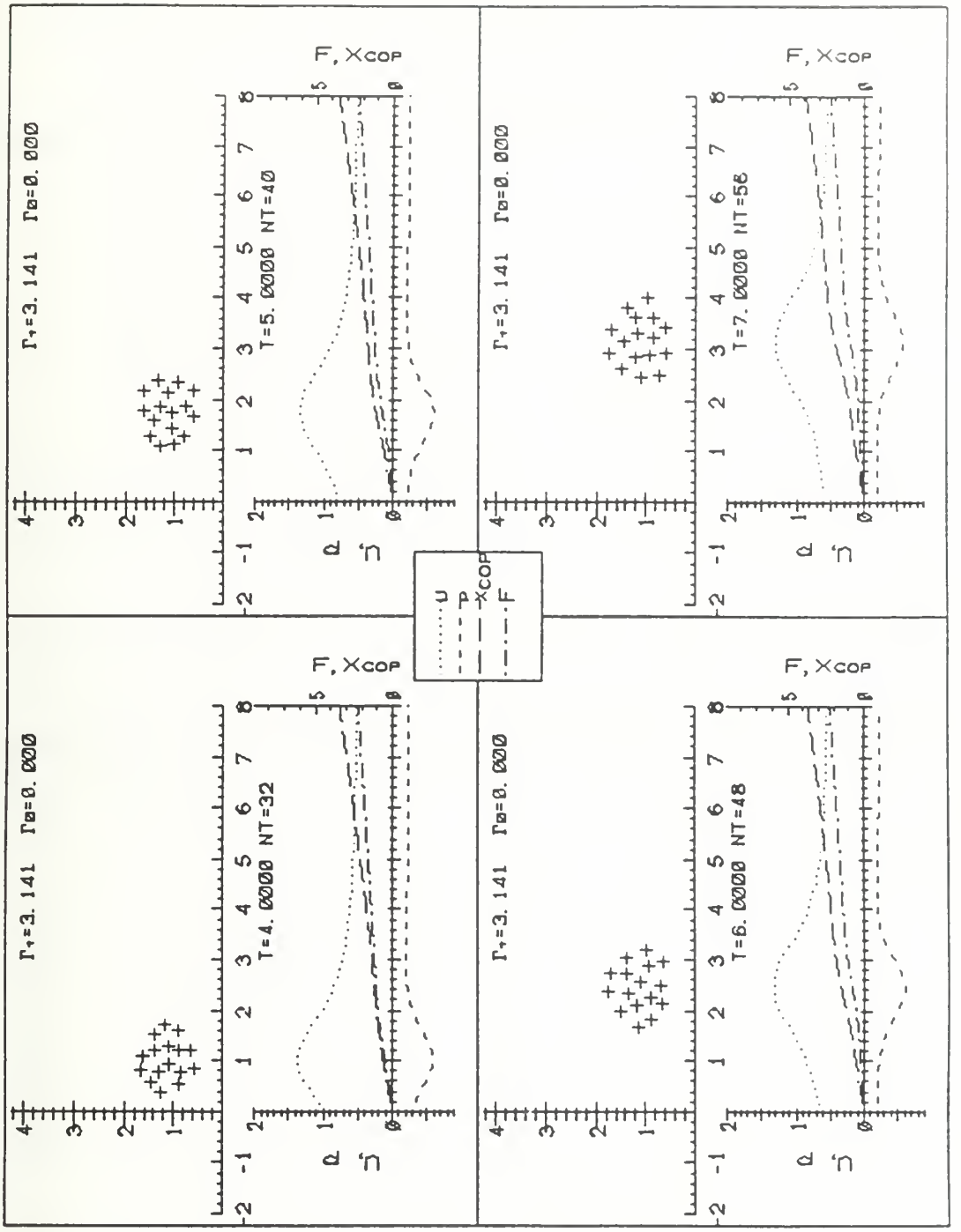


Figure 5.11(con't.) Potential flow with primary vortex discretized: $U_\infty = 1.0$.

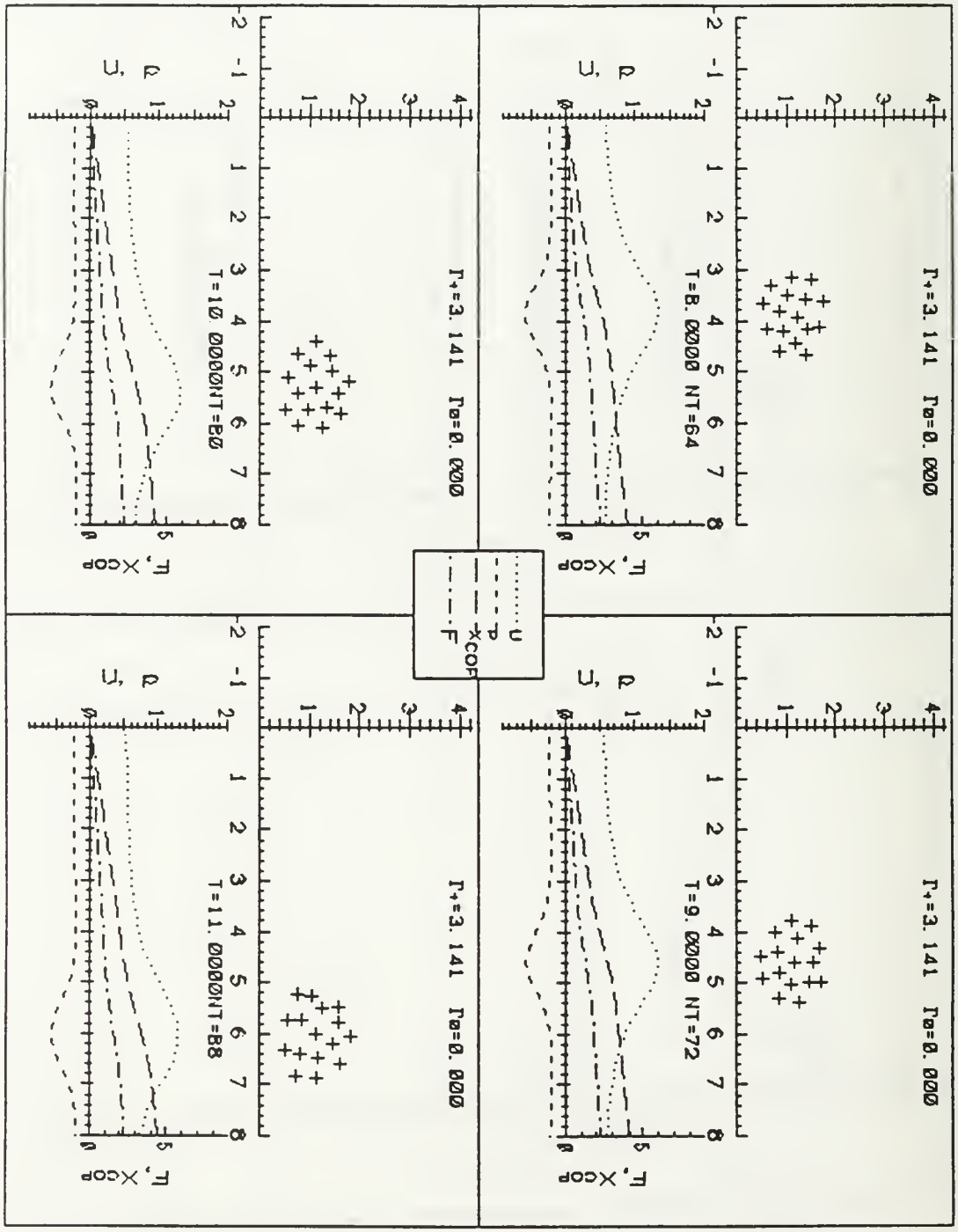


Figure 5.11(con't.) Potential flow with primary vortex discretized: $U_\infty = 1.0$.

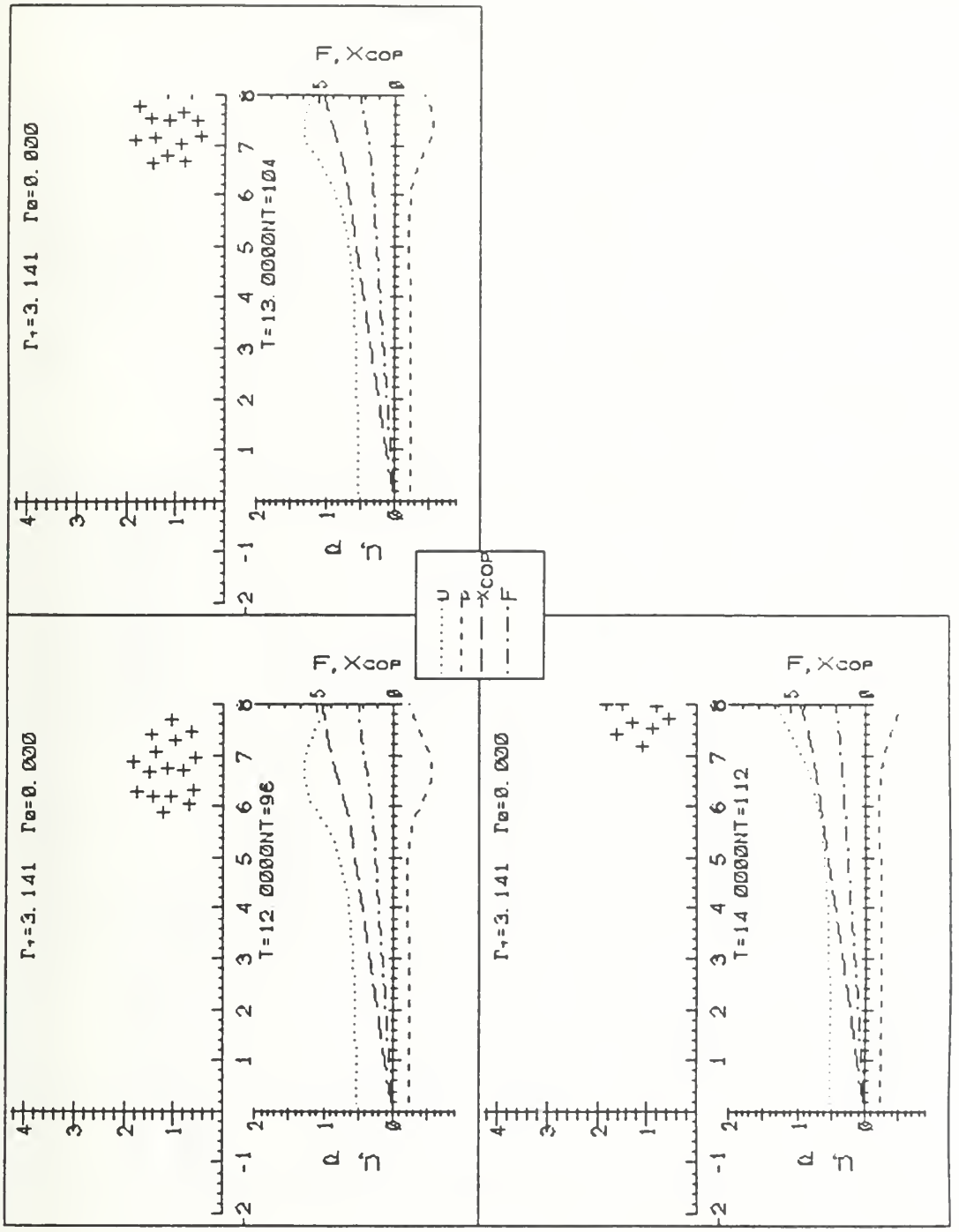


Figure 5.11(con't.) Potential flow with primary vortex discretized: $U_\infty = 1.0$.

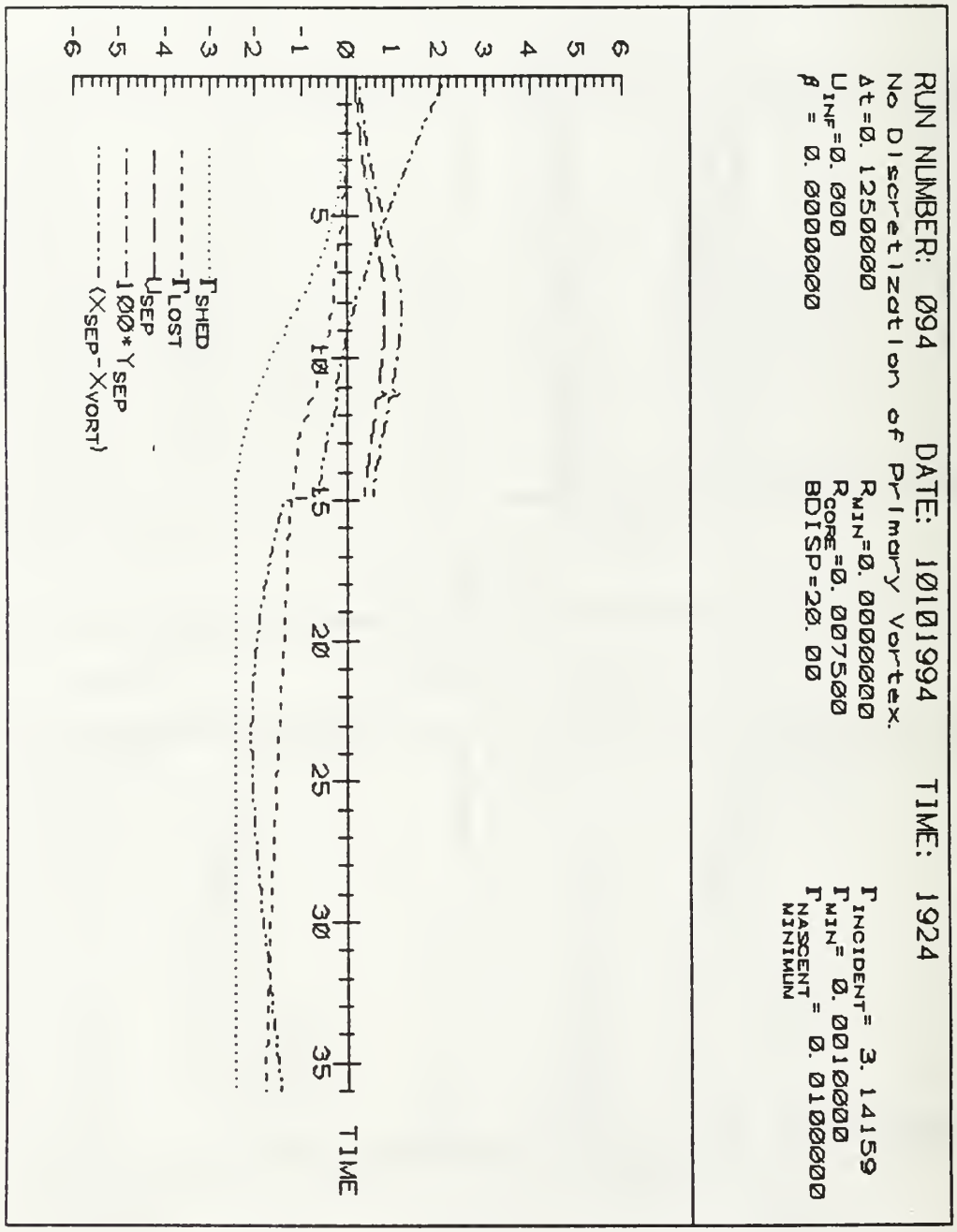


Figure 5.12 Viscous flow with no discretization of primary vortex: $U_\infty = 0$.

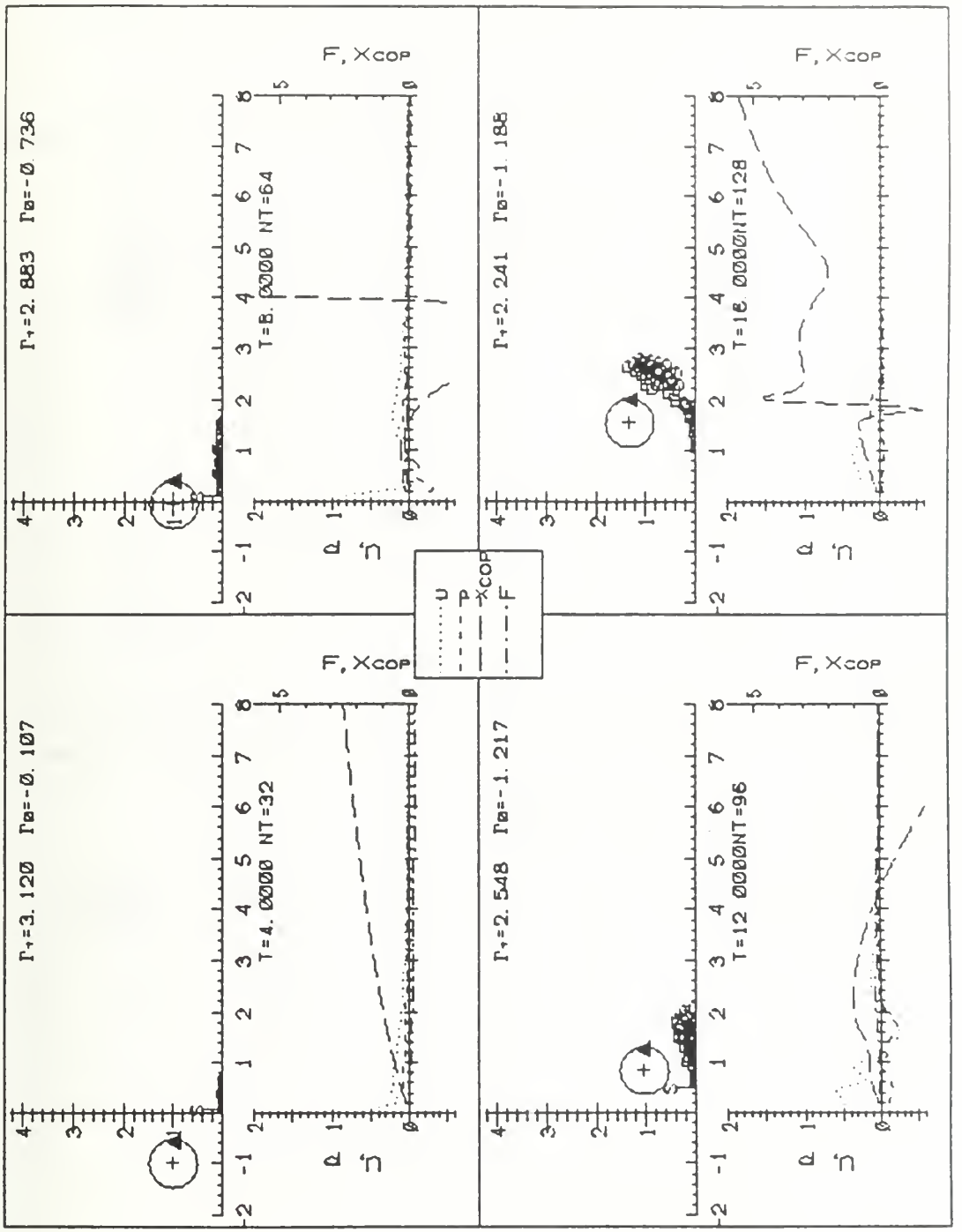


Figure 5.12 (con't.) Viscous flow with no discretization of primary vortex: $U_\infty = 0$.

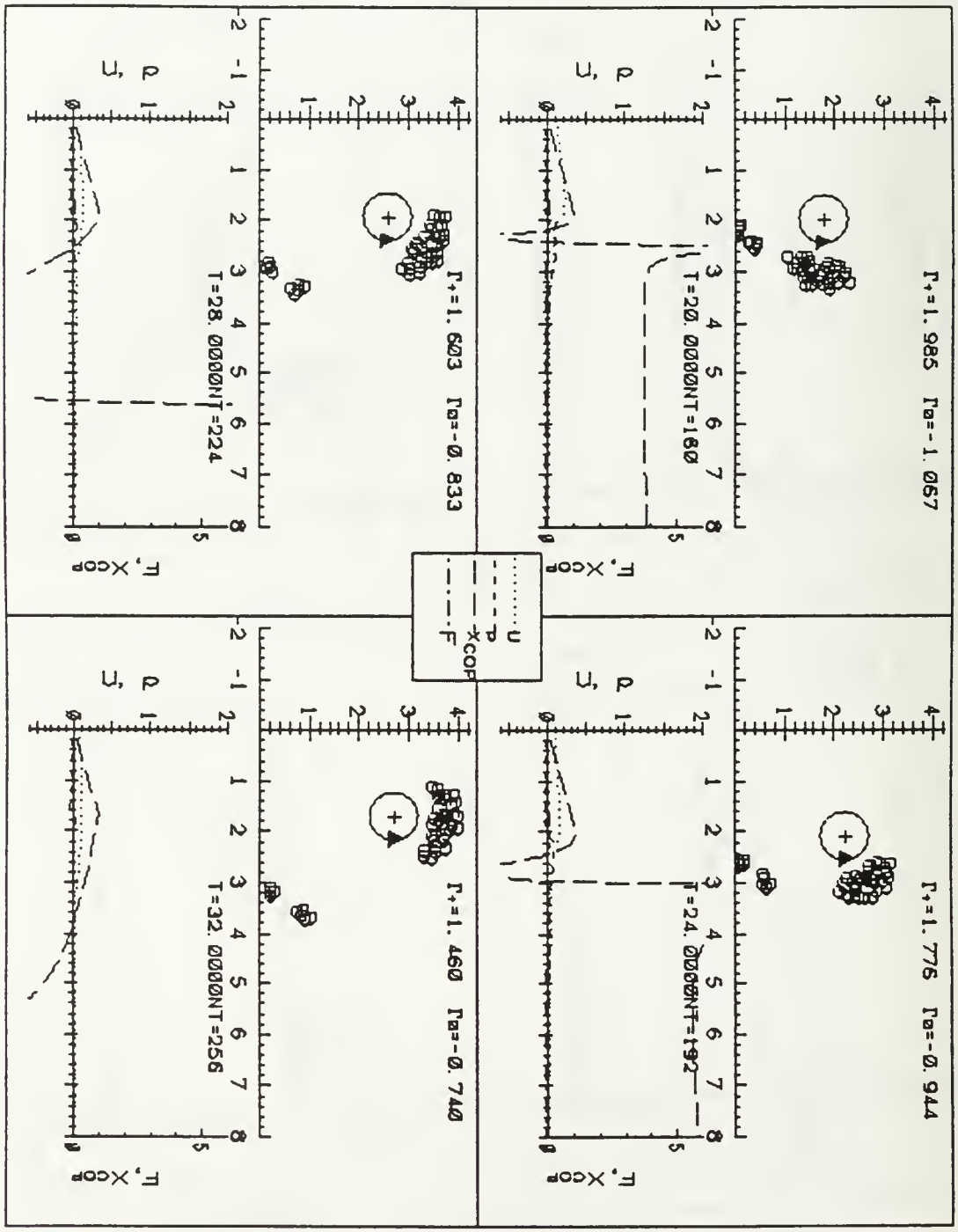


Figure 5.12 (con't.) Viscous flow with no discretization of primary vortex: $U_\infty = 0$.

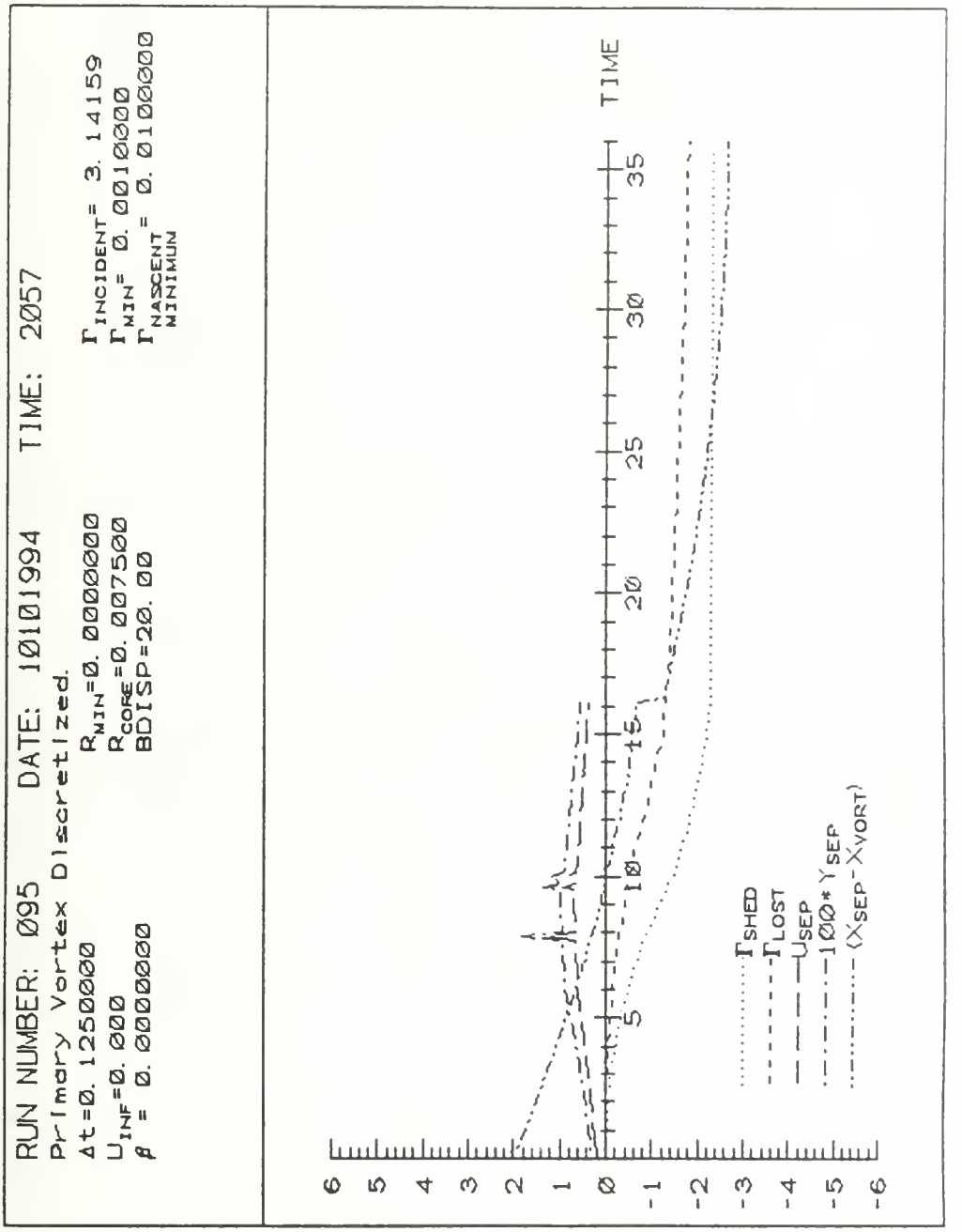


Figure 5.13 Viscous flow with primary vortex:discretized $U_\infty = 0$.

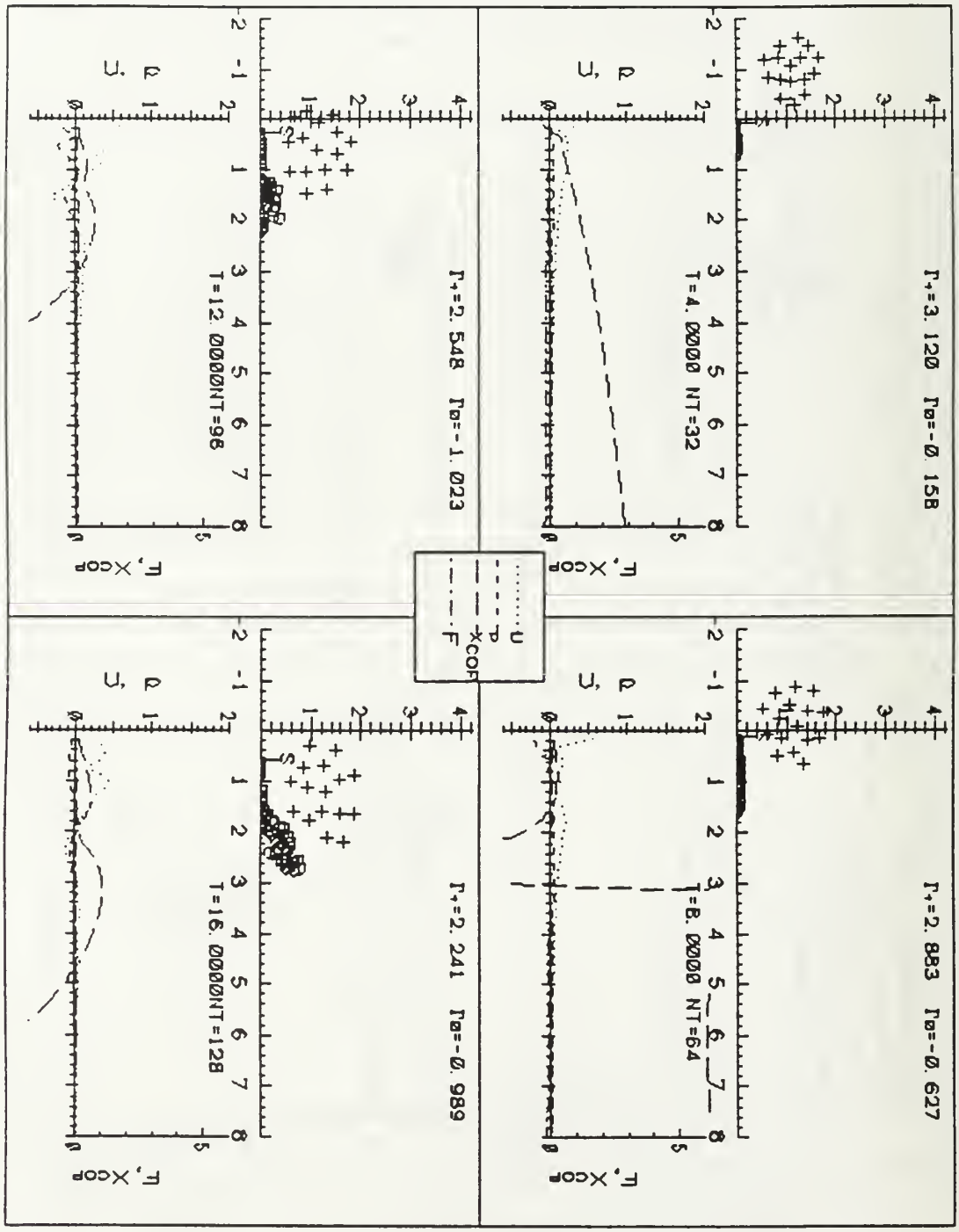


Figure 5.13 (con't.) Viscous flow with primary vortex:discretized $U_\infty = 0$.

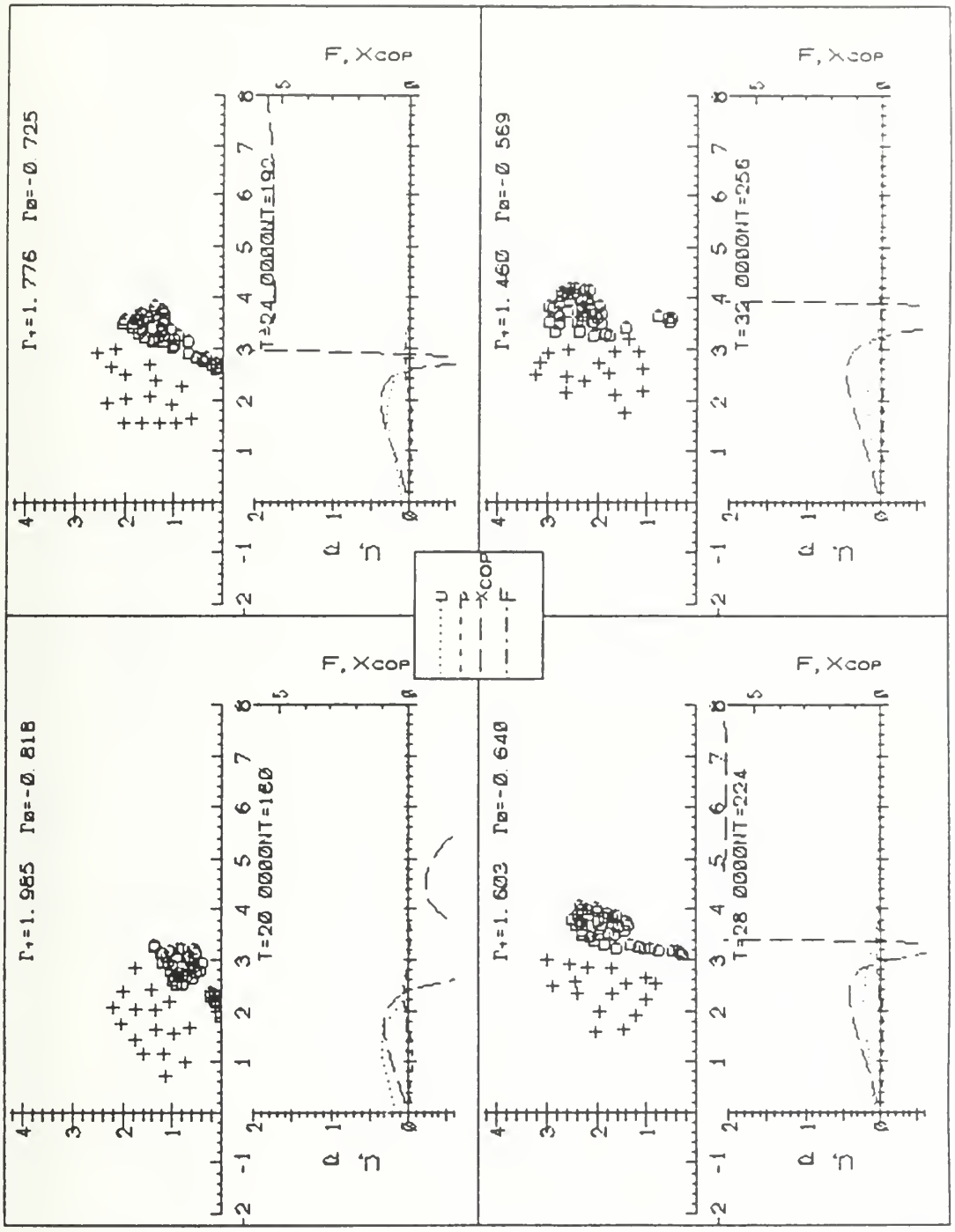


Figure 5.13 (con't.) Viscous flow with primary vortex:discretized $U_\infty = 0$.

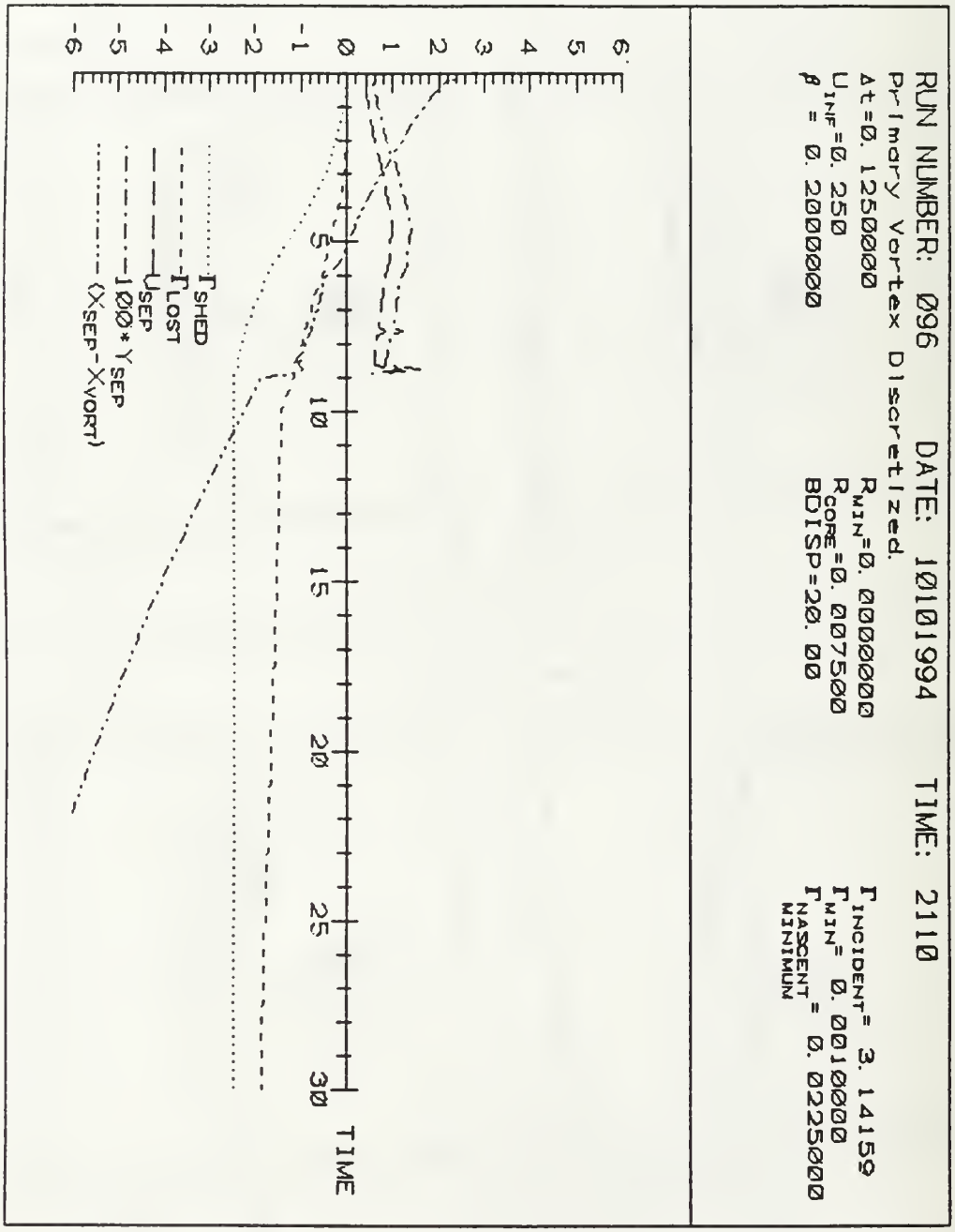


Figure 5.14 Viscous flow with primary vortex:discretized $U_\infty = 0.25$.

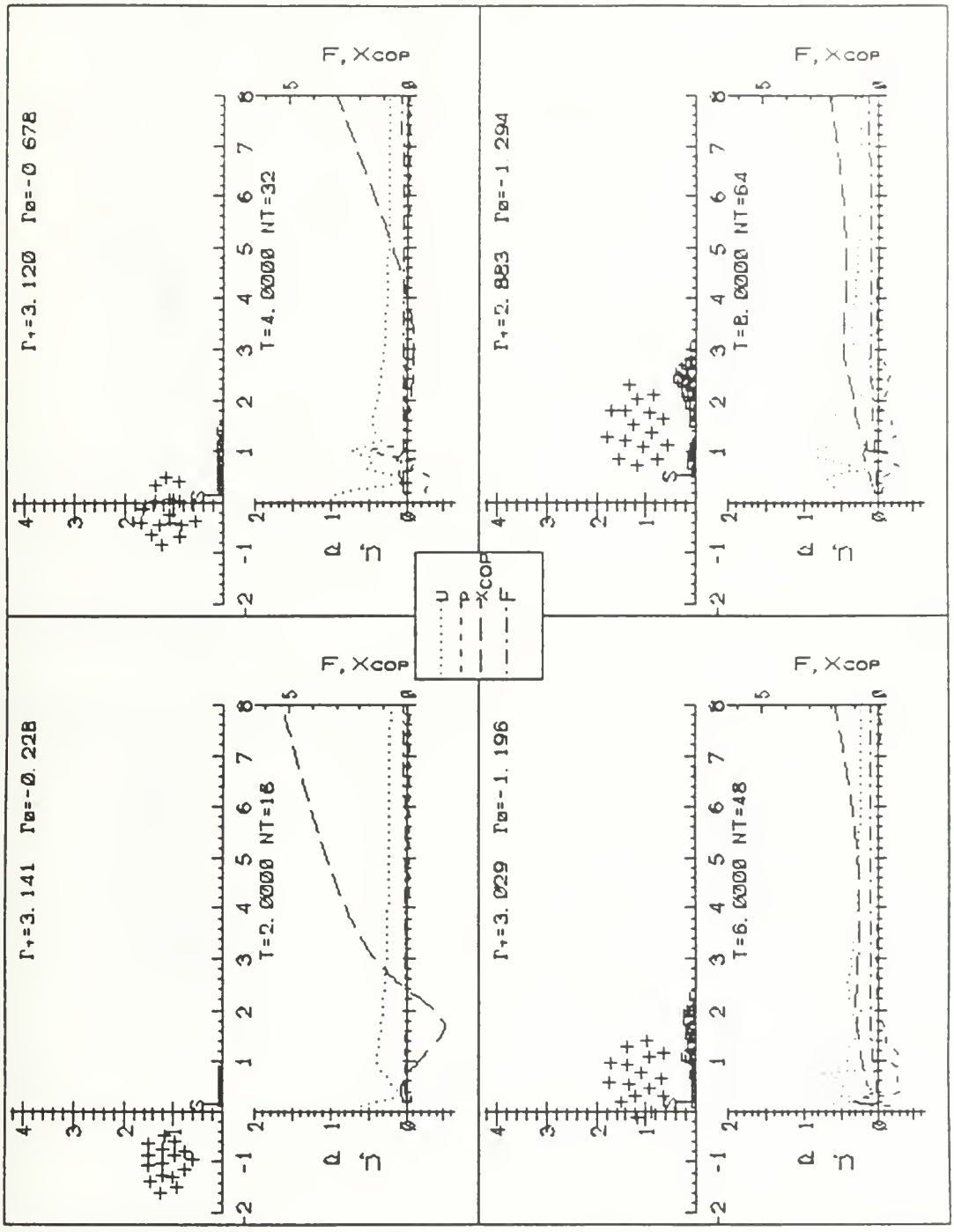


Figure 5 .14 (con't.) Viscous flow with primary vortex:discretized $U_\infty = 0.25$.

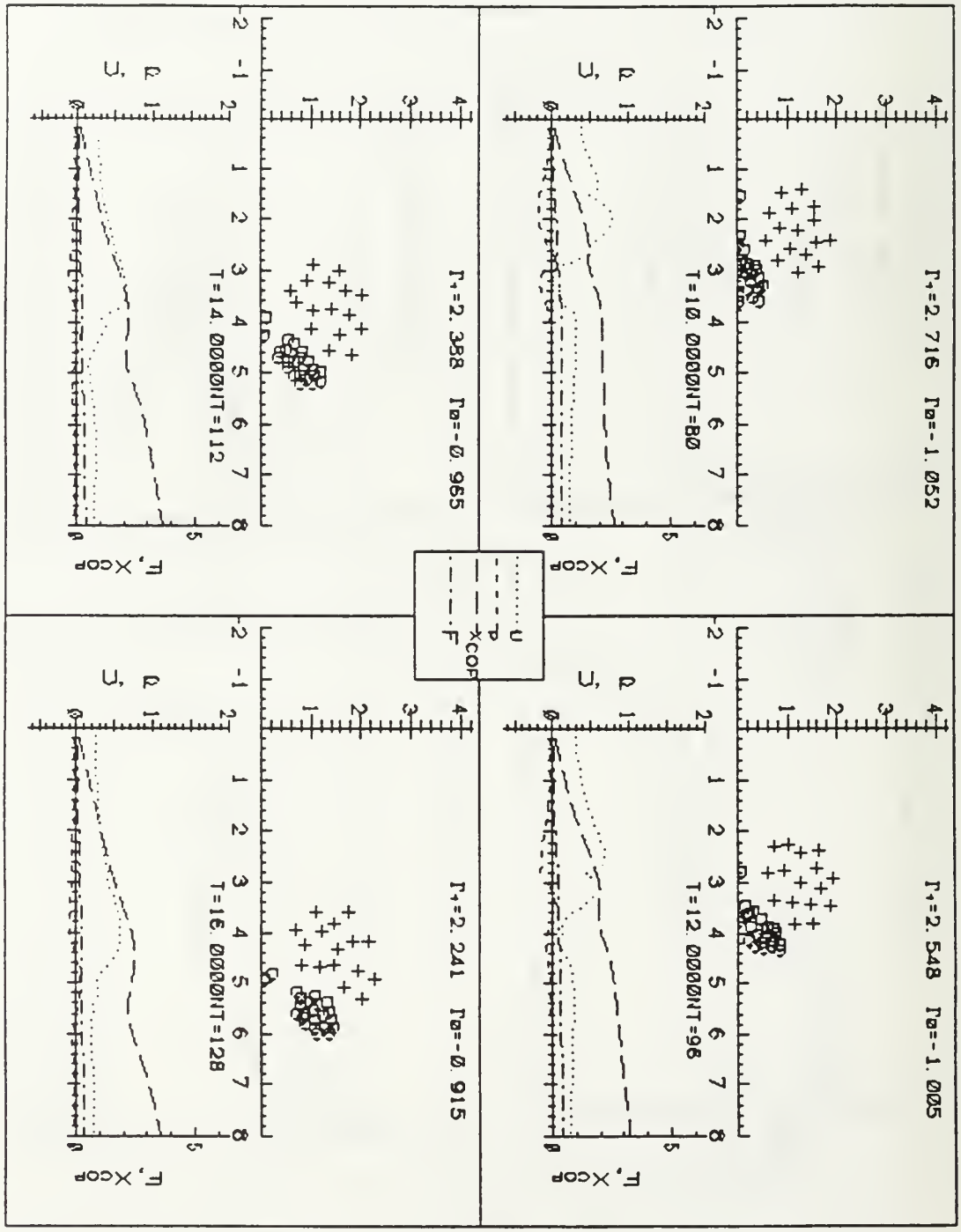


Figure 5.14 (con't.) Viscous flow with primary vortex:discretized $U_\infty = 0.25$.

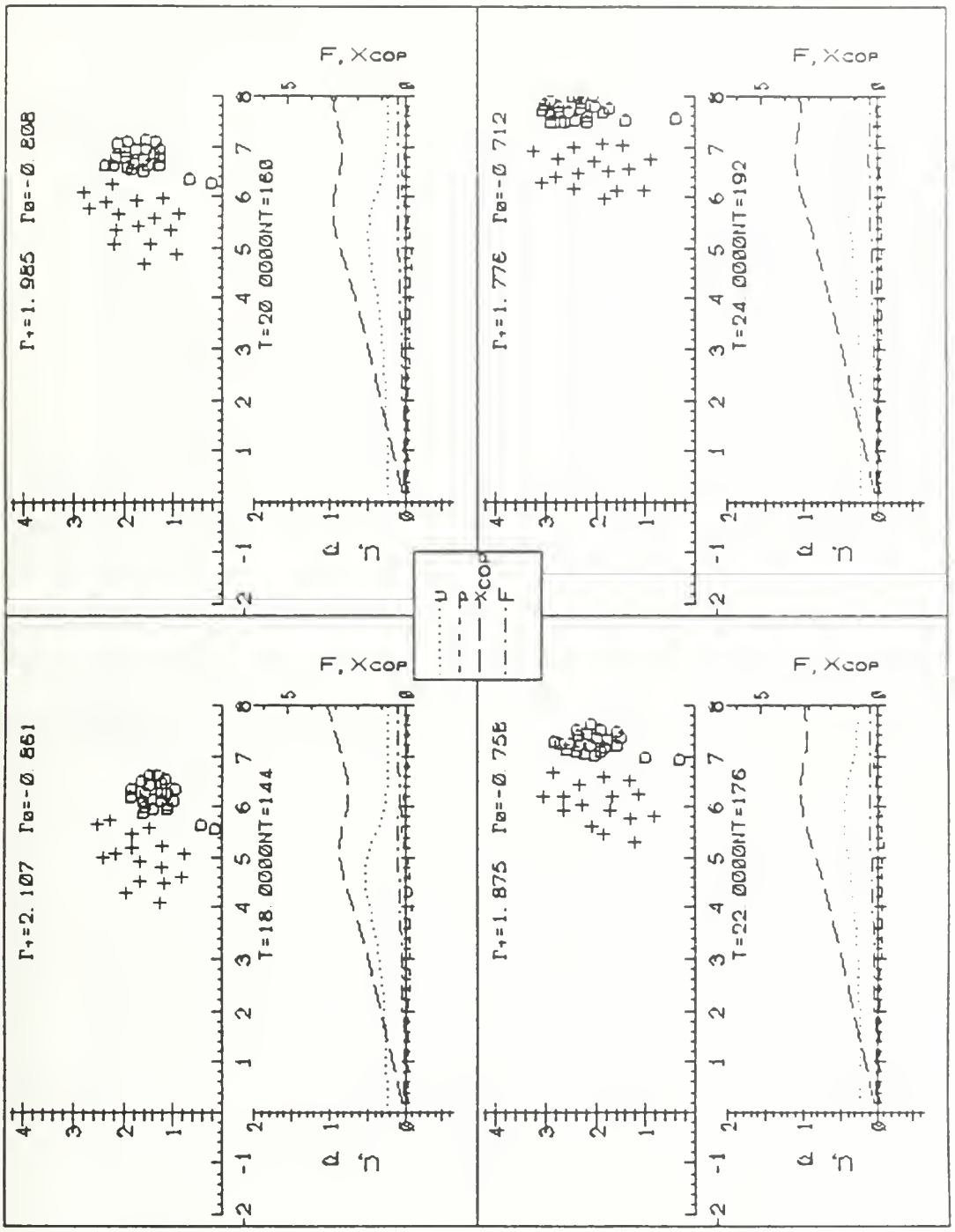


Figure 5.14 (con't.) Viscous flow with primary vortex:discretized $U_\infty = 0.25$.

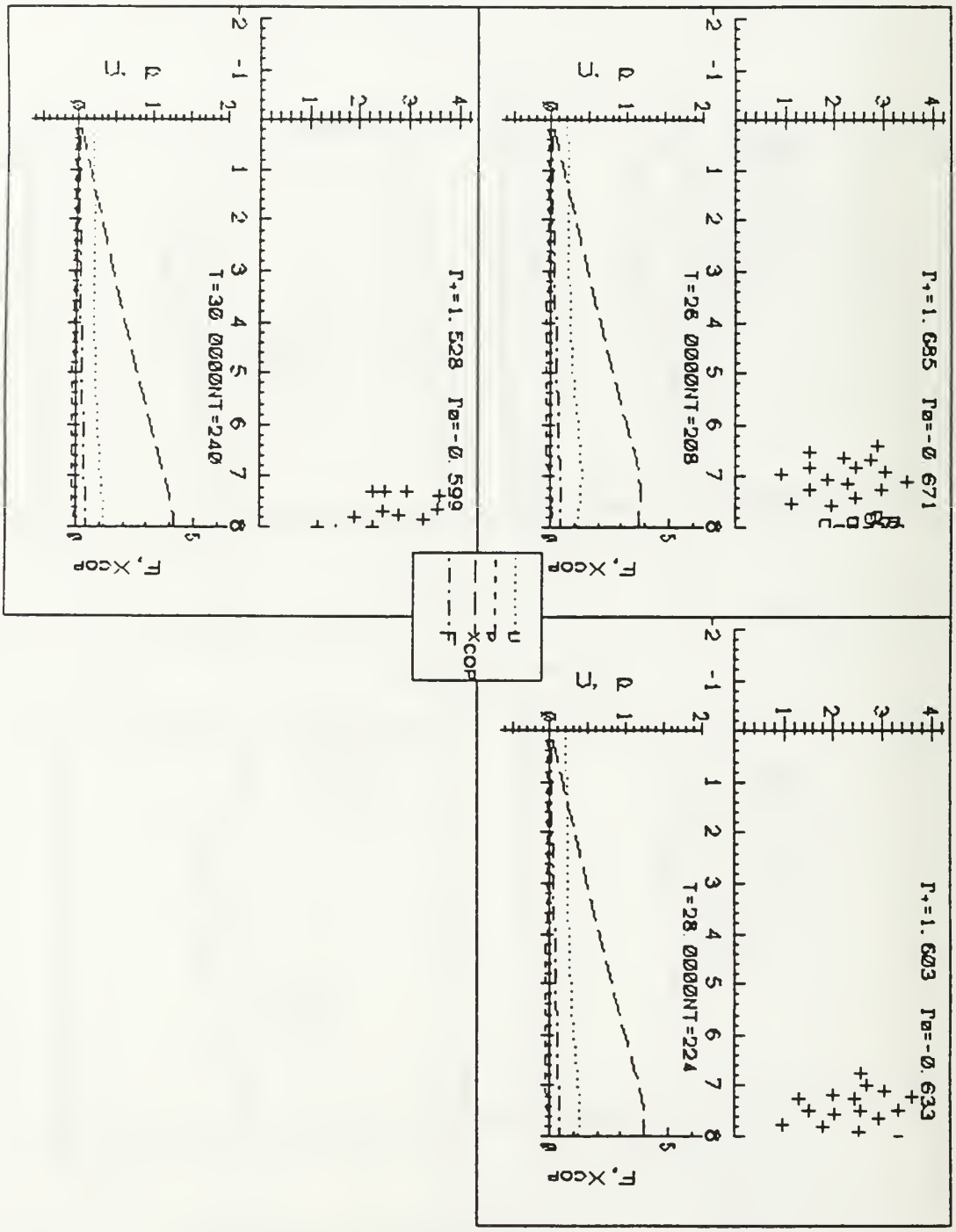


Figure 5.14 (con't.) Viscous flow with primary vortex:discretized $U_\infty = 0.25$.

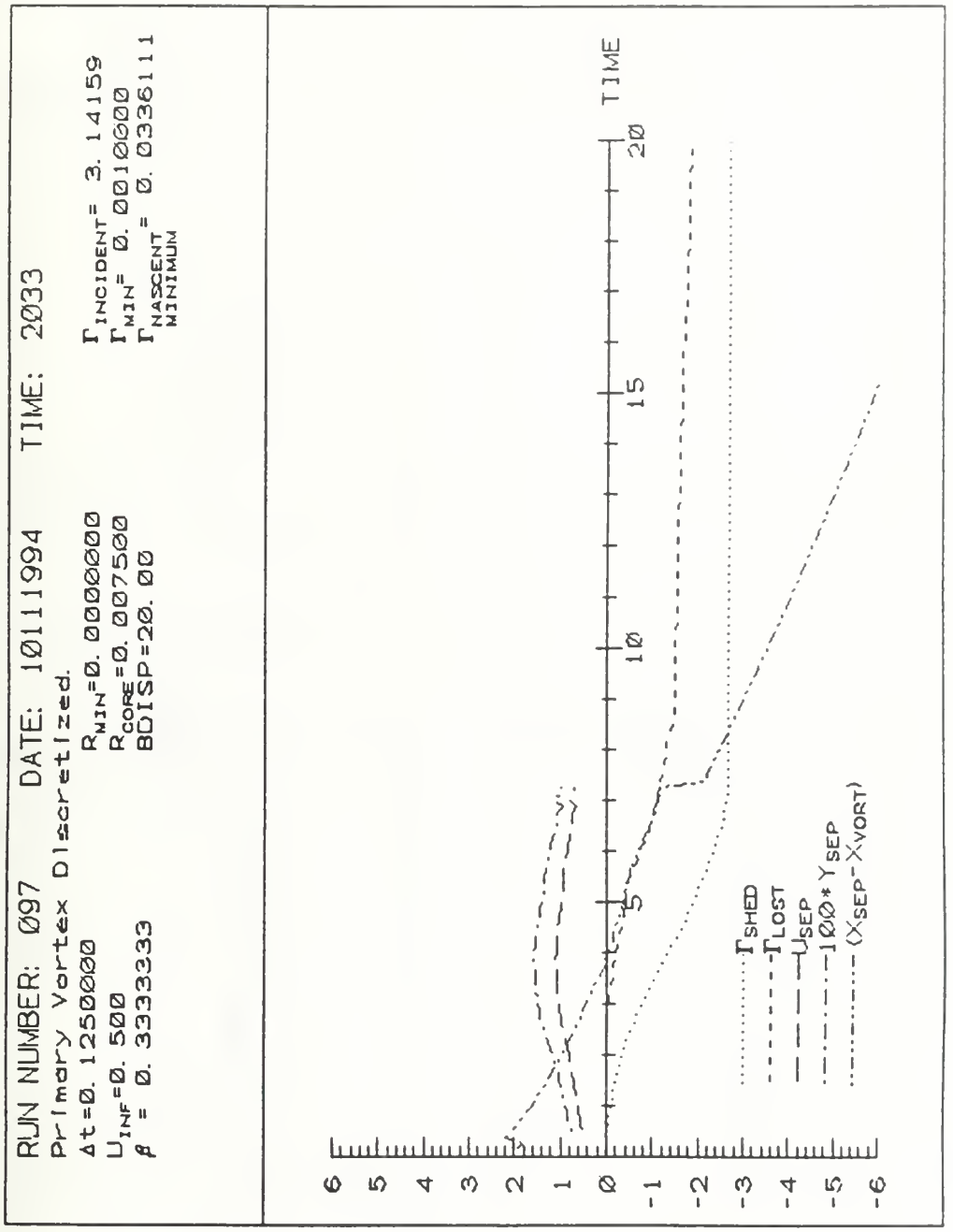


Figure 5.15 Viscous flow with primary vortex:discretized $U_\infty = 0.50$.

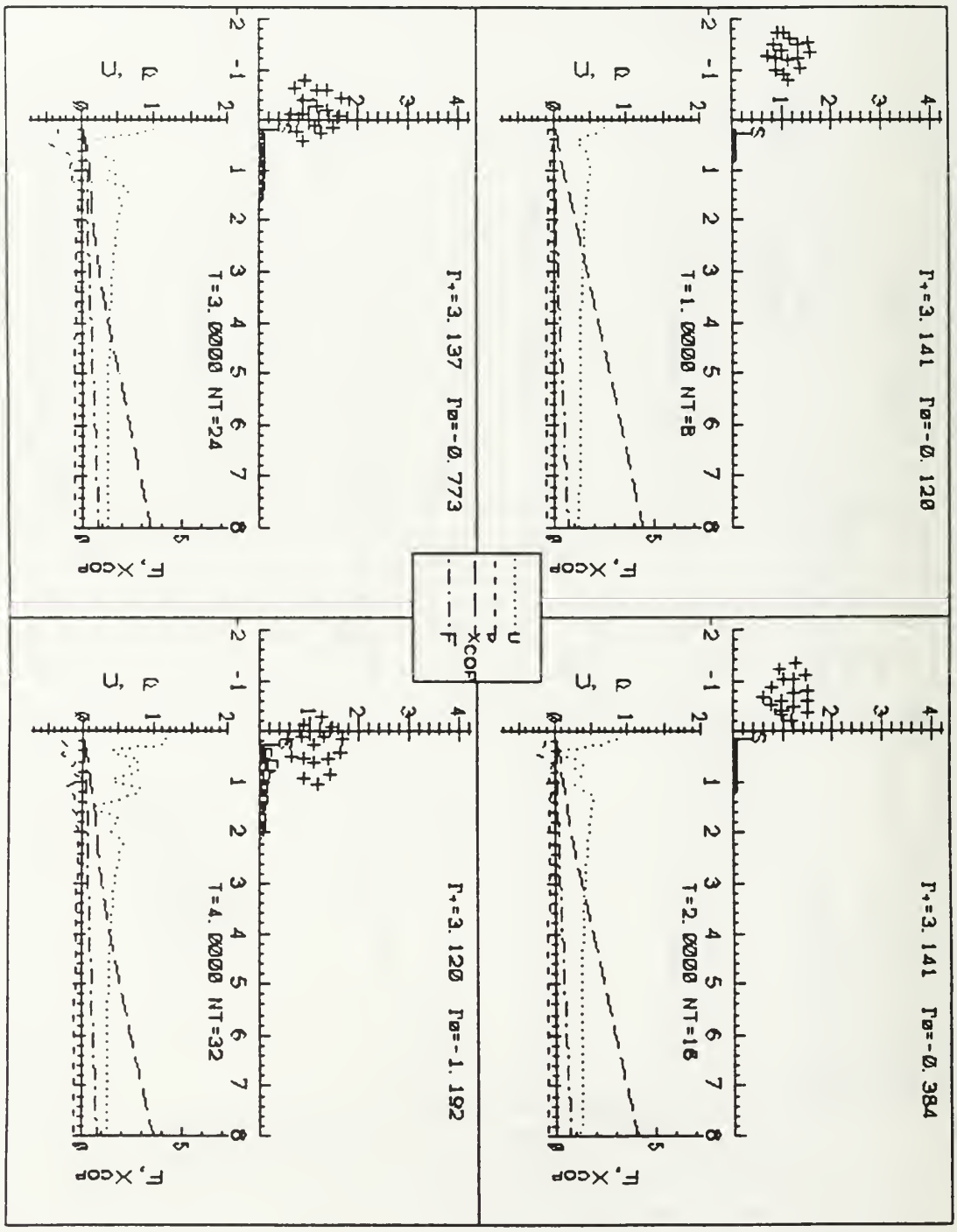


Figure 5.15 (con't.) Viscous flow with primary vortex:discretized $U_\infty = 0.50$.

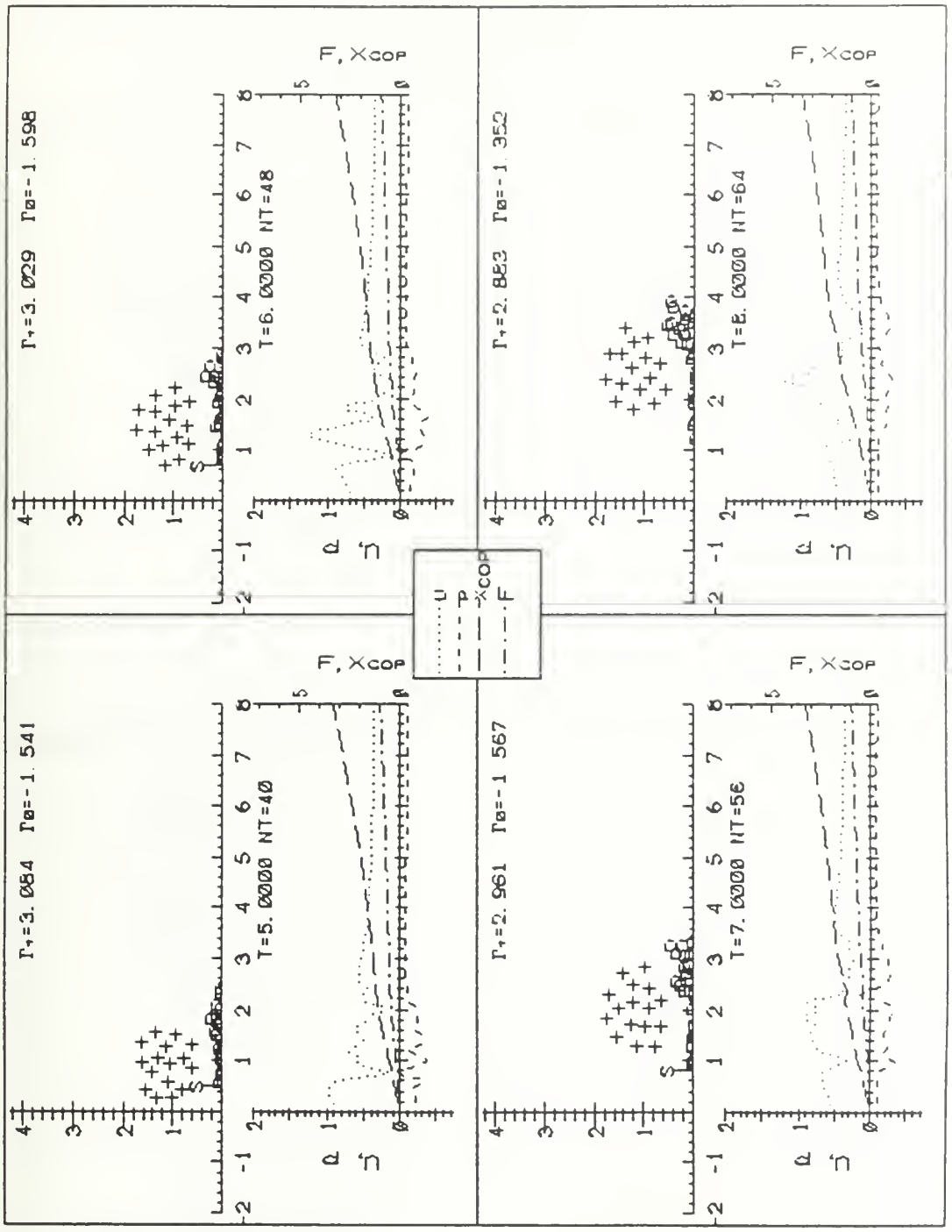


Figure 5.15 (con't.) Viscous flow with primary vortex:discretized $U_\infty = 0.50$.

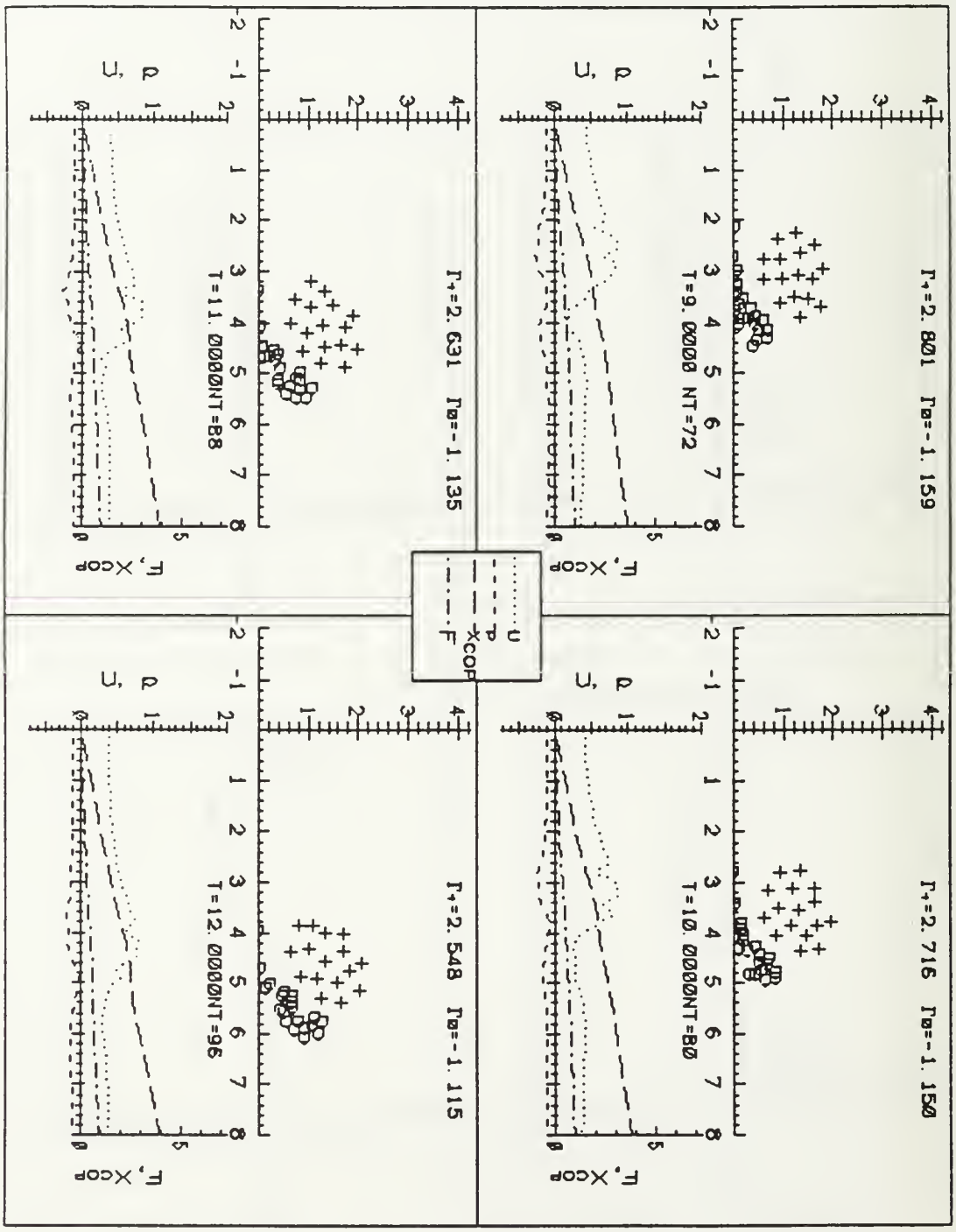


Figure 5.15 (con't.) Viscous flow with primary vortex:discretized $U_\infty = 0.50$.

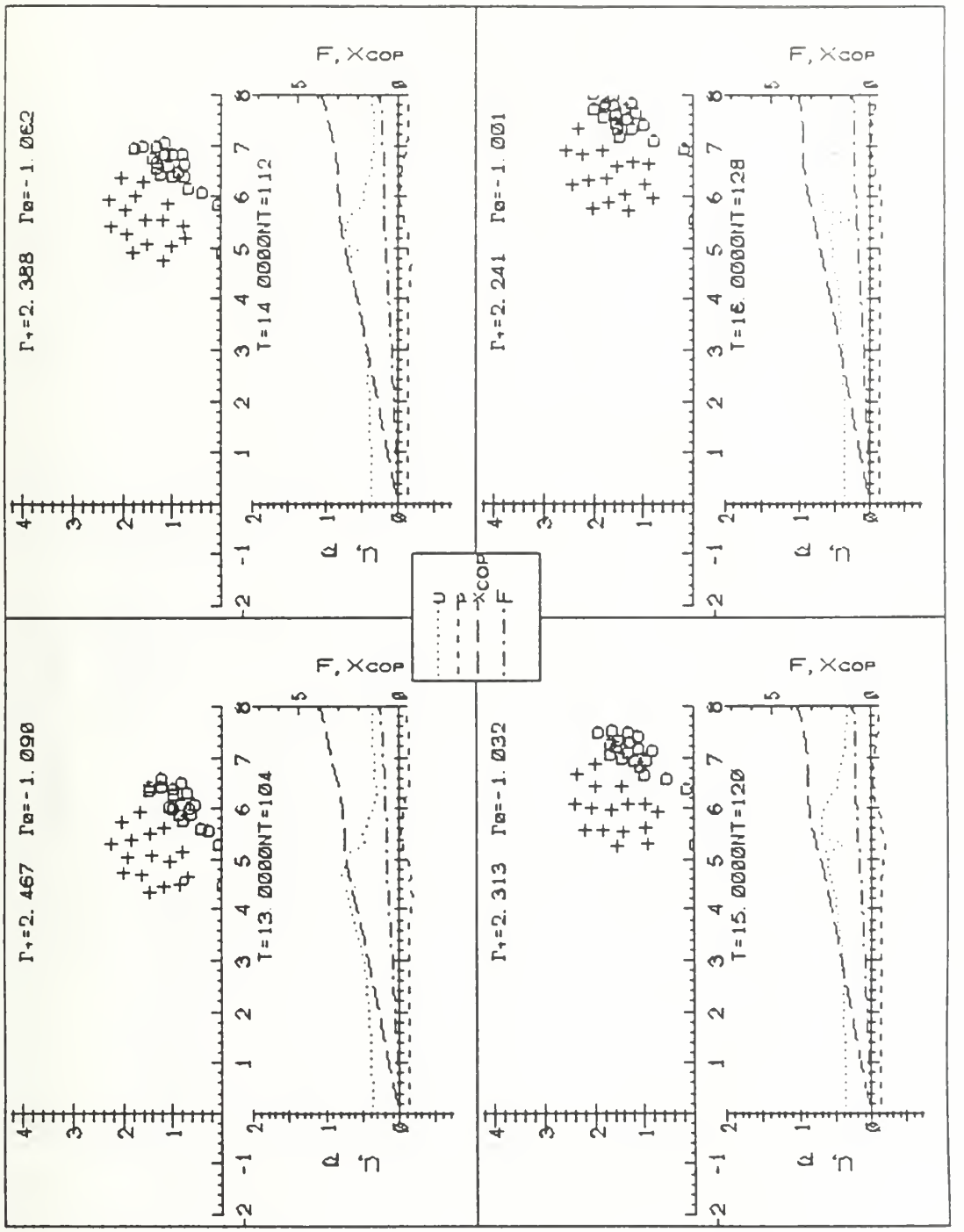


Figure 5.15 (con't.) Viscous flow with primary vortex:discretized $U_\infty = 0.50$.

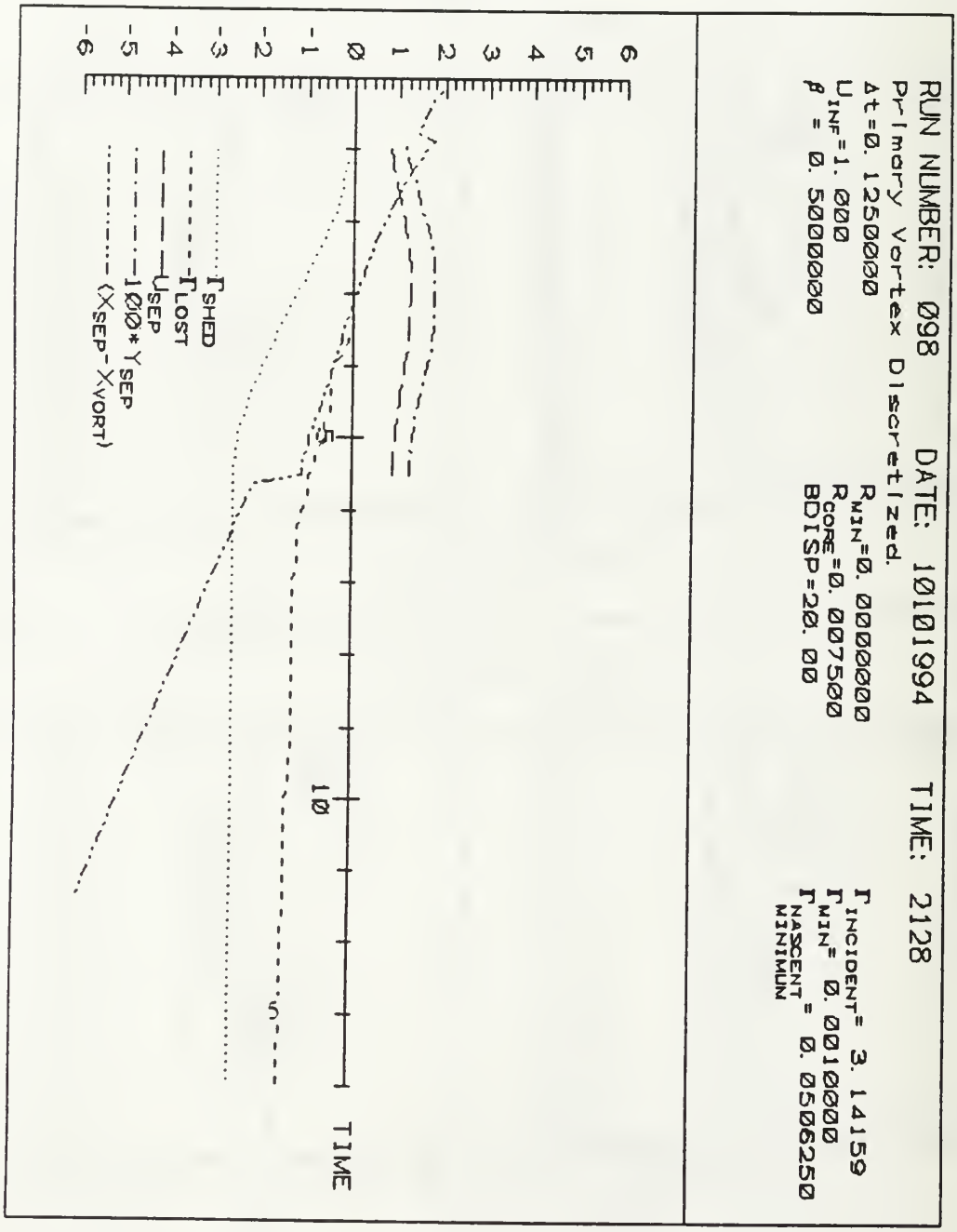


Figure 5.16 Viscous flow with primary vortex:discretized $U_\infty = 1.0$.

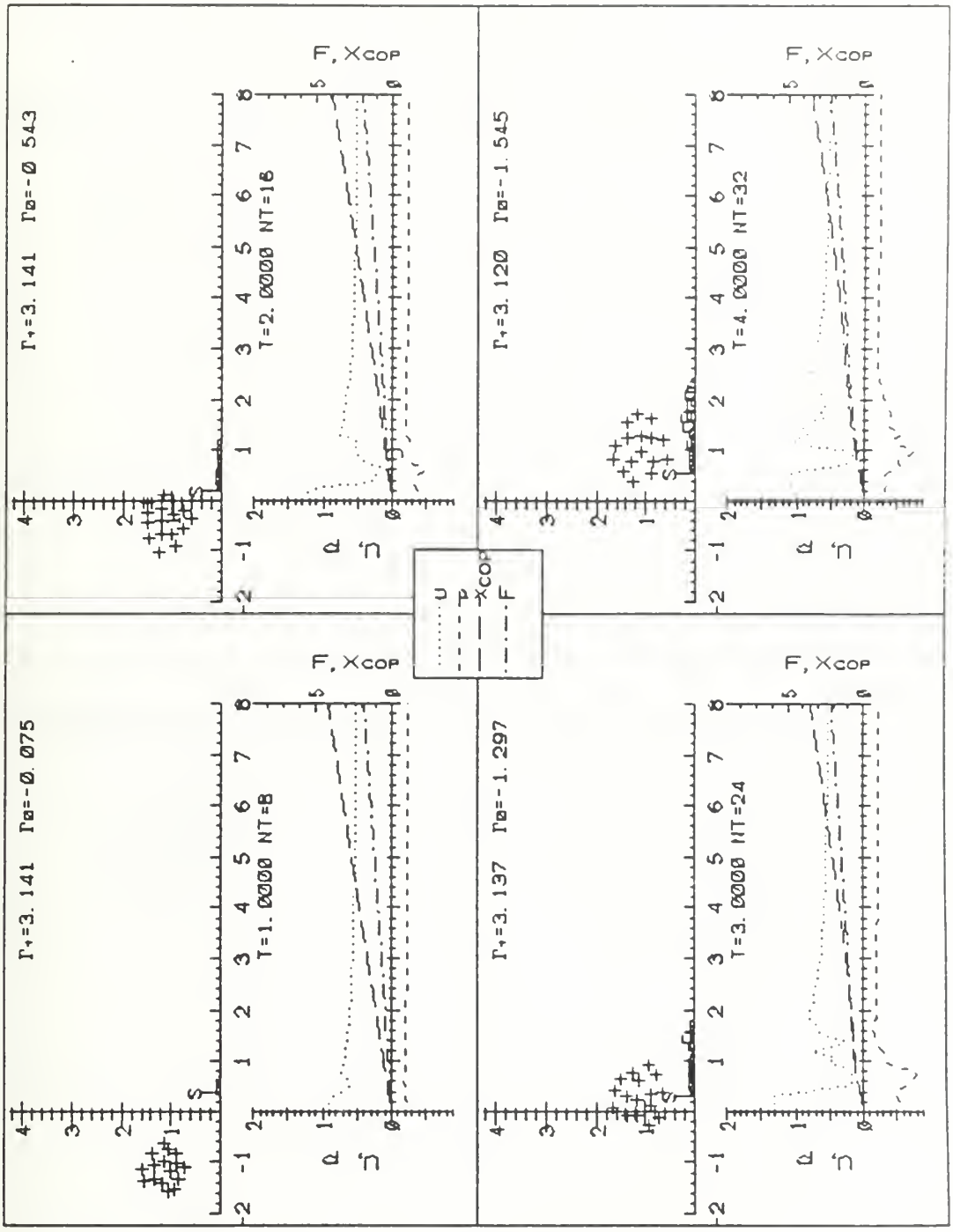


Figure 5.16 (con't.) Viscous flow with primary vortex:discretized $U_\infty = 1.0$.

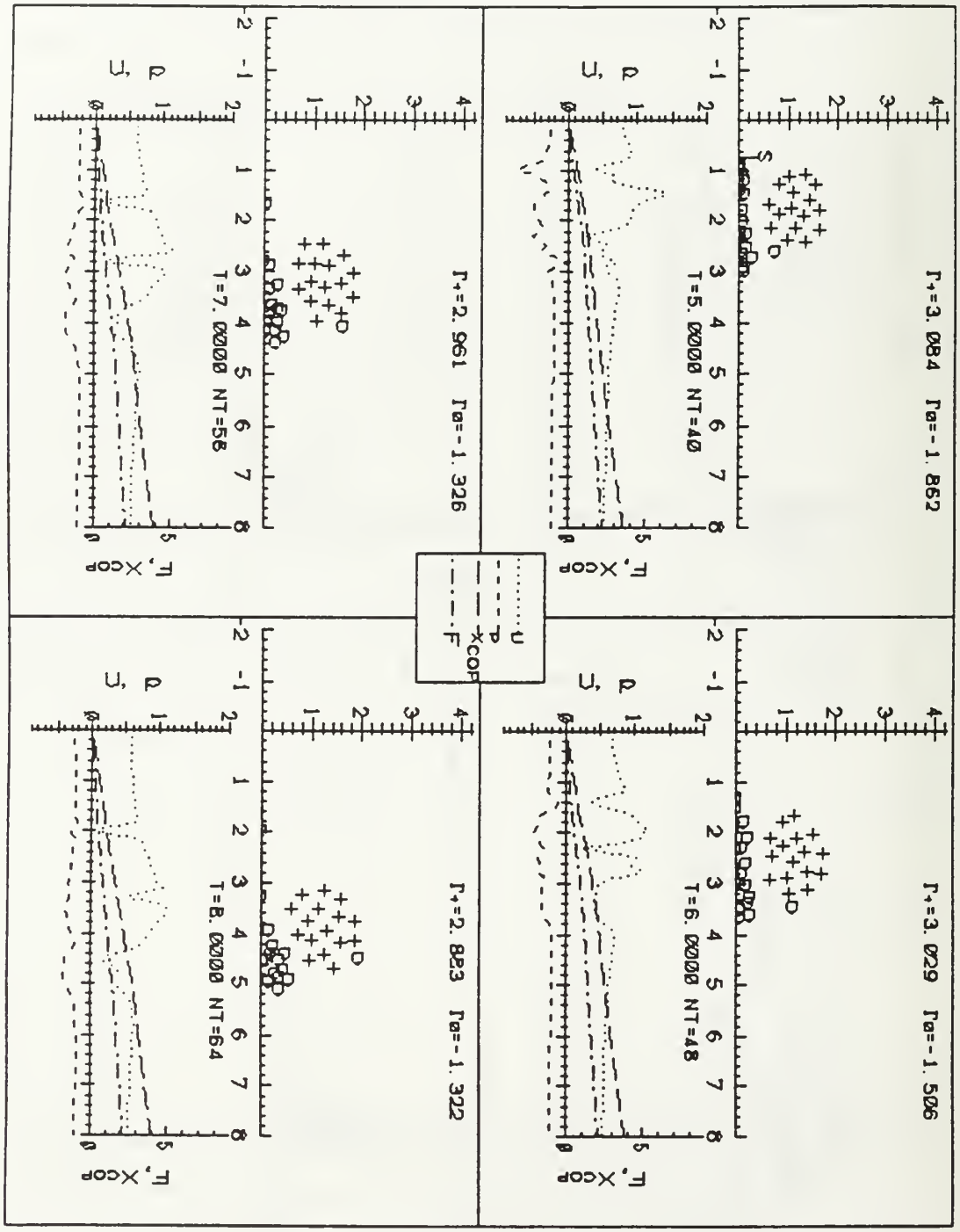


Figure 5.16 (con't.) Viscous flow with primary vortex:discretized $U_\infty = 1.0$.

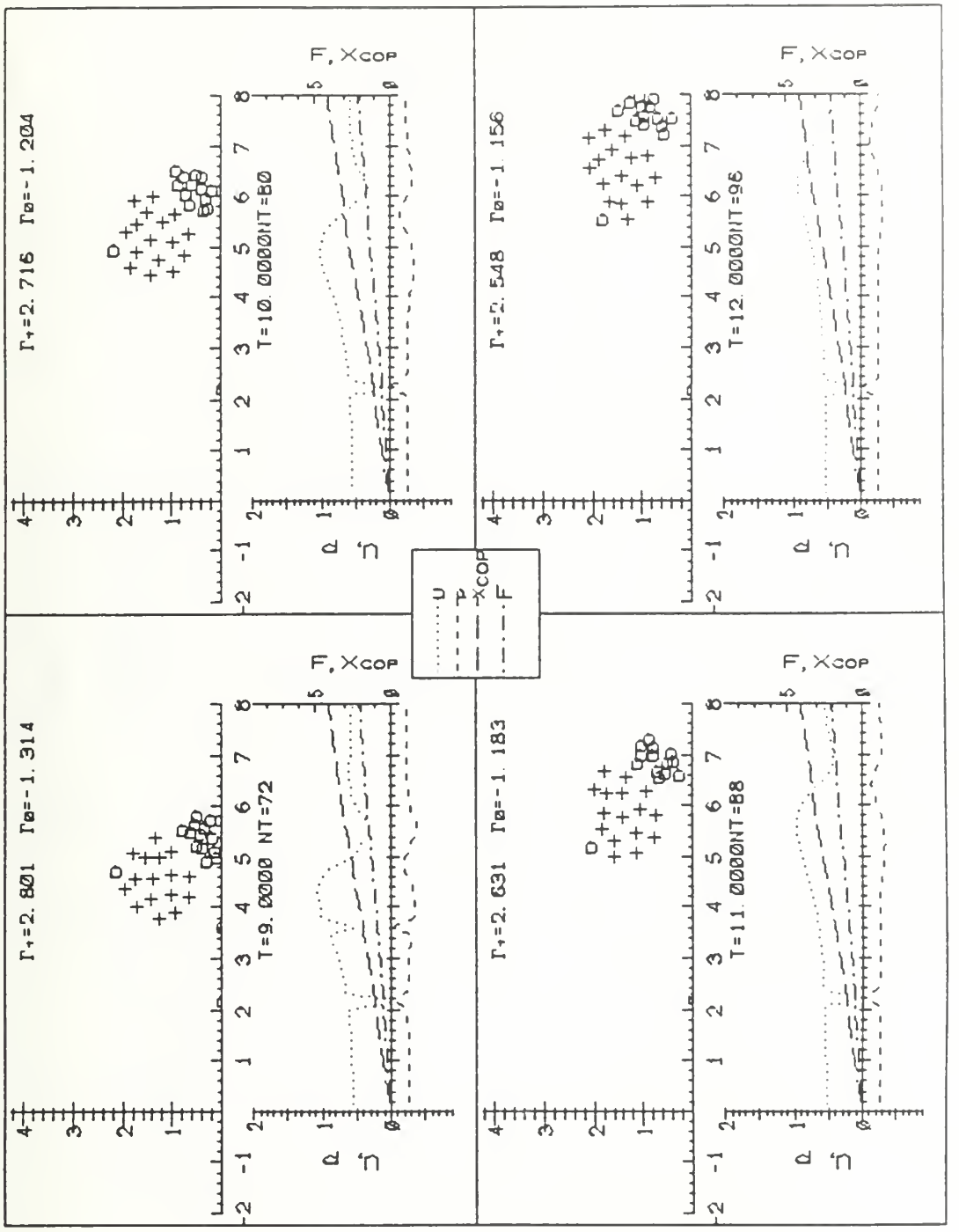


Figure 5.16 (con't.) Viscous flow with primary vortex:discretized $U_\infty = 1.0$.

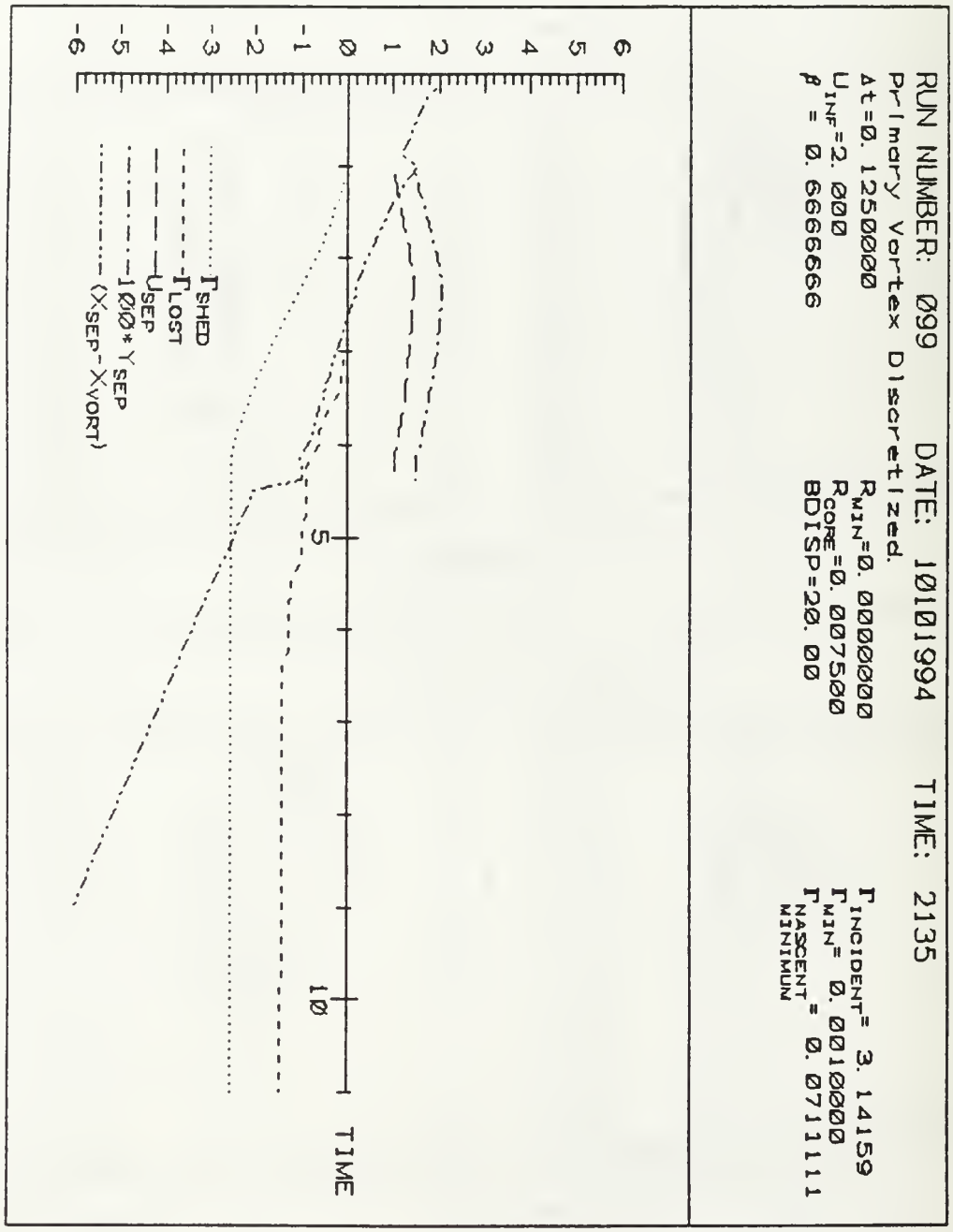


Figure 5.17 Viscous flow with primary vortex:discretized $U_\infty = 2.0$.

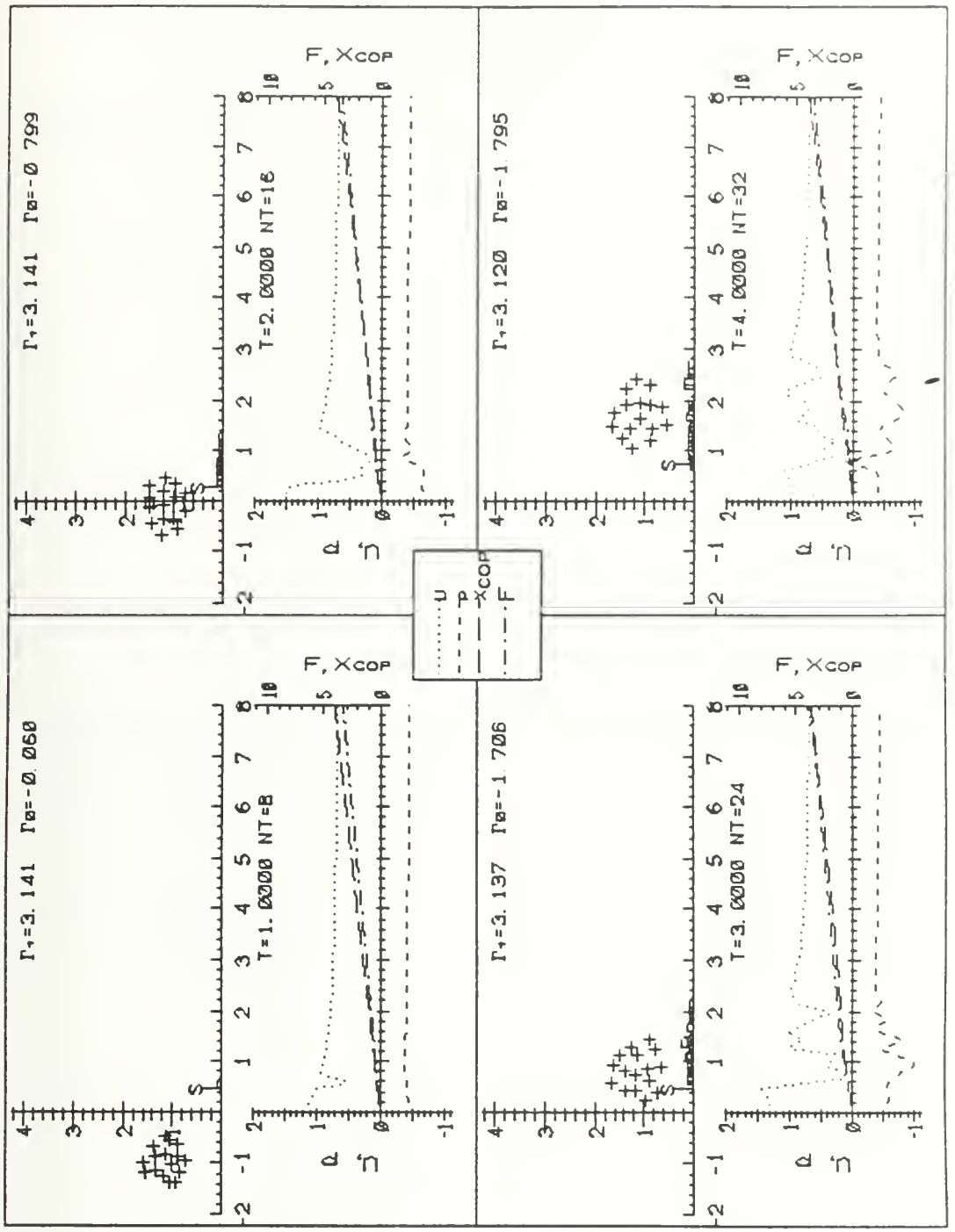


Figure 5.17 (con't.) Viscous flow with primary vortex:discretized $U_\infty = 2.0$.

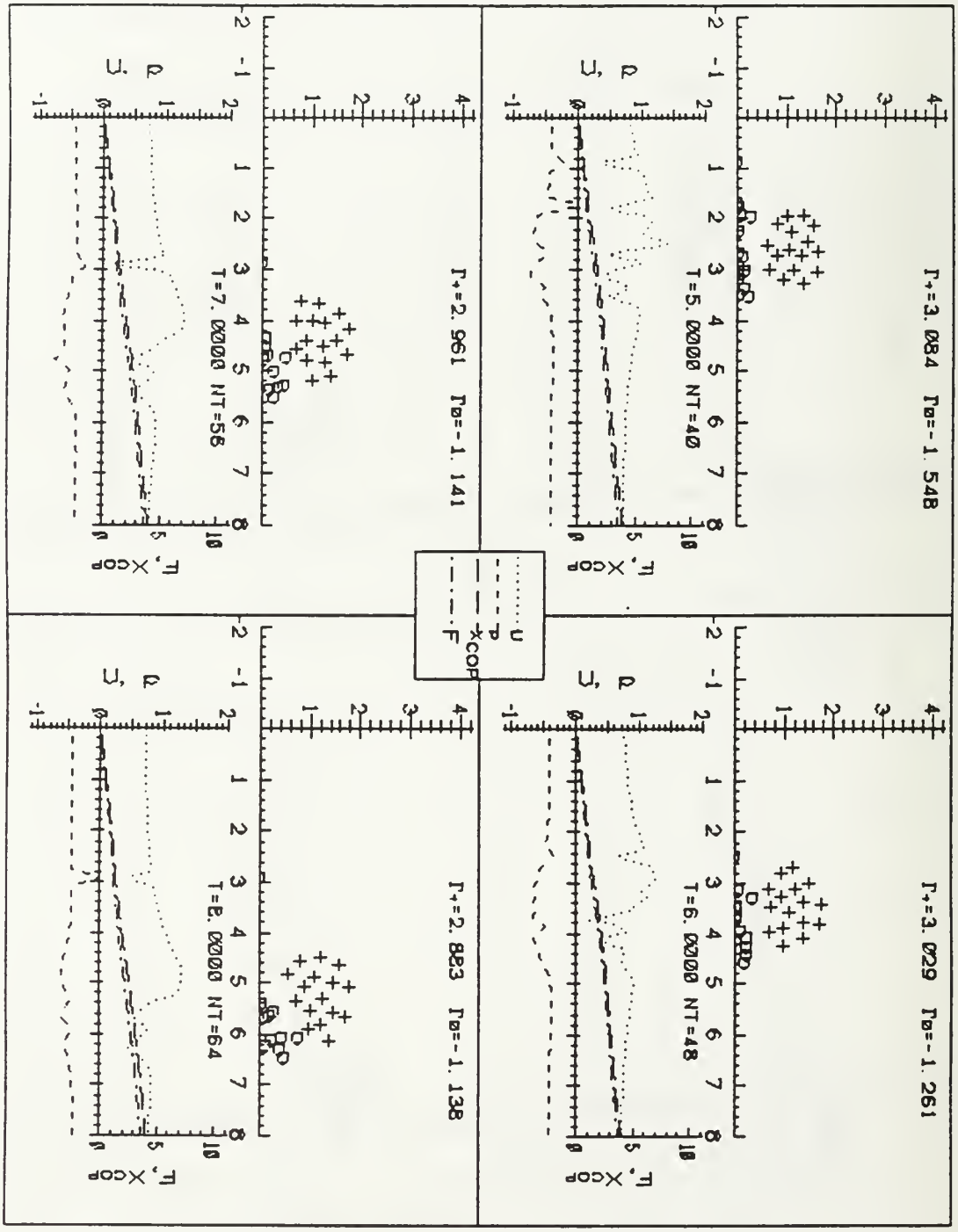


Figure 5.17 (con't.) Viscous flow with primary vortex:discretized $U_\infty = 2.0$.

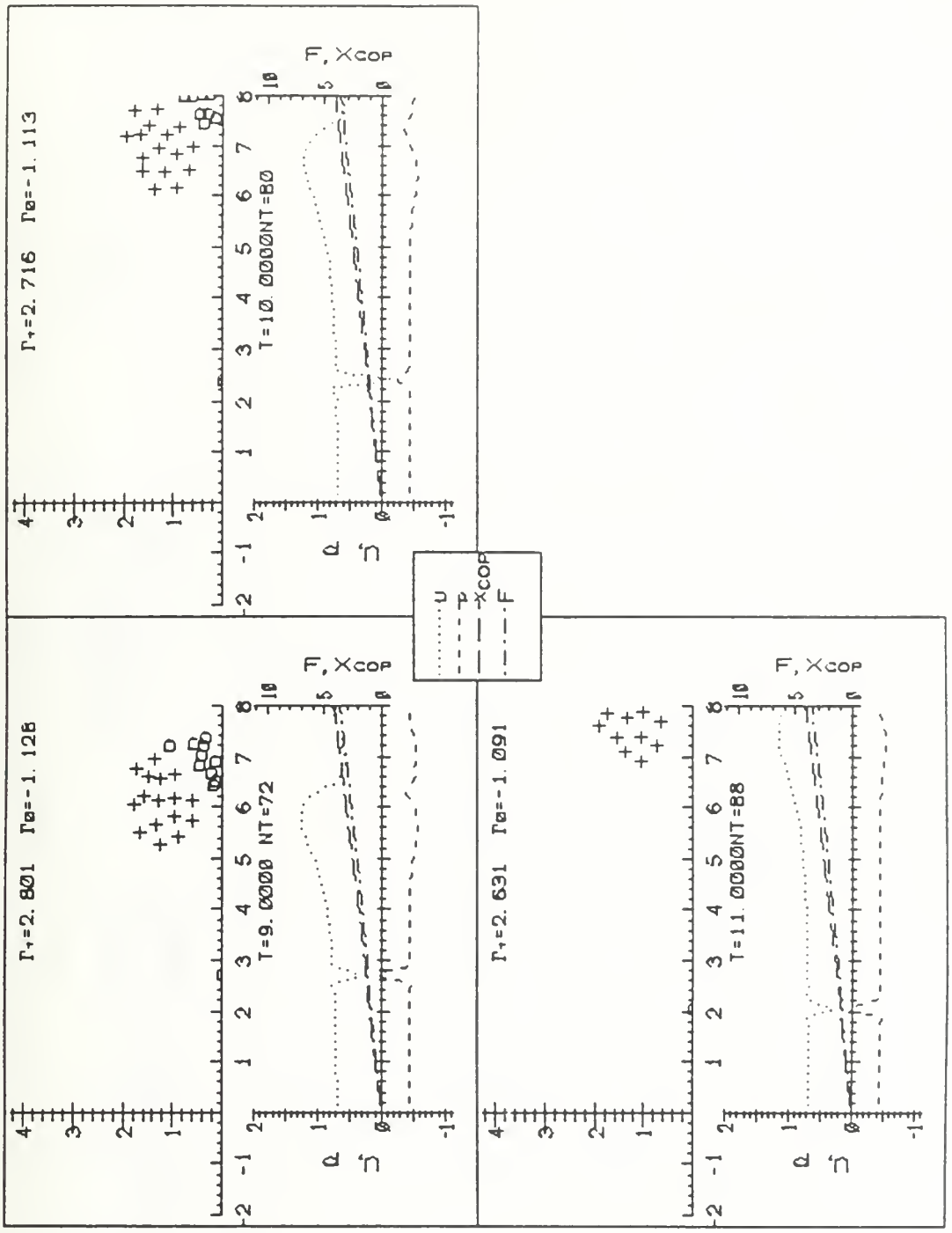


Figure 5.17 (con't.) Viscous flow with primary vortex:discretized $U_\infty = 2.0$.

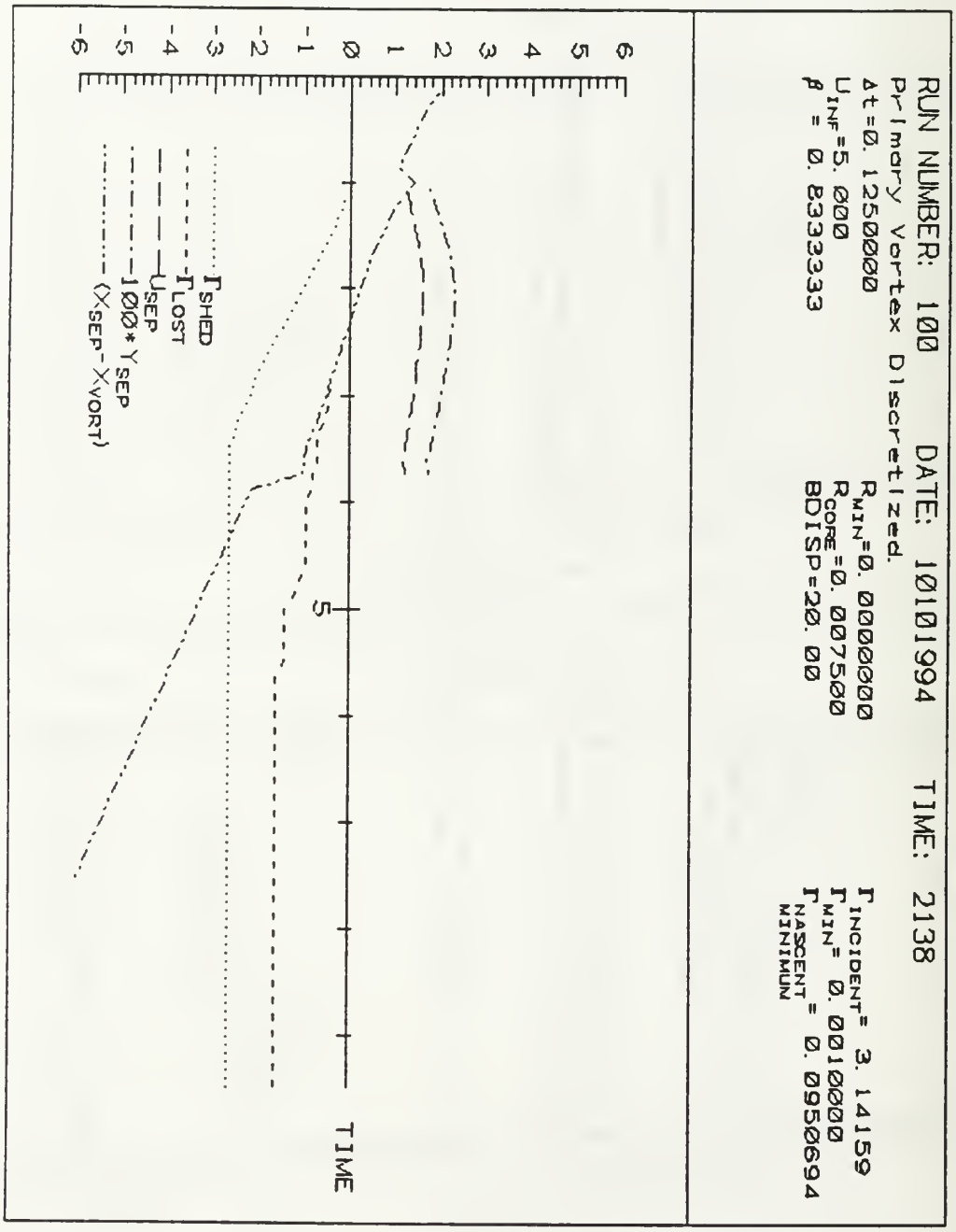


Figure 5.18 Viscous flow with primary vortex:discretized $U_\infty = 5.0$.

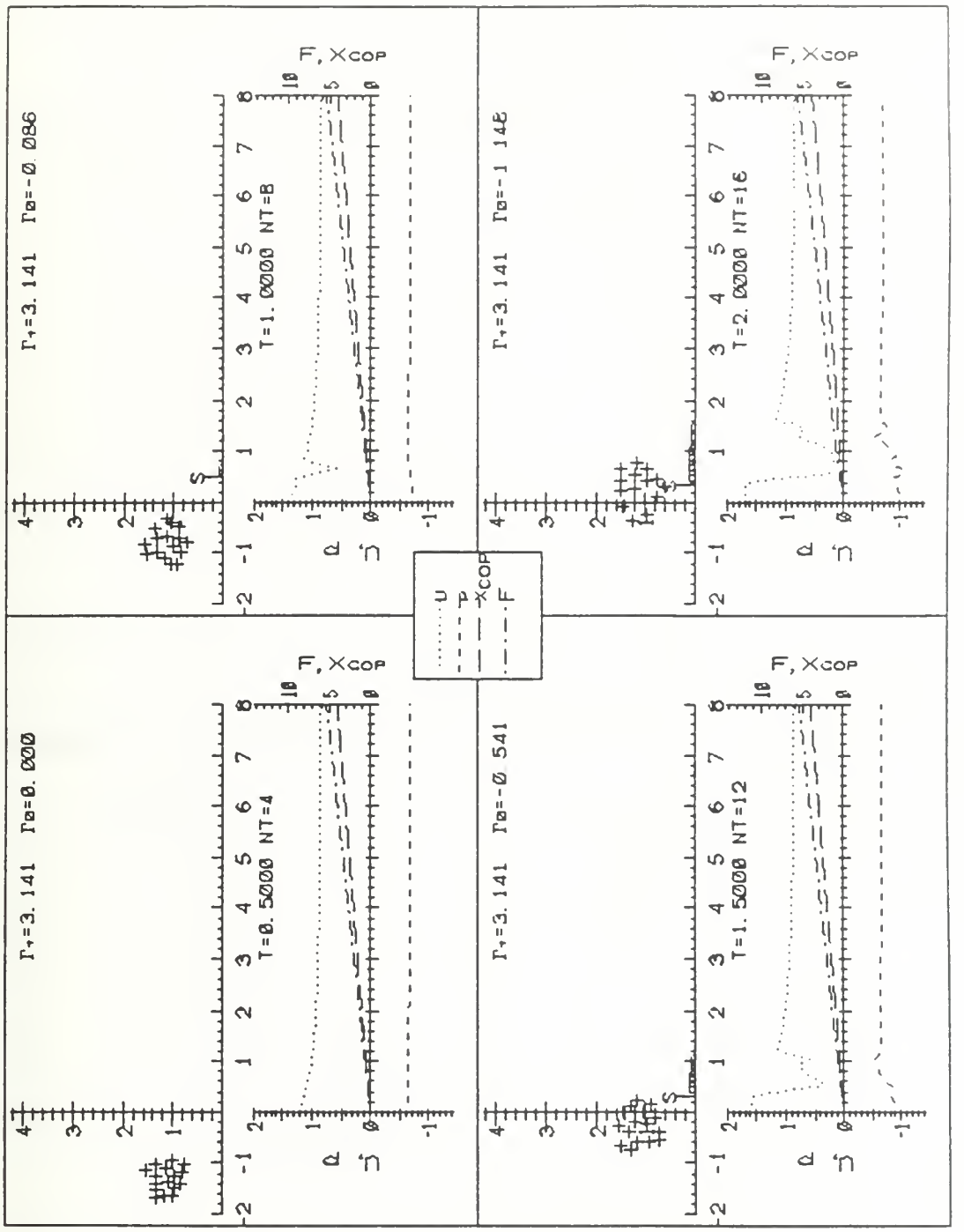


Figure 5.18 (con't.) Viscous flow with primary vortex:discretized $U_\infty = 5.0$.

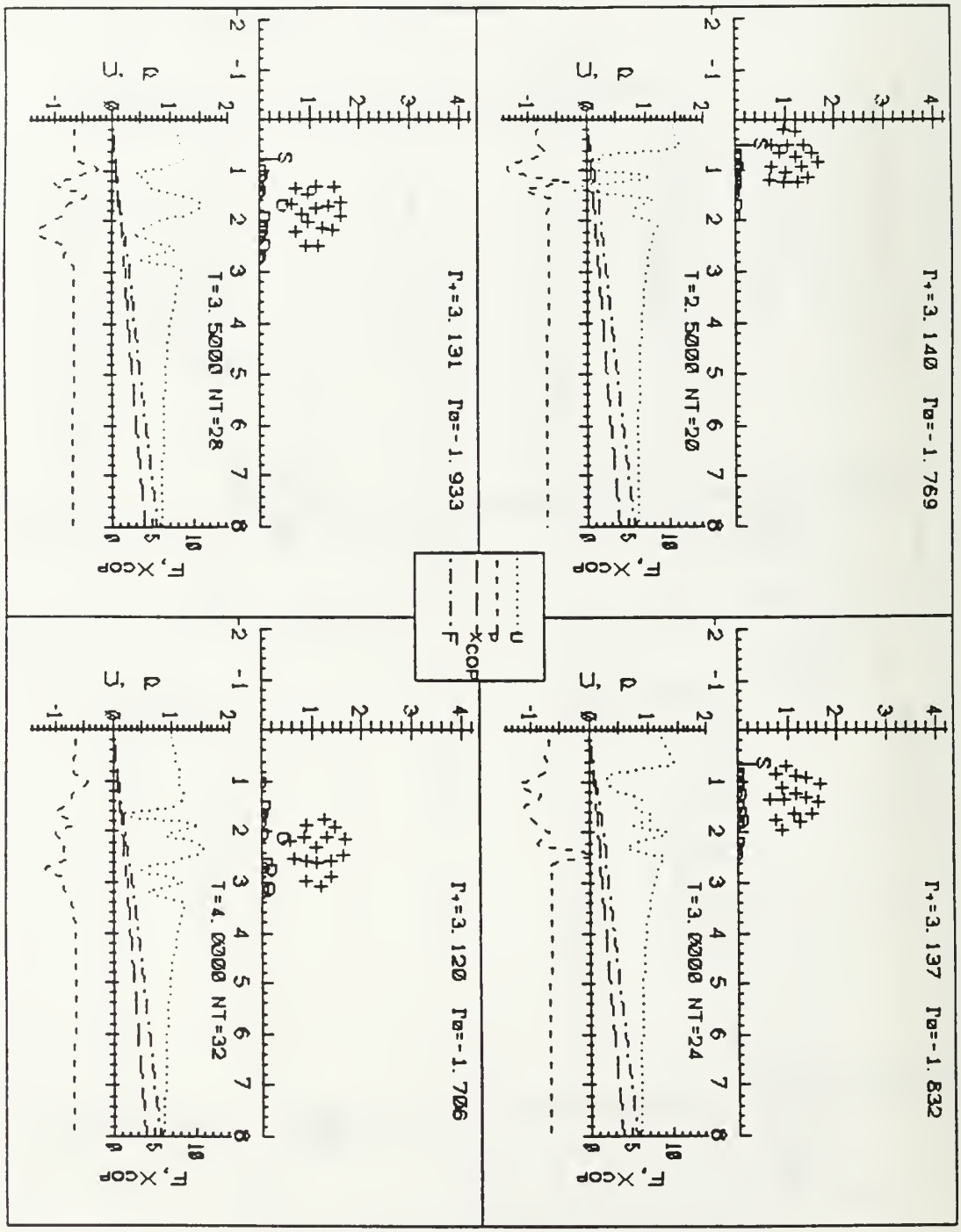


Figure 5.18 (con't.) Viscous flow with primary vortex:discretized $U_\infty = 5.0$.

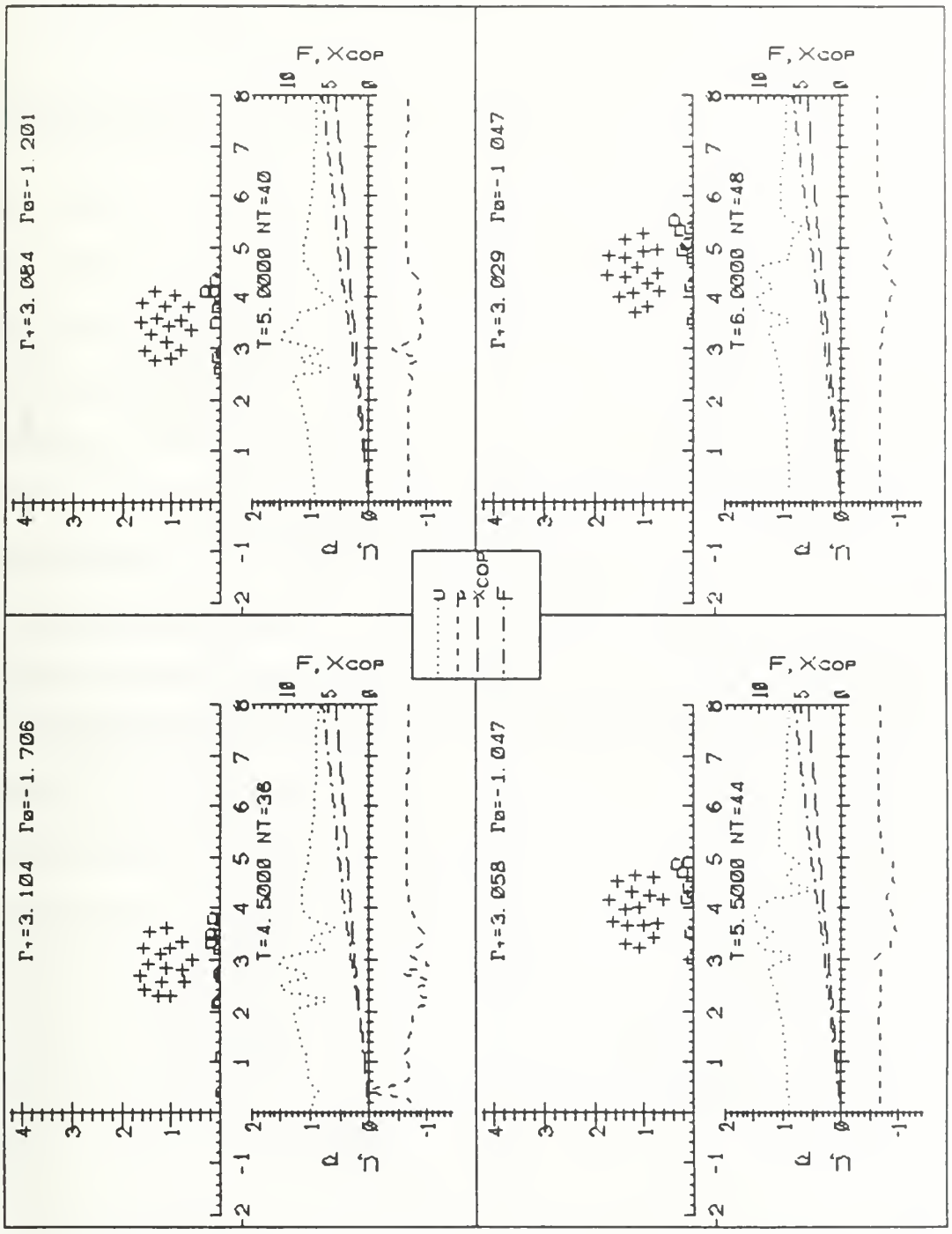


Figure 5.18 (con't.) Viscous flow with primary vortex:discretized $U_\infty = 5.0$.

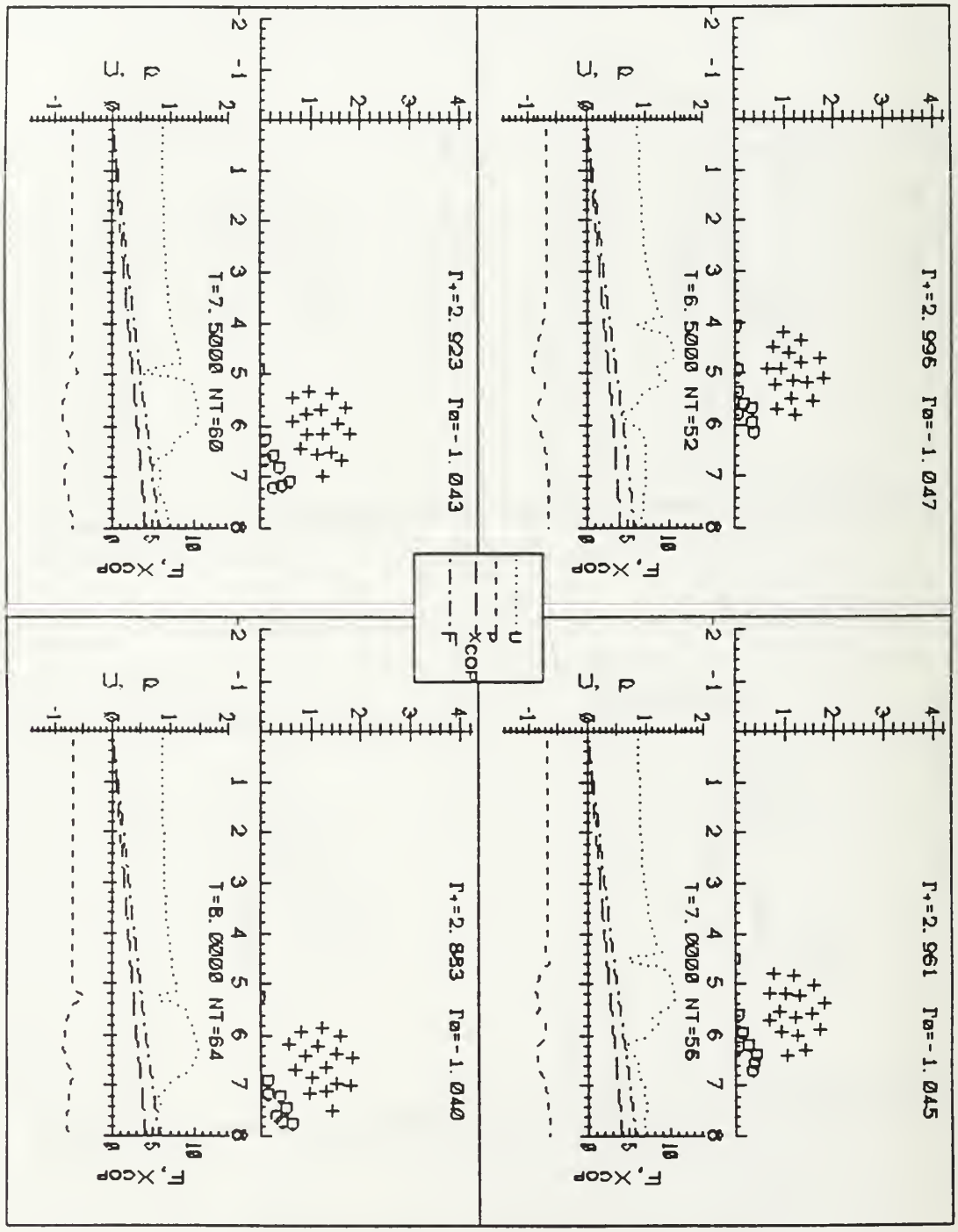


Figure 5.18 (con't.) Viscous flow with primary vortex:discretized $U_\infty = 5.0$.

# VI. CONCLUSIONS

This chapter will synopsize the concluding remarks on harmonic flow (Chapter IV) and blade-vortex interaction (Chapter V), and will suggest areas for further work.

A brief review of the literature has pointed out the strengths and shortcomings of both the finite difference and discrete vortex methods in the solution of unsteady flow problems. Two-dimensional finite difference codes are most appropriate for low Reynolds number flows, but computational constraints, stability problems, and implementation of boundary conditions and artificial viscosity are but a few problems which limit its effectiveness in the analysis of many situations of practical interest. Although the discrete vortex method has been shown to avoid many of these problems, it is not without its own: separation point prediction and the consequent introduction of vorticity, computer time required for convection of the vortices, and the requirements for artificial dissipation.

The discrete vortex method in the harmonic flow application is fraught with difficulties, chief of which is the determination of separation points on bluff bodies. Several boundary layer criteria and ad hoc methods all failed to reproduce the vortex kinematics observed experimentally. It was found that countervorticity was a requirement for the smooth transition in in-line force from one half cycle to the next. Although the model predicted the in-line force reasonably well, the lift force was not in agreement with experimental data. Complex flow instabilities, spanwise coherence, and a host of other problems render high Reynolds number harmonic flow difficult to analyze by any computational method.

At this point, it was realized that the interaction of a vortex with a boundary layer warranted analysis in a much simpler flow situation; the blade-vortex interaction problem proved to be ideal. A boundary layer code which predicted separation on an infinite flat plate under the influence of a line vortex (Sherman [1990]) was adapted to the BVI problem, so that it could be used with a semi-infinite plate in a flow field comprised of a free stream and numerous discrete vortices. Although data are not readily available for the comparison of force and moment data on a semi-infinite flat plate, the kinematics resulting from the interaction of the primary vortex and the shed vorticity are most encouraging. The

kinematics and approximate strengths of the shed vortices are in agreement with the observations of several researchers.

Having illustrated the importance of secondary vorticity and cluster representation of vortical structures, several other areas warrant additional research:

- different boundary layer separation prediction methods.
- effect of different vortex core structure geometries and sizes.
- effect of primary vortices of opposite sense (i.e., clockwise rotation).
- implementation of arrays of approaching primary vortices.
- different surface geometries (finite flat plate, airfoils, etc.) at a variety of angles of attack.
- investigation of direct vortex impingement and subsequent splitting.

It is hoped that by conducting additional work on the BVI, sufficient insight will be gained to provide inroads to the case of harmonic flow about circular cylinders. As with every successful and meaningful implementation of the discrete vortex model, it will have to be tailored for its specific application, taking into account unique aspects of the flow while making a minimum of assumptions.

# APPENDIX A. VORTEX-DRIVEN BOUNDARY LAYERS

## A. INTRODUCTION

The details of the algorithm utilized to predict boundary layer separation in the blade-vortex interaction analyzed in Chapter V are adapted from Sherman [1990]. The FORTRAN code for the basic problem of boundary layer separation on an infinite plate under a stationary vortex is presented in Appendix B of Sherman [1990], and is based on the material presented in Chapters 10 and 12 of the text; the basic differences which are required to modify the procedure for a semi-infinite flat plate are presented in Chapter 12 of his text, along with the results, but no modifications to the FORTRAN code are provided. After modifying the code and verifying its ability to replicate Sherman's tabulated results for a semi-infinite plate, the current analysis incorporates modifications for a vortex moving in a free stream above a semi-infinite flat plate; additionally, a numerical integration technique is utilized to facilitate the evaluation of Thwaites' integral when a field of many vortices is present above the plate. The details of this procedure are presented herein, and a listing of the FORTRAN code is contained in Appendix B.

## B. CLOSED FORM SOLUTION FOR SELF-SIMILAR BOUNDARY LAYERS

The simplest treatment of the problem of a vortex-driven boundary layer begins with the x-momentum equation and the continuity equation:

$$u_{,t}+uu_{,x}+vu_{,y}+p_{,x}=\nu u_{,yy} \tag{A.1}$$

$$u_{,x}+v_{,y}=0 \tag{A.2}$$

Thwaites [1949] related the tangential pressure gradient in the boundary layer to the tangential speed of the external potential flow by the Euler equation

$$p_{,x}=-\left(U_{,t}+UU_{,x}\right), \tag{A.3}$$

and introduced it into the x-momentum equation to obtain

$$u_{,t}+uu_{,x}+vu_{,y}-(U_{,t}+UU_{,x})=\nu u_{,yy} \tag{A.4}$$

Multiplying the continuity equation by u-U, adding it to Equation (A.4), and then integrating from $y = 0$ to $y = \infty$ (with the assumption that $u\text{-}U \to 0$ and $u_{,yy} \to 0$ quickly enough to allow all integrals to possess finite values), Thwaites obtained

$$\left(U\delta^*\right)_{,t} + \left(U^2\theta\right)_{,x} + UU_{,x}\,\delta^* = \frac{\tau_w}{\rho}. \tag{A.5}$$

Here, the following definitions are germane:

$$\text{momentum thickness:} \quad \theta = \int_0^\infty \frac{u}{U}\left(1 - \frac{u}{U}\right) dy \tag{A.6}$$

$$\text{displacement thickness:} \quad \delta^* = \int_0^\infty \left(1 - \frac{u}{U}\right) dy \tag{A.7}$$

$$\text{skin friction:} \quad \tau_w = \mu u_{,y}\,(x,0) \tag{A.8}$$

The dimensionless shape factors $H = \delta^*/\theta$ and $T = \tau_w\theta/\mu U$ do not depend on the thickness of the boundary layer, but rather on the shape of the boundary layer velocity profile. In the most general sense, they are functions of x and t; for the current analysis, $\partial/\partial t = 0$ and $v_w = 0$, so that Equation (A.5) becomes

$$\left(\frac{\theta^2}{\nu}\right)_{,x} + \frac{2}{U}\left[(2+H)U_{,x}\left(\frac{\theta^2}{\nu}\right) - T\right] = 0. \tag{A.9}$$

Were H and T constant, this last equation would be easily integrable, and the analysis would be restricted to boundary layer velocity profiles of constant shape, thus precluding many situations of practical interest. Several researchers noticed, however, that H and T are almost entirely dependent upon the dimensionless quantity $\lambda = U_{,x}\,\theta^2/\nu$. Specifically, Thwaites [1949] noticed that

$$2T - 2(H+2)\lambda = 0.45 - 6.0\lambda \tag{A.10}$$

so that Equation (A.9) becomes

$$\left(\frac{\theta^2}{\nu}\right)_{,x} = \frac{0.45 - 6U_{,x}\,(\theta^2/\nu)}{U} \tag{A.11}$$

$$\frac{\theta^2(x)}{\nu} = C\left[\frac{U(x_0)}{U(x)}\right]^6 + \frac{0.45}{U(x)}\int_{x_0}^{x}\left[\frac{U(x')}{U(x)}\right]^5 dx'. \tag{A.12}$$

Here, $x_o$ is the upstream starting value of x, x′ is a dummy variable of integration, and C is a constant of integration.

For the case of a stationary rectilinear vortex of strength Γ at a distance a above an infinite flat plate (see Figure A.1 ), we have

$$U(\xi) = \frac{\Gamma}{\pi}\frac{1}{\left(1+\xi^2\right)}, \quad \xi = \frac{x}{a} \tag{A.13}$$

The boundary layer starts at $x = -\infty$ where $U(x) = 0$, so that $C = 0$ and, therefore, only the second term of Equation (A.12) is required. If a reference velocity of $U_o = \Gamma/\pi a$ is defined, then we have

$$U(\xi) = \frac{U_0}{1+\xi^2} \tag{A.14}$$

$$U_{,\xi} = -U_0\frac{2\xi}{\left(1+\xi^2\right)^2}. \tag{A.15}$$

Equation (A.12) then becomes

$$\frac{\theta^2 U_0}{\nu a} = \frac{0.45}{384}\xi\left(1+\xi^2\right)^2\left[279+511\xi^2+385\xi^4+105\xi^6+\left(\frac{105}{\xi}\right)\left(1+\xi^2\right)^4\left(\arctan\xi+\frac{\pi}{2}\right)\right] \tag{A.16}$$

For $\xi << -1$, this simplifies to

$$\frac{\theta^2 U_0}{\nu a} \cong -0.050\xi^3\left[1+\frac{21}{11}\xi^{-2}+\ldots\right] \tag{A.17}$$

Additionally, the parameter λ becomes

$$\lambda = -\frac{0.90}{384}\xi^2\left[279+511\xi^2+385\xi^4+105\xi^6+\left(\frac{105}{\xi}\right)\left(1+\xi^2\right)^4\left(\arctan\xi+\frac{\pi}{2}\right)\right] \tag{A.18}$$

and for the region far upstream ($\xi << -1$)

$$\lambda \cong 0.100\left[1-\frac{1}{11}\xi^{-2}+\ldots\right] \tag{A.19}$$

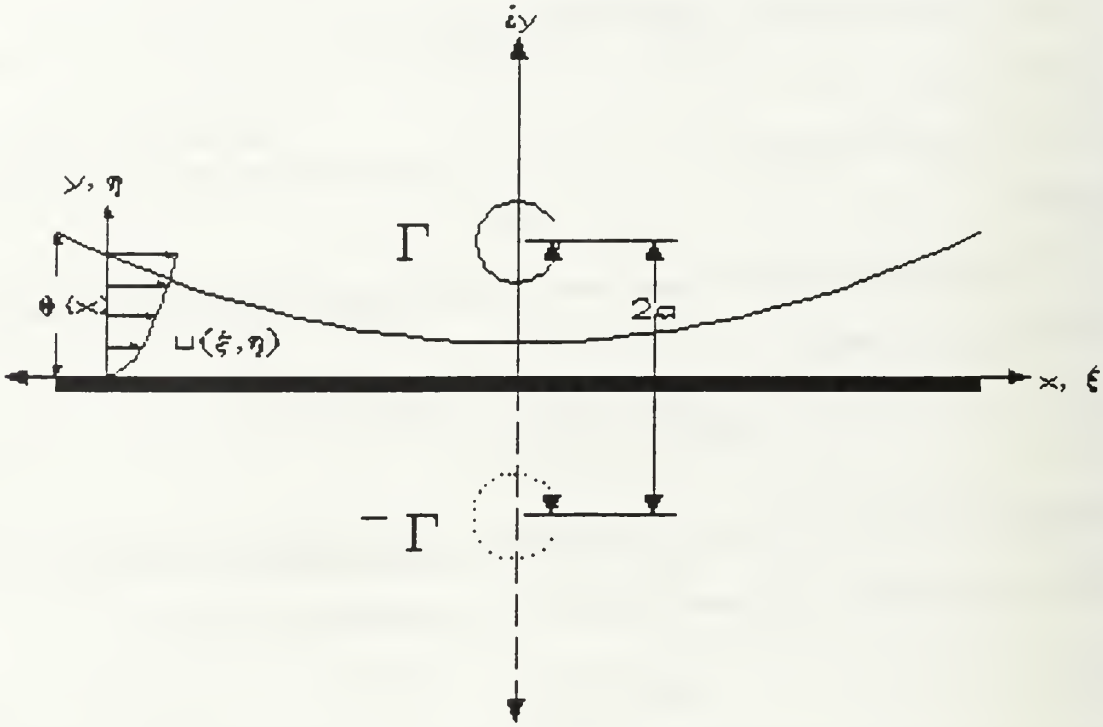


Figure A.1 Boundary layer on an infinite flat plate under the influence of a stationary line vortex (not to scale).

Directly beneath the vortex ($\xi = 0$), we have $\theta^2 U_o / \nu a = 0.194$; $\theta_{min}$ is reached at $\xi = -0.429$, where $U(\xi) = 0.845\ U(0)$. Most importantly, separation occurs at $\xi_{sep} = 0.157$, where $U(\xi) = 0.976\ U(0)$[1]. We have thus arrived at a first estimate at predicting separation, albeit beneath a stationary vortex over an infinite flat plate, with the relatively crude assumption of a self-similar boundary layer velocity profile.

## C. NUMERICAL SOLUTION OF NONSIMILAR BOUNDARY LAYERS OVER AN INFINITE FLAT PLATE

This section will describe the numerical technique employed by Sherman [1990] to allow for nonsimilar boundary layer velocity profiles; the following sections will then concern themselves with the

[1] Utilizing curve fits, White[1986] showed that shear stress disappears for $\lambda = -0.09$, which is the cirterion for predicting separation.

modifications required to analyze semi-infinite flat plates. Finally, a free stream and multiple vortices are introduced, and the code validation is described.

Beginning with the boundary-layer equations (Equations (A.1) and (A.2)), we introduce dimensionless, scaled variables $\xi = \xi(x)$ and $\eta = \eta(x, y) = y/g(x)$, where $g(x)$ is a measure of local boundary layer thickness. Also of use is the definition of a scaled, dimensionless stream function $f(\xi, \eta)$,

$$\Psi(x,y) = Q(x)\, f(\xi,\eta) \tag{A.20}$$

where $Q(x) = U(x)\, g(x)$ may be likened to the flow in the boundary layer at a particular streamwise station at x. We now use an asterisk to denote physical velocity components (primes connote derivatives with respect to x, except that $f' = f_{,\eta}$):

$$u^* = Uf' \tag{A.21}$$

$$v^* = -Ug\left[f_{,\xi}\,\xi' + f'\eta_{,x} + (\ln Q)'\, f\right] \tag{A.22}$$

$$u^*_{,x} = U\left[f'_{,\xi}\,\xi' + f''\eta_{,x}\right] + f'U' \tag{A.23}$$

$$u^*_{,y} = \frac{Uf''}{g} \tag{A.24}$$

$$u^*_{,yy} = \frac{Uf'''}{g^2} \tag{A.25}$$

Substituting Equations (A.21) through (A.25) into Equation (A.1), the steady form of the x-momentum equation becomes

$$u'' + \gamma(\xi)u'f + \delta(\xi)\left(1-u^2\right) = \psi(\xi)\left[uu_{,\xi} - u'f_{,\xi}\right] \tag{A.26}$$

where the $\xi$-dependent coefficients are defined as

$$\gamma = \frac{g^2U}{\nu}(\ln Q)' \qquad \delta = \frac{g^2U}{\nu}(\ln U)' \qquad \psi = \frac{g^2U}{\nu}\xi' \tag{A.27}$$

We note here that $\gamma$ is proportional to the percentage rate of increase of the nominal flowrate in the boundary layer, and $\delta$ is proportional to the percentage rate of increase of U. Note also that $\psi$ is not the same as the stream function, $\Psi$. Finally, Equation (A.26) is subject to the following boundary conditions:

$$\text{no slip:} \quad u(\xi,0) = 0$$

$$\text{matching (outer) potential flow:} \quad u(\xi,\infty) = 1 \tag{A.28}$$

$$\text{impermeable wall:} \quad f(\xi,0) = 0.$$

Having transformed the boundary layer equations through this change of variables, it is now a matter of choosing the most appropriate forms for $\xi$ and $\eta$. Before the advent of computers, the choice of $\xi$ and $\eta$ usually was made to show that two apparently different boundary layer problems could be transformed into the same mathematical formulation. With the rise of finite difference techniques, the impetus turned to transformations which retained the boundary layer's natural growth; the computer was then left to account for minor changes in the boundary layer velocity profiles. To balance programming considerations and accurate boundary layer velocity profile portrayal, Sherman [1990] chose to set g proportional to boundary layer thickness and $\xi$ proportional to streamwise distance, x:

$$g(x) = A\,\theta(x) \qquad\qquad \xi(x) = \frac{x}{a} \tag{A.29}$$

The choice of the constant A determines the range of $\eta$ which will be considered by the computer code. The solution is iterative, and will begin with an initial profile which corresponds to a self-similar solution; it will, therefore, be most convenient to use the value of A which will give give the coefficients $\gamma$ and $\delta$ initial values which will make the initial profile numerically identical to the self-similar solution.

Using Thwaites' approximation (Equations (A.10) and (A.11)), we obtain

$$\left(\frac{g^2}{\nu}\right)' = \frac{0.45\,A^2 - 6(g^2/\nu)U'}{U}, \tag{A.30}$$

which can be used in conjunction with Equations (A.27) to obtain

$$\delta = \frac{g^2 U'}{\nu} = A^2\lambda \qquad\qquad \gamma = 0.225\,A^2 - 2\delta \tag{A.31}$$

For self-similar boundary layers, u ($\xi$ , $\eta$) would reduce to a function of $\eta$ alone, and both $\gamma$ and $\delta$ would be independent of x. The initial velocity profile chosen to begin the numerical procedure should be

identical to the solution of the ordinary differential equation obtained when the right hand side of Equation (A.26) is set equal to zero. A somewhat incorrect initial profile may be tolerated, however, if the calculations are commenced sufficiently far upstream, and the outer flow is an accelerating potential flow which allows the initial conditions to be forgotten.

The more general case of Falkner-Skan flows involves boundary layers which begin at $x = 0$ and grow continuously thereafter, so that Q is monotonically increasing with x, and $\gamma$ is positive. Recall that the arbitrary constant, A, was involved in the definition of the function g (x) to adjust the range of $\eta$-values used in the boundary layer calculations; from Equations (A.27), it can be seen that the choice of A directly influences the values of $\gamma$, $\delta$, and $\psi$. It will turn out that it is most convenient to choose A so that $\gamma = 1$. The shape of the boundary layer velocity profile is determined by the ratio of $\gamma$ to $\delta$, which is found to be

$$\frac{\gamma}{\delta} = \frac{(\ln Q)'}{(\ln U)'} = 1 + \frac{Ug'}{U'g} \tag{A.32}$$

For the Falkner-Skan family, we also have

$$U(x) \propto x^{m} \qquad\qquad g(x) \propto x^{(1-m)/2} \tag{A.33}$$

which, if $\gamma$ is set equal to unity, results in

$$\delta = \frac{2\,m}{1+m} \tag{A.34}$$

The classic case of the Blasius boundary layer on a flat plate is obtained from this last set of equations if m is set equal to 0, resulting in $\delta = 0$ and $\gamma = 1$.

The vortex-driven boundary layer, however, is born at $x = -\infty$, and begins to ingest fluid with increasing x, so that $\gamma$ is positive. The boundary layer is only asymptotically self-similar, in the region where $(-x/a) >> 1$, so that $(\ln U)' = -2/\xi$ and $(\ln Q)' = -1/2\xi$. Again, choosing A such that $\gamma = 1$ results in a value of $\delta = 4$. In fact, although its physical origins are different, the vortex-driven boundary layer is mathematically a member of the Falkner-Skan family.

Returning to the nonsimilar boundary layer, we recall that, at large negative values of x, the shape-determining factor $\lambda = U_x\theta^2/\nu$ approaches a constant value in the integral-momentum analysis. It is, therefore, reasonable to expect that a Falkner-Skan type profile can be used as a close approximation to the boundary layer at large, but finite values of x, with $\gamma = 1$ and $\delta = 4$. To confirm this, a power-series expansion will be employed to prove that the calculations may commence with a similarity solution. Recalling the series expansion for $\lambda$ at far upstream conditions (Equation (A.19)) and choosing $A^2 = 40$, we find that Equations (A.27 ) become

$$\delta = 4 - \frac{4}{11}\xi^{-2} + \ldots \qquad \gamma = 1 + \frac{8}{11}\xi^{-2} + \ldots \qquad \psi = -2\xi - \frac{20}{11}\xi^{-1} + \ldots \tag{A.35}$$

It is seen that at far upstream conditions, the values of $\gamma$ and $\delta$ approach constant values (a necessary condition for the existence of a self-similar solution), but $\psi \to \infty$. It is, therefore, necessary to show that the right hand side of Equation (A.26 ) vanishes as $\xi \to -\infty$, so that it will be permissible to solve ordinary differential equations in calculating starting profiles of f and u.

To this end, a Blasius (power) series expansion (see Schlichting [1968] ) will be assumed to represent f and u

$$\begin{aligned} f(\xi,\eta) &= f_0(\eta) + f_1(\eta)\xi^{-2} + \ldots \\ u(\xi,\eta) &= u_0(\eta) + u_1(\eta)\xi^{-2} + \ldots \end{aligned} \tag{A.36}$$

so that

$$\begin{aligned} f_{,\xi} &= -2 f_1(\eta)\xi^{-3} + \ldots \\ u_{,\xi} &= -2 u_1(\eta)\xi^{-3} + \ldots \end{aligned} \tag{A.37}$$

Inserting Equations (A.35) through (A.37) into Equation (A.26), and evaluating the resulting expression in the limit of $\xi \to -\infty$, the result obtained is precisely that for the self-similar solution (e.g., Equation (A.26) with the right hand side set equal to zero):

$$u_0'' + f_0 u_0' + 4\left(1 - u_0^2\right) = 0 \qquad\qquad f_0' = u_0$$

subject to (A.38)

$$f_0(0) = 0 \qquad\qquad u_0(0) = 0 \qquad\qquad u_0(\infty) = 1.$$

Next, we investigate the terms which are coefficients of $\xi^{-2}$, which results in the boundary value problem

$$u_1'' + f_0 u_1' - 12\, u_0 u_1 + 5\, u_0' f_1 = -\frac{8}{11} f_0 u_0' + \frac{4}{11}\left(1 - u_0^2\right) \qquad\qquad f_0' = u_0$$

subject to (A.39)

$$f_1(0) = 0 \qquad\qquad u_1(0) = 0 \qquad\qquad u_1(\infty) = 0.$$

The Blasius series representation has led to a well-defined series of boundary value problems (Equations (A.38) and (A.39)), so that it would appear that this will be useful. It is assumed that the two-term solution resulting from these equations will provide a reasonable degree of accuracy when a starting value of, say, $\xi_0 = -10$ is chosen to begin the calculations.

What is required next is a scheme which can be used to represent $u_{,\xi}(\xi, \eta)$ and $f_{,\xi}(\xi, \eta)$ for boundary layers which develop in a decelerating potential outer flow, and which are, therefore, exceedingly sensitive to their upstream histories. A second-order formula which lends itself to easy implementation with the above linearization process is the three-point trailing difference formula of the form

$$u_{,\xi}(\xi, \eta) = au(\xi, \eta) + bu(\xi - d\xi_1, \eta) + cu(\xi - d\xi_1 - d\xi_2, \eta) \tag{A.40}$$

For upstream calculations, a constant value of $d\xi$ may be utilized, so that (a, b, c) = (3, -4, 1)/2$d\xi$. As the calculations near the separation point, $d\xi$ is successively halved, so that $d\xi_1 = ½ d\xi_2$, and (a, b, c) = (8, -9, 1)/6$d\xi_1$.

The right-hand side of Equation (A.26) also requires linearization. We begin by noting that

$$\begin{aligned} u &= u^* + (u - u^*) \\ f &= f^* + (f - f^*), \end{aligned} \tag{A.41}$$

where the asterisked quantities denote approximate values. When squaring these last two equations and dropping higher order terms, we obtain

$$u^2 \approx 2uu^* - u^{*2}$$
$$v^2 \approx 2vv^* - v^{*2}. \tag{A.42}$$

Using these, the following components of Equation (A.26) are obtained:

$$uu_{,\xi} \approx u(\xi,\eta)\left[2au^*(\xi,\eta) + bu(\xi - d\xi_1,\eta) + cu(\xi - d\xi_1 - d\xi_2,\eta)\right] - au^{*2}(\xi,\eta) \tag{A.43}$$

$$u'f \approx -u'^*f^* + fu'^* + f^*u' \tag{A.44}$$

$$\begin{aligned} u'f_{,\xi} \approx\ & u'(\xi,\eta)\left[af^*(\xi,\eta) + bf(\xi - d\xi_1,\eta) + cf(\xi - d\xi_1 - d\xi_2,\eta)\right] \\ & + au'^*(\xi,\eta)f(\xi,\eta) - au'^*(\xi,\eta)f^*(\xi,\eta) \end{aligned} \tag{A.45}$$

$$\delta(1-u^2) \approx \delta(1+u^{*2}) - 2\delta u^* u \tag{A.46}$$

Inserting all of these into Equation (A.26) results in

$$\begin{aligned} u'' + u'\left[\gamma f^* + \psi(af^* + bf^- + cf^=)\right] + u\left[-2\delta u^* - \psi(2au^* + bu^- + cu^=)\right] + f\left[u'\gamma + u'^*\psi\right] = \\ -\delta(1+u^{*2}) + \gamma u'^*f^* - a\psi u^{*2} + \psi af^*u'^* \end{aligned} \tag{A.47}$$

where the following shorthand has been employed:

$$\begin{aligned} u^- &= u(\xi - d\xi_1,\eta) & f^- &= f(\xi - d\xi_1,\eta) \\ u^= &= u(\xi - d\xi_1 - d\xi_2,\eta) & f^= &= f(\xi - d\xi_1 - d\xi_2,\eta). \end{aligned} \tag{A.48}$$

Equation (A.47) is of the form

$$u'' + u'r_n + us_n + fw_n = t_n \tag{A.49}$$

where

$$r_n = \gamma f^* + \psi(af^* + bf^- + cf^=) \tag{A.50}$$

$$s_n = -2\delta u^* - \psi(2au^* + bu^- + cu^=) \tag{A.51}$$

$$w_n = u'^*(\gamma + a\psi) \tag{A.52}$$

$$t_n = \gamma u'^* f^* - \delta(1 + u^{*2}) + \psi a(u'^* f^* - u^{*2}) \tag{A.53}$$

and the following boundary conditions apply:

$$u(0) = 0 \qquad u(\infty) = 1 \qquad f(0) = 0. \tag{A.54}$$

In conjunction with $f' = u$, we now have a pair of coupled equations which may be solved numerically.

With central differences, the first of these two (Equation (A.49)) becomes

$$\frac{u_{n+1} - 2u_n + u_{n-1}}{h^2} + r_n \frac{u_{n+1} - u_{n-1}}{2h} + s_n u_n + w_n f_n = t_n \tag{A.55}$$

$$u_{n-1}\left[\frac{1}{h^2} - \frac{r_n}{2h}\right] + u_n\left[-\frac{2}{h^2} + s_n\right] + u_{n+1}\left[\frac{1}{h^2} + \frac{r_n}{2h}\right] + f_{n-1}[0] + f_n\left[w_n\right] + f_{n+1}[0] = t_n \tag{A.56}$$

$$A_{11} \qquad B_{11} \qquad C_{11} \qquad A_{12} \qquad B_{12} \qquad C_{12} \quad D_1$$

and the second equation becomes

$$u - f' = 0 \tag{A.57}$$

$$\frac{u_{n-1} + u_n}{2} - \frac{f_n - f_{n-1}}{h} = 0 \tag{A.58}$$

$$u_{n-1}\left[\frac{1}{2}\right] + u_n\left[\frac{1}{2}\right] + u_{n+1}[0] + f_{n-1}\left[\frac{1}{h}\right] + f_n\left[-\frac{1}{h}\right] + f_{n+1}[0] = 0. \tag{A.59}$$

$$A_{21} \qquad B_{21} \qquad C_{21} \qquad A_{22} \qquad B_{22} \qquad C_{22} \quad D_2$$

Here, $h = \Delta\eta$. Also, central differences were not used in the finite difference representation of the second equation since that would have involved a term $f_{n+1}$, which, at the outer limit of the boundary layer, is not known.

These two finite difference equations are of the form

$$A\hat{y}_{n-1} + B\hat{y}_n + C\hat{y}_{n+1} = \hat{D}, \tag{A.60}$$

where A, B, and C are 2 x 2 coefficient matrices, and the $\hat{y}_i$ are two-element column vectors:

$$A = \begin{bmatrix} A_{11} & A_{12} \\ A_{21} & A_{22} \end{bmatrix} \qquad \hat{y}_n = \begin{Bmatrix} u_n \\ f_n \end{Bmatrix}. \tag{A.61}$$

These equations can be solved with the triangularization and back-substitution of the Thomas algorithm (see, e.g., Gerrard [1978] ). A back-substitution formula of the form

$$\hat{y}_n = E_n \hat{y}_{n+1} + \hat{F}_n \tag{A.62}$$

will be employed; when this is written for $\hat{y}_{n-1}$ and inserted into Equation (A.60), we obtain

$$(A_n E_{n-1} + B_n)\hat{y}_n = -C_n \hat{y}_{n+1} + (\hat{D}_n - A_n \hat{F}_{n-1}). \tag{A.63}$$

Next, Equation (A.62) is multiplied by $(A_n E_{n-1} + B_n)$, resulting in

$$(A_n E_{n-1} + B_n)\hat{y}_n = (A_n E_{n-1} + B_n)E_n \hat{y}_{n+1} + (A_n E_{n-1} + B_n)\hat{F}_n. \tag{A.64}$$

Comparing Equations (A.63) and (A.64), the $E_n$ and $\hat{F}_n$ are obtained by equating like terms:

$$(A_n E_{n-1} + B_n)E_n = -C_n \qquad\qquad (A_n E_{n-1} + B_n)\hat{F}_n = \hat{D}_n - A_n \hat{F}_{n-1} \tag{A.65}$$

If the order of the coefficient matrix were two or three, Cramer's Rule could be utilized. For more realistic problems where many stations are utilized across the boundary layer velocity profile, a Gauss-Jordan matrix inversion routine is more expedient. In fact, 81 stations were found to be the minimum number of stations across the boundary layer required to maintain reasonable accuracy. Let $G = A_n E_{n-1} + B_n$ so that Equation (A.65) may be recast as

$$E_n = -G^{-1} C_n \qquad\qquad \hat{F}_n = G^{-1}(\hat{D}_n - A_n \hat{F}_{n-1}). \tag{A.66}$$

Here, G has four components, and the components of $G^{-1}$ are

$$G_{11}^{-1} = \frac{G_{22}}{G_{11}G_{22} - G_{12}G_{21}} \qquad G_{12}^{-1} = \frac{-G_{12}}{G_{11}G_{22} - G_{12}G_{21}}$$

$$G_{21}^{-1} = \frac{-G_{21}}{G_{11}G_{22} - G_{12}G_{21}} \qquad G_{22}^{-1} = \frac{G_{11}}{G_{11}G_{22} - G_{12}G_{21}} \tag{A.67}$$

Note that the second column of $E_n$ will always be zero since $C_{12} = C_{22} = 0$.

For the triangularization of the matrix, iteration begins by setting

$$E_1 = \begin{bmatrix} 0 & 0 \\ 0 & 0 \end{bmatrix} \qquad \text{and} \qquad \hat{F}_1 = \begin{Bmatrix} 0 \\ 0 \end{Bmatrix} \tag{A.68}$$

to satisfy the boundary conditions $u = f = 0$ at the wall. The calculations continue across the boundary layer until a suitably large value of $\eta = \eta^*$ is reached, at which it is assumed that $u_N = 1$ for the leading term of the Blasius series (see Equation (A.38) ), or $u_N = 0$ for the second term (see Equation (A.39) ).

For the case at hand (i.e., the boundary layer on an infinite wall under a stationary vortex), a value of $\eta^* = 3.6$ was found to be sufficient. Were a value of $\eta^*$ chosen to be much larger than 3.6, there would be wasted calculations; too small a value of $\eta^*$ would result in loss of accuracy.

At this point, the back-substitution begins, with calculations continuing as the velocity profile and stream function are obtained from Equation (A.62). Note that, in the linearization of Equation (A.26), a convenient function was chosen to represent a first-guess at the boundary layer velocity profile which satisfied all the boundary conditions. A parabolic velocity profile is utilized in the calculations:

$$f^*(\eta) = \left[\left(\frac{\eta}{\eta^*}\right)^2 - \frac{1}{3}\left(\frac{\eta}{\eta^*}\right)^3\right]\eta^*$$

$$u^*(\eta) = 2\left(\frac{\eta}{\eta^*}\right) - \left(\frac{\eta}{\eta^*}\right)^2 \tag{A.69}$$

$$u'^*(\eta) = \frac{2}{\eta^*}\left[1 - \left(\frac{\eta}{\eta^*}\right)\right].$$

For the second and subsequent iterations, the values of u and f obtained from the previous iteration are used as the current estimates, $u^*$ and $f^*$, respectively.

Synopsizing the numerical procedure for the case of a stationary vortex over an infinite flat plate, we have:

1. At $\xi = -\infty$, self-similar velocity profiles are calculated iteratively to obtain the first terms in the Blasius series representations for $f_0(\eta)$, $u_0(\eta)$, and $u_0'(\eta)$. This process begins with values of $\gamma = 1$, $\delta = 4$, and $\psi = 0$, in conjunction with a parabolic first-guess estimate of the boundary layer velocity profile (Equation (A.69)). From one iteration (using the Thomas algorithm) to the next, the output values of f, u, and u′ are then employed as the estimated values for the next iteration, $f^*$, $u^*$, and $u'^*$. Seven iterations are usually sufficient to obtain convergence to five decimal places, and these functions ($f_0(\eta)$, $u_0(\eta)$, and $u_0'(\eta)$) are retained for later combination with their respective second terms of the

Blasius series representations. Finally, dimensionless integrals of momentum and displacement thicknesses are calculated, along with the shape factors H and T.

2. Now that the coefficients have been obtained in Equation (A.39), the Thomas algorithm is employed to solve for $f_1(\eta)$, $u_1(\eta)$, and $u_1'(\eta)$. Since Equation (A.39) is linear, no iteration is required.

3. Two-term Blasius series representations are now available for use as starting profiles for f, u, and u′ at a position ($\xi = \xi_0$) sufficiently far upstream of the vortex position. Values of momentum and displacement thicknesses and skin friction are calculated.

4. A streamwise step size, $d\xi$, is chosen, and the streamwise calculations are begun at $\xi = \xi_0 + 2d\xi$. Equations (A.16), (A.31), and (A.27) are then utilized to calculate $g^2$, $\delta$, $\gamma$, and $\psi$.

5. The Thomas algorithm now utilizes these values to produce (normally with only two iterations) estimates of f, u, and u′. In the first cycle of iteration, the values of f, u, and u′ are approximated by the values at $\xi = \xi_0 + d\xi$.

6. The converged values of f, u, and u′ are used to calculate the shape factors (H and T), displacement and momentum thicknesses, and skin friction.

7. In anticipation of the next step downstream, the profiles for u and f at $\xi_0 + d\xi$ and $\xi_0 + 2d\xi$ are shifted into storage arrays as the two most recent sets of calculated profiles.

8. Steps 4 through 7 are repeated as $\xi$ is incremented. The process is repeated until a negative value of skin friction is obtained, thereby indicating boundary layer separation.

Using this procedure (and the NEWBL code provided in Sherman [1990] ) with a vortex strength of $\Gamma = \pi$ and with calculations beginning at $\xi_0 = -10.0$, it is found that separation occurs at $\xi_{sep} = 0.176$,

with a momentum thickness of $\theta_0 = 0.471$ beneath the vortex and $\theta_{sep} = 0.608$ at separation. By varying the position at which calculations begin, it was found that these values did not vary at the third decimal place until calculations were begun at $\xi_0 = -2.0$. It is evident that the boundary layer rapidly forgets its upstream history as long as it is forming in a favorable pressure gradient. Hand in hand with this conclusion is the fact that the flow becomes increasingly unstable in the region of decelerating potential flow. To maintain accuracy, it was necessary to begin halving the streamwise step size ($d\xi$) as separation was approached (beginning at approximately $\xi = -2.0$), with successive halvings at judiciously selected points until separation was achieved.

## D. LEADING EDGE AT FINITE $\xi$

In this instance, we have $\theta = 0$ at the leading edge $\xi = \xi_0$ (see Figure A.2), so that Equation (A.12) becomes (with the change of variable $\xi = x/a$)

$$\frac{\theta^2(\xi)U_0}{\nu a} = 0.45(1+\xi^2)^6\left[F(\xi) - F(\xi_0)\right], \tag{A.70}$$

where

$$F(\xi) = \frac{1}{384}\left[48\xi(1+\xi^2)^{-4} + 56\xi(1+\xi^2)^{-3} + 70\xi(1+\xi^2)^{-2} + 105\xi(1+\xi^2)^{-1} + 105\arctan(\xi)\right] \tag{A.71}$$

From Equations (A.27), the following relationships are derived after choosing $A^2 = 40/9$:

$$\delta = -4\xi_0(1+\xi_0^2)^{-1}(\xi - \xi_0) \tag{A.72}$$

$$\psi = 2(\xi - \xi_0) \tag{A.73}$$

$$\gamma = 1 + 8\xi_0(1+\xi_0^2)^{-1}(\xi - \xi_0). \tag{A.74}$$

Additionally, a new two-term Blasius series is required to represent the velocity and stream functions. As suggested by Sherman [1990], a successful form is

$$u(\xi,\eta) = u_0(\eta) + u_1(\eta)(\xi - \xi_0) + u_2(\eta)\frac{(\xi - \xi_0)^2}{2} + \ldots \tag{A.75}$$

$$u_{,\xi}(\xi,\eta) = u_1(\eta) + u_2(\eta)(\xi - \xi_0) + \ldots \tag{A.76}$$

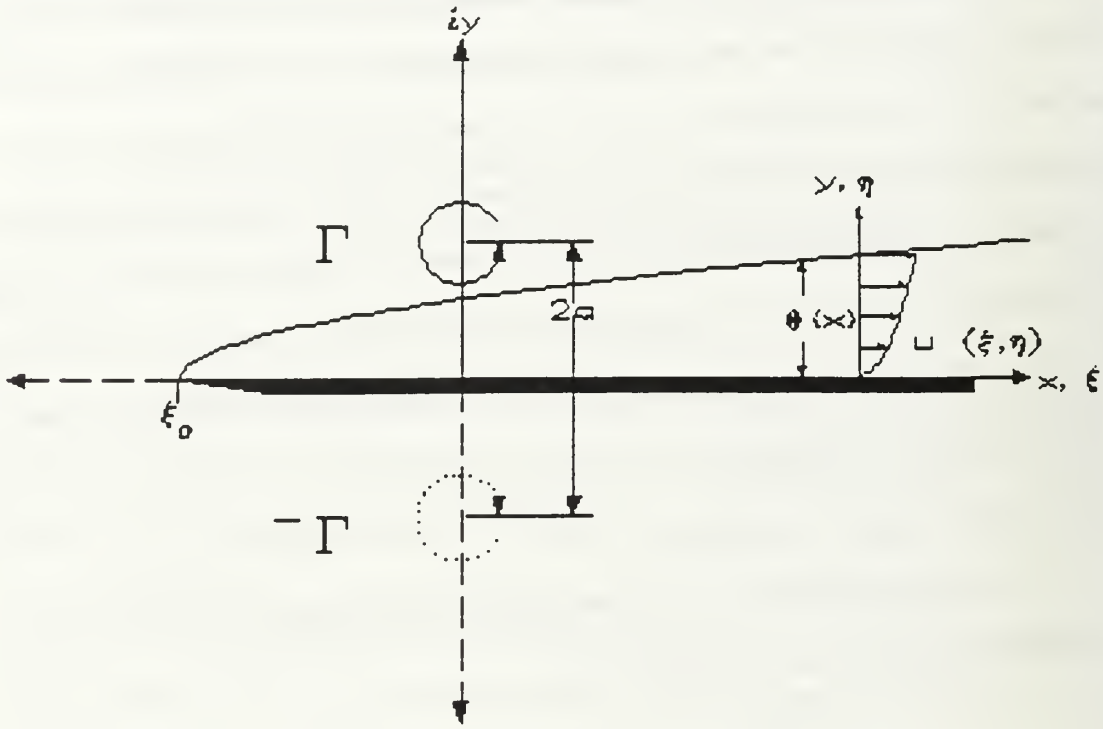


Figure A.2 Boundary layer on a semi-infinite flat plate under the influence of a stationary line vortex (not to scale ).

$$f(\xi,\eta) = f_0(\eta) + f_1(\eta)(\xi-\xi_0) + f_2(\eta)\frac{(\xi-\xi_0)}{2} + \ldots \tag{A.77}$$

$$f_{,\xi}(\xi,\eta) = f_1(\eta) + f_2(\eta)(\xi-\xi_0) + \ldots \tag{A.78}$$

With all of the foregoing in place, attention returns to Equation (A.26), where the appropriate substitutions are made. Collecting terms which are associated with $(\xi - \xi_0)^0$, we obtain

$$u_0'' + f_0 u_0' = 0.^2 \tag{A.79}$$

This is of the form of Equation (A.26) where $\gamma = 1$ and $\delta = \psi = 0$. Next, the terms associated with$(\xi - \xi_0)^1$ are found to be

$$u_1'' + (f_0)u_1' - (2u_0)u_1 + (3u_0')f_1 = \frac{4\xi_0}{1+\xi_0^2}\left[1 - u_0^2 - 2f_0 u_0'\right] \tag{A.80}$$

[2] Note that this may be recast as the classic Blasius function, $f_0''' + f_0 f_0'' = 0$.

The parenthesized terms and the entire right-hand side of the last equation are all known quantities after having solved the first term of the Blasius series. The process continues with a finite difference representation of the last equation to obtain

$$\underbrace{u_{n-1}\left[\frac{1}{h^2}-\frac{f_0}{2h}\right]}_{A_{11}}+\underbrace{u_n\left[-\frac{2}{h^2}-2u_0\right]}_{B_{11}}+\underbrace{u_{n+1}\left[\frac{1}{h^2}+\frac{f_0}{2h}\right]}_{C_{11}}+\underbrace{f_{n-1}[0]}_{A_{12}}+\underbrace{f_n\left[3u_0'\right]}_{B_{12}}+\underbrace{f_{n+1}[0]}_{C_{12}}=\underbrace{\frac{4\xi_0}{1+\xi_0^2}\left(1-u_0^2-2f_0u_0^2\right)}_{D_1}$$

In this last equation, $B_{11}$, $B_{12}$, and $D_1$ are the only terms which are different from those in Equation (A.56) for the infinite flat plate. We note also that the second equation to describe this physical situation is identical to that for the infinite flat plate, Equations (A.57) through (A.59), so that the coefficients are also identical. Finally, the boundary conditions which are applicable for this situation are $f_1(0) = u_1(0) = u_1(\infty) = 0$, $f_0(0) = u_0(0) = 0$, and $u_0(\infty) = 1$.

Computer coding for the case of a finite plate was not included in Sherman [1990], but the NEWBL code was modified for this case and run for various distances of the leading edge upstream of the stationary vortex. A value of $\eta^* = 6.5$ was required to capture the full shape of the velocity profile across the boundary layer. With the vortex at $\xi = 0$ and the leading edge at $\xi_0 = -10$, the same values of momentum thickness directly under the vortex ($\theta(0) = 0.471$) and at separation ($\theta_{sep} = 0.608$), and the same location for separation ($\xi_{sep} = 0.176$) were obtained as for the infinite plate case. Very little change (down to the third decimal place) was noted until the leading edge was closer than $\xi_0 = -2.0$. When the vortex was directly over the leading edge, $\xi_{sep} = 0.291$, $\theta(0) = 0$, and $\theta_{sep} = 0.433$. The strong upstream favorable pressure gradient results in almost complete loss of memory in the flow when the leading edge is far upstream. The current analysis produced values of $\theta_0$ and $\xi_{sep}$ which agreed well with values provided in Table 12.1 of Sherman [1990].

## E. INCORPORATION OF FREE STREAM AND NUMEROUS VORTICES

To make the code applicable to more realistic flow situations, the outer (potential) flow was modified to include a free stream and several vortices. Additionally, numerical integration was utilized to

calculate Thwaites' integral (Equation (A.12)) in lieu of using the series expansion (Equations (A.16) or (A.17)), which would significantly increase program execution time. Specifically, a Romberg integration routine was employed (see, e.g., Kuo [1972] ). Again, the assumption is made that the flow is quasi-steady, so that the Sherman boundary layer technique can be used to predict separation on a flat plate beneath a vortex field in the presence of a free stream.

## F. PROGRAM VERIFICATION

At this stage, the code was verified by limiting the flow field to a single stationary ($U_\infty = 0$) vortex above a semi-infinite flat plate whose leading edge was varied from $\xi_0 = -10$ (essentially an infinite flat plate) to $\xi_0 = 0$. The results (first column of Table A.1) agree with Sherman's results to the third decimal place. Numerical (Romberg) integration of Thwaites' integral was as accurate as the series expansion.

Next, the code was tested with a free stream and no vortices in the flow field. The velocity profile at all streamwise positions proved to be precisely the Blasius velocity profile, the solution to Equation (A.79). Finally, the code was tested with a single vortex and successively larger free stream velocities at a variety of leading edge locations. For all cases, higher free stream velocities resulted in a delay of separation and a thinner boundary layer at separation, agreeing with intuition. For situations where the leading edge was located at a position $-2 < \xi_0 < 0$, the boundary layer momentum thickness directly beneath the vortex decreased uniformly with increasing free stream velocity.

| | | $U_\infty = 0.00$ | $U_\infty = 0.25$ | $U_\infty = 0.50$ | $U_\infty = 0.75$ | $U_\infty = 1.00$ |
|---|---|---|---|---|---|---|
| $\xi_0 = 0.0$ | $\theta(0)$ | 0.000 | 0.000 | 0.000 | 0.000 | 0.000 |
| | $\xi_{sep}$ | 0.291 | 0.321 | 0.344 | 0.361 | 0.370 |
| | $\theta_{sep}$ | 0.433 | 0.412 | 0.408 | 0.378 | 0.383 |
| $\xi_0 = -0.2$ | $\theta(0)$ | 0.290 | 0.266 | 0.253 | 0.245 | 0.239 |
| | $\xi_{sep}$ | 0.223 | 0.252 | 0.273 | 0.283 | 0.293 |
| | $\theta_{sep}$ | 0.465 | 0.462 | 0.456 | 0.436 | 0.435 |
| $\xi_0 = -0.5$ | $\theta(0)$ | 0.409 | 0.381 | 0.366 | 0.356 | 0.349 |
| | $\xi_{sep}$ | 0.190 | 0.212 | 0.225 | 0.239 | 0.245 |
| | $\theta_{sep}$ | 0.561 | 0.532 | 0.513 | 0.502 | 0.498 |
| $\xi_0 = -1$ | $\theta(0)$ | 0.460 | 0.441 | 0.430 | 0.422 | 0.417 |
| | $\xi_{sep}$ | 0.179 | 0.200 | 0.206 | 0.216 | 0.221 |
| | $\theta_{sep}$ | 0.603 | 0.573 | 0.559 | 0.553 | 0.546 |
| $\xi_0 = -2$ | $\theta(0)$ | 0.471 | 0.462 | 0.457 | 0.454 | 0.452 |
| | $\xi_{sep}$ | 0.176 | 0.192 | 0.203 | 0.212 | 0.211 |
| | $\theta_{sep}$ | 0.610 | 0.594 | 0.585 | 0.577 | 0.571 |
| $\xi_0 = -4$ | $\theta(0)$ | 0.471 | 0.468 | 0.469 | 0.471 | 0.472 |
| | $\xi_{sep}$ | 0.176 | 0.190 | 0.201 | 0.207 | 0.209 |
| | $\theta_{sep}$ | 0.610 | 0.596 | 0.598 | 0.596 | 0.591 |
| $\xi_0 = -10$ | $\theta(0)$ | 0.471 | 0.472 | 0.480 | 0.489 | 0.497 |
| | $\xi_{sep}$ | 0.176 | 0.189 | 0.203 | 0.203 | 0.207 |
| | $\theta_{sep}$ | 0.610 | 0.527 | 0.605 | 0.611 | 0.618 |

Table A.1 Parametric analysis conducted for verification of boundary layer code.

# APPENDIX B: PROGRAM PLATE.FOR

```
CCCCCCCCCCCCCCCCCCCCCCCCCCCCCCCCCCCCCCCCCCCCCCCCCCCCCCCCCCCCCCCCCCCCCCCC
CCCCCCCCCCCCCCCCCCCCCCCCCCCCCCCCCCCCCCCCCCCCCCCCCCCCCCCCCCCCCCCCCCCCCCCC
      IMPLICIT COMPLEX(C,Z),INTEGER(I-N)
      CHARACTER RUNNO*3,FILM*7,RECAP*8,CHECK*1,RMNDR*59,KILL*1
      CHARACTER DISCRT*1,POT*1
      CHARACTER*60 COMNTS(5)
      COMMON/VORTEX/ZV(300,4),CV(300,4),GV(300,4),GV0(300,4),
     1              DGDT(300,4),AGE(300,4),GSHED(800,4),GLOST(800,4),
     2              GVMIN,GV0MIN,NNV(4),NNB,NVMAX
      COMMON/SAVE/XVORT(800),YVORT(800),XSEP(800),YSEP(800),USEP(800)
      COMMON/TIMES/DELT,T(800),NT,NTMAX,NTSTOP
      COMMON/CONST/ZONE,ZERO,ZFAC,ZI,ZPI,PI,TWOPI,PI90,PI180,OV2PI
      COMMON/SURFCE/Q(200),PTOTAL(200),PVORT(200),PVELO(200),
     1              DX,NDX,XMAX,X(200),XI(500),TAU(500),BLDISP(500),
     2              BLMOM(500),MSEP,FY(800),XBAR(800)
      COMMON/FLOW/RCORE,CINF,VINF,RMIN,BDISP,NOTOCH,AGECHK
      COMMON/MISC/RUNNO,NPLOTS,NCOMNT,COMNTS
      COMMON/MISC1/NHICUP
CCCCCCCCCCCCCCCCCCCCCCCCCCCCCCCCCCCCCCCCCCCCCCCCCCCCCCCCCCCCCCCCCCCCCCCC
C
C     THIS CODE IS THE LATEST IN A SERIES OF PROGRAMS WHOSE ORIGIN WAS
C     DEVELOPED BY PROF T. SARPKAYA IN THE EARLY 1960'S.  IT HAS
C     UNDERGONE NUMEROUS REVISIONS AND REFINEMENTS AS MANY STUDENTS
C     HAVE UTILIZED IT IN CONJUNCTION WITH RESEARCH INVOLVING THE
C     DISCRETE VORTEX MODEL.  ITS CURRENT USE SIMULATES VORTEX FLOW
C     PAST A SEMI-INFINITE FLAT PLATE, AND MAY INCLUDE VISCOUS EFFECTS
C     AND CONSEQUENT SECONDARY VORTEX GENERATION.  THE CURRENT VERSION
C     WAS WRITTEN AND COMPILED WITH MICROSOFT FORTRAN POWERSTATION
C     VERSION 1.0; THE ACCOMPANYING PROGRAM IN APPENDIX C WAS UTILIZED
C     TO PRODUCE GRAPHIC AND TABULAR OUTPUT.  BOTH PROGRAMS WERE
C     COMPILED AND EXECUTED ON A COMPAQ CONTURA 486DX LAPTOP RUNNING
C     AT 25 MHZ.BOTH PROGRAMS PROMPT THE USER FOR VARIOUS RUNTIME
C     PARAMETERS, SO THAT COMPILATION WAS NOT REQUIRED PRIOR TO EACH
C     EXECUTION.  WRITTEN BY CAPT MICHAEL R. MAIXNER, DEC 1994, IN
C     CONJUNCTION WITH DOCTORAL DISSERTATION AT NAVAL POSTGRADUATE
C     SCHOOL, MONTEREY, CA.
C
CCCCCCCCCCCCCCCCCCCCCCCCCCCCCCCCCCCCCCCCCCCCCCCCCCCCCCCCCCCCCCCCCCCCCCCC
C
C     INPUT RUN NUMBER AND ANY OTHER INFORMATION REQUIRED; CONSTRUCT
C     DATA FILE NAMES
C
      WRITE(6,10)
   10 FORMAT(' INPUT THREE-DIGIT RUN NUMBER')
      READ(5,5)RUNNO
    5 FORMAT(A3)
      FILM= RUNNO//'FILM'
      RECAP=RUNNO//'RECAP'
      WRITE(6,11)
   11 FORMAT(' INPUT FREE STREAM VELOCITY')
      READ(5,*)VINF
      BETA=VINF/(1.+VINF)
      NCOMNT=0
```

```
   15 WRITE(6,20)
   20 FORMAT(' INPUT <= 5 LINES OF COMNTS.IF NO ADDTNL LINES,INPUT 0.')
      READ(5,21)CHECK,RMNDR
   21 FORMAT(A1,A59)
      IF (CHECK.EQ.'0') GO TO 25
      NCOMNT=NCOMNT+1
      COMNTS(NCOMNT)=CHECK//RMNDR
      IF((NCOMNT+1).GT.5)GO TO 25
      GO TO 15
   25 CONTINUE
CCCCCCCCCCCCCCCCCCCCCCCCCCCCCCCCCCCCCCCCCCCCCCCCCCCCCCCCCCCCCCCCCCCCCCC
C
C     COMPUTE NECESSARY PARAMETERS AND INITIALIZE ARRAYS
C
      DELT=0.125
      PI=4.0*ATAN(1.0)
      PI90=PI/90.
      PI180=PI/180.
      TWOPI=2.0*PI
      OV2PI=1./TWOPI
      DEGNAS=32.0
      ANGNAS=DEGNAS*PI180
      ZERO=CMPLX(0.0,0.0)
      ZONE=CMPLX(1.0,0.0)
      ZI=CMPLX(0.0,1.0)
      ZFAC=CMPLX(0.0,OV2PI)
      ZPI=CMPLX(PI,0.0)
      NPLOTS=0
      XSTOP=0.06
      WRITE(6,40)
      YINITL=1.0
   40 FORMAT(' INPUT BEGINNING X-COORDINATE FOR MAJOR VORTEX')
      READ(5,*)XINITL
      WRITE(6,50)
   50 FORMAT(' INPUT MAXIMUM X-VALUE FOR MAJOR VORTEX TRAVEL')
      READ(5,*)XSTOP
      WRITE(6,55)
   55 FORMAT(' DO YOU WANT PURELY POTENTIAL RUN?')
      READ(5,73)POT
      IF(POT.EQ.'y')POT='Y'
      BDISP=20.0
      DX=0.05
      XMAX=10.0
      NDX=XMAX/DX
      RMAX=0.4
      WRITE(6,64)
   64 FORMAT(' DO YOU WANT MAJOR VORTEX DISCRETIZED?')
      READ(5,73)DISCRT
   73 FORMAT(A1)
      IF(DISCRT.EQ.'y')DISCRT='Y'
      IF(DISCRT.NE.'Y')GO TO 68
      IGAMMA=4
   68 RCORE=0.0075
      RMIN=RCORE
      NHICUP=0
      NOTOCH=(0.125/DELT)*15
```

```
      AGECHK=NOTOCH*DELT
      CINF=CMPLX(BETA,0.0)
      IPRT=1
      WRITE(6,70)
   70 FORMAT(' INPUT FREQUENCY OF PLOTTING AND PRINTING')
      READ(5,*)IPRT
      KILL='Y'
      IF (KILL.EQ.'y')KILL='Y'
      DV=0.4
      NNB=2
      NNV(1)=0
      NNV(2)=0
      NNV(3)=0
      NNV(4)=0
      NSUMRY=8
      NMOVIE=7
      NTMAX=300
CCCCCCCCCCCCCCCCCCCCCCCCCCCCCCCCCCCCCCCCCCCCCCCCCCCCCCCCCCCCCCCCCCCCCCCC
C     UNFORMATTED DATA FILES ARE UTILIZED TO MINIMIZE TIME TO READ/WRITE,
C     AND TO MINIMIZE DATA FILE SIZE.
C
      OPEN(7,FILE=FILM,FORM='UNFORMATTED')
      OPEN(8,FILE=RECAP,FORM='UNFORMATTED')
      NVMAX=300
      DO 80 I=1,NTMAX
      DO 75 NB=1,NNB
      GLOST(I,NB)=0.0
   75 GSHED(I,NB)=0.0
      GSHED(I,1)=PI
      XSEP(I)=0.0
      YSEP(I)=0.0
      USEP(I)=0.0
      XVORT(I)=0.0
      YVORT(I)=0.0
      XBAR(I)=0.0
      FY(I)=0.0
   80 CONTINUE
      DO 90 NB=1,NNB
      DO 90 NV=1,NVMAX
      ZV(NV,NB)=ZERO
      CV(NV,NB)=ZERO
      GV(NV,NB)=0.0
      GV0(NV,NB)=0.0
      DGDT(NV,NB)=0.0
      AGE(NV,NB)=0.0
   90 CONTINUE
      DO 100 I=1,NDX
      X(I)=I*DX
      Q(I)=0.0
      PTOTAL(I)=0.0
      PVORT(I)=0.0
      PVELO(I)=0.0
  100 CONTINUE
CCCCCCCCCCCCCCCCCCCCCCCCCCCCCCCCCCCCCCCCCCCCCCCCCCCCCCCCCCCCCCCCCCCCCCCC
C
C    START THE CALCULATIONS
```

```
C
      NNV(1)=1
      ZV(1,1)=CMPLX(XINITL,YINITL)
      GV(1,1)=PI
      GV0(1,1)=GV(1,1)
      GVMIN=0.001
      IBLSTP=0
      IBLMAX=3
      T(1)=DELT
      NT=0
 9999 NTP1=NT+1
      IF(NTP1.GT.NTMAX)GO TO 10001
      NT=NTP1
      GAMMA=GV(1,1)
      ZIN=ZV(1,1)
CCCCCCCCCCCCCCCCCCCCCCCCCCCCCCCCCCCCCCCCCCCCCCCCCCCCCCCCCCCCCCCCCCCCCCCC
C     IF DISCRETIZING PRIMARY VORTEX, THIS "EXPLODES" IT INTO A CLUSTER
C
      IF((NT.EQ.2).AND.(DISCRT.EQ.'Y'))
     1   CALL EXPLOD(1,GAMMA,ZIN,RMAX,IGAMMA)
      IF (NT.EQ.1) GO TO 105
      T(NT)=T(NT-1)+DELT
      DO 102 NB=1,NNB
  102 GLOST(NT,NB)=GLOST(NT-1,NB)
  105 JPRT=0
      IF (MOD(NT,IPRT).EQ.0) JPRT=1
CCCCCCCCCCCCCCCCCCCCCCCCCCCCCCCCCCCCCCCCCCCCCCCCCCCCCCCCCCCCCCCCCCCCCCCC
C     CALCULATE CENTROID OF PRIMARY VORTEX CLUSTER.
C
      CALL AMALG(1,1,ZCNTRD,GTOTAL)
      XVORT(NT)=REAL(ZCNTRD)
      YVORT(NT)=AIMAG(ZCNTRD)
          WRITE(6,*)ZCNTRD
CCCCCCCCCCCCCCCCCCCCCCCCCCCCCCCCCCCCCCCCCCCCCCCCCCCCCCCCCCCCCCCCCCCCCCCC
C
C     DETERMINE VELOCITY DISTRIBUTION ON PLATE AND COMPUTE
C     SEPARATION POINT AND VELOCITY AT SEPARATION POINT (USEP)
C

      IF(POT.EQ.'Y')GO TO 119
      IF(IBLSTP.LT.IBLMAX)CALL NEWBL(XVORT(NT),XSEP(NT),USEP(NT))
      IF(NT.EQ.1)WRITE(6,110)XSEP(NT)
  110 FORMAT(' FIRST SEPARATION POINT IS AT X=',F8.4)
CCCCCCCCCCCCCCCCCCCCCCCCCCCCCCCCCCCCCCCCCCCCCCCCCCCCCCCCCCCCCCCCCCCCCCCC
C
C     CREATE NEW NASCENT VORTEX AND INTRODUCE AT COMPUTED SEPARATION
C     POINT AND AT A DISTANCE TO SATISFY KUTTA CONDITION; CALCULATE
C     VELOCITY AT SEPARATION POINT AND THEN NASCENT VORTEX STRENGTH.
C
      NNV(2)=NNV(2)+1
      NV=NNV(2)
      GV(NV,2)=-0.5*USEP(NT)*USEP(NT)*DELT
      IF (USEP(NT).LT.0.0001)GO TO 115
      R=ABS(GV(NV,2))*COS(ANGNAS)/(PI*USEP(NT))
      GO TO 116
  115 R=0.0
```

```
  116 XV=R*SIN(ANGNAS)
      YV=R*COS(ANGNAS)
      XV=XV+XSEP(NT)
      YSEP(NT)=YV
      GV0MIN=0.0
      IF(XVORT(NT).GT.0.5)
     1      GV0MIN=DELT*0.5*(BETA+DV)**2
      IF ((KILL.EQ.'Y').AND.(ABS(GV(NV,2)).LT.GV0MIN))
     1   GV(NV,2)=0.0
      GV0(NV,2)=GV(NV,2)
CCCCCCCCCCCCCCCCCCCCCCCCCCCCCCCCCCCCCCCCCCCCCCCCCCCCCCCCCCCCCCCCCCCCCCCCCCCC
C
C     IF THE NASCENT VORTEX HASN'T SATISFIED THE MINIMUM STRENGTH
C     CRITERION (SET FOR THE CASE WHERE THE VORTEX HAS GONE AT LEAST
C     TO X=0.5), THEN ADD 1 TO THE COUNTER.  WHEN THE COUNTER HITS A
C     CERTAIN TALLY (IBLMAX), THEN IT'S HIGHLY UNLIKELY THAT THE BL
C     WILL BE INTRODUCING ANY MORE VORTICITY TO THE FLOW, AND
C     COMPUTATION TIME CAN BE SAVED BY BYPASSING THE SEPARATION
C     POINT CALCULATION.
C
      IF((GV(NV,2).EQ.0.0).AND.(GV0MIN.GT.0.0))IBLSTP=IBLSTP+1
      ZV(NV,2)=CMPLX(XV,YV)
  119 WRITE(6,120) NT,T(NT),GV(NV,2),XSEP(NT),YSEP(NT),REAL(ZCNTRD)
  120 FORMAT(1X,'NT=',I3,' T=',F6.3,' G=',F6.3,' XSEP=',F6.3,
     1      ' YSEP=',F6.4,' XVORT=',F6.3)
      IF (NT.EQ.1) GO TO 2005
      GSHED(NT,2)=GSHED(NT-1,2)+GV(NV,2)
      GO TO 2010
 2005 GSHED(NT,2)=GV(NV,2)
 2010 CONTINUE
CCCCCCCCCCCCCCCCCCCCCCCCCCCCCCCCCCCCCCCCCCCCCCCCCCCCCCCCCCCCCCCCCCCCCCCCCCCC
C
C     DETERMINE VELOCITIES AT EACH VORTEX POSITION AND CONVECT
C     VORTICES DOWNSTREAM
C
      CALL MOVE
      NB1=1
      NB2=NNB
      CALL CNCL(NB1,NB2,NCL)
      IF (NCL.LT.1) GO TO 2065
      DO 2050 NB=1,NNB
      CALL PACK(NB)
 2050 CONTINUE
 2065 CONTINUE
CCCCCCCCCCCCCCCCCCCCCCCCCCCCCCCCCCCCCCCCCCCCCCCCCCCCCCCCCCCCCCCCCCCCCCCCCCCC
C
C     DISSIPATE VORTICITY
C
 2070 IF(POT.NE.'Y')CALL DISP
CCCCCCCCCCCCCCCCCCCCCCCCCCCCCCCCCCCCCCCCCCCCCCCCCCCCCCCCCCCCCCCCCCCCCCCCCCCC
C
C     COMPUTE SURFACE PRESSURE AND VELOCITY DISTRIBUTIONS
C
      CALL PRVEL
CCCCCCCCCCCCCCCCCCCCCCCCCCCCCCCCCCCCCCCCCCCCCCCCCCCCCCCCCCCCCCCCCCCCCCCCCCCC
C
```

```
C     STORE OUTPUT DATA
C
      IF (JPRT.NE.1)GO TO 5900
      CALL MOVIE(NMOVIE)
      REWIND(NSUMRY)
      CALL SUMARY(NSUMRY)
 5900 CONTINUE
      IF (REAL(ZCNTRD).GT.XSTOP) GO TO 10001
      GO TO 9999
10001 IF (JPRT.EQ.1)GO TO 10002
      CALL MOVIE(NMOVIE)
      CALL SUMARY(NSUMRY)
10002 CLOSE(7,STATUS='KEEP')
      CLOSE(8,STATUS='KEEP')
      STOP
      END
CCCCCCCCCCCCCCCCCCCCCCCCCCCCCCCCCCCCCCCCCCCCCCCCCCCCCCCCCCCCCCCCCCCCCCCCCCC
CCCCCCCCCCCCCCCCCCCCCCCCCCCCCCCCCCCCCCCCCCCCCCCCCCCCCCCCCCCCCCCCCCCCCCCCCCC
      SUBROUTINE PRVEL
      IMPLICIT COMPLEX(C,Z),INTEGER(I-N)
      COMMON/VORTEX/ZV(300,4),CV(300,4),GV(300,4),GV0(300,4),
     1              DGDT(300,4),AGE(300,4),GSHED(800,4),GLOST(800,4),
     2              GVMIN,GV0MIN,NNV(4),NNB,NVMAX
      COMMON/TIMES/DELT,T(800),NT,NTMAX,NTSTOP
      COMMON/SURFCE/Q(200),PTOTAL(200),PVORT(200),PVELO(200),
     1              DX,NDX,XMAX,X(200),XI(500),TAU(500),BLDISP(500),
     2              BLMOM(500),MSEP,FY(800),XBAR(800)
      COMMON/FLOW/RCORE,CINF,VINF,RMIN,BDISP,NOTOCH,AGECHK
CCCCCCCCCCCCCCCCCCCCCCCCCCCCCCCCCCCCCCCCCCCCCCCCCCCCCCCCCCCCCCCCCCCCCCCCCCC
C
C     CALCULATES PRESSURE AND VELOCITY ON PLATE SURFACE.
C
C     NOTE:  THIS IS WHERE SMOOTHING/FORCE/MOMENT ROUTINE WOULD
C            BE PLACED, IF THEY ARE MOVED FROM THE GRAPHICS
C            SUBROUTINE.
C
      DO 100 I=1,NDX
      CALL PRESUR(X(I),PVORT(I),PVELO(I),PTOTAL(I),Q(I))
  100 CONTINUE
      RETURN
      END
CCCCCCCCCCCCCCCCCCCCCCCCCCCCCCCCCCCCCCCCCCCCCCCCCCCCCCCCCCCCCCCCCCCCCCCCCCC
CCCCCCCCCCCCCCCCCCCCCCCCCCCCCCCCCCCCCCCCCCCCCCCCCCCCCCCCCCCCCCCCCCCCCCCCCCC
      SUBROUTINE PRESUR(X,PV,PQ,PT,Q)
      IMPLICIT COMPLEX(C,Z),INTEGER(I-N)
      COMMON/VORTEX/ZV(300,4),CV(300,4),GV(300,4),GV0(300,4),
     1              DGDT(300,4),AGE(300,4),GSHED(800,4),GLOST(800,4),
     2              GVMIN,GV0MIN,NNV(4),NNB,NVMAX
      COMMON/CONST/ZONE,ZERO,ZFAC,ZI,ZPI,PI,TWOPI,PI90,PI180,OV2PI
CCCCCCCCCCCCCCCCCCCCCCCCCCCCCCCCCCCCCCCCCCCCCCCCCCCCCCCCCCCCCCCCCCCCCCCCCCC
C
C     DOES DETAILED VELOCITY AND PRESSURE CALCULATIONS.
C
      Q=UTAN(X)
      ZZ=CMPLX(X,0.0)
      ZPSUM=ZERO
```

```
      ZHOLD=ZERO
      DO 3000 NB=1,NNB
      NV2=NNV(NB)
      IF (NV2.LT.1) GO TO 3000
      DO 2000 NV=1,NV2
      ZK=ZV(NV,NB)
      DKRATE=DGDT(NV,NB)
      ZKIMAG=CONJG(ZK)
      GAMA=GV(NV,NB)
      ZDIFRL=ZZ-ZK
      ZDIFIM=ZZ-ZKIMAG
      CVELRL=CV(NV,NB)
      CVCONJ=CONJG(CV(NV,NB))
      ZPSUM=ZPSUM+DKRATE*CLOG(ZDIFRL/ZDIFIM)
      ZHOLD=ZHOLD+GAMA*(-CVELRL/ZDIFRL+CVCONJ/ZDIFIM)
 2000 CONTINUE
 3000 CONTINUE
      ZPSUM=ZI*(ZPSUM+ZHOLD)
      PV=REAL(ZPSUM)/PI
      PQ=-Q*Q
      PT=PV+PQ
      RETURN
      END
CCCCCCCCCCCCCCCCCCCCCCCCCCCCCCCCCCCCCCCCCCCCCCCCCCCCCCCCCCCCCCCCCCCCCCCCCCC
CCCCCCCCCCCCCCCCCCCCCCCCCCCCCCCCCCCCCCCCCCCCCCCCCCCCCCCCCCCCCCCCCCCCCCCCCCC
      FUNCTION UTAN(X)
      IMPLICIT COMPLEX(C,Z),INTEGER(I-N)
CCCCCCCCCCCCCCCCCCCCCCCCCCCCCCCCCCCCCCCCCCCCCCCCCCCCCCCCCCCCCCCCCCCCCCCCCCC
C
C     CALCULATES COMPLEX VELOCITY ON PLATE SURFACE
C
      Z=CMPLX(X,0.0)
      CALL CVELP(Z,0,0,0,C)
      UTAN=REAL(C)
      RETURN
      END
CCCCCCCCCCCCCCCCCCCCCCCCCCCCCCCCCCCCCCCCCCCCCCCCCCCCCCCCCCCCCCCCCCCCCCCCCCC
CCCCCCCCCCCCCCCCCCCCCCCCCCCCCCCCCCCCCCCCCCCCCCCCCCCCCCCCCCCCCCCCCCCCCCCCCCC
      SUBROUTINE MOVE
      IMPLICIT COMPLEX(C,Z),INTEGER(I-N)
      COMMON/VORTEX/ZV(300,4),CV(300,4),GV(300,4),GV0(300,4),
     1              DGDT(300,4),AGE(300,4),GSHED(800,4),GLOST(800,4),
     2              GVMIN,GV0MIN,NNV(4),NNB,NVMAX
      COMMON/SAVE/XVORT(800),YVORT(800),XSEP(800),YSEP(800),USEP(800)
      COMMON/TIMES/DELT,T(800),NT,NTMAX,NTSTOP
      COMMON/CONST/ZONE,ZERO,ZFAC,ZI,ZPI,PI,TWOPI,PI90,PI180,OV2PI
      COMMON/FLOW/RCORE,CINF,VINF,RMIN,BDISP,NOTOCH,AGECHK
CCCCCCCCCCCCCCCCCCCCCCCCCCCCCCCCCCCCCCCCCCCCCCCCCCCCCCCCCCCCCCCCCCCCCCCCCCC
C!!!!!!!!!!!!!!!!!!!!!!!!!!!!!!!!!!!!!!!!!!!!!!!!!!!!!!!!!!!!!!!!!!!!!!!!!
C     N.B.:  IF NO NASCENT VORTEX IS INTRODUCED, THEN THE LAST VORTEX
C     SHED IS TREATED AS THE NASCENT VORTEX--IF THIS SITUATION IS
C     ALLOWED TO OCCUR, CODE NEEDS TO BE MODIFIED TO INCLUDE THE
C     VELOCITIES INDUCED BY THE LAST VORTEX SHED!!!!  THIS CAN BE
C     CIRCUMVENTED BY ENSURING THAT, EVEN IF A VORTEX IS NOT INPUT, A
C     "DUMMY" VORTEX OF ZERO STRENGTH IS INPUT IN THE MAIN PROGRAM,
C     CONVECTED, AND THEN REMOVED FROM THE FLOW IN SUBROUTINE CNCL.
```

```
C!!!!!!!!!!!!!!!!!!!!!!!!!!!!!!!!!!!!!!!!!!!!!!!!!!!!!!!!!!!!!!!!!!!!!!!!!
C
C     COMPUTE VELOCITIES OF ALL VORTICES.  VELOCITY OF NASCENT VORTEX
C     IS DETERMINED AS A SPECIAL CASE.  VORTICES ARE CONVECTED
C     WITHOUT THE EFFECTS OF THE NASCENT VORTICES.
C
      DO 3035 NB=1,NNB
CCCCCCCCCCCCCCCCCCCCCCCCCCCCCCCCCCCCCCCCCCCCCCCCCCCCCCCCCCCCCCCCCCCCCCCCC
C
C     TEMPORARILY REMOVE THE NASCENT VORTEX FROM THE CALCULATIONS
C
      IF (NB.EQ.2) NNV(NB)=NNV(NB)-1
      NV2=NNV(NB)
      IF (NV2.LT.1) GO TO 3035
      DO 3030 NV=1,NV2
 3025 CALL CVELP (ZV(NV,NB),1,NV,NB,C)
      CV(NV,NB)=C
 3030 CONTINUE
 3035 CONTINUE
      NV=NNV(2)+1
CCCCCCCCCCCCCCCCCCCCCCCCCCCCCCCCCCCCCCCCCCCCCCCCCCCCCCCCCCCCCCCCCCCCCCCCC
C
C     THE NASCENT VORTEX IS CONVECTED WITHOUT THE INFLUENCE OF
C     ITS IMAGE
C
 3037 CALL CVELP(ZV(NV,2),0,0,0,CV(NV,2))
 3039 NNV(2)=NNV(2)+1
CCCCCCCCCCCCCCCCCCCCCCCCCCCCCCCCCCCCCCCCCCCCCCCCCCCCCCCCCCCCCCCCCCCCCCCCC
C
C     CONVECT VORTICES AND INCREASE THEIR AGES BY ONE TIMESTEP.
C
      DO 3050 NB=1,NNB
      NV2=NNV(NB)
      IF (NV2.LT.1) GO TO 3050
      DO 3040 NV=1,NV2
      AGE(NV,NB)=AGE(NV,NB)+DELT
 3333 ZV(NV,NB)=ZV(NV,NB)+DELT*CV(NV,NB)
 3040 CONTINUE
 3050 CONTINUE
CCCCCCCCCCCCCCCCCCCCCCCCCCCCCCCCCCCCCCCCCCCCCCCCCCCCCCCCCCCCCCCCCCCCCCCCC
C
C     ENSURE THAT NO VORTICES ARE CONVECTED ACROSS THE PLATE.
C     ANNIHILATE THOSE VORTICES TOO CLOSE TO THE PLATE.
C     DO NOT CONSIDER THE VORTICES NEAR THE SEPARATION REGIONS.
C     THE FIRST FIFTEEN (FOR DELT=0.125) VORTICES ARE CONSIDERED
C     TO BE IN THIS 'EXCLUSION ZONE.'  IF DELT=0.0625 IS USED,
C     THE NUMBER OF EXEMPTED VORTICES IS 30, AND SO ON.
C
      YMIN=RCORE
      DO 3070 NB=1,NNB
      NV2=NNV(NB)
      IF (NV2.LT.1)GO TO 3070
      KEY=0
      DO 3060 NV=1,NV2
      IF(NB.EQ.1)GO TO 3053
      IF(ABS(GV(NV,NB)).LT.GVMIN)KEY=1
```

```
CCCCCCCCCCCCCCCCCCCCCCCCCCCCCCCCCCCCCCCCCCCCCCCCCCCCCCCCCCCCCCCCCCCC
C
C     CHECK TO SEE IF ANY VORTICES HAVE BEEN "SHOT" FORWARD OF THE
C     CALCULATED SEPARATION POINT; IF SO, REMOVE FROM THE FLOW AND
C     ADD TO THE GLOST TALLY.  DO NOT CONSIDER VORTICES IN THE
C     MAJOR VORTEX SHEET--THEY CAN APPROACH THE LEADING EDGE FROM
C     AN UPSTREAM POSITION!  ALSO, ONLY REMOVE THOSE VORTICES WHICH
C     ARE CLOSE (Y<0.5) TO THE PLATE.
C
      X=REAL(ZV(NV,NB))
      Y=AIMAG(ZV(NV,NB))
      IF ((X.GE.XSEP(NT)).OR.(Y.GE.0.5))GO TO 3053
      WRITE(6,3052)NV,NB
 3052 FORMAT(16H VORTEX NUMBER (,I3,1H,,I2,18H) IS AHEAD OF XSEP)
      GLOST(NT,NB)=GLOST(NT,NB)+GV(NV,NB)
      GV(NV,NB)=0.0
      KEY=1
      GO TO 3060
CCCCCCCCCCCCCCCCCCCCCCCCCCCCCCCCCCCCCCCCCCCCCCCCCCCCCCCCCCCCCCCCCCCCCC
C
C     FOR THOSE VORTICES WHICH ARE NOT AHEAD OF THE SEPARATION REGION,
C     AND WHICH ARE NOT IN THE FIRST 15 VORTICES, CHECK TO SEE IF THEY
C     ARE WITHIN A CORE RADIUS OF THE PLATE; IF SO, REMOVE FROM THE
C     FLOW AND ADD TO THE GLOST TALLY.
C
 3053 IF(AGE(NV,NB).LE.AGECHK)GO TO 3060
      Y=AIMAG(ZV(NV,NB))
      IF (Y.GT.YMIN) GO TO 3060
      WRITE(6,2)NV,NB
    2 FORMAT(16H VORTEX NUMBER (,I3,1H,,I2,23H) HAS CROSSED THE PLATE)
      GLOST(NT,NB)=GLOST(NT,NB)+GV(NV,NB)
      GV(NV,NB)=0.0
      KEY=1
 3060 CONTINUE
      IF (KEY.EQ.1) CALL PACK (NB)
 3070 CONTINUE
      RETURN
      END
CCCCCCCCCCCCCCCCCCCCCCCCCCCCCCCCCCCCCCCCCCCCCCCCCCCCCCCCCCCCCCCCCCCCCC
CCCCCCCCCCCCCCCCCCCCCCCCCCCCCCCCCCCCCCCCCCCCCCCCCCCCCCCCCCCCCCCCCCCCCC
      SUBROUTINE CVELP(Z,KEY,NV1,NB1,C)
      IMPLICIT COMPLEX(C,Z),INTEGER(I-N)
      COMMON/VORTEX/ZV(300,4),CV(300,4),GV(300,4),GV0(300,4),
     1              DGDT(300,4),AGE(300,4),GSHED(800,4),GLOST(800,4),
     2              GVMIN,GV0MIN,NNV(4),NNB,NVMAX
      COMMON/TIMES/DELT,T(800),NT,NTMAX,NTSTOP
      COMMON/CONST/ZONE,ZERO,ZFAC,ZI,ZPI,PI,TWOPI,PI90,PI180,OV2PI
      COMMON/FLOW/RCORE,CINF,VINF,RMIN,BDISP,NOTOCH,AGECHK
CCCCCCCCCCCCCCCCCCCCCCCCCCCCCCCCCCCCCCCCCCCCCCCCCCCCCCCCCCCCCCCCCCCCCC
C
C     VELOCITY CALCULATION
C
C     KEY=0 DENOTES CALCULATION ASSOICATED WITH CONVECTION OF NASCENT
C     VORTEX, THE SOLID SURFACE, OR, IN THE MOST GENERAL SENSE, AT SOME
C     POINT WHICH IS NOT A VORTEX.
C
```

```
      C=ZERO
      DO 1200 NB=1,NNB
      IF (KEY.EQ.0) GO TO 1020
      IF (NB.EQ.NB1) GO TO 1200
 1020 NV2=NNV(NB)
      IF (NV2.LT.1) GO TO 1200
      DO 1100 NV=1,NV2
      ZN=ZV(NV,NB)
      C=C+CVRANK(Z,ZN,GV(NV,NB),0)
 1100 CONTINUE
 1200 CONTINUE
      IF (KEY.EQ.0) GO TO 1500
      NB=NB1
      IF (NNV(NB).LT.1) GO TO 1500
      I1=1
      I2=NV1-1
      I3=NV1+1
      I4=NNV(NB1)
      IF (I2.LT.I1) GO TO 1310
      DO 1300 NV=I1,I2
      ZN=ZV(NV,NB)
      C=C+CVRANK(Z,ZN,GV(NV,NB),0)
 1300 CONTINUE
 1310 IF (I4.LT.I3) GO TO 1420
      DO 1400 NV=I3,I4
      ZN=ZV(NV,NB)
      C=C+CVRANK(Z,ZN,GV(NV,NB),0)
 1400 CONTINUE
CCCCCCCCCCCCCCCCCCCCCCCCCCCCCCCCCCCCCCCCCCCCCCCCCCCCCCCCCCCCCCCCCCCCCCCCCCCCCCCCC
C
C     INCLUDE THE EFFECT OF THE IMAGE OF THE VORTEX BEING
C     CONVECTED
C
 1420 C=C+CVRANK(Z,ZV(NV1,NB1),GV(NV1,NB1),1)
 1500 CONTINUE
      C=C*ZFAC
      C=CMPLX(-REAL(C),AIMAG(C))
      C=C+CINF
      RETURN
      END
CCCCCCCCCCCCCCCCCCCCCCCCCCCCCCCCCCCCCCCCCCCCCCCCCCCCCCCCCCCCCCCCCCCCCCCCCCCCCCCCC
CCCCCCCCCCCCCCCCCCCCCCCCCCCCCCCCCCCCCCCCCCCCCCCCCCCCCCCCCCCCCCCCCCCCCCCCCCCCCCCCC
      FUNCTION CVRANK(Z,ZN,GV,KEY)
      IMPLICIT COMPLEX(C,Z),INTEGER(I-N)
      COMMON/CONST/ZONE,ZERO,ZFAC,ZI,ZPI,PI,TWOPI,PI90,PI180,OV2PI
      COMMON/FLOW/RCORE,CINF,VINF,RMIN,BDISP,NOTOCH,AGECHK
CCCCCCCCCCCCCCCCCCCCCCCCCCCCCCCCCCCCCCCCCCCCCCCCCCCCCCCCCCCCCCCCCCCCCCCCCCCCCCCCC
C     RANKINE VORTEX VELOCITY CALCULATION.
C
C     KEY=0:  MOST GENERAL CONDITION
C        =1:  CONVECTION OF A VORTEX POSITION, WHEREIN SELF-INDUCED
C             VELOCITY IS SKIPPED, AND ONLY THE CONTRIBUTION OF THE
C             IMAGE IS INCLUDED.
C
      ZNCONJ=CONJG(ZN)
      ZDIFRL=Z-ZN
```

```
      ZDIFIM=Z-ZNCONJ
      RREAL=CABS(ZDIFRL)
      RIMAG=CABS(ZDIFIM)
      CREAL=ZERO
      IF(KEY.EQ.1)GO TO 100
      IF(RREAL.GT.RCORE)GO TO 50
      IF(RREAL.LT.0.00001)GO TO 100
      ZCORE=(ZDIFRL/RREAL)*RCORE
      CREAL=(1.0/ZCORE)*(RREAL/RCORE)
      GO TO 100
   50 CREAL=1.0/ZDIFRL
  100 CIMAG=ZERO
      IF(RIMAG.GT.RCORE) GO TO 150
      IF(RIMAG.LT.0.00001)GO TO 200
      ZCORE=(ZDIFIM/RIMAG)*RCORE
      CIMAG=(1.0/ZDIFIM)*(RIMAG/RCORE)
      GO TO 200
  150 CIMAG=1.0/ZDIFIM
  200 CVRANK=GV*(CREAL-CIMAG)
      RETURN
      END
CCCCCCCCCCCCCCCCCCCCCCCCCCCCCCCCCCCCCCCCCCCCCCCCCCCCCCCCCCCCCCCCCCCCCCCCCC
CCCCCCCCCCCCCCCCCCCCCCCCCCCCCCCCCCCCCCCCCCCCCCCCCCCCCCCCCCCCCCCCCCCCCCCCCC
      SUBROUTINE DISP
      IMPLICIT COMPLEX(C,Z),INTEGER(I-N)
      COMMON/VORTEX/ZV(300,4),CV(300,4),GV(300,4),GV0(300,4),
     1              DGDT(300,4),AGE(300,4),GSHED(800,4),GLOST(800,4),
     2              GVMIN,GV0MIN,NNV(4),NNB,NVMAX
      COMMON/TIMES/DELT,T(800),NT,NTMAX,NTSTOP
      COMMON/FLOW/RCORE,CINF,VINF,RMIN,BDISP,NOTOCH,AGECHK
CCCCCCCCCCCCCCCCCCCCCCCCCCCCCCCCCCCCCCCCCCCCCCCCCCCCCCCCCCCCCCCCCCCCCCCCCC
C
C     DISSIPATES EACH DISCRETE VORTEX'S STRENGTH.
C
      DO 1200 NB=1,NNB
      T0=0.0
      NV2=NNV(NB)
      IF(NB.EQ.1)GO TO 100
      NV2=NNV(NB)
      IF(NV2.LT.1)GO TO 1200
      T0=AGECHK
  100 DO 1100 NV=1,NV2
      IF(AGE(NV,NB).LE.AGECHK)GO TO 1100
      GHOLD=GV(NV,NB)
      TDIFF=AGE(NV,NB)-T0
      IF(TDIFF.LT.DELT)TDIFF=DELT
      EXPONE=EXP(-BDISP/TDIFF)
      GV(NV,NB)=GV0(NV,NB)*(1.0-EXPONE)
      GDIFF=GHOLD-GV(NV,NB)
      DGDT(NV,NB)=GDIFF/DELT
      GLOST(NT,NB)=GLOST(NT,NB)+GDIFF
 1100 CONTINUE
 1200 CONTINUE
      RETURN
      END
CCCCCCCCCCCCCCCCCCCCCCCCCCCCCCCCCCCCCCCCCCCCCCCCCCCCCCCCCCCCCCCCCCCCCCCCCC
```

```
CCCCCCCCCCCCCCCCCCCCCCCCCCCCCCCCCCCCCCCCCCCCCCCCCCCCCCCCCCCCCCCCCCCCCCCCCCCC
      SUBROUTINE PACK(NB)
      IMPLICIT COMPLEX(C,Z),INTEGER(I-N)
      COMMON/VORTEX/ZV(300,4),CV(300,4),GV(300,4),GV0(300,4),
     1              DGDT(300,4),AGE(300,4),GSHED(800,4),GLOST(800,4),
     2              GVMIN,GV0MIN,NNV(4),NNB,NVMAX
      COMMON/CONST/ZONE,ZERO,ZFAC,ZI,ZPI,PI,TWOPI,PI90,PI180,OV2PI
CCCCCCCCCCCCCCCCCCCCCCCCCCCCCCCCCCCCCCCCCCCCCCCCCCCCCCCCCCCCCCCCCCCCCCCCCCCC
C
C     CONSOLIDATES VORTEX ARRAYS, IF ANY VORTICES HAVE BEEN PREVIOUSLY
C     REMOVED FROM THE FLOWFIELD
C
      KNT=0
      NN=NNV(NB)
      DO 1020 N=1,NN
      TEST=ABS(GV(N,NB))-GVMIN
      IF (TEST)1020,1010,1010
 1010 KNT=KNT+1
      IF (KNT.EQ.N) GO TO 1020
      ZV(KNT,NB)=ZV(N,NB)
      GV(KNT,NB)=GV(N,NB)
      CV(KNT,NB)=CV(N,NB)
      GV0(KNT,NB)=GV0(N,NB)
      DGDT(KNT,NB)=DGDT(N,NB)
      AGE(KNT,NB)=AGE(N,NB)
 1020 CONTINUE
      N1=KNT+1
      DO 1030 N=N1,NVMAX
      ZV(N,NB)=ZERO
      CV(N,NB)=ZERO
      GV(N,NB)=0.0
      GV0(N,NB)=0.0
      DGDT(N,NB)=0.0
      AGE(N,NB)=0.0
 1030 CONTINUE
      NNV(NB)=KNT
      RETURN
      END
CCCCCCCCCCCCCCCCCCCCCCCCCCCCCCCCCCCCCCCCCCCCCCCCCCCCCCCCCCCCCCCCCCCCCCCCCCCC
CCCCCCCCCCCCCCCCCCCCCCCCCCCCCCCCCCCCCCCCCCCCCCCCCCCCCCCCCCCCCCCCCCCCCCCCCCCC
      SUBROUTINE CNCL(NNB1,NNB2,NCL)
      IMPLICIT COMPLEX(C,Z),INTEGER(I-N)
      COMMON/VORTEX/ZV(300,4),CV(300,4),GV(300,4),GV0(300,4),
     1              DGDT(300,4),AGE(300,4),GSHED(800,4),GLOST(800,4),
     2              GVMIN,GV0MIN,NNV(4),NNB,NVMAX
      COMMON/TIMES/DELT,T(800),NT,NTMAX,NTSTOP
      COMMON/CONST/ZONE,ZERO,ZFAC,ZI,ZPI,PI,TWOPI,PI90,PI180,OV2PI
      COMMON/FLOW/RCORE,CINF,VINF,RMIN,BDISP,NOTOCH,AGECHK
CCCCCCCCCCCCCCCCCCCCCCCCCCCCCCCCCCCCCCCCCCCCCCCCCCCCCCCCCCCCCCCCCCCCCCCCCCCC
C
C     COMBINES VORTICES IN CLOSE PROXIMITY TO ONE ANOTHER.
C
      NCL=0
      DO 1400 NB1=NNB1,NNB2
      NNV1=NNV(NB1)
      IF (NNV1.LT.1) GO TO 1400
```

```
      DO 1300 NV1X=1,NNV1
      NV1=NNV1-NV1X+1
      G1=GV(NV1,NB1)
      Z1=ZV(NV1,NB1)
      DO 1200 NB2=NNB1,NNB2
      NNV2=NNV(NB2)
      IF (NNV2.LT.1) GO TO 1200
      DO 1100 NV2X=1,NNV2
      NV2=NNV2-NV2X+1
      IF (NB1.NE.NB2) GO TO 1010
      IF (NV1.EQ.NV2) GO TO 1100
 1010 G2=GV(NV2,NB2)
      Z2=ZV(NV2,NB2)
      Z=Z1-Z2
      R=CABS(Z)
      IF (R-RMIN) 1030,1030,1100
 1030 IF ((G1*G2).LT.0.0) GO TO 1100
      G=G1+G2
      IF (ABS(G).GT.GVMIN) GO TO 1040
      GV(NV1,NB1)=0.0
      GV(NV2,NB2)=0.0
      ZV(NV1,NB1)=ZERO
      ZV(NV2,NB2)=ZERO
      CV(NV1,NB1)=ZERO
      CV(NV2,NB2)=ZERO
      GV0(NV1,NB1)=0.0
      GV0(NV2,NB2)=0.0
      DGDT(NV1,NB1)=0.0
      DGDT(NV2,NB2)=0.0
      AGE(NV1,NB1)=0.0
      AGE(NV2,NB2)=0.0
      NCL=NCL+1
      GO TO 1300
 1040 CONTINUE
      Z=(Z1*G1+Z2*G2)/G
      ZV(NV1,NB1)=Z
      GV(NV1,NB1)=G
      CV(NV1,NB1)=ZERO
      GV0(NV1,NB1)=GV0(NV1,NB1)+GV0(NV2,NB2)
      DGDT(NV1,NB1)=DGDT(NV1,NB1)+DGDT(NV2,NB2)
      AGE1=AGE(NV1,NB1)
      AGE2=AGE(NV2,NB2)
      AGE(NV1,NB1)=(AGE1*ABS(G1)+AGE2*ABS(G2))/(ABS(G1)+ABS(G2))
      IF(AGE(NV1,NB1).LT.AGECHK)AGE(NV1,NB1)=AGECHK
      GV(NV2,NB2)=0.0
      ZV(NV2,NB2)=ZERO
      CV(NV2,NB2)=ZERO
      GV0(NV2,NB2)=0.0
      DGDT(NV2,NB2)=0.0
      AGE(NV2,NB2)=0.0
      G1=G
      Z1=Z
      NCL=NCL+1
 1100 CONTINUE
 1200 CONTINUE
 1300 CONTINUE
```

```
 1400 CONTINUE
      RETURN
      END
CCCCCCCCCCCCCCCCCCCCCCCCCCCCCCCCCCCCCCCCCCCCCCCCCCCCCCCCCCCCCCCCCCCCCCCC
CCCCCCCCCCCCCCCCCCCCCCCCCCCCCCCCCCCCCCCCCCCCCCCCCCCCCCCCCCCCCCCCCCCCCCCC
      SUBROUTINE MOVIE(M)
      IMPLICIT COMPLEX(C,Z),INTEGER(I-N)
      CHARACTER RUNNO*3,FILM*7,RECAP*8,CHECK*1
      CHARACTER*60 COMNTS(5)
      COMMON/VORTEX/ZV(300,4),CV(300,4),GV(300,4),GV0(300,4),
     1              DGDT(300,4),AGE(300,4),GSHED(800,4),GLOST(800,4),
     2              GVMIN,GV0MIN,NNV(4),NNB,NVMAX
      COMMON/TIMES/DELT,T(800),NT,NTMAX,NTSTOP
      COMMON/SURFCE/Q(200),PTOTAL(200),PVORT(200),PVELO(200),
     1              DX,NDX,XMAX,X(200),XI(500),TAU(500),BLDISP(500),
     2              BLMOM(500),MSEP,FY(800),XBAR(800)
      COMMON/MISC/RUNNO,NPLOTS,NCOMNT,COMNTS
CCCCCCCCCCCCCCCCCCCCCCCCCCCCCCCCCCCCCCCCCCCCCCCCCCCCCCCCCCCCCCCCCCCCCCCC
C
C     WRITES DATA FOR EACH TIMESTEP TO AN UNFORMATTED FILE:  VORTEX
C     INFORMATION, PLATE PRESSURE/VELOCITY DISTRIBUTIONS, ETC.
C
      NPLOTS=NPLOTS+1
      WRITE(M)NT,T(NT)
      DO 300 NB=1,NNB
      WRITE(M) NNV(NB)
      DO 300 NV=1,NNV(NB)
  300 WRITE(M) ZV(NV,NB),GV(NV,NB),GV0(NV,NB),DGDT(NV,NB)
      DO 1000 I=1,NDX
 1000 WRITE(M)X(I),Q(I),PVELO(I),PVORT(I),PTOTAL(I)
      WRITE(M)MSEP
      DO 2000 I=1,MSEP
 2000 WRITE(M)XI(I),TAU(I),BLDISP(I),BLMOM(I)
      RETURN
      END
CCCCCCCCCCCCCCCCCCCCCCCCCCCCCCCCCCCCCCCCCCCCCCCCCCCCCCCCCCCCCCCCCCCCCCCC
CCCCCCCCCCCCCCCCCCCCCCCCCCCCCCCCCCCCCCCCCCCCCCCCCCCCCCCCCCCCCCCCCCCCCCCC
      SUBROUTINE SUMARY(M)
      IMPLICIT COMPLEX(C,Z),INTEGER(I-N)
      CHARACTER RUNNO*3,FILM*7,RECAP*8,CHECK*1
      CHARACTER*60 COMNTS(5)
      COMMON/VORTEX/ZV(300,4),CV(300,4),GV(300,4),GV0(300,4),
     1              DGDT(300,4),AGE(300,4),GSHED(800,4),GLOST(800,4),
     2              GVMIN,GV0MIN,NNV(4),NNB,NVMAX
      COMMON/SAVE/XVORT(800),YVORT(800),XSEP(800),YSEP(800),USEP(800)
      COMMON/TIMES/DELT,T(800),NT,NTMAX,NTSTOP
      COMMON/CONST/ZONE,ZERO,ZFAC,ZI,ZPI,PI,TWOPI,PI90,PI180,OV2PI
      COMMON/SURFCE/Q(200),PTOTAL(200),PVORT(200),PVELO(200),
     1              DX,NDX,XMAX,X(200),XI(500),TAU(500),BLDISP(500),
     2              BLMOM(500),MSEP,FY(800),XBAR(800)
      COMMON/FLOW/RCORE,CINF,VINF,RMIN,BDISP,NOTOCH,AGECHK
      COMMON/MISC/RUNNO,NPLOTS,NCOMNT,COMNTS
      COMMON/MISC1/NHICUP
CCCCCCCCCCCCCCCCCCCCCCCCCCCCCCCCCCCCCCCCCCCCCCCCCCCCCCCCCCCCCCCCCCCCCCCC
C
C     WRITES SUMMARY INFORMATION TO AN UNFORMATTED FILE.
```

```
C
      NTSTOP=NT
      CALL GETTIM(IHR,IMIN,ISEC,I100TH)
      CALL GETDAT(IYR,IMO,IDAY)
      ITIME=IHR*100+IMIN
      IDATE=IMO*10**6+IDAY*10**4+IYR
      WRITE(M)IDATE,ITIME
      WRITE(M)NCOMNT
      IF (NCOMNT.EQ.0) GO TO 40
      DO 25 J=1,NCOMNT
   25 WRITE(M)COMNTS(J)
   40 WRITE(M)RUNNO,DELT,RCORE,GVMIN,GV0MIN,BDISP
      WRITE(M)NHICUP
      WRITE(M)NPLOTS
      WRITE(M)NNB
      WRITE(M)VINF,XMAX,DX,NDX
      WRITE(M)NTSTOP
      DO 400 I=1,NTSTOP
  400 WRITE(M)T(I),(GSHED(I,NB),GLOST(I,NB),NB=1,NNB),XSEP(I),YSEP(I),
     1        USEP(I),XVORT(I),YVORT(I),FY(I),XBAR(I)
      RETURN
      END
CCCCCCCCCCCCCCCCCCCCCCCCCCCCCCCCCCCCCCCCCCCCCCCCCCCCCCCCCCCCCCCCCCCCCCCC
CCCCCCCCCCCCCCCCCCCCCCCCCCCCCCCCCCCCCCCCCCCCCCCCCCCCCCCCCCCCCCCCCCCCCCCC
      SUBROUTINE NEWBL(XVORT,XSEP,USEP)
      DIMENSION ETA(121),U0(121),F0(121),S0(121),YOT(121),VOR(121)
      COMMON/INTEG/MT,ITER,NM,NN,IBL,IFL
      COMMON/REAL/DEL,GAM,PSI,HI,HI2,A21,A22,B21,B22,SUM,SF,DEL1,H,T
      COMMON/REAL1/ETAMAX,DN
      COMMON/ALG/E11(121),E21(121),F1(121),F2(121),FMN2(121)
      COMMON/SOLN/UM(121),FM(121),S(121),UMN1(121),FMN1(121),UMN2(121)
      COMMON/FINITE/XILE,VINF
      COMMON/CONST/ZONE,ZERO,ZFAC,ZI,ZPI,PI,TWOPI,PI90,PI180,OV2PI
      COMMON/SURFCE/Q(200),PTOTAL(200),PVORT(200),PVELO(200),
     1             DX,NDX,XMAX,X(200),XXI(500),TTAU(500),BLDISP(500),
     2             BLMOM(500),MSEP,FY(800),XBAR(800)
      COMMON/MISC1/NHICUP
CCCCCCCCCCCCCCCCCCCCCCCCCCCCCCCCCCCCCCCCCCCCCCCCCCCCCCCCCCCCCCCCCCCCCCCC
C
C THIS SUBROUTINE INTEGRATES THE LAMINAR BOUNDARY-LAYER EQUATIONS FOR
C PLANE, STEADY, INCOMPRESSIBLE FLOW.  IT EMPLOYS A TRANSFORMATION
C OF VARIABLES THAT IS BASED ON THWAITES' ANALYSIS OF THE MOMENTUM-
C INTEGRAL EQUATION, AND EMBODIES A TWO-TERM BLASIUS SERIES TO START
C THE CALCULATION.  THREE-POINT TRAILING DIFFERENCES ARE SUBSEQUENTLY
C USED FOR SECOND-ORDER ACCURACY IN XI.  THE FLOW IS THAT UNDER A LINE
C VORTEX PLACED AT XI=0.0, WHERE THE LEADING EDGE OF THE PLATE IS AT
C XI=XILE.THIS CORRECTS ERRORS IN BOOK VERSION OF THE PROGRAM, BASED
C UPON COMMUNICATIONS WITH SHERMAN. (VISCOUS FLOW, BY FREDERICK S.
C SHERMAN, MCGRAW-HILL PUBLISHING CO., 1990).
C
      REAL MOM,ATEMP(12)
      COMPLEX ZONE,ZERO,ZFAC,ZI,ZPI
      EXTERNAL FOFX
CCCCCCCCCCCCCCCCCCCCCCCCCCCCCCCCCCCCCCCCCCCCCCCCCCCCCCCCCCCCCCCCCCCCCCCC
C
C  ASSIGN VALUES TO CONSTANTS
```

```
C
        XILE=0.00001
        NN=81
        EPSLON=.0010
        HPI=0.50*PI
        ETAMAX=6.50
        NM=NN-1
        RNM=NM
        DN=ETAMAX/RNM
        HI=1.0/DN
        HI2=HI*HI
        A21=.50
        A22=HI
        B21=.50
        B22=-HI
CCCCCCCCCCCCCCCCCCCCCCCCCCCCCCCCCCCCCCCCCCCCCCCCCCCCCCCCCCCCCCCCCCCCCCCCCCCCCCC
C
C    SET UP ETA(N) AND FIRST-GUESS INITIAL PROFILES OF UM, S, AND FM.
C    THESE WILL BE REFINED BY ITERATION.  PARABOLIC FIRST GUESS.
C
      DO 10 N=1,NN
        ETA(N)=(N-1)*DN
        G=ETA(N)/ETAMAX
        UM(N)=G*(2.0-G)
        S(N)=2.0*(1.0-G)/ETAMAX
        FM(N)=G*G*(1.0-G/3.0)*ETAMAX
        UMN1(N)=UM(N)
        FMN1(N)=FM(N)
        UMN2(N)=UM(N)
        FMN2(N)=FM(N)
   10  CONTINUE
CCCCCCCCCCCCCCCCCCCCCCCCCCCCCCCCCCCCCCCCCCCCCCCCCCCCCCCCCCCCCCCCCCCCCCCCCCCCCCC
C
C    CALCULATE U0 AND F0 OF STARTING PROFILE
C
        GAM=1.0
        DEL=0.0
        PSI=0.0
        E11(1)=0.0
        E21(1)=0.0
        F1(1)=0.0
        F2(1)=0.0
        ITER=1
        MT=1
        IBL=0
        CALL THOMAS
      DO 31 N=1,NN
         U0(N)=UM(N)
         F0(N)=FM(N)
         S0(N)=S(N)
   31 CONTINUE
         SF0=SF
         DEL0=DEL1
         SUM0=SUM
CCCCCCCCCCCCCCCCCCCCCCCCCCCCCCCCCCCCCCCCCCCCCCCCCCCCCCCCCCCCCCCCCCCCCCCCCCCCCCC
C
```

```
C     CALCULATE U1 AND F1 IN THE BLASIUS-SERIES REPRESENTATION
C
          E11(1)=0.0
          E21(1)=0.0
          F1(1)=0.0
          F2(1)=0.0
          ITER=10
          MT=1
          M=1
          IBL=1
          CALL THOMAS
   32 CONTINUE
CCCCCCCCCCCCCCCCCCCCCCCCCCCCCCCCCCCCCCCCCCCCCCCCCCCCCCCCCCCCCCCCCCCCCCCCCCCCCCC
C
C       INITIALIZE XI.  SET THE INITIAL SIZE OF DXI.
C
          XI=XILE
          DXI=0.0031250
          IF (XVORT.GT.0.0)DXI=0.006250
          IF (XVORT.GT.0.5)DXI=0.012500
          IF (XVORT.GT.1.0)DXI=0.025000
          IF (XVORT.GT.2.0)DXI=0.050000
CCCCCCCCCCCCCCCCCCCCCCCCCCCCCCCCCCCCCCCCCCCCCCCCCCCCCCCCCCCCCCCCCCCCCCCCCCCCCCC
C
C       COMBINE U0 AND U1, ETC, TO GET INITIAL PROFILES.
C
          IF (ABS(XI).LT.EPSLON) XI=EPSLON
          Z=XI-XILE
          ZZ=XI-XILE+DXI
          ZZZ=XI-XILE+2.0*DXI
          ALIMIT=XILE
          BLIMIT=XI
          CALL ROM(ALIMIT,BLIMIT,EPSLON,ANS,FOFX,ATEMP)
          G2=ANS
          XX=XI
          V=UTAN(XX)
          VSQR=V*V
          V6=VSQR*VSQR*VSQR
          G2=G2*2.0/V6
          DVDXI=DERIV(XX)
          IF(G2.GT.0.0)GO TO 30
          NHICUP=NHICUP+1
          G2=ABS(G2)
          WRITE(6,50)NHICUP
   30     DYDETA=SQRT(G2)
          DEL=G2*DVDXI
          GAM=1.0-2.0*DEL
          SUM=0.0
       DO 33 N=2,NN
          UMN2(N)=U0(N)+Z*UM(N)
          FMN2(N)=F0(N)+Z*FM(N)
          UMN1(N)=U0(N)+ZZ*UM(N)
          FMN1(N)=F0(N)+ZZ*FM(N)
          UM(N)=U0(N)+ZZZ*UM(N)
          FM(N)=F0(N)+ZZZ*FM(N)
          S(N)=S0(N)+ZZZ*S(N)
```

```
         SUM=SUM+0.50*DN*(UM(N)+UM(N-1))*(1.0-0.50*(UM(N)+UM(N-1)))
  33  CONTINUE
         DEL1=ETA(NM)-FM(NM)
         SF=UM(2)*HI+.500*DN*DEL
         UM(1)=0.0
         FM(1)=0.0
         S(1)=SF
         T=SF*SUM
         H=DEL1/SUM
         DISPL=DYDETA*DEL1
         MOM=DYDETA*SUM
         TAU=V*SF/DYDETA
         XXI(1)=XI
         BLDISP(1)=DISPL
         BLMOM(1)=MOM
         TTAU(1)=TAU
CCCCCCCCCCCCCCCCCCCCCCCCCCCCCCCCCCCCCCCCCCCCCCCCCCCCCCCCCCCCCCCCCCCCCCCC
C
C      START THE MARCHING LOOP.  SPECIFY DXI FOR VARIOUS RANGES OF XI.
C      CALCULATE QUANTITIES THAT DEPEND ONLY ON XI.
C
         IBL=2
         M=1
 1000    M=M+1
         MT=M
       DXIB4=DXI
       XDIFF=XI-XVORT
       DXI=0.05
       IF (XDIFF.GE.-2.00)DXI=0.0250
       IF (XDIFF.GE.-1.00)DXI=0.01250
       IF (XDIFF.GE.-0.50)DXI=0.006250
       IF (XDIFF.GE.-0.00)DXI=0.0031250
       IF (DXI.NE.DXIB4) IFL=1
         XI=XI+DXI
         XX=XI
         V=UTAN(XX)
         DVDXI=DERIV(XX)
      BLIMIT=XI
      CALL ROM(ALIMIT,BLIMIT,EPSLON,ANS,FOFX,ATEMP)
      G2=ANS
      VSQR=V*V
      V6=VSQR*VSQR*VSQR
      G2=G2*2.0/V6
      IF(G2.GT.0.0)GO TO 44
      G2=ABS(G2)
      NHICUP=NHICUP+1
      WRITE(6,50)NHICUP
   50 FORMAT(' THWAITES INTEGRAL < 0, OCCURRENCE NUMBER',I4)
   44  DYDETA=SQRT(G2)
       DEL=G2*DVDXI
       GAM=1.0-2.0*DEL
       PSI=G2*V/DXI
CCCCCCCCCCCCCCCCCCCCCCCCCCCCCCCCCCCCCCCCCCCCCCCCCCCCCCCCCCCCCCCCCCCCCCCC
C
C      SET WALL BOUNDARY CONDITIONS.
C
```

```
          E11(1)=0.0
          E21(1)=0.0
          F1(1)=0.0
          F2(1)=0.0
CCCCCCCCCCCCCCCCCCCCCCCCCCCCCCCCCCCCCCCCCCCCCCCCCCCCCCCCCCCCCCCCCCCCCCCC
C
C      SET ITERATION COUNTER.  CALCULATE PROFILES AT NEW VALUE OF XI.
C
          ITER=1
          CALL THOMAS
CCCCCCCCCCCCCCCCCCCCCCCCCCCCCCCCCCCCCCCCCCCCCCCCCCCCCCCCCCCCCCCCCCCCCCCC
C
C      UNWIND TRANSFORMATION
C
       DISPL=DYDETA*DEL1
       MOM=DYDETA*SUM
       TAU=V*SF/DYDETA
       BLDISP(M)=DISPL
       BLMOM(M)=MOM
       XXI(M)=XI
       TTAU(M)=TAU
CCCCCCCCCCCCCCCCCCCCCCCCCCCCCCCCCCCCCCCCCCCCCCCCCCCCCCCCCCCCCCCCCCCCCCCC
C
C     LOGIC TO DETERMINE SEPARATION POINT, BASED UPON ZERO
C     SHEAR CRITERION FOR STEADY FLOW.
C
      IF (M.LE.3) GO TO 101
CCCCCCCCCCCCCCCCCCCCCCCCCCCCCCCCCCCCCCCCCCCCCCCCCCCCCCCCCCCCCCCCCCCCCCCC
C
C     IF TAU CHANGES TO NEGATIVE VALUE, INTERPOLATE
C
      IF (TTAU(M)*TTAU(M-1).LT.0.0) GO TO 80
CCCCCCCCCCCCCCCCCCCCCCCCCCCCCCCCCCCCCCCCCCCCCCCCCCCCCCCCCCCCCCCCCCCCCCCC
C
C     IF MOST RECENT TAU IS < THAN PREVIOUS, CONTINUE MARCH DOWNSTRM
C
      IF (TTAU(M).LT.TTAU(M-1)) GO TO 101
CCCCCCCCCCCCCCCCCCCCCCCCCCCCCCCCCCCCCCCCCCCCCCCCCCCCCCCCCCCCCCCCCCCCCCCC
C
C     WE'VE NOW REACHED A POINT WHERE THE LATEST TAU IS GREATER THAN
C     THE PREVIOUS VALUE.  IF TWICE THE DISTANCE BETWEEN PREVIOUS
C     TWO POINTS ADDED TO THE MOST RECENT INDICATES THAT SHEAR
C     SHOULD'VE GONE NEGATIVE, IGNORE THE MOST RECENT AND EXTRAPOLATE
C     FROM THE LAST MONOTONICALLY DECREASING VALUE. IF THE EXTRAPOLATED
C     VALUE ISN'T NEGATIVE, WE'RE PROBABLY ON THE UPWARD SLOPE BEFORE
C     TAU PEAKS OUT.
C
      IF (TTAU(M-1)-2.0*(TTAU(M-2)-TTAU(M-1)).GT.0.0) GO TO 101
      XSEP=XXI(M-1)+(XXI(M-1)-XXI(M-2))*TTAU(M-1)/(TTAU(M-2)-TTAU(M-1))
      USEP=UTAN(XSEP)
      M=M-1
      MSEP=M
      RETURN
   80 XSEP=XXI(M-1)+(XXI(M)-XXI(M-1))*TTAU(M-1)/(TTAU(M-1)-TTAU(M))
      USEP=UTAN(XSEP)
      M=M-1
```

```
      MSEP=M
      RETURN
CCCCCCCCCCCCCCCCCCCCCCCCCCCCCCCCCCCCCCCCCCCCCCCCCCCCCCCCCCCCCCCCCCCCCCCCCCCC
C
C     IF PRINCIPAL VORTEX IS UPSTREAM OF LEADING EDGE, AND CALCULATION
C     HAS CARRIED ON TO XI=0.5, ASSUME NO SEPARATION WILL OCCUR
C
  101 IF ((XVORT.LT.0.0).AND.(XXI(M).GT.0.5))GO TO 103
      XCALC=XXI(M)-XVORT
      IF ((XVORT.GE.0.0).AND.(XCALC.GT.1.0)) GO TO 103
CCCCCCCCCCCCCCCCCCCCCCCCCCCCCCCCCCCCCCCCCCCCCCCCCCCCCCCCCCCCCCCCCCCCCCCCCCCC
C
C     IF VORTEX HAS PASSED THE LEADING EDGE AND CALCULATION HAS
C     PROCEEDED ONE NONDIMENSIONAL UNIT DOWNSTREAM OF THE VORTEX,
C     ASSUME NO SEPARATION WILL OCCUR.
C
  102 IF (M.LT.500) GO TO 1000
CCCCCCCCCCCCCCCCCCCCCCCCCCCCCCCCCCCCCCCCCCCCCCCCCCCCCCCCCCCCCCCCCCCCCCCCCCCC
C
C     SEPARATION IS ASSUMED NOT TO HAVE OCCURRED IF XSEP=USEP=0.0
C
  103 USEP=0.0
      XSEP=0.0
      MSEP=M
      RETURN
      END
CCCCCCCCCCCCCCCCCCCCCCCCCCCCCCCCCCCCCCCCCCCCCCCCCCCCCCCCCCCCCCCCCCCCCCCCCCCC
CCCCCCCCCCCCCCCCCCCCCCCCCCCCCCCCCCCCCCCCCCCCCCCCCCCCCCCCCCCCCCCCCCCCCCCCCCCC
      FUNCTION FOFX(X)
CCCCCCCCCCCCCCCCCCCCCCCCCCCCCCCCCCCCCCCCCCCCCCCCCCCCCCCCCCCCCCCCCCCCCCCCCCCC
C
C     THIS IS THE INTEGRAND INVOLVED IN THWAITES' METHOD
C
      V=UTAN(X)
      VSQR=V*V
      V5=VSQR*VSQR*V
      FOFX=V5
      RETURN
      END
CCCCCCCCCCCCCCCCCCCCCCCCCCCCCCCCCCCCCCCCCCCCCCCCCCCCCCCCCCCCCCCCCCCCCCCCCCCC
CCCCCCCCCCCCCCCCCCCCCCCCCCCCCCCCCCCCCCCCCCCCCCCCCCCCCCCCCCCCCCCCCCCCCCCCCCCC
      FUNCTION DERIV(X)
      IMPLICIT COMPLEX(C,Z),INTEGER(I-N)
      COMMON/VORTEX/ZV(300,4),CV(300,4),GV(300,4),GV0(300,4),
     1              DGDT(300,4),AGE(300,4),GSHED(800,4),GLOST(800,4),
     2              GVMIN,GV0MIN,NNV(4),NNB,NVMAX
      COMMON/CONST/ZONE,ZERO,ZFAC,ZI,ZPI,PI,TWOPI,PI90,PI180,OV2PI
CCCCCCCCCCCCCCCCCCCCCCCCCCCCCCCCCCCCCCCCCCCCCCCCCCCCCCCCCCCCCCCCCCCCCCCCCCCC
C
C     TAKES DERIVATIVE OF VELOCITY DISTRIBUTION AT THE PLATE
C

      DVDX=0.0
      DO 1200 NB=1,NNB
      NV2=NNV(NB)
      IF (NV2.LT.1) GO TO 1200
```

```
      DO 1100 NV=1,NV2
      XDIFF=X-REAL(ZV(NV,NB))
      YDIFF=-AIMAG(ZV(NV,NB))
      XSQ=XDIFF*XDIFF
      YSQ=YDIFF*YDIFF
      SUM=XSQ+YSQ
      DVDX=DVDX+2.0*GV(NV,NB)*XDIFF*YDIFF/(PI*SUM*SUM)
 1100 CONTINUE
 1200 CONTINUE
      DERIV=DVDX
      RETURN
      END
CCCCCCCCCCCCCCCCCCCCCCCCCCCCCCCCCCCCCCCCCCCCCCCCCCCCCCCCCCCCCCCCCCCCCCCCCCC
CCCCCCCCCCCCCCCCCCCCCCCCCCCCCCCCCCCCCCCCCCCCCCCCCCCCCCCCCCCCCCCCCCCCCCCCCCC
      SUBROUTINE ROM(ALIMIT,BLIMIT,EPSLON,ANS,FUNCT,ATEMP)
      EQUIVALENCE (I,N)
      DIMENSION ATEMP(12)
CCCCCCCCCCCCCCCCCCCCCCCCCCCCCCCCCCCCCCCCCCCCCCCCCCCCCCCCCCCCCCCCCCCCCCCCCCC
C
C     NUMERICAL INTEGRATION ROUTINE AS OBTAINED FROM COMPUTER
C     APPLICATIONS OF NUMERICAL METHODS, BY SHAN S. KUO, ADDISON-
C     WESLEY PUBLISHING CO., 1972.USER MUST CODE FUNCTION SUBPROGRAM
C     FUNCT(X). THE UPWARD DIAGONAL ELEMENTS ARE COMPUTED AND STORED
C     IN ATEMP.
C
      I=1
      ATEMP(1)=0.5*(FUNCT(BLIMIT)+FUNCT(ALIMIT))
CCCCCCCCCCCCCCCCCCCCCCCCCCCCCCCCCCCCCCCCCCCCCCCCCCCCCCCCCCCCCCCCCCCCCCCCCCC
C
C     INTERVAL (WIDTH) MUST NOT BE ZERO.
C
      WIDTH=BLIMIT-ALIMIT
      ZL=WIDTH
CCCCCCCCCCCCCCCCCCCCCCCCCCCCCCCCCCCCCCCCCCCCCCCCCCCCCCCCCCCCCCCCCCCCCCCCCCC
C
C     POWER USED TO COMPUTE 2**(I-1)
C     JJ USED TO CONTROL DO LOOP 12 BELOW.
C
      POWER=1.
      JJ=1
CCCCCCCCCCCCCCCCCCCCCCCCCCCCCCCCCCCCCCCCCCCCCCCCCCCCCCCCCCCCCCCCCCCCCCCCCCC
C
C     BEGIN THE OUTERMOST LOOP
C
  711 I=I+1
      ANS=ATEMP(1)
CCCCCCCCCCCCCCCCCCCCCCCCCCCCCCCCCCCCCCCCCCCCCCCCCCCCCCCCCCCCCCCCCCCCCCCCCCC
C
C     FOLLOWING 10 STATEMENTS COMPUTE A NEW A(I,1) BY TRAPEZOIDAL RULE.
C      EQN.(12.19B)
C
      TEMPL=ZL
      ZL=0.5*ZL
      POWER=0.5*POWER
      X=ALIMIT+ZL
      SUM=0.0
```

```
      DO 12 JCOUNT=1,JJ
      SUM=SUM+FUNCT(X)
   12 X=X+TEMPL
      ATEMP(I)=0.5*ATEMP(I-1)+SUM*POWER
CCCCCCCCCCCCCCCCCCCCCCCCCCCCCCCCCCCCCCCCCCCCCCCCCCCCCCCCCCCCCCCCCC
C
C     NEXT 9 STATEMENTS USED TO CALCULATE A(N,M) BY EQN.(12.19A).
C      M IS NOT EQUAL TO 1.
C
      R=1.0
      NM1=N-1
      DO 16 KOUNT=1,NM1
      KK=N-KOUNT
      R=R+R
      R=R+R
      ATEMP(KK)=ATEMP(KK+1)+(ATEMP(KK+1)-ATEMP(KK))/(R-1.)
      M=KOUNT+1
   16 CONTINUE
      DELTA=ABS((ATEMP(1)/ANS)-1.)
      IF (DELTA-EPSLON) 40,40,30
   30 JJ=JJ+JJ
      GO TO 711
Y   40 ANS=ATEMP(1)*WIDTH
      RETURN
      END
CCCCCCCCCCCCCCCCCCCCCCCCCCCCCCCCCCCCCCCCCCCCCCCCCCCCCCCCCCCCCCCCCCCCC
CCCCCCCCCCCCCCCCCCCCCCCCCCCCCCCCCCCCCCCCCCCCCCCCCCCCCCCCCCCCCCCCCCCCC
      SUBROUTINE THOMAS
      COMMON/INTEG/MT,ITER,NM,NN,IBL,IFL
      COMMON/REAL/DEL,GAM,PSI,HI,HI2,A21,A22,B21,B22,SUM,SF,DEL1,H,T
      COMMON/REAL1/ETAMAX,DN
      COMMON/ALG/E11(121),E21(121),F1(121),F2(121),FMN2(121)
      COMMON/SOLN/UM(121),FM(121),S(121),UMN1(121),FMN1(121),UMN2(121)
      COMMON/FINITE/XILE,VINF
CCCCCCCCCCCCCCCCCCCCCCCCCCCCCCCCCCCCCCCCCCCCCCCCCCCCCCCCCCCCCCCCCCCCC
C
C     IMPLEMENTATION OF THE THOMAS ALGORITHM TO SOLVE COEFF MATRIX.
C     THIS CORRECTS TEXT VERSION OF THE PROGRAM, BASED UPON COMMENTS
C     RECEIVED FROM SHERMAN.  PROGRAM MODIFIED FOR SEMI-INFINITE
C     FLAT PLATE.
C
C      START THOMAS ALGORITHM.  TRIANGULARIZE.
C

1000  DO 20 N=2,NM
         IF (IFL.EQ.1) GO TO 10
         A=1.50
         B=-2.0
         C=.50
         GO TO 15
10       A=4.0/3.0
         B=-1.50
         C=1.0/6.0
15       X=GAM*FM(N)+PSI*(A*FM(N)+B*FMN1(N)+C*FMN2(N))
         Y=-2.0*DEL*UM(N)-PSI*(2.0*A*UM(N)+B*UMN1(N)+C*UMN2(N))
         IF (IBL.EQ.1) X=FM(N)
```

```
         IF (IBL.EQ.1) Y=-2.0*UM(N)
         A11=HI2-.50*HI*X
         C11=HI2+.50*HI*X
         B11=-2.0*HI2+Y
         B12=(GAM+A*PSI)*S(N)
         IF (IBL.EQ.1) B12=3.0*S(N)
         D1=GAM*FM(N)*S(N)-DEL*(1.0+UM(N)*UM(N))+PSI*A*(S(N)*FM(N)-
     1   UM(N)*UM(N))
         IF (IBL.EQ.1) D1=4.0*XILE/(1.0+XILE*XILE)*
     1                    (1.0-UM(N)*UM(N)-2.0*FM(N)*S(N))
         G11=A11*E11(N-1)+B11
         G12=B12
         G21=A21*E11(N-1)+A22*E21(N-1)+B21
         G22=B22
         DENO=G11*G22-G12*G21
         GI11=G22/DENO
         GI12=-G12/DENO
         GI21=-G21/DENO
         GI22=G11/DENO
         E11(N)=-GI11*C11
         E21(N)=-GI21*C11
         F1(N)=GI11*(D1-A11*F1(N-1))-GI12*(A21*F1(N-1)+A22*F2(N-1))
         F2(N)=GI21*(D1-A11*F1(N-1))-GI22*(A21*F1(N-1)+A22*F2(N-1))
20    CONTINUE

CCCCCCCCCCCCCCCCCCCCCCCCCCCCCCCCCCCCCCCCCCCCCCCCCCCCCCCCCCCCCCCCCCCCCCCCCCC
C      SET OUTER BOUNDARY CONDITION.
C
        UM(NN)=1.0
        IF (IBL.EQ.1) UM(NN)=0.0
CCCCCCCCCCCCCCCCCCCCCCCCCCCCCCCCCCCCCCCCCCCCCCCCCCCCCCCCCCCCCCCCCCCCCCCCCCC
C
C      BACK-SUBSTITUTE TO FIND UM AND FM.
C
      DO 30 N=1,NM
         K=NN-N
         UM(K)=E11(K)*UM(K+1)+F1(K)
         FM(K)=E21(K)*UM(K+1)+F2(K)
30    CONTINUE
         FM(NN)=FM(NM)+.50*DN*(UM(NN)+UM(NM))
CCCCCCCCCCCCCCCCCCCCCCCCCCCCCCCCCCCCCCCCCCCCCCCCCCCCCCCCCCCCCCCCCCCCCCCCCCC
C
C      UPDATE S(N).
C
      DO 40 N=2,NM
         S(N)=.50*HI*(UM(N+1)-UM(N-1))
40    CONTINUE

CCCCCCCCCCCCCCCCCCCCCCCCCCCCCCCCCCCCCCCCCCCCCCCCCCCCCCCCCCCCCCCCCCCCCCCCCCC
C
C      ADVANCE AND CHECK ITERATION COUNTER.
C
         ITER=ITER+1
         IF (MT.EQ.1.AND.ITER.LT.10) GO TO 1000
         IF (MT.GT.1.AND.ITER.LT.3) GO TO 1000
CCCCCCCCCCCCCCCCCCCCCCCCCCCCCCCCCCCCCCCCCCCCCCCCCCCCCCCCCCCCCCCCCCCCCCCCCCC
```

```
C
C      CALCULATE B.L. THICKNESSES, SHAPE FACTORS, AND SKIN
C      FRICTION.  UPDATE UMN1 AND FMN1.
C
          SUM=0.0
       DO 50 N=2,NM
          SUM=SUM+0.50*DN*(UM(N)+UM(N-1))*(1.0-0.50*(UM(N)+UM(N-1)))
          UMN2(N)=UMN1(N)
          FMN2(N)=FMN1(N)
          UMN1(N)=UM(N)
          FMN1(N)=FM(N)
50     CONTINUE
          SF=UM(2)*HI+.500*DN*DEL
          S(1)=SF
          DEL1=ETAMAX-DN-FM(NM)
          H=DEL1/SUM
          T=SF*SUM
       IFL=0
       RETURN
       END
CCCCCCCCCCCCCCCCCCCCCCCCCCCCCCCCCCCCCCCCCCCCCCCCCCCCCCCCCCCCCCCCCCCCCCCC
CCCCCCCCCCCCCCCCCCCCCCCCCCCCCCCCCCCCCCCCCCCCCCCCCCCCCCCCCCCCCCCCCCCCCCCC
       SUBROUTINE EXPLOD(NB,GAMMA,ZCNTR,RMAX,IGAMMA)
       IMPLICIT COMPLEX(C,Z),INTEGER(I-N)
       COMMON/VORTEX/ZV(300,4),CV(300,4),GV(300,4),GV0(300,4),
      1              DGDT(300,4),AGE(300,4),GSHED(800,4),GLOST(800,4),
      2              GVMIN,GV0MIN,NNV(4),NNB,NVMAX
       COMMON/TIMES/DELT,T(800),NT,NTMAX,NTSTOP
       COMMON/CONST/ZONE,ZERO,ZFAC,ZI,ZPI,PI,TWOPI,PI90,PI180,OV2PI
       DIMENSION R(4),NVRING(4)
CCCCCCCCCCCCCCCCCCCCCCCCCCCCCCCCCCCCCCCCCCCCCCCCCCCCCCCCCCCCCCCCCCCCCCCC
C
C      DISCRETIZES PRIMARY VORTEX; METHOD SELECTABLE BY USER:
C
C      IF IGAMMA=1:  POLLING VORTICITY DISTRIBUTION WITHIN RMAX
C               =2:  RANDOM VORTEX DISTRIBUTION AND STRENGTH WITHIN RMAX
C               =3:  RANDOM DISTRIBUTION, EQUAL STRENGTHS WIHIN RMAX
C               =4:  EVENLY RANDOM DISTRIBUTION (I.E., NO CONCENTRATION
C                    AT CENTER), EQUAL STRENGTHS WITHIN RMAX
C
       AGE0=AGE(1,NB)
       DGDT0=DGDT(1,NB)
       GV00=GV0(1,NB)
       IF(IGAMMA.EQ.1)GO TO 100
       IF(IGAMMA.EQ.2)GO TO 2000
       IF(IGAMMA.EQ.3)GO TO 4500
       IF(IGAMMA.EQ.4)GO TO 6000
       GO TO 9999
CCCCCCCCCCCCCCCCCCCCCCCCCCCCCCCCCCCCCCCCCCCCCCCCCCCCCCCCCCCCCCCCCCCCCCCC
C
C      DISTRIBUTION AND STRENGTHS AS PER POLING
C
  100  R(1)=0.0
       R(2)=0.50*RMAX
       R(3)=0.75*RMAX
       R(4)=     RMAX
```

```
      NVRING(1)=1
      NVRING(2)=8
      NVRING(3)=12
      NVRING(4)=24
      NV=1
      ZV(1,NB)=ZCNTR
      GV(1,NB)=GAMMA/4.0
      DO 1000 NRING=2,4
      THETA=0.0
      IF(NRING.EQ.2)GRING=3.0*GAMMA/8.0
      IF(NRING.EQ.3)GRING=2.0*GAMMA/8.0
      IF(NRING.EQ.4)GRING=1.0*GAMMA/8.0
      DTHETA=TWOPI/NVRING(NRING)
      DO 500 I=1,NVRING(NRING)
      NV=NV+1
      THETA=THETA+DTHETA
      XV=R(NRING)*COS(THETA)
      YV=R(NRING)*SIN(THETA)
      ZV(NV,NB)=ZCNTR+CMPLX(XV,YV)
      GV(NV,NB)=GRING/NVRING(NRING)
  500 CONTINUE
 1000 CONTINUE
      NNV(NB)=NV
      GO TO 8888
CCCCCCCCCCCCCCCCCCCCCCCCCCCCCCCCCCCCCCCCCCCCCCCCCCCCCCCCCCCCCCCCCCCCCC
C
C     RANDOM LOCATIONS AND RANDOM STRENGTH
C
 2000 CALL SEED(RND$TIMESEED)
      GSUM=0.0
      GMAX=0.2*DELT/0.125
      NEQSTR=INT(GAMMA/GMAX)
      NTOPS=5*NEQSTR
CCCCCCCCCCCCCCCCCCCCCCCCCCCCCCCCCCCCCCCCCCCCCCCCCCCCCCCCCCCCCCCCCCCCCC
C
C     NOTE:  CONCENTRATION OF VORTICITY AT CENTER.  IF A MORE EVEN
C            DISTRIBUTION OF VORTICITY IS DESIRED, USE A CARTESIAN
C            PLACMENT SCHEME, DISCARDING VORTICES WHICH FALL OUTSIDE
C            A CIRCLE OF RADIUS=RMAX.
C
      DO 3000 NV=1,NTOPS
      CALL RANDOM(RADIAL)
      RADIUS=RMAX*RADIAL
      CALL RANDOM(ANGULR)
      THETA=TWOPI*ANGULR
      XV=RADIUS*COS(THETA)
      YV=RADIUS*SIN(THETA)
      ZV(NV,NB)=ZCNTR+CMPLX(XV,YV)
      IF((GAMMA-GSUM).GT.GMAX)GO TO 2500
      GV(NV,NB)=GAMMA-GSUM
      GO TO 4000
 2500 CALL RANDOM(SIZE)
      GV(NV,NB)=GMAX*SIZE
      GSUM=GSUM+GV(NV,NB)
 3000 CONTINUE
      WRITE(6,3500)NB
```

```
 3500 FORMAT(' NOT ENOUGH VORTICITY IN SHEET NUMBER',I2)
 4000 NNV(NB)=NV
      GO TO 8888
CCCCCCCCCCCCCCCCCCCCCCCCCCCCCCCCCCCCCCCCCCCCCCCCCCCCCCCCCCCCCCCCCCCCC
C
C     RANDOM LOCATION AND EQUAL STRENGTH
C
 4500 CALL SEED(RND$TIMESEED)
      GVORT=0.2*DELT/0.125
      NVORTS=INT(GAMMA/GVORT)
      NVORTS=NVORTS+1
      GVORT=GAMMA/NVORTS
      DO 5000 NV=1,NVORTS
      CALL RANDOM(RADIAL)
      RADIUS=RMAX*RADIAL
      CALL RANDOM(ANGULR)
      THETA=TWOPI*ANGULR
      XV=RADIUS*COS(THETA)
      YV=RADIUS*SIN(THETA)
      ZV(NV,NB)=ZCNTR+CMPLX(XV,YV)
      GV(NV,NB)=GVORT
 5000 CONTINUE
      NNV(NB)=NVORTS
      GO TO 8888
 6000 CALL SEED(RND$TIMESEED)
      GVORT=0.2*DELT/0.125
      NVORTS=INT(GAMMA/GVORT)
      NVORTS=NVORTS+1
      RMAX2=2.0*RMAX
      GVORT=GAMMA/NVORTS
      ZCORNR=ZCNTR-CMPLX(RMAX,RMAX)
      DO 7000 NV=1,NVORTS
 6500 CALL RANDOM(XV)
      CALL RANDOM(YV)
      ZVRTX=CMPLX(XV,YV)+ZCNTR
      ZDIFF=ZVRTX-ZCNTR
      IF(CABS(ZDIFF).GT.RMAX)GO TO 6500
      ZV(NV,NB)=ZVRTX
      GV(NV,NB)=GVORT
 7000 CONTINUE
      NNV(NB)=NVORTS
 8888 DO 9000 NV=1,NNV(NB)
      AGE(NV,NB)=AGE0
      DGDT(NV,NB)=DGDT0*GV(NV,NB)/GAMMA
      GV0(NV,NB)=GV00*GV(NV,NB)/GAMMA
 9000 CONTINUE
 9999 RETURN
      END
CCCCCCCCCCCCCCCCCCCCCCCCCCCCCCCCCCCCCCCCCCCCCCCCCCCCCCCCCCCCCCCCCCCCCCCCC
CCCCCCCCCCCCCCCCCCCCCCCCCCCCCCCCCCCCCCCCCCCCCCCCCCCCCCCCCCCCCCCCCCCCCCCCC
      SUBROUTINE AMALG(NB,IDOIT,ZAMALG,GAMALG)
      IMPLICIT COMPLEX(C,Z),INTEGER(I-N)
      COMMON/VORTEX/ZV(300,4),CV(300,4),GV(300,4),GV0(300,4),
     1              DGDT(300,4),AGE(300,4),GSHED(800,4),GLOST(800,4),
     2              GVMIN,GV0MIN,NNV(4),NNB,NVMAX
      COMMON/CONST/ZONE,ZERO,ZFAC,ZI,ZPI,PI,TWOPI,PI90,PI180,OV2PI
```

```
CCCCCCCCCCCCCCCCCCCCCCCCCCCCCCCCCCCCCCCCCCCCCCCCCCCCCCCCCCCCCCCCCCCCCCCC
C
C     CONDUCTS CENTROID CALCULATION TO AID IN TRACKING VORTEX CLUSTER
C     TRAVEL.  CODE WRITTEN TO ALLOW ACTUAL AMALGAMATION IF REQUIRED
C     IN FUTURE PROGRAM MODIFICATIONS.
C
C     IDOIT=1:  MERELY CENTROID CALCULATION
C          =2:  FULL AMALGAMATION
C
      IF(NNV(NB).LT.0)GO TO 9000
      GAMALG=0.0
      ZMOMNT=ZERO
      AGEPRD=0.0
      DGDTSM=0.0
      GV0SUM=0.0
      DO 1000 NV=1,NNV(NB)
      GAMALG=GAMALG+GV(NV,NB)
      ZMOMNT=ZMOMNT+GV(NV,NB)*ZV(NV,NB)
      IF(IDOIT.NE.2)GO TO 1000
      GV(NV,NB)=0.0
      AGEPRD=AGEPRD+AGE(NV,NB)*GV(NV,NB)
      DGDTSM=DGDTSM+DGDT(NV,NB)
      GV0SUM=GV0SUM+GV0(NV,NB)
 1000 CONTINUE
      ZAMALG=ZMOMNT/GAMALG
      IF(IDOIT.NE.2)GO TO 9999
      NNV(NB)=1
      ZV(1,NB)=ZAMALG
      GV(1,NB)=GAMALG
      AGE(1,NB)=AGEPRD/GAMALG
      GV0(1,NB)=GV0SUM
      DGDT(1,NB)=DGDTSM
      GO TO 9999
 9000 WRITE(6,9010)NB
 9010 FORMAT(' NO VORTICES IN SHEET ',I2,' WHEN TRYING TO AMALGAMATE')
 9999 RETURN
      END
CCCCCCCCCCCCCCCCCCCCCCCCCCCCCCCCCCCCCCCCCCCCCCCCCCCCCCCCCCCCCCCCCCCCCCCC
CCCCCCCCCCCCCCCCCCCCCCCCCCCCCCCCCCCCCCCCCCCCCCCCCCCCCCCCCCCCCCCCCCCCCCCC
```

# APPENDIX C. PLTPLT.FOR

```
CCCCCCCCCCCCCCCCCCCCCCCCCCCCCCCCCCCCCCCCCCCCCCCCCCCCCCCCCCCCCCCCCCCCCCCC
CCCCCCCCCCCCCCCCCCCCCCCCCCCCCCCCCCCCCCCCCCCCCCCCCCCCCCCCCCCCCCCCCCCCCCCC
      IMPLICIT COMPLEX(C,Z),INTEGER(I-N)
      INTEGER*2 K,JGRK,JSMPLX
      CHARACTER RUNNO*3, KEYCHR*1,TITLE*80
      CHARACTER*1 COMNTS(61,5),VORANS,PRSANS,SMOOTH
      REAL PLOT1(800),PLOT2(800),CHRSZ
      COMMON/VORTEX/ZV(300,4),CV(300,4),GV(300,4),GV0(300,4),
     1              DGDT(300,4),AGE(300,4),GSHED(800,4),GLOST(800,4),
     2              GVMIN,GV0MIN,NNV(4),NNB,NVMAX
      COMMON/SAVE/XVORT(800),YVORT(800),XSEP(800),YSEP(800),USEP(800)
      COMMON/TIMES/DELT,T(800),NT,NTMAX,NTSTOP
      COMMON/CONST/ZONE,ZERO,ZFAC,ZI,ZPI,PI,TWOPI,PI90,PI180,OV2PI,
     1             FOURPI
      COMMON/SURFCE/Q(200),PTOTAL(200),PVORT(200),PVELO(200),
     1              DX,NDX,XMAX,X(200),XI(500),TAU(500),BLDISP(500),
     2              BLMOM(500),MSEP,F(200),XBAR(200)
      COMMON/FLOW/RCORE,CINF,VINF,RMIN,BDISP,NOTOCH,AGECHK
      COMMON/MISC/RUNNO,NPLOTS,NCOMNT,COMNTS,IDATE,ITIME
      COMMON/MISC1/NHICUP
CCCCCCCCCCCCCCCCCCCCCCCCCCCCCCCCCCCCCCCCCCCCCCCCCCCCCCCCCCCCCCCCCCCCCCCC
C
C     THIS CODE WAS WRITTEN TO READ UNFORMATTED DATA PROVIDED BY
C     PROGRAM PLATE.FOR (APPENDIX B).  IT WAS WRITTEN AND COMPILED
C     IN MICROSOFT FORTRAN POWERSTATION VERSION 1.0, WITH INGRAF
C     LIBRARY ROUTINES PURCHASED FROM SUTRASOFT.  THE USER IS PROMPTED
C     FOR VARIOUS RUNTIME ROUTINES WHICH ASK WHETHER OR NOT PLOT
C     SMOOTHING AND/OR TABULAR PRINTOUT OF VORTEX INFORMATION, AND/OR
C     A TABULAR PRINTOUT OF VARIOUS PARAMETERS UTILIZED IN SEPARATION
C     POINT PREDICTION.  WRITTEN BY CAPT MICHAEL R. MAIXNER, DEC 1994
C     IN CONJUNCTION WITH DOCTORAL DISSERTATION FROM NAVAL POSTGRADUATE
C     SCHOOL, MONTEREY, CA.
C
      PI=4.*ATAN(1.)
      WRITE(6,*)(' INPUT THREE DIGITS FOR RUN NUMBER')
      READ(5,100)RUNNO
      MPRS=9
      MVOR=10
  100 FORMAT(A3)
      OPEN(7,FORM='UNFORMATTED',FILE=RUNNO//'FILM')
      OPEN(8,FORM='UNFORMATTED',FILE=RUNNO//'RECAP')
CCCCCCCCCCCCCCCCCCCCCCCCCCCCCCCCCCCCCCCCCCCCCCCCCCCCCCCCCCCCCCCCCCCCCCCC
C
C     GET SUMMARY INFORMATION TO ALLOW ACCESS TO INDIVIDUAL
C     PICTURE FRAMES
C
      CALL SUMARY(8)
      BETA=VINF/(1.+VINF)
CCCCCCCCCCCCCCCCCCCCCCCCCCCCCCCCCCCCCCCCCCCCCCCCCCCCCCCCCCCCCCCCCCCCCCCC
C
C     SEE IF SMOOTHED PRESSURE DATA ARE DESIRED.
C
      WRITE(6,*)(' DO YOU WANT DATA SMOOTHED?')
```

```
      READ(5,190)SMOOTH
      IF(SMOOTH.EQ.'y')SMOOTH='Y'
CCCCCCCCCCCCCCCCCCCCCCCCCCCCCCCCCCCCCCCCCCCCCCCCCCCCCCCCCCCCCCCCCCCCCCCC
C
C     DO YOU WANT TO OBTAIN A PRINTOUT OF ONLY VORTEX POSITIONAL
C     INFORMATION WITHOUT ALL OF THE PRESSURE, SHEAR, MOMENTUM
C     THICKNESS, ETC. INFORMATION?
C
      WRITE(6,*)(' DO YOU WANT A VORTEX POSITION PRINTOUT?')
      READ(5,190)VORANS
      WRITE(6,*)(' DO YOU WANT A PRESSURE PRINTOUT?')
      READ(5,190)PRSANS
  190 FORMAT(A1)
      IF(VORANS.EQ.'y')VORANS='Y'
      IF(PRSANS.EQ.'y')PRSANS='Y'
      IF((PRSANS.EQ.'Y').OR.(VORANS.EQ.'Y'))GO TO 200
      GO TO 300
  200 IF (VORANS.EQ.'Y')OPEN(MVOR,FILE=RUNNO//'VOR')
      IF (PRSANS.EQ.'Y')OPEN(MPRS,FILE=RUNNO//'PRS')
CCCCCCCCCCCCCCCCCCCCCCCCCCCCCCCCCCCCCCCCCCCCCCCCCCCCCCCCCCCCCCCCCCCCCCCC
C
C     BEGIN TO PRINT POSITION INFORMATION, TIMSTEP BY TIMESTEP
C
      CALL MOVIE(7)
      REWIND(7)
CCCCCCCCCCCCCCCCCCCCCCCCCCCCCCCCCCCCCCCCCCCCCCCCCCCCCCCCCCCCCCCCCCCCCCCC
C
C     BEGIN THE FIRST PAGE OF PLOTTING
C
  300 CALL GOPEN('VGA2\0','CON:\0',K)
      CALL GETFNT('COMPLEX2.FNT\0',JGRK)
      CALL GETFNT('SIMPLEX1.FNT\0',JSMPLX)
      CALL SETFNT(JSMPLX)
      CALL NEWWND(0.0,0.0,9.0,5.0,2)
      CALL NEWPEN(2)
      CALL LTYPE(0)
      CALL WFRAME
      XX=9.0
      YY=7.0
      CALL PLIMIT(0.5,0.5,7.5,4.0,2)
      CALL SETPU
      XMIN=0.0
      XMAX=T(NTSTOP)
      IF (XMAX.LT.1.0)XMAX=1.0
      YMIN=-6.0
      YMAX=6.0
      CHRSZ=0.1
      THRQTR=0.75*CHRSZ
      HALFSZ=0.5*CHRSZ
      QTRSZ=0.25*CHRSZ
      SUBSZ=THRQTR
      TICMAJ=0.1
      TICMIN=TICMAJ/2.0
      CALL CSIZE(CHRSZ,CHRSZ)
      DWNSPC=-1.4
      XLINE=1.0
```

```
CCCCCCCCCCCCCCCCCCCCCCCCCCCCCCCCCCCCCCCCCCCCCCCCCCCCCCCCCCCCCCCCCCCCCCCC
C
C     BEGIN BY WRITING THE LEGEND FOR THE SUMMARY PLOT
C
      CALL CLIPOF

      CALL MOVE(2.0,1.5)
      CALL QCPOS(XHOME,YHOME)
      CALL NEWPEN(7)
      CALL LTYPE(1)
      CALL RLINE(-XLINE,0.0)
      CALL MOVE(XHOME,YHOME)
      CALL LBLORG(2)
      CALL SETFNT(JGRK)
      CALL LABEL(CHAR(71)//'\0')
      CALL CMOVE(1.0,0.0)
      CALL CSIZE(SUBSZ,SUBSZ)
      CALL SETFNT(JSMPLX)
      CALL LABEL('SHED\0')
      CALL CSIZE(CHRSZ,CHRSZ)
      CALL MOVE(XHOME,YHOME)
      CALL CMOVE(0.0,DWNSPC)

      CALL QCPOS(XHOME,YHOME)
      CALL NEWPEN(7)
      CALL LTYPE(2)
      CALL RLINE(-XLINE,0.0)
      CALL MOVE(XHOME,YHOME)
      CALL LBLORG(2)
      CALL SETFNT(JGRK)
      CALL LABEL(CHAR(71)//'\0')
      CALL CMOVE(1.0,0.0)
      CALL CSIZE(SUBSZ,SUBSZ)
      CALL SETFNT(JSMPLX)
      CALL LABEL('LOST\0')
      CALL CSIZE(CHRSZ,CHRSZ)
      CALL MOVE(XHOME,YHOME)
      CALL CMOVE(0.0,DWNSPC)

      CALL QCPOS(XHOME,YHOME)
      CALL NEWPEN(3)
      CALL LTYPE(3)
      CALL RLINE(-XLINE,0.0)
      CALL MOVE(XHOME,YHOME)
      CALL LABEL('U\0')
      CALL CMOVE(1.0,0.0)
      CALL CSIZE(SUBSZ,SUBSZ)
      CALL LABEL('SEP\0')
      CALL CSIZE(CHRSZ,CHRSZ)
      CALL MOVE(XHOME,YHOME)
      CALL CMOVE(0.0,DWNSPC)

      CALL QCPOS(XHOME,YHOME)
      CALL NEWPEN(4)
      CALL LTYPE(4)
      CALL RLINE(-XLINE,0.0)
```

```
      CALL MOVE(XHOME,YHOME)
      CALL LABEL('100*Y\0')
      CALL CMOVE(5.0,0.0)
      CALL CSIZE(SUBSZ,SUBSZ)
      CALL LABEL('SEP\0')
      CALL CSIZE(CHRSZ,CHRSZ)
      CALL MOVE(XHOME,YHOME)
      CALL CMOVE(0.0,DWNSPC)

      CALL QCPOS(XHOME,YHOME)
      CALL NEWPEN(5)
      CALL LTYPE(5)
      CALL RLINE(-XLINE,0.0)
      CALL MOVE(XHOME,YHOME)
      CALL LABEL('(X\0')
      CALL CMOVE(2.0,0.0)
      CALL CSIZE(SUBSZ,SUBSZ)
      CALL LABEL('SEP\0')
      CALL CMOVE(3.0,0.0)
      CALL CSIZE(CHRSZ,CHRSZ)
      CALL CMOVE(0.0,0.6)
      CALL LABEL('-X\0')
      CALL CMOVE(2.0,0.0)
      CALL CSIZE(SUBSZ,SUBSZ)
      CALL LABEL('VORT\0')
      CALL CMOVE(4.0,0.0)
      CALL CSIZE(CHRSZ,CHRSZ)
      CALL CMOVE(0.0,0.6)
      CALL LABEL(')\0')
      CALL MOVE(XHOME,YHOME)
      CALL CMOVE(0.0,DWNSPC)

      CALL CLIPON

      CALL SCALE(XMIN,XMAX,YMIN,YMAX)
      CALL SETSU
      CALL SETDEG

CCCCCCCCCCCCCCCCCCCCCCCCCCCCCCCCCCCCCCCCCCCCCCCCCCCCCCCCCCCCCCCCCCCCCCCCCCCCCCCC
C
C     SET UP THE AXES
C
      CALL LTYPE(0)
      CALL NEWPEN(2)
      CALL XTSIZE(TICMAJ,TICMAJ,TICMIN,TICMIN)
      CALL AXES(XMAX,SPCNG,DELORD,NSPCS)
      CALL XAXIS(XMIN,XMAX,0.0,SPCNG,NSPCS)
      CALL YAXIS(YMIN,YMAX,0.0,0.2,5)
      CALL LBLORG(8)
      CALL LBLDIR(0.0)
      Y=YMIN
 2000 CALL MOVE(XMIN,Y)
      CALL CMOVE(-1.0,0.0)
      CALL NLABEL(Y,-1)
      Y=Y+1.0
```

```
      IF (Y.LE.YMAX) GO TO 2000
      CALL LBLORG(6)
      CALL LBLDIR(0.0)

      XX=XMIN+DELORD
 3000 CALL MOVE(XX,0.0)
      CALL CMOVE(0.0,-1.0)
      IF(XMAX.GE.2.0)CALL NLABEL(XX,-1)
      IF(XMAX.LT.2.0)CALL NLABEL(XX, 1)
      XX=XX+DELORD
      IF (XX.LE.XMAX) GO TO 3000

CCCCCCCCCCCCCCCCCCCCCCCCCCCCCCCCCCCCCCCCCCCCCCCCCCCCCCCCCCCCCCCCCCCCCCCCCC
C
C     LABEL THE X-AXIS
C
      CALL MOVE(XMAX,0.0)
      CALL LBLORG(2)
      CALL LBLDIR(0.0)
      CALL CMOVE(2.0,0.0)
      CALL LABEL('TIME\0')

CCCCCCCCCCCCCCCCCCCCCCCCCCCCCCCCCCCCCCCCCCCCCCCCCCCCCCCCCCCCCCCCCCCCCCCCCC
C
C     SCALE THE SEPARATION INFORMATION RELATIVE TO MAJOR VORTEX
C     POSITION
C
      DO 3100 I=1,NTSTOP
 3100 PLOT1(I)=(XSEP(I)-XVORT(I))*1.0

CCCCCCCCCCCCCCCCCCCCCCCCCCCCCCCCCCCCCCCCCCCCCCCCCCCCCCCCCCCCCCCCCCCCCCCCCC
C
C     PLOT THE CURVES
C
      CALL LTYPE(1)
      CALL NEWPEN(7)
      CALL NOZERO(T,GSHED(NT,2),NTSTOP)

      CALL LTYPE(2)
      CALL NEWPEN(7)
      CALL NOZERO(T,GLOST(NT,2),NTSTOP)

      CALL LTYPE(3)
      CALL NEWPEN(3)
      CALL NOZERO(T,USEP,NTSTOP)

CCCCCCCCCCCCCCCCCCCCCCCCCCCCCCCCCCCCCCCCCCCCCCCCCCCCCCCCCCCCCCCCCCCCCCCCCC
C
C     SCALE THE VERTICAL POSITION INFORMATION FOR THE SEPARATION
C     POINT
C
      DO 3110 I=1,NTSTOP
 3110 YSEP(I)=YSEP(I)*100.0

CCCCCCCCCCCCCCCCCCCCCCCCCCCCCCCCCCCCCCCCCCCCCCCCCCCCCCCCCCCCCCCCCCCCCCCCCC
C
```

```
C     CONTINUE PLOTTING
C
      CALL LTYPE(4)
      CALL NEWPEN(4)
      CALL NOZERO(T,YSEP,NTSTOP)

      CALL LTYPE(5)
      CALL NEWPEN(5)
      CALL NOZERO(T,PLOT1,NTSTOP)

CCCCCCCCCCCCCCCCCCCCCCCCCCCCCCCCCCCCCCCCCCCCCCCCCCCCCCCCCCCCCCCCCCCCCCCCCCCC
C
C     ADD NEW FRAME TO FIRST PAGE WITH ALL INFORMATION ON IT
C     FOR SUMMARY.
C
      CALL NEWWND(0.0,5.0,9.0,1.9,2)
      CALL SETFNT(JSMPLX)
      CALL NEWPEN(2)
      CALL LTYPE(0)
      CALL WFRAME
      CALL PLIMIT(0.0,0.0,9.0,2.5,2)
      CALL SCALE (0.0,9.0,0.0,2.5)
      CALL SETSU
      CALL MOVE(0.5,2.2)
      CALL QCPOS(XHOME,YHOME)
      CALL LBLORG(1)
CCCCCCCCCCCCCCCCCCCCCCCCCCCCCCCCCCCCCCCCCCCCCCCCCCCCCCCCCCCCCCCCCCCCCCCCCCCC
C
C     DO TITLE
C
      TITLE='RUN NUMBER: '//RUNNO//'\0'
      CALL CSIZE(CHRSZ,1.5*CHRSZ)
      CALL LABEL(TITLE)
      CALL CMOVE(16.0,0.0)
      CALL LABEL('    DATE: \0')
      CALL CMOVE(10.0,0.0)
      RIDATE=IDATE
      CALL NLABEL(RIDATE,-1)
      CALL CMOVE(8.0,0.0)
      CALL LABEL('    TIME: \0')
      CALL CMOVE(10.0,0.0)
      RITIME=ITIME
      CALL NLABEL(RITIME,-1)
      CALL CSIZE(CHRSZ,CHRSZ)
CCCCCCCCCCCCCCCCCCCCCCCCCCCCCCCCCCCCCCCCCCCCCCCCCCCCCCCCCCCCCCCCCCCCCCCCCCCC
C
C     RETURN FOR SECOND AND SUBSEQUENT LINES
C
      CALL MOVE(XHOME,YHOME)
      CALL CMOVE(0.0,DWNSPC)
      CALL QCPOS(XHOME,YHOME)
      DO 3150 J=1,NCOMNT
      CALL LABEL(COMNTS(1,J))
      CALL MOVE(XHOME,YHOME)
      CALL CMOVE(0.0,DWNSPC)
 3150 CALL QCPOS(XHOME,YHOME)
```

```
      YCOL1=YHOME
      XCOL1=XHOME

      CALL SETFNT(JGRK)
      CALL LABEL(CHAR(68)//'\0')
      CALL CMOVE(1.0,0.0)
      CALL SETFNT(JSMPLX)
      CALL LABEL('t=\0')
      CALL CMOVE(2.0,0.0)
      CALL NLABEL(DELT,7)
      CALL MOVE(XHOME,YHOME)
      CALL CMOVE(0.0,DWNSPC)
      CALL QCPOS(XHOME,YHOME)

      CALL LABEL('U\0')
      CALL CMOVE(1.0,0.0)
      CALL CSIZE(SUBSZ,SUBSZ)
      CALL CMOVE(0.0,-0.5)
      CALL LABEL('INF\0')
      CALL CMOVE(3.0,0.5)
      CALL CSIZE(CHRSZ,CHRSZ)
      CALL LABEL('=\0')
      CALL CMOVE(1.0,0.0)
      CALL NLABEL(VINF,3)
      CALL MOVE(XHOME,YHOME)
      CALL CMOVE(0.0,DWNSPC)
      CALL QCPOS(XHOME,YHOME)

      CALL SETFNT(JGRK)
      CALL LABEL(CHAR(98)//'\0')
      CALL CSIZE(CHRSZ,CHRSZ)
      CALL SETFNT(JSMPLX)
      CALL CMOVE(2.0,0.0)
      CALL LABEL('=\0')
      CALL CMOVE(2.0,0.0)
      CALL NLABEL(BETA,7)
      CALL MOVE(XHOME,YHOME)
      CALL CMOVE(0.0,-2.0*SUBSZ)
      CALL QCPOS(XHOME,YHOME)

CCCCCCCCCCCCCCCCCCCCCCCCCCCCCCCCCCCCCCCCCCCCCCCCCCCCCCCCCCCCCCCCCCCCCC
C
C     START SECOND COLUMN
C
      YCOL2=YCOL1
      XCOL2=XCOL1+3.0
      CALL MOVE(XCOL2,YCOL2)
      CALL QCPOS(XHOME,YHOME)
      CALL LABEL('R\0')
      CALL CMOVE(1.0,0.0)
      CALL CSIZE(SUBSZ,SUBSZ)
      CALL CMOVE(0.0,-0.5)
      CALL LABEL('MIN\0')
      CALL CMOVE(3.0,0.5)
      CALL CSIZE(CHRSZ,CHRSZ)
      CALL LABEL('=\0')
```

```
      CALL CMOVE(1.0,0.0)
      CALL NLABEL(RMIN,7)
      CALL MOVE(XHOME,YHOME)
      CALL CMOVE(0.0,DWNSPC)
      CALL QCPOS(XHOME,YHOME)

      CALL LABEL('R\0')
      CALL CMOVE(1.0,0.0)
      CALL CSIZE(SUBSZ,SUBSZ)
      CALL CMOVE(0.0,-0.5)
      CALL LABEL('CORE\0')
      CALL CMOVE(4.0,0.5)
      CALL CSIZE(CHRSZ,CHRSZ)
      CALL LABEL('=\0')
      CALL CMOVE(1.0,0.0)
      CALL NLABEL(RCORE,6)
      CALL MOVE(XHOME,YHOME)
      CALL CMOVE(0.0,DWNSPC)

      CALL LABEL('BDISP=\0')
      CALL CMOVE(6.0,0.0)
      CALL NLABEL(BDISP,2)

CCCCCCCCCCCCCCCCCCCCCCCCCCCCCCCCCCCCCCCCCCCCCCCCCCCCCCCCCCCCCCCCCCC
C
C     START THIRD COLUMN
C
      YCOL3=YCOL1
      XCOL3=XCOL2+3.0
      CALL MOVE(XCOL3,YCOL3)
      CALL QCPOS(XHOME,YHOME)
      CALL SETFNT(JGRK)
      CALL LABEL(CHAR(71)//'\0')
      CALL CMOVE(1.0,0.0)
      CALL SETFNT(JSMPLX)
      CALL CSIZE(SUBSZ,SUBSZ)
      CALL CMOVE(0.0,-0.5)
      CALL LABEL('INCIDENT\0')
      CALL CMOVE(8.0,0.5)
      CALL CSIZE(CHRSZ,CHRSZ)
      CALL LABEL('=\0')
      CALL CMOVE(2.0,0.0)
      CALL NLABEL(PI,5)
      CALL MOVE(XHOME,YHOME)
      CALL CMOVE(0.0,DWNSPC)
      CALL QCPOS(XHOME,YHOME)

      CALL SETFNT(JGRK)
      CALL LABEL(CHAR(71)//'\0')
      CALL CMOVE(1.0,0.0)
      CALL SETFNT(JSMPLX)
      CALL CSIZE(SUBSZ,SUBSZ)
      CALL CMOVE(0.0,-0.5)
      CALL LABEL('MIN\0')
      CALL CMOVE(3.0,0.5)
      CALL CSIZE(CHRSZ,CHRSZ)
```

```
      CALL LABEL('=\0')
      CALL CMOVE(2.0,0.0)
      CALL NLABEL(GVMIN,7)
      CALL MOVE(XHOME,YHOME)
      CALL CMOVE(0.0,DWNSPC)
      CALL QCPOS(XHOME,YHOME)

      CALL SETFNT(JGRK)
      CALL LABEL(CHAR(71)//'\0')
      CALL CMOVE(1.0,0.0)
      CALL SETFNT(JSMPLX)
      CALL CSIZE(SUBSZ,SUBSZ)
      CALL CMOVE(0.0,-0.5)
      CALL QCPOS(XHOME1,YHOME1)
      CALL LABEL('NASCENT\0')
      CALL MOVE(XHOME1,YHOME1)
      CALL CMOVE(0.0,DWNSPC/1.5)
      CALL LABEL('MINIMUM\0')
      CALL MOVE(XHOME1,YHOME1)
      CALL CMOVE(7.0,0.8)
      CALL CSIZE(CHRSZ,CHRSZ)
      CALL LABEL('=\0')
      CALL CMOVE(2.0,0.0)
      CALL NLABEL(GV0MIN,7)
      CALL MOVE(XHOME,YHOME)
      CALL CMOVE(0.0,-2.0*SUBSZ)
      CALL QCPOS(XHOME,YHOME)

CCCCCCCCCCCCCCCCCCCCCCCCCCCCCCCCCCCCCCCCCCCCCCCCCCCCCCCCCCCCCCCCCCCCCC
C
C     SEE IF PRINTOUT IS DESIRED
C
      CALL INKEY(KEYCHR,K)
      IF(KEYCHR.EQ.'p')KEYCHR='P'
      IF(KEYCHR.EQ.'n')KEYCHR='N'
      IF(KEYCHR.EQ.'a')KEYCHR='A'
      IF((KEYCHR.EQ.'P').OR.(KEYCHR.EQ.'A'))GO TO 5450
      IF(KEYCHR.EQ.'0')GO TO 5460
      IF((KEYCHR.EQ.'Q').OR.(KEYCHR.EQ.'q'))GO TO 17860
      GO TO 5460

 5450 CALL PGRAF(4,'PRN:\0')

 5460 NFRAME=10
CCCCCCCCCCCCCCCCCCCCCCCCCCCCCCCCCCCCCCCCCCCCCCCCCCCCCCCCCCCCCCCCCCCCCC
C
C     MAXIMUM OF FOUR FRAMES PER PAGE
C
      MAXFRM=4
CCCCCCCCCCCCCCCCCCCCCCCCCCCCCCCCCCCCCCCCCCCCCCCCCCCCCCCCCCCCCCCCCCCCCC
C
C     CLOSE THE FIRST PLOT
C
      CALL GCLOSE
CCCCCCCCCCCCCCCCCCCCCCCCCCCCCCCCCCCCCCCCCCCCCCCCCCCCCCCCCCCCCCCCCCCCCC
C
```

```
C     PLOT, FRAME BY FRAME
C
      DO 9999 I=1,NPLOTS
      NFRAME=NFRAME+1
      IF (NFRAME.LE.MAXFRM) GO TO 5500
      NFRAME=1
      XCNTR=4.8
      YCNTR=3.7
      XWIDTH=1.0
      YWIDTH=1.0
 5500 IF ((NFRAME.EQ.1).OR.(NFRAME.EQ.2)) Y0=YCNTR
      IF ((NFRAME.EQ.3).OR.(NFRAME.EQ.4)) Y0=0.0
      IF ((NFRAME.EQ.1).OR.(NFRAME.EQ.3)) X0=0.0
      IF ((NFRAME.EQ.2).OR.(NFRAME.EQ.4)) X0=XCNTR
      IF(NFRAME.GT.1)GO TO 5550
      CALL GOPEN('VGA2\0','CON:\0',K)
      CALL GETFNT('COMPLEX2.FNT\0',JGRK)
      CALL GETFNT('SIMPLEX1.FNT\0',JSMPLX)
 5550 CALL SETFNT(JSMPLX)
      CALL NEWWND(X0,Y0,XCNTR,YCNTR,2)
      NPEN=3
      CALL NEWPEN(NPEN)
      CALL LTYPE(0)
      CALL MOVIE(7)
      CALL WFRAME
CCCCCCCCCCCCCCCCCCCCCCCCCCCCCCCCCCCCCCCCCCCCCCCCCCCCCCCCCCCCCCCCCCCCCCCCCCCC
C
C     SET UP UPPER PLOT
C
      X1=0.1
      XLENTH=4.0
      Y1=2.0
      YLENTH=1.7
      RATIO=XLENTH/YLENTH
      CALL PLIMIT(X1,Y1,XLENTH,YLENTH,2)
      CALL SETPU
      CALL CSIZE(CHRSZ,CHRSZ)
CCCCCCCCCCCCCCCCCCCCCCCCCCCCCCCCCCCCCCCCCCCCCCCCCCCCCCCCCCCCCCCCCCCCCCCCCCCC
C
C     DO VORTEX POSITION PLOTS
C
      XMIN=-2.0
      YMIN=0.0
      XMAX=8.0
      YMAX=(XMAX-XMIN)/RATIO+YMIN

      CALL SCALE(XMIN,XMAX,YMIN,1.03*YMAX)
      CALL SETSU
      CALL SETMRK(1)
      DO 5560 NV=1,NNV(1)
      PLOT1(NV)=REAL(ZV(NV,1))
 5560 PLOT2(NV)=AIMAG(ZV(NV,1))
      CALL SCATER(PLOT1,PLOT2,NNV(1))

CCCCCCCCCCCCCCCCCCCCCCCCCCCCCCCCCCCCCCCCCCCCCCCCCCCCCCCCCCCCCCCCCCCCCCCCCCCC
C
```

```
C     DRAW ARROW ON PRINCIPAL VORTEX ONLY IF MAJOR VORTEX IS AN
C     AMALGAMATED ONE
C
      IF(NNV(1).GT.1)GO TO 6450
      RADIUS=0.5
      RAD=RADIUS*XLENTH/(XMAX-XMIN)
      CALL CIRCLE(PLOT1(1),PLOT2(1),RAD)
      FACTOR=3.0
      HEIGHT=0.1*FACTOR
      WIDTH =0.1*FACTOR
      ZCNTR= ZV(1,1)+CMPLX(.9*RADIUS,0.0)
      ZTOP = ZCNTR+CMPLX(0.0,HEIGHT/2.0)
      ZLEFT= ZCNTR+CMPLX(-WIDTH/2.0,-HEIGHT/2.0)
      ZRIGHT=ZCNTR+CMPLX( WIDTH/2.0,-HEIGHT/2.0)
      PLOT1(1)=REAL(ZTOP)
      PLOT1(2)=REAL(ZLEFT)
      PLOT1(3)=REAL(ZRIGHT)
      PLOT2(1)=AIMAG(ZTOP)
      PLOT2(2)=AIMAG(ZLEFT)
      PLOT2(3)=AIMAG(ZRIGHT)
      CALL FPOLY(NPEN,PLOT1,PLOT2,3)
 6450 DO 6500 NV=1,NNV(2)
      PLOT1(NV)=REAL(ZV(NV,2))
      PLOT2(NV)=AIMAG(ZV(NV,2))
 6500 CONTINUE
      CALL SETMRK(4)
      CALL CLIPON
      CALL SCATER(PLOT1,PLOT2,NNV(2))
      CALL CLIPOF
      CALL SETMRK(0)

CCCCCCCCCCCCCCCCCCCCCCCCCCCCCCCCCCCCCCCCCCCCCCCCCCCCCCCCCCCCCCCCCCCCCCCC
C
C     LABEL PLOT WITH TIME AND TIMESTEP NUMBER.
C
      CALL CLIPOF
      CALL LBLORG(1)
      CALL SETDEG
      CALL LBLDIR(0.0)
      CALL CSIZE(.75*CHRSZ,CHRSZ)
      CALL MOVE(3.0,-1.0)
      CALL QCPOS(XHOME,YHOME)
      CALL LABEL('T=\0')
      CALL CMOVE(2.0,0.0)
      CALL NLABEL(T(NT),4)
      CALL MOVE(XHOME,YHOME)
      CALL CMOVE(9.0,0.0)
      CALL LABEL('NT= \0')
      CALL CMOVE(3.0,0.0)
      RNT=NT
      CALL NLABEL(RNT,-1)
      CALL CSIZE(CHRSZ,CHRSZ)
      CALL CLIPON

CCCCCCCCCCCCCCCCCCCCCCCCCCCCCCCCCCCCCCCCCCCCCCCCCCCCCCCCCCCCCCCCCCCCCCCC
C
```

```
C     LABEL PLOT WITH VORTEX CLUSTER SUMS
C
      CALL CSIZE(.75*CHRSZ,CHRSZ)
      CALL MOVE(3.0,3.8)
      CALL SETFNT(JGRK)
      CALL LABEL (CHAR(71)//'\0')
      CALL CMOVE(1.0,0.0)
      CALL CSIZE(SUBSZ,SUBSZ)
      CALL SETFNT(JSMPLX)
      CALL LABEL('+\0')
      CALL CMOVE(1.0,0.0)
      CALL CSIZE(.75*CHRSZ,CHRSZ)
      CALL LABEL('=\0')
      CALL CMOVE(1.0,0.0)
      SIGMAP=SIGMA(1)
      CALL NLABEL(SIGMAP,3)
      CALL CMOVE(7.0,0.0)
      CALL SETFNT(JGRK)
      CALL LABEL(CHAR(71)//'\0')
      CALL CMOVE(1.0,0.0)
      CALL CSIZE(SUBSZ,SUBSZ)
      CALL SETFNT(JSMPLX)
      CALL LABEL('0\0')
      CALL CMOVE(1.0,0.0)
      CALL CSIZE(.75*CHRSZ,CHRSZ)
      CALL LABEL('=\0')
      CALL CMOVE(1.0,0.0)
      SIGMAM=SIGMA(2)
      CALL NLABEL(SIGMAM,3)

CCCCCCCCCCCCCCCCCCCCCCCCCCCCCCCCCCCCCCCCCCCCCCCCCCCCCCCCCCCCCCCCCCCCCCC
C
C     DO THE AXES
C
      CALL LTYPE(0)
      CALL NEWPEN(NPEN)
      TICMAJ=0.1
      TICMIN=TICMAJ/2.0
      CALL XTSIZE(TICMAJ,TICMAJ,TICMIN,TICMIN)
      CALL XAXIS(XMIN,XMAX,0.0,0.2,5)
      CALL YTSIZE(TICMAJ,TICMAJ,TICMIN,TICMIN)
      CALL YAXIS(0.0,YMAX,0.0,0.2,5)
      CALL YAXIS(0.0,YMIN,0.0,0.2,5)
      CALL LBLORG(8)
      CALL LBLDIR(0.0)
      Y=0.0
 7000 CALL MOVE(0.0,Y)
      CALL CMOVE(-1.0,0.0)
      IF (Y.NE.0.0) CALL NLABEL(Y,-1)
      Y=Y+1.0
      IF (Y.LE.YMAX) GO TO 7000
      CALL LBLORG(6)
      CALL LBLDIR(0.0)
      XX=XMIN
 7500 CALL MOVE(XX,0.0)
      CALL CMOVE(0.0,-1.0)
```

```
      IF(XX.NE.0.0) CALL NLABEL(XX,-1)
      XX=XX+1.0
      IF (XX.LE.XMAX) GO TO 7500

CCCCCCCCCCCCCCCCCCCCCCCCCCCCCCCCCCCCCCCCCCCCCCCCCCCCCCCCCCCCCCCCCCCCCCCCCCCC
C
C     MARK THE SEPARATION POINT WITH A SMALL VERTICAL LINE.
C
      IF(XSEP(NT).EQ.0.0)GO TO 7510
      CALL LBLORG(4)
      YHT=0.4
      CALL MOVE(XSEP(NT),0.0)
      CALL LINE(XSEP(NT),YHT)
      CALL MOVE(XSEP(NT),YHT)
      CALL LABEL('S\0')
CCCCCCCCCCCCCCCCCCCCCCCCCCCCCCCCCCCCCCCCCCCCCCCCCCCCCCCCCCCCCCCCCCCCCCCCCCCC
C
C     DO PRESSURE, VELOCITY, AND OTHER PLOTS.
C
 7510 CALL SETPU
      Y1=0.2
      YLENTH=1.6
CCCCCCCCCCCCCCCCCCCCCCCCCCCCCCCCCCCCCCCCCCCCCCCCCCCCCCCCCCCCCCCCCCCCCCCCCCCC
C
C     KEEP VALUES FOR X1 AND XLENTH FROM VORTEX POSITION PLOT.
C
      CALL PLIMIT(X1,Y1,XLENTH,YLENTH,2)
      QMIN=-2.0
      QMAX=BETA*1.5
      IF(QMAX.LT.2.0)QMAX=2.0
      PMIN=-BETA**2-0.5
      PMIN=1.2*PMIN
      PMAX=2.0
      YMIN=PMIN
      YMAX=QMAX

      CALL SCALE(XMIN,XMAX,YMIN,1.03*YMAX)
      CALL SETSU
      CHRSZ=0.1
      CALL CSIZE(CHRSZ,CHRSZ)
      DWNSPC=-1.4
      XLINE=1.0

 7550 CONTINUE
CCCCCCCCCCCCCCCCCCCCCCCCCCCCCCCCCCCCCCCCCCCCCCCCCCCCCCCCCCCCCCCCCCCCCCCCCCCC
C
C     DO THE CURVE PLOTTING
C
      CALL CLIPON
      IF(SMOOTH.EQ.'Y') GO TO 7560

      CALL LTYPE(2)
      CALL NEWPEN(2)
      CALL APOLY(X,PTOTAL,NDX)

      CALL SETSU
```

```
      CALL LTYPE(1)
      CALL NEWPEN(7)
      CALL APOLY(X,Q,NDX)

      GO TO 7561

 7560 CALL PSMUTH(QMIN,QMAX,Q      ,Q      ,NDX)
      CALL PSMUTH(PMIN,PMAX,PTOTAL,PTOTAL,NDX)

      CALL LTYPE(2)
      CALL NEWPEN(2)
      CALL APOLY(X,PTOTAL,NDX)

      CALL SETSU
      CALL LTYPE(1)
      CALL NEWPEN(7)
      CALL APOLY(X,Q,NDX)

 7561 CALL FORMOM
CCCCCCCCCCCCCCCCCCCCCCCCCCCCCCCCCCCCCCCCCCCCCCCCCCCCCCCCCCCCCCCCCCCCCCCCCCCCCCCC
C
C     SCALE THE CENTER OF PRESSURE AND FORCE DATA.
C
      XBARMX=5.0
      FMAX=-PMIN*X(NDX)
      IF(FMAX.LT.XBARMX)FMAX=XBARMX

      DO 7580 L=1,NDX
      XBAR(L)=XBAR(L)*YMAX/FMAX
 7580 F(L)=F(L)*YMAX/FMAX

      IF(SMOOTH.EQ.'Y')GO TO 7600

      CALL LTYPE(3)
      CALL NEWPEN(3)
      CALL APOLY(X,XBAR,NDX)

      CALL LTYPE(4)
      CALL NEWPEN(4)
      CALL APOLY(X,F,NDX)

      GO TO 7650

 7600 CALL PSMUTH(-1.0,11.0,    F,    F,NDX)
      CALL PSMUTH(-1.0, 6.0,XBAR,XBAR,NDX)

      CALL LTYPE(3)
      CALL NEWPEN(3)
      CALL APOLY(X,XBAR,NDX)

      CALL LTYPE(4)
      CALL NEWPEN(4)
      CALL APOLY(X,F,NDX)

 7650 CONTINUE
```

```
      CALL PRNTIT(MPRS,MVOR,PRSANS,VORANS)
CCCCCCCCCCCCCCCCCCCCCCCCCCCCCCCCCCCCCCCCCCCCCCCCCCCCCCCCCCCCCCCCCCCCCCCC
C
C     DO THE AXES
C
      CALL LTYPE(0)
      CALL NEWPEN(NPEN)
      TICMAJ=0.5*TICMAJ
      TICMIN=TICMAJ/2.0
      CALL XTSIZE(TICMAJ,TICMAJ,TICMIN,TICMIN)
      CALL XAXIS(0.0,XMAX,0.0,0.2,5)
      CALL YTSIZE(TICMAJ,TICMAJ,TICMIN,TICMIN)
      BIGEST=YMAX
      BIGEST=MAX(BIGEST,ABS(YMIN))
      CALL AXES(BIGEST,SPCNG,DELORD,NSPCS)
      SPCNG=0.1
      NSPCS=5
      CALL YAXIS(0.0,YMAX,0.0,SPCNG,NSPCS)
      CALL YAXIS(0.0,YMIN,0.0,SPCNG,NSPCS)
      CALL LBLORG(8)
      CALL LBLDIR(0.0)
      CALL CSIZE(HALFSZ,CHRSZ)
      Y=0.0
 7700 CALL MOVE(0.0,Y)
      CALL CMOVE(-1.0,0.0)
      CALL NLABEL(Y,-1)
      Y=Y+DELORD
      IF (Y.LE.YMAX) GO TO 7700
      Y=0.0
 7710 CALL MOVE(0.0,Y)
      CALL CMOVE(-1.0,0.0)
      CALL NLABEL(Y,-1)
      Y=Y-DELORD
      IF(Y.GE.YMIN)GO TO 7710
      CALL LBLORG(6)
      CALL LBLDIR(0.0)
      XX=0.0
 7750 CALL MOVE(XX,YMIN)
      XX=XX+1.0
      IF (XX.LE.XMAX) GO TO 7750

      CALL LBLDIR(0.0)
      CALL LBLORG(2)
      CALL AXES(FMAX,SPCNG,DELORD,NSPCS)
      CALL YAXIS(0.0,YMAX,XMAX,SPCNG*YMAX/FMAX,NSPCS)
      CALL CSIZE(HALFSZ,CHRSZ)
      Y=0.0
      YLABEL=0.0
 7800 CALL MOVE(XMAX,Y)
      CALL CMOVE(1.0,0.0)
      CALL NLABEL(YLABEL,-1)
      Y=Y+(YMAX)*DELORD/FMAX
      YLABEL=YLABEL+DELORD
      IF(Y.LE.YMAX)GO TO 7800
      CALL CSIZE(CHRSZ,CHRSZ)
CCCCCCCCCCCCCCCCCCCCCCCCCCCCCCCCCCCCCCCCCCCCCCCCCCCCCCCCCCCCCCCCCCCCCCCC
```

```
C
C     LABEL THE VERTICAL AXES
C
      CALL SETDEG
      CALL MOVE(0.0,(YMAX+YMIN)/2.0)
      CALL CMOVE(-2.5,0.0)
      CALL LBLDIR(90.0)
      CALL LBLORG(4)
      CALL NEWPEN(7)
      CALL LABEL('U, \0')
      CALL NEWPEN(2)
      CALL LABEL('p\0')

      CALL MOVE(XMAX,.7*YMAX/2.0)
      CALL CMOVE(2.1,0.0)
      CALL LBLDIR(270.0)
      CALL LBLORG(7)
      CALL NEWPEN(4)
      CALL LABEL('F,\0')
      CALL LBLORG(1)
      CALL NEWPEN(3)
      CALL LABEL('X\0')
      CALL CMOVE(0.0,-1.0)
      CALL CSIZE(SUBSZ,SUBSZ)
      CALL LABEL('COP\0')
CCCCCCCCCCCCCCCCCCCCCCCCCCCCCCCCCCCCCCCCCCCCCCCCCCCCCCCCCCCCCCCCCCCCCCCCCCCC
C
C     PUT THE LEGEND IN THE CENTER OF THE PAGE
C
      CALL LBLDIR(0.0)
      IF(I.EQ.NPLOTS)GO TO 7810
      IF(NFRAME.NE.MAXFRM)GO TO 9999
 7810 CALL NEWPEN(2)
      CALL LTYPE(0)
      CALL NEWWND(XCNTR-XWIDTH/2.0,YCNTR-YWIDTH/2.0,XWIDTH,YWIDTH,2)
      CALL FILWND(0)
      CALL WFRAME
      CALL PLIMIT(0.0,0.0,XWIDTH,YWIDTH,2)
      CALL SCALE(0.0,XWIDTH,0.0,YWIDTH)
      CALL SETSU
      CALL LBLORG(2)

      CALL MOVE(0.62*XWIDTH,0.8*YWIDTH)
      CALL NEWPEN(7)
      CALL LTYPE(1)
      CALL QCPOS(XHOME,YHOME)
      CALL RLINE(-XLINE,0.0)
      CALL MOVE(XHOME,YHOME)
      CALL CMOVE(XSHIFT,0.0)
      CALL LABEL('U\0')
      CALL MOVE(XHOME,YHOME)
      CALL CMOVE(0.0,DWNSPC)

      CALL NEWPEN(2)
      CALL LTYPE(2)
      CALL QCPOS(XHOME,YHOME)
```

```
      CALL RLINE(-XLINE,0.0)
      CALL MOVE(XHOME,YHOME)
      CALL CMOVE(XSHIFT,0.0)
      CALL LABEL('p\0')
      CALL MOVE(XHOME,YHOME)
      CALL CMOVE(0.0,DWNSPC)

      CALL NEWPEN(3)
      CALL LTYPE(3)
      CALL QCPOS(XHOME,YHOME)
      CALL RLINE(-XLINE,0.0)
      CALL MOVE(XHOME,YHOME)
      CALL CMOVE(XSHIFT,0.0)
      CALL LABEL('X\0')
      CALL CMOVE(1.0,0.0)
      CALL CSIZE(SUBSZ,SUBSZ)
      CALL LABEL('COP\0')
      CALL CSIZE(CHRSZ,CHRSZ)
      CALL MOVE(XHOME,YHOME)
      CALL CMOVE(0.0,DWNSPC)

      CALL NEWPEN(4)
      CALL LTYPE(4)
      CALL QCPOS(XHOME,YHOME)
      CALL RLINE(-XLINE,0.0)
      CALL MOVE(XHOME,YHOME)
      CALL CMOVE(XSHIFT,0.0)
      CALL LABEL('F\0')
      CALL SETFNT(JSMPLX)

      IF(KEYCHR.EQ.'A')GO TO 7850
      CALL INKEY(KEYCHR,K)
      IF(KEYCHR.EQ.'p')KEYCHR='P'
      IF(KEYCHR.EQ.'n')KEYCHR='N'
      IF(KEYCHR.EQ.'a')KEYCHR='A'
      IF((KEYCHR.EQ.'P').OR.(KEYCHR.EQ.'A'))GO TO 7850
      IF((KEYCHR.EQ.'Q').OR.(KEYCHR.EQ.'q'))GO TO 17860
      IF(KEYCHR.EQ.'0')GO TO 7860
      GO TO 7860

 7850 CALL PGRAF(4,'PRN:\0')
 7860 CALL GCLOSE
 9999 CONTINUE
      IF (NFRAME.EQ.MAXFRM)GO TO 17860

      IF(KEYCHR.EQ.'A')GO TO 17850
      CALL INKEY(KEYCHR,K)
      IF(KEYCHR.EQ.'p')KEYCHR='P'
      IF(KEYCHR.EQ.'n')KEYCHR='N'
      IF(KEYCHR.EQ.'a')KEYCHR='A'
      IF((KEYCHR.EQ.'P').OR.(KEYCHR.EQ.'A'))GO TO 17850
      IF(KEYCHR.EQ.'0')GO TO 17860
      GO TO 17860

17850 CALL PGRAF(4,'PRN:\0')
      CALL GCLOSE
```

```
17860 CLOSE(7,STATUS='KEEP')
      CLOSE(8,STATUS='KEEP')
      IF(VORANS.EQ.'Y')CLOSE(MVOR,STATUS='KEEP')
      IF(PRSANS.EQ.'Y')CLOSE(MPRS,STATUS='KEEP')
      CALL NEWPEN(0)
      CALL HOME
      CALL GCLOSE
      CALL SETTXT
      STOP
      END
CCCCCCCCCCCCCCCCCCCCCCCCCCCCCCCCCCCCCCCCCCCCCCCCCCCCCCCCCCCCCCCCCCCCCCCCCCCC
CCCCCCCCCCCCCCCCCCCCCCCCCCCCCCCCCCCCCCCCCCCCCCCCCCCCCCCCCCCCCCCCCCCCCCCCCCCC
      SUBROUTINE MOVIE(M)
      IMPLICIT COMPLEX(C,Z),INTEGER(I-N)
      CHARACTER RUNNO*3, KEYCHR*1,TITLE*80,BOGUS*1
      CHARACTER*1 COMNTS(61,5)
      COMMON/VORTEX/ZV(300,4),CV(300,4),GV(300,4),GV0(300,4),
     1              DGDT(300,4),AGE(300,4),GSHED(800,4),GLOST(800,4),
     2              GVMIN,GV0MIN,NNV(4),NNB,NVMAX
      COMMON/SAVE/XVORT(800),YVORT(800),XSEP(800),YSEP(800),USEP(800)
      COMMON/TIMES/DELT,T(800),NT,NTMAX,NTSTOP
      COMMON/CONST/ZONE,ZERO,ZFAC,ZI,ZPI,PI,TWOPI,PI90,PI180,OV2PI,
     1             FOURPI
      COMMON/SURFCE/Q(200),PTOTAL(200),PVORT(200),PVELO(200),
     1              DX,NDX,XMAX,X(200),XI(500),TAU(500),BLDISP(500),
     2              BLMOM(500),MSEP,F(200),XBAR(200)
      COMMON/FLOW/RCORE,CINF,VINF,RMIN,BDISP,NOTOCH,AGECHK
      COMMON/MISC/RUNNO,NPLOTS,NCOMNT,COMNTS,IDATE,ITIME
CCCCCCCCCCCCCCCCCCCCCCCCCCCCCCCCCCCCCCCCCCCCCCCCCCCCCCCCCCCCCCCCCCCCCCCCCCCC
C
C     READS UNFORMATTED DATA FOR EACH TIMESTEP
C
      READ(M)NT,T(NT)
      DO 300 NB=1,NNB
      READ(M) NNV(NB)
      DO 300 NV=1,NNV(NB)
  300 READ(M) ZV(NV,NB),GV(NV,NB),GV0(NV,NB),DGDT(NV,NB)
      DO 1000 I=1,NDX
 1000 READ(M)X(I),Q(I),PVELO(I),PVORT(I),PTOTAL(I)
      READ(M)MSEP
      DO 2000 I=1,MSEP
 2000 READ(M)XI(I),TAU(I),BLDISP(I),BLMOM(I)
      RETURN
      END
CCCCCCCCCCCCCCCCCCCCCCCCCCCCCCCCCCCCCCCCCCCCCCCCCCCCCCCCCCCCCCCCCCCCCCCCCCCC
CCCCCCCCCCCCCCCCCCCCCCCCCCCCCCCCCCCCCCCCCCCCCCCCCCCCCCCCCCCCCCCCCCCCCCCCCCCC
      SUBROUTINE SUMARY(M)
      IMPLICIT COMPLEX(C,Z),INTEGER(I-N)
      CHARACTER RUNNO*3,KEYCHR*1,TITLE*80
      CHARACTER*1 COMNTS(61,5)
      COMMON/VORTEX/ZV(300,4),CV(300,4),GV(300,4),GV0(300,4),
     1              DGDT(300,4),AGE(300,4),GSHED(800,4),GLOST(800,4),
     2              GVMIN,GV0MIN,NNV(4),NNB,NVMAX
      COMMON/SAVE/XVORT(800),YVORT(800),XSEP(800),YSEP(800),USEP(800)
      COMMON/TIMES/DELT,T(800),NT,NTMAX,NTSTOP
      COMMON/CONST/ZONE,ZERO,ZFAC,ZI,ZPI,PI,TWOPI,PI90,PI180,OV2PI,
```

```
     1             FOURPI
      COMMON/SURFCE/Q(200),PTOTAL(200),PVORT(200),PVELO(200),
     1             DX,NDX,XMAX,X(200),XI(500),TAU(500),BLDISP(500),
     2             BLMOM(500),MSEP,F(200),XBAR(200)
      COMMON/FLOW/RCORE,CINF,VINF,RMIN,BDISP,NOTOCH,AGECHK
      COMMON/MISC/RUNNO,NPLOTS,NCOMNT,COMNTS,IDATE,ITIME
      COMMON/MISC1/NHICUP
CCCCCCCCCCCCCCCCCCCCCCCCCCCCCCCCCCCCCCCCCCCCCCCCCCCCCCCCCCCCCCCCCCCCCC
C
C     READS SUMMARY DATA
C
      READ(M)IDATE,ITIME
      READ(M)NCOMNT
      IF (NCOMNT.EQ.0) GO TO 40
      DO 25 J=1,NCOMNT
      READ(M)(COMNTS(I,J),I=1,60)
   25 COMNTS(61,J)=0
   40 READ(M)RUNNO,DELT,RCORE,GVMIN,GV0MIN,BDISP
      READ(M)NHICUPS
      READ(M)NPLOTS
      READ(M)NNB
      READ(M)VINF,XMAX,DX,NDX
      READ(M)NTSTOP
      DO 400 I=1,NTSTOP
      READ(M)T(I),(GSHED(I,NB),GLOST(I,NB),NB=1,NNB),XSEP(I),YSEP(I),
     1      USEP(I),XVORT(I),YVORT(I)
  400 CONTINUE
      RETURN
      END
CCCCCCCCCCCCCCCCCCCCCCCCCCCCCCCCCCCCCCCCCCCCCCCCCCCCCCCCCCCCCCCCCCCCCC
CCCCCCCCCCCCCCCCCCCCCCCCCCCCCCCCCCCCCCCCCCCCCCCCCCCCCCCCCCCCCCCCCCCCCC
      SUBROUTINE PRNTIT(MPRS,MVOR,PRSANS,VORANS)
      IMPLICIT COMPLEX(C,Z),INTEGER(I-N)
      CHARACTER RUNNO*3
      CHARACTER*1 COMNTS(61,5),PRSANS,VORANS
      COMMON/VORTEX/ZV(300,4),CV(300,4),GV(300,4),GV0(300,4),
     1             DGDT(300,4),AGE(300,4),GSHED(800,4),GLOST(800,4),
     2             GVMIN,GV0MIN,NNV(4),NNB,NVMAX
      COMMON/SAVE/XVORT(800),YVORT(800),XSEP(800),YSEP(800),USEP(800)
      COMMON/TIMES/DELT,T(800),NT,NTMAX,NTSTOP
      COMMON/SURFCE/Q(200),PTOTAL(200),PVORT(200),PVELO(200),
     1             DX,NDX,XMAX,X(200),XI(500),TAU(500),BLDISP(500),
     2             BLMOM(500),MSEP,F(200),XBAR(200)
      COMMON/MISC/RUNNO,NPLOTS,NCOMNT,COMNTS,IDATE,ITIME
CCCCCCCCCCCCCCCCCCCCCCCCCCCCCCCCCCCCCCCCCCCCCCCCCCCCCCCCCCCCCCCCCCCCCC
C
C     PRINTS OUT DATA WHEN SO DIRECTED BY USER.
C
      REAL GTOTAL(4)
      IF(VORANS.NE.'Y')GO TO 450
      WRITE(MVOR,50)
   50 FORMAT(5(5H*****,5H00000))
      WRITE(MVOR,100)NT,T(NT)
      WRITE(MVOR,75)XSEP(NT)
   75 FORMAT(2X,16HSEPARATION AT X=,F7.4)
  100 FORMAT(2X,16HTIMESTEP NUMBER ,I3,5X,5HTIME=,F8.4)
```

```
      NV2=0
      DO 200 NB=1,NNB
      IF(ABS(GSHED(NT,NB)).LT.0.00001)GSHED(NT,NB)=-0.00001
      NV3=NNV(NB)
      IF (NV3.LT.1)GO TO 200
      GTOTAL(NB)=0.0
      DO 190 NV=1,NV3
  190 GTOTAL(NB)=GTOTAL(NB)+GV(NV,NB)
  200 NV2=MAX0(NV2,NNV(NB))
      IF (NNB.EQ.2)WRITE(MVOR,272)
      IF (NNB.EQ.3)WRITE(MVOR,273)
      IF (NNB.EQ.4)WRITE(MVOR,274)
  272 FORMAT(8X,2HNV,2X,2(6X,8HPOSITION,6X,5HGAMMA,3X))
  273 FORMAT(8X,2HNV,2X,3(6X,8HPOSITION,6X,5HGAMMA,3X))
  274 FORMAT(8X,2HNV,2X,4(6X,8HPOSITION,6X,5HGAMMA,3X))
  290 IF(NV2.LT.1)GO TO 450
      DO 300 NV=1,NV2
      WRITE(MVOR,310)NV,(ZV(NV,NB),GV(NV,NB),NB=1,NNB)
  300 CONTINUE
  310 FORMAT(7X,I3,2X,4(F8.4,1H,,F8.4,1X,F7.4,3X))
      IF (NNB.EQ.2)WRITE(MVOR,352)(GTOTAL(NB),
     1     (100.*GTOTAL(NB)/GSHED(NT,NB)),NB=1,NNB)
      IF (NNB.EQ.3)WRITE(MVOR,353)(GTOTAL(NB),
     1     (100.*GTOTAL(NB)/GSHED(NT,NB)),NB=1,NNB)
      IF (NNB.EQ.4)WRITE(MVOR,354)(GTOTAL(NB),
     1     (100.*GTOTAL(NB)/GSHED(NT,NB)),NB=1,NNB)
  352 FORMAT(1X,12HGTOTAL/%RMNG,2(14X,F7.4,'/',F5.1,'%'))
  353 FORMAT(1X,12HGTOTAL/%RMNG,3(14X,F7.4,'/',F5.1,'%'))
  354 FORMAT(1X,12HGTOTAL/%RMNG,4(14X,F7.4,'/',F5.1,'%'))
  450 IF(PRSANS.NE.'Y')GO TO 999
      WRITE(MPRS,50)
      WRITE(MPRS,100)NT,T(NT)
      WRITE(MPRS,500)
  500 FORMAT(/3X,3H I ,4X,    10H     X    ,3X,10H     Q    ,3X,
     1       10H  PVELO   ,3X,10H  PVORT   ,3X,10H  PTOTAL  ,3X,
     2       10H     F    ,3X,10H    XBAR  )
      DO 1000 I=1,NDX
 1000 WRITE(MPRS,600)I,X(I),Q(I),PVELO(I),PVORT(I),PTOTAL(I),F(I),
     1                XBAR(I)
  600 FORMAT(2X,I3,7(3X,F10.4))
      WRITE(MPRS,650)MSEP
  650 FORMAT(/2X,I3,' POINTS USED IN CALCULATING SEPARATION POINT')
      WRITE(MPRS,700)
  700 FORMAT(/2X,3HSTN,3X,10H    XI    ,3X,10H    TAU   ,3X,
     1       10H  BLDISP  ,3X,10H   BLMOM  )
      DO 2000 I=1,MSEP
 2000 WRITE(MPRS,800)I,XI(I),TAU(I),BLDISP(I),BLMOM(I)
  800 FORMAT(2X,I3,4(3X,F10.4))
  999 RETURN
      END
CCCCCCCCCCCCCCCCCCCCCCCCCCCCCCCCCCCCCCCCCCCCCCCCCCCCCCCCCCCCCCCCCCCCCCCCCC
CCCCCCCCCCCCCCCCCCCCCCCCCCCCCCCCCCCCCCCCCCCCCCCCCCCCCCCCCCCCCCCCCCCCCCCCCC
      SUBROUTINE FIVEPT(PIN,POUT,NDIM)
      DIMENSION PIN(200),POUT(200)
CCCCCCCCCCCCCCCCCCCCCCCCCCCCCCCCCCCCCCCCCCCCCCCCCCCCCCCCCCCCCCCCCCCCCCCCCC
C
```

```
C     SMOOTHING ROUTINE PROPOSED BY LONGUET-HIGGINS AND COCKELET
C     (1976) PROC. ROY. SOC. SER. A, 350, PP. 1-26.
C
      DO 100 I=1,NDIM
  100 POUT(I)=PIN(I)
      DO 200 I=3,NDIM-2
      PM2=PIN(I-2)
      PM1=PIN(I-1)
      P  =PIN(I)
      PP1=PIN(I+1)
      PP2=PIN(I+2)
  200 POUT(I)=(-PM2+4.*PM1+10.*P+4.*PP1-PP2)/16.
      RETURN
      END
CCCCCCCCCCCCCCCCCCCCCCCCCCCCCCCCCCCCCCCCCCCCCCCCCCCCCCCCCCCCCCCCCCCCCCCCCCC
CCCCCCCCCCCCCCCCCCCCCCCCCCCCCCCCCCCCCCCCCCCCCCCCCCCCCCCCCCCCCCCCCCCCCCCCCCC
      SUBROUTINE PSMUTH(PLOWER,PUPPER,PIN,POUT,NDIM)
      DIMENSION PIN(200),POUT(200),P1(200),P2(200)
CCCCCCCCCCCCCCCCCCCCCCCCCCCCCCCCCCCCCCCCCCCCCCCCCCCCCCCCCCCCCCCCCCCCCCCCCCC
C
C     SMOOTHING ROUTINE, ORIGINALLY DEVELOPED FOR THE PRESSURE
C     DISTRIBUTION, BUT APPROPRIATE FOR ANY CURVE TO BE SMOOTHED.
C     LOOK AT PROBLEM IN TERMS OF MAXIMUM PRESSURE MAGNITUDE WHICH
C     COULD BE PRODUCED IN INVISCID CASE AS MAJOR VORTEX PASSES OVER
C     PLATE.  LOP OFF THESE EXCURSIONS BEFORE UTILIZING A SMOOTHING
C     ROUTINE TO FURTHER IMPROVE THE DATA FOR INTEGRATION.  PUPPER AND
C     PLOWER ARE THE LIMITS SET FOR REALISTIC DATA, SPECIFIED AS INPUT
C     ARGUMENTS WHEN CALLING PSMUTH.
C
      ITS=10
      FACTOR=0.8
      DO 50 I=1,NDIM
      P1(I)=PIN(I)
   50 P2(I)=PIN(I)
      DO 150 I=1,ITS
      IF(P1(1)  .GT.PUPPER)P1(1)   =
     1  FACTOR*PUPPER*P1(1)   /ABS(P1(1   ))
      IF(P1(1)  .LT.PLOWER)P1(1)   =
     1  FACTOR*PLOWER*P1(1)   /ABS(P1(1   ))
      IF(P1(NDIM).GT.PUPPER)P1(NDIM)=
     1  FACTOR*PUPPER*P1(NDIM)/P1(NDIM)
      IF(P1(NDIM).LT.PLOWER)P1(NDIM)=
     1  FACTOR*PLOWER*P1(NDIM)/P1(NDIM)
      KGOOD=1
      DO 100 K=1,NDIM
      IF((P1(K).GT.PUPPER).OR.(P1(K).LT.PLOWER))GO TO 100
      IF(KGOOD.EQ.(K-1).OR.K.EQ.1)GO TO 90
      DO 60 J=KGOOD,(K-1)
   60 P2(J)=P1(KGOOD)
   90 KGOOD=K
  100 CONTINUE
      CALL FIVEPT(P2,P2,NDIM)
      DO 140 K=2,NDIM-1
  140 P1(K)=P2(K)
  150 CONTINUE
      DO 160 I=1,NDIM
```

```
  160 POUT(I)=P1(I)
      RETURN
      END
CCCCCCCCCCCCCCCCCCCCCCCCCCCCCCCCCCCCCCCCCCCCCCCCCCCCCCCCCCCCCCCCCCCCCCCC
CCCCCCCCCCCCCCCCCCCCCCCCCCCCCCCCCCCCCCCCCCCCCCCCCCCCCCCCCCCCCCCCCCCCCCCC
      SUBROUTINE FORMOM
      COMMON/SURFCE/Q(200),PTOTAL(200),PVORT(200),PVELO(200),
     1              DX,NDX,XMAX,X(200),XI(500),TAU(500),BLDISP(500),
     2              BLMOM(500),MSEP,F(200),XBAR(200)
CCCCCCCCCCCCCCCCCCCCCCCCCCCCCCCCCCCCCCCCCCCCCCCCCCCCCCCCCCCCCCCCCCCCCCCC
C
C     CALCULATES FORCE AND MOMENT FOR DURATION OF THE RUN
C
      FMIN=0.001
      FORCE=0.0
      RMOMNT=0.0
      DO 200 I=1,NDX
      FORCE=FORCE+PTOTAL(I)
      RMOMNT=RMOMNT+PTOTAL(I)*X(I)
      F(I)=-FORCE*DX
      IF(ABS(FORCE).LT.FMIN)FORCE=SIGN(FMIN,FORCE)
  200 XBAR(I)=RMOMNT/FORCE
      RETURN
      END
CCCCCCCCCCCCCCCCCCCCCCCCCCCCCCCCCCCCCCCCCCCCCCCCCCCCCCCCCCCCCCCCCCCCCCCC
CCCCCCCCCCCCCCCCCCCCCCCCCCCCCCCCCCCCCCCCCCCCCCCCCCCCCCCCCCCCCCCCCCCCCCCC
      SUBROUTINE AXES(AMAX,SPCNG,DELORD,NSPCS)
      DELORD=1.0
CCCCCCCCCCCCCCCCCCCCCCCCCCCCCCCCCCCCCCCCCCCCCCCCCCCCCCCCCCCCCCCCCCCCCCCC
C
C     PERFORMS INTELLIGENT SCALING OF THE AXES, BASED UPON DATA TO BE
C     PLOTTED.
C
      SPCNG=0.2
      NSPCS=5
      ORDMAX=ABS(AMAX)

      IF(ORDMAX.GE.5.0)SPCNG=1.0
      IF(ORDMAX.GE.5.0)NSPCS=5
      IF(ORDMAX.GE.5.0)DELORD=5.0

      IF(ORDMAX.GE.10.0)SPCNG=1.0
      IF(ORDMAX.GE.10.0)NSPCS=5
      IF(ORDMAX.GE.10.0)DELORD=5.0

      IF(ORDMAX.GE.50.0)SPCNG=5.0
      IF(ORDMAX.GE.50.0)NSPCS=2
      IF(ORDMAX.GE.50.0)DELORD=10.0

      IF(ORDMAX.GE.100.0)SPCNG=10.0
      IF(ORDMAX.GE.100.0)NSPCS=5
      IF(ORDMAX.GE.100.0)DELORD=50.0

      IF(ORDMAX.GE.200.0)SPCNG=10.0
      IF(ORDMAX.GE.200.0)NSPCS=5
      IF(ORDMAX.GE.200.0)DELORD=50.0
```

```
      RETURN
      END
CCCCCCCCCCCCCCCCCCCCCCCCCCCCCCCCCCCCCCCCCCCCCCCCCCCCCCCCCCCCCCCCCCCCCCCC
CCCCCCCCCCCCCCCCCCCCCCCCCCCCCCCCCCCCCCCCCCCCCCCCCCCCCCCCCCCCCCCCCCCCCCCC
      FUNCTION SIGMA(NB)
      IMPLICIT COMPLEX(C,Z),INTEGER(I-N)
      COMMON/VORTEX/ZV(300,4),CV(300,4),GV(300,4),GV0(300,4),
     1              DGDT(300,4),AGE(300,4),GSHED(800,4),GLOST(800,4),
     2              GVMIN,GV0MIN,NNV(4),NNB,NVMAX
CCCCCCCCCCCCCCCCCCCCCCCCCCCCCCCCCCCCCCCCCCCCCCCCCCCCCCCCCCCCCCCCCCCCCCCC
C
C     SUMS VORTICITY WITHIN THE DESIRED CLUSTER.
C
      SUM=0.0
      IF(NNV(NB).LT.1)GO TO 200
      DO 100 NV=1,NNV(NB)
      SUM=SUM+GV(NV,NB)
  100 CONTINUE
  200 SIGMA=SUM
      RETURN
      END
CCCCCCCCCCCCCCCCCCCCCCCCCCCCCCCCCCCCCCCCCCCCCCCCCCCCCCCCCCCCCCCCCCCCCCCC
CCCCCCCCCCCCCCCCCCCCCCCCCCCCCCCCCCCCCCCCCCCCCCCCCCCCCCCCCCCCCCCCCCCCCCCC
      SUBROUTINE NOZERO(X,Y,NDIM)
      DIMENSION X(800),Y(800)
CCCCCCCCCCCCCCCCCCCCCCCCCCCCCCCCCCCCCCCCCCCCCCCCCCCCCCCCCCCCCCCCCCCCCCCC
C
C     REMOVES ZERO DATA POINTS FROM THE DATA TO FACILITATE PRINTOUT OF
C     THE DATA.
C
      DO 100 I=1,NDIM-1
      CALL MOVE(X(I),Y(I))
      IF((Y(I).EQ.0.0).OR.(Y(I+1).EQ.0.0))GO TO 100
      CALL LINE(X(I+1),Y(I+1))
  100 CONTINUE
      RETURN
      END
CCCCCCCCCCCCCCCCCCCCCCCCCCCCCCCCCCCCCCCCCCCCCCCCCCCCCCCCCCCCCCCCCCCCCCCC
CCCCCCCCCCCCCCCCCCCCCCCCCCCCCCCCCCCCCCCCCCCCCCCCCCCCCCCCCCCCCCCCCCCCCCCC
```

# LIST OF REFERENCES


Baker, G.R. 1979. The "Cloud in Cell" Technique Applied to the Roll Up of Vortex Sheets. *Journal of Computational Physics*. **31** (1): 76-95.

Baker, G.R. 1980. A Test of the Method of Fink & Soh for Following Vortex-Sheet Motion. *Journal of Fluid Mechanics*. **100** (1): 209-20.

Basuk, J., and Graham, J.M.R. 1987. Discrete Vortex Computation of Separated Airfoil Flow. *AIAA Journal*. **25** (11): 1409-10.

Bellamy-Knights, P.G. 1967. Analytical Study of Symmetrical Separated Flow About a Circular Cylinder. Master's Thesis, University of Manchester.

Bènard, H. 1908. Formation de Centres de Gyration a l'arrière d'un Obstacle en Mouvement. *Comptes Rendus*. **147**: 839-42.

Bergson, A.J., and Porter, J.D. 1960. *An Investigation of the Flow Around Slender Delta Wings with Leading Edge Separation*. Report No. 510, Princeton University.

Birkhoff, G. 1950. *Hydrodynamics: A Study in Logic, Fact and Similitude*. Princeton, N.J.: Princeton University Press.

Bloor, M.S., and Gerrard, J.H. 1966. Measurements on Turbulent Vortices in a Cylinder Wake. *Proceedings of the Royal Society A*. **294** (1438): 319-42.

Cebeci, T. 1978. *A Computer Program for Calculating Incompressible Laminar and Turbulent Boundary Layers on Plane and Axisymmetric Bodies with Surface Roughness*. Report No. TR-78-1, Department of Mechanical Engineering, California State University at Long Beach, Long Beach, Ca.

Cebeci, T., and Carr, L.W. 1984. Description of a Computer Program for Calculating Time-Dependent Boundary Layers with Flow Reversal. Unpublished Computer Program.

Chaplin, J.R. 1973. Computer Model of Vortex Shedding from a Cylinder. *Proceedings of the American Society of Civil Engineers. Journal of the Hydraulics Division*. **99** (HY1): 155-65. Chorin, A.J. 1973. Numerical Study of Slightly Viscous Flow. *Journal of Fluid Mechanics*. **57** (4): 785-96.

Chorin, A.J. 1973. Numerical Study of Slightly Viscous Flow. *Journal of Fluid Mechanics*. **57**(4): 785-96.

Chorin, A.J. 1978. Vortex Sheet Approximation of Boundary Layers. *Journal of Computational Physics.* **27**(3): 428-42.

Chu, C.C. and Falco, R.E. 1988. Vortex Ring/Viscous Wall Layer Interaction Model of the Turbulence Production Process Near Walls. *Exp. Fluids.* **6**: 305-15.

Chuang, F.-S. and Conlisk, A.T. 1989. The Effect of Interaction on the Boundary Layer Induced by a Convected Rectilinear Vortex. *Journal of Fluid Mechanics.* **200**: 337-65.

Clements, R.R. 1977. Flow Representation, Including Separated Regions, Using Discrete Vortices. *AGARD Lecture Series No. 86 on Computational Fluid Dynamics.*

Conlisk, A.T., and Rockwell, D. 1981. Modelling of Vortex-Corner Interaction Using Point Vortices. *Physics of Fluids.* **24** (12): 2133-42.

Conlisk, A.T. and Veley, D. 1985. The Generation of Noise in Impinging Vortex Motion Past a Step. *Physics of Fluids.* **28**: 3004-12.

Davis, M.D. 1969. An Analytical Study of Separated Flow About a Circular Cylinder. Master's Thesis, Naval Postgraduate School, Monterey, Ca.

Deffenbaugh, F.D., and Marshall, F.J. 1976. Time Development of the Flow About an Impulsively Started Cylinder. *AIAA Journal.* **14** (7): 908-13.

Doligalski, T.L. and Walker, J.D.A. 1984. The Boundary Layer Induced by a Convected Two-Dimensional Vortex. *Journal of Fluid Mechanics.* **139**: 1-28.

Doligalski, T.L., Smith, C.R., and Walker, J.D.A. 1994. Vortex Interactions with Walls. *Annual Reviews of Fluid Mechanics.* **26**: 573-616.

Elliott, J.W., Cowley, S.J., and Smith, F.T. 1983. Breakdown of Boundary Layers: (i) On Moving Surfaces; (ii) In Self-Similar Unsteady Flows; (iii) In Fully Unsteady Flows. *Geophys. Astrophys. Fluid Dyn.* **25**: 77-138.

Ersoy, S. and Walker, J.D.A. 1985. Viscous Flow Induced by Counter-Rotating Vortices. *Physics of Fluids.* **28**: 2687-98.

Ersoy, S. and Walker, J.D.A. 1986. Flow Induced at a Wall by a Vortex Pair. *AIAA Journal.* **24** (10): 1597-1605.

Ersoy, S. and Walker, J.D.A. 1987. The Boundary Layer Due to a Three-Dimensional Vortex Loop. *Journal of Fluid Mechanics.* **185**: 569-98.

Fage, A., and Johansen, F.C. 1928. *The Structure of Vortex Sheets.* Great Britain Aeronautical Research Council R&M 1143 (Ae. 311). (see also: *Philosophical Magazine.* series 7, 5 (28): 417–41.)

Falco, R.E. 1991. A Coherent Sturcture Model of the Turbulent Boundary Layer and Its Ability to Predict Reynolds Number Dependence. *Phil. Trans. R. Soc. London Ser. A.* **336**: 103-29.

Fink, P.T., and Soh, W.K. 1974a. Calculation of Vortex Sheets in Unsteady Flow and Applications in Ship Hydrodynamics. *Tenth Symposium Naval Hydrodynamics,* 1974, Cambridge, Ma. 1976: Office of Naval Research: 463-87; discussion: 488-91.

Fink, P.T., and Soh, W.K. 1974b *On an Anomalous Result in Linearised Slender Lifting Surface Theory.* Report NAV/ARCH 74/6, University of New South Wales, 9 pp. (see also: *Fifth Australaisan Conference on Hydraulics and Fluid Mechanics.* Institution of Engineers Australia: 9pp.)

Fink, P.T., and Soh, W.K. 1978. A New Approach to Roll-Up Calculations of Vortex Sheets. *Proceedings of the Royal Society A.* **362**: 195-209.

Franks, C.B. 1983. *Sensitivity Studies of Methods for Predicting Separation in Discrete Vortex Models.* Report DTNSRDC-83/093, David W. Taylor Naval Ship Research and Development Center, Bethesda, Md.

Frederickson, K.A. 1990. Numerical Study of Non-Impulsively Started Flow Around a Circular Cylinder. Master's Thesis, Naval Postgraduate School, Monterey, Ca.

Gerald, C.F. 1978. *Applied Numerical Analysis.* Reading, Ma.: Addison-Wesley.

Gerrard, J.H. 1966. The Mechanics of the Formation Region of Vortices Behind Bluff Bodies. *Journal of Fluid Mechanics.* **25** (2): 401-13.

Gerrard, J.H. 1967. Numerical Computation of the Magnitude and Frequency of the Lift on a Circular Cylinder. *Philosophical Transactions of the Royal Society A.* London. **261** (1118): 137-62.

Grass, A.J., and Kemp, P.H. 1979. Flow Visualization Studies of Oscillatory Flow Past Smooth and Rough Circular Cylinders. *Mechanics of Wave-Induced Forces on Cylinders* (ed. T.L. Shaw), Marshfield, Ma.: Pitman: 406-20.

Hardin, J.C. and Lamkin, S.L. 1984. Aeroacoustic Interaction of a Distributed Vortex with a Lifting Joukowski Airfoil. Paper AIAA-84-2287.

Harvey, J.K. and Perry, F.J. 1971. Flowfield Produced by Trailing Vortices in the Vicinity of the Ground. *AIAA Journal.* **9** (12): 1659-60.

Higdon, J.J.L., and Pozrikidis, C. 1985. The Self-Induced Motion of Vortex Sheets. *Journal of Fluid Mechanics.* **150**: 203-31.

Hoeijmakers, H.W. M., and Vaastra, W. 1983. A Higher-Order Panel Method Applied to Vortex Sheet Roll-up. *AIAA Journal.* **21**: 516-23.

Ikeda, Y. 1984. *Calculation of Lift Force Acting on Circular Cylinder in Oscillating Flow.* TUB/ISM-Bericht Nr. 84/12, Technische Universität Berlin, Institut für Schiffs-und Merestechnik.

Ikeda, Y., and Himeno, Y. 1981. Calculation of Vortex-Shedding Flow Around Oscillating Circular and Lewis-Form Cylinders. *Proceedings Third International Conference on Numerical Ship Hydrodynamics.* Paris: Bassin d' Essais des Carènes: 335-46.

Inamuro, T.; Adachi, T.; and Sakata, H. 1983. A Numerical Analysis of Unsteady Separated Flow by Vortex Shedding Model. *Bulletin of Japan Society of Mechanical Engineers.* **26** (222): 2106-12.

Inamuro, T.; Saito, T.; and Adachi, T. 1984. A Numerical Analysis of Unsteady Separated Flow by the Discrete Vortex Method Combined with the Singularity Method. *Computers & Structures.* **19** (1/2): 75-84.

Izumi, K.; Kuwahara, K.; Horiuti, K.; and Oshima, K. 1982. Flow Past an Elliptic Cylinder Started Impulsively. *Flow Visualization II,* Proceedings of the Second International Symposium on Flow Visualization (ed. W. Merzkirch). New York: Hemisphere Publishing Corporation: 343-7.

von Kármán, T. 1911. Über den Mechanismus des Widerstandes, den ein bewegter Körper in einer Flüssigkeit erfährt. *Nachrichten von der Königlichen Gesellschaft der Wissenschaften zu Göttingen. Mathematisch-physikalische Klasse:* 509-17.

Katz, J. 1981. A Discrete Vortex Method for the Non-Steady Separated Flow Over an Airfoil. *Journal of Fluid Mechanics.* **102**: 315-28.

Kaya, M. 1992. Discrete Vortex Mehtod Simulation of Kármán Vortex Street-Edge Interaction. Ph.D. Dissertation, Istanbul Technical University.

Kaykayoglu, C.R. 1987. Modeling of Unsteady Pressure Fields Due to Vortex-Curved Surface Interactions by the Method of Discrete Vortices. *Bulletin of the Technical University of Instanbul.* **40**(4): 679-703.

Kaykayoglu, C.R. and Graham, J.M.R. 1989. Vortex-Sharp Edge Interactions. Aero. Report. Aero. Tech. No. 89-001, Imperial College.

Kaykayoglu, C.R. and Kaya, M.O. 1992. Vortex Method Simulation of a Self Sustained Wake-Edge Interaction: Unsteaady Loading. ASME Symposium on Flow-Inudced Vibration and Noise--Volume 7. AMD **151**/PVP **247**: 35-62.

Kaykayoglu, R., and Rockwell, D. 1985. Vortices Incident Upon a Leading Edge. Instantaneous Pressure Fields. *Journal of Fluid Mechanics.* **156**: 439-61.

Keulegan, G.H., and Carpenter, L.H. 1956. *Forces on Cylinders and Plates in an Oscillating Fluid.* Report No. 4821, National Bureau of Standards. (see also: 1958. *Journal of Research of the National Bureau of Standards.* **60** (5): 423-40.)

Kimura, T., and Tsutahara, M. 1987. Flows About a Rotating Circular Cylinder by the Discrete-Vortex Method. *AIAA Journal.* **25** (1): 182-84.

Kiya, M., and Arie, M. 1977. A Contribution to an Inviscid Vortex-Shedding Model for an Inclined Flat Plate in Uniform Flow. *Journal of Fluid Mechanics.* **82** (2): 3-40.

Kiya, M. and Arie, M. 1980. Discrete-Vortex Simulation of Unsteady Separated Flow Behind a Nearly Normal Plate. *Bulletin of Japan Society of Mechanical Engineers.* **23** (183): 1451-8.

Kiya, M.; Sasaki, K.; and Arie, M. 1982. Discrete-Vortex Simulation of a Turbulent Separation Bubble. *Journal of Fluid Mechanics.* **120**: 219-44.

Krasny, R. A Study of Singularity Formation in a Vortex Sheet by the Point Vortex Approximation. *Journal of Fluid Mechanics.* **167**: 65-93.

Kudo, K. 1979. An Inviscid Model of Discrete-Vortex Shedding for Two-Dimensional Oscillating Flow Around a Flat Plate. *Journal of the Society of Naval Architects of Japan.* **145**: 54-62.

Kudo, K. 1981. Hydrodynamic Forces of the Oscillating Flat Plate. *Proceedings Third International Conference on Numerical Ship Hydrodynamics.* Paris: Bassin d' Essais des Carènes: 347-57; discussion: 358.

Kuo, S.S. 1972. *Computer Applications of Numerical Methods.* Reading, Ma.: Addison-Wesley.

Kuwahara, K. 1973. Numerical Study of Flow Past an Inclined Flat Plate by an Inviscid Model. *Journal of the Physical Society of Japan.* **35** (5): 1545-51.

Kuwahara, K. 1978. Study of Flow Past a Circular Cylinder by an Inviscid Model. *Journal of the Physical Society of Japan.* **45** (1): 292-7.

Laird, A.D.K. 1971. Eddy Formation Behind Circular Cylinders. *Proceedings of the American Society of Civil Engineers. Journal of the Hydraulics Division.* **97** (HY6): 763-75.

Lamb, Sir H. 1932. *Hydrodynamics,* 6th ed. Cambridge, England: Cambridge University Press.

Lee, D.J. and Smith, C.A. 1991. Effect of Vortex Core Distortion on Blade-Vortex Interaction. *AIAA Journal.* **29** (9): 1355-62.

Loitsianskii, L.G. 1941. Integral Methods in the Theory of the Boundary Layer. *Priladnaia Mathematika I Mekhanika.* **V** (3): 453-70. (translated as 1944. National Advisory Committee for Aeronautics TM 1070.)

Longuet-Higgins, M.S. 1981. Oscillating Flow Over Steep Sand Ripples. *Journal of Fluid Mechanics.* **107**: 1-35.

Lugt, H.J. 1981. Numerical Modelling of Vortex Flows in Ship Hydrodynamics--A Review. *Proceedings Third International Conference on Numerical Ship Hydrodynamics.* Paris: Bassin d' Essais des Carènes: 297-316; discussion: 317.

Milne-Thomson, L.M. 1966. *Theoretical Aerodynamics,* 4th ed. London: Macmillan.

Milne-Thomson, L.M. 1968. *Theoretical Hydrodynamics,* 5th ed. London: Macmillan.

Moorty, S., and Olson, M.D. 1989. A Numerical Study of Low Reynolds Number Fluid-Structure Interaction. *Journal of Fluids and Structures.* **3**: 37-60.

Morison, J.R.; O'Brien, M.P.; Johnson, J.W.; and Schaff, S.A. 1950. The Force Exerted by Surface Waves on Piles. *Petroleum Transactions, AIME.* **189**: 149-54.

Mostafa, S.I.M. 1987. Numerical Simulation of Unsteady Separated Flows. Ph.D. Dissertation, Naval Postgraduate School, Monterey, Ca.

Munz, P.D. 1987. Unsteady Flow About Cambered Plates. Master's Thesis, Naval Postgraduate School, Monterey, Ca.

Nagano, S.; Naito, M.; and Takata, H. 1981. Analysis of the Flow Past Rectangular Cylinders by the Discrete Vortex Model (in Japanese). *Transactions of the Japan Society of Mechanical Engineers.* **47**: 32-43.

Nagano, S.; Naito, M.; and Takata, H. 1982. A Numerical Analysis of Two-Dimensional Flow Past a Rectangular Prism by a Discrete Vortex Model. *Computers and Fluids.* **10** (4): 243-59.

Nielsen, J. 1960. *Missile Aerodynamics.* New York: McGraw-Hill.

Ogawa, T. 1984. Theoretical Study on the Flow About Savonius Rotor. *ASME Journal of Fluids Engineering.* **106** (1): 85-91.

Ohring, S. 1986. Calculation of Self-Excited Impinging Jet Flow. *Journal of Fluid Mechanics.* **163**: 69-89.

Panaras, A.G. 1985. Pressure Pulses Generated by the Interaction of a Discrete Vortex with an Edge. *Journal of Fluid Mechanics.* **154**: 445-62.

Panaras, A.G. 1987. Numerical Modelling of the Vortex/Airfoil Interaction. *AIAA Journal.* **25** (1): 5-11.

Panaras, A.G. 1990. Shear-Layer-Edge Interaction: Simulation by Finite-Area Vortices. *AIAA Journal.* **28** (9): 1557-64.

Park, J-H and Lee, D-J. 1994. Numerical Simulation of Vortex-Edge Interaction. *AIAA Journal.* **32** (6): 1126-34.

Pattani, P.G., and Olson, M.D. 1988. Forces on Oscillating Bodies in Viscous Fluids. *International Journal for Numerical Methods in Fluids.* **8**: 519-36.

Peridier, V.J., Smith, F.T., and Walker, J.D.A. 1991a. Vortex-Induced Boundary Layer Separation. Part 1. The Unsteady Limit Problem **Re**$\rightarrow\infty$. *Journal of Fluid Mechanics.* **232**: 99-131.

Peridier, V.J., Smith, F.T., and Walker, J.D.A. 1991b. Vortex-Induced Boundary Layer Separation. Part 2. Unsteady Interacting Boundary Layer Theory. *Journal of Fluid Mechanics.* **232**: 133-65

Pohlhausen, K. 1921. Zur Näherungsweisen Integration des Differentialgleichungen der laminaren Grenzschict, *Zeitschrift für angewandte Mathematick und Mechanik.* **1**: 252-68. (translation by R.C. Roland. 1965. *The Approximate Integration of the Differential Equation for the Laminar Boundary Layer.* Gainesville: Department of Aerospace Engineering, University of Florida: 36 pp.)

Poling, D.R., Dadone, L., and Telionis, D.P. 1987. Blade-Vortex Interaction. Paper AIAA-87-0497.

Poling, D.R. and Telionis, D.P. 1986. The Response of Airfoils to Periodic Disturbances--The Unsteady Kutta Condition. *AIAA Journal.* **24**: 193-9.

Poling, D.R., Wilder, M.C., and Telionis, D.P. 1988. Two-Dimensional Interaction of Vortices with a Blade. Paper AIAA-88-0044.

Poling, D.R., Wilder, M.C., and Telionis, D.P. 1991. Fundamental Research in Helicopter Rotor Blade-Vortex Interaction Modeling. Paper 47th Annual Forum of the American Helicopter Society. Phoenix, Az. May.

Putzig, C.J. 1991. Numerical Experiments in Unsteady Flows Through the Use of Full Navier-Stokes Equations. Engineer's Thesis, Naval Postgraduate School, Monterey, Ca.

Robertson, J.M. 1965. *Hydrodynamics in Theory and Application.* Englewood Cliffs, N.J.: Prentice-Hall.

Rockwell, D. 1983. Oscillation of Impinging Shear Layers. *AIAA Journal.* **21** (5): 645-64.

Rockwell, D., Kaykayoglu, C.R., Sohn, D., and Kuo, C.H. 1985. An Assessment of Some Vorticity Field-Leading Edge Interactions. *Shear Flow-Structure Phenomena.* ASME NCA **1**: 79-88.

Rosenhead, L. 1931. The Formation of Vortices from a Surface of Discontinuity. *Proceedings of the Royal Society A.* **134** (823): 170-92.

Roshko, A. 1954. On the Wake and Drag of Bluff Bodies. *Journal of the Aeronautical Sciences.* **22** (2): 124-32.

Sarpkaya, T. 1963 Lift, Drag, and Added-Mass Coefficients for a Circular Cylinder Immersed in a Time-Dependent Flow. *Journal of Applied Mechanics.* **30** (1): 13-15.

Sarpkaya, T. 1968. An Analytical Study of Separated Flow About Circular Cylinders. *ASME Journal of Basic Engineering.* **90**: 511-20.

Sarpkaya, T. 1975 An Inviscid Model of Two-Dimensional Vortex Shedding for Transient and Asymptotically Steady Separated Flow over an Inclined Flat Plate. *Journal of Fluid Mechanics.* **68** (1): 109-28.

Sarpkaya, T. 1976. *Vortex Shedding and Resistance in Harmonic Flow About Smooth and Rough Circular Cylinders at High Reynolds Numbers.* Report No. NPS-59SL76021, Naval Postgraduate School, Monterey, Ca.

Sarpkaya, T. 1978. *Impulsive Flow About a Circular Cylinder.* Report No. NPS-69SL787008, Naval Postgraduate School, Monterey, Ca.

Sarpkaya, T. 1981a. *Morison's Equation and the Wave Forces on Offshore Structures.* Report CR 82.008, Naval Civil Engineering Laboratory, Port Hueneme, Ca.

Sarpkaya, T. 1981b. A Critical Assessment of Morison's Equation. *Proceedings of the International Symposium on Hydrodynamics in Ocean Engineering*. Trondheim: Norwegian Hydrodynamic Laboratories: 447-67.

Sarpkaya, T. 1985. Past Progress and Outstanding Problems in Time-Dependent Flows About Ocean Structures. *Separated Flow Around Marine Structures*. Trondheim: The Norwegian Institute of Technology: 1-36.

Sarpkaya, T. 1989. Computational Methods with Vortices--The 1988 Freeman Scholar Lecture. *ASME Journal of Fluids Engineering*. **111**: 5-52.

Sarpkaya, T. 1992. Brief Reviews of Some Time-Dependent Flows. *ASME Journal of Fluids Engineering*. **114**: 283-98.

Sarpkaya, T. 1994. Vortex Element Methods for Flow Simulation. *Advances in Applied Mechanics* **(31)**: 113-247.

Sarpkaya , T., and Butterworth, W. 1992. Separation Points on a Cylinder in Oscillating Flow. *ASME Journal of Offshore Mechanics and Arctic Engineering*. **114**: 28-35.

Sarpkaya, T., Putzig, C., Gordon, D., Wang, X., and Dalton, D. 1992. Vortex Trajectories Around a Circular Cylinder in Oscillatory Plus Mean Flow. *ASME Journal of Offshore Mechanics and Arctic Engineering*. **114**: 291-98.

Sarpkaya, T., and Henderson, D.O., Jr. Free Surface Scars and Striations Due to Trailing Vortices Generated by a Submerged Lifting Surface. Paper AIAA-85-0445.

Sarpkaya, T., and Ihrig, C.J. 1986. Impulsively Started Flow About Rectangular Prisms: Experiments and Discrete Vortex Analysis. *ASME Journal of Fluids Engineering*. **(108)**: 47-54.

Sarpkaya, T., and Isaacson, M. 1981. *Mechanics of Wave Forces on Offshore Structures*. New York: Van Nostrand Reinhold.

Sarpkaya, T., Mostafa, S.I.M., and Munz, P.D. 1987 *Unsteady Flow About Cambered Plates*. Report No. NPS-69-87-012, Naval Postgraduate School, Monterey, Ca.

Sarpkaya, T., and Shoaff, R.L. 1979. *A Discrete Vortex Analysis of Flow About Stationary and Transversely Oscillating Circular Cylinders*. Report No. NPS-69SL79011, Naval Postgraduate School, Monterey, Ca. (see also: Inviscid Model of Two-Dimensional Vortex Shedding by a Circular Cylinder *AIAA Journal*. **17** (11): 1193-1200.).

Sarpkaya, T., and Wilson, J.R. Pressure Distribution on Smooth and Rough Cylinders in Harmonic Flow. *Proceedings Ocean Structural Dynamics Symposium '84.* Corvalis: Oregon State University: 341-55.

Sawaragi, T., and Nakamura, T. 1979. Analytical Study of Wave Force on a Cylinder in Oscillatory Flow. *Coastal Structures '79,* **I**. New York: American Society of Civil Engineers: 154-73.

Schlichting, H. 1932. Berechnung ebener periodischer Grenzschichtströmungen. *Physikalischer Zeitschrift.* **XXXIII**: 327-35.

Schlichting, H. 1968. *Boundary Layer Theory,* 6th ed. New York: McGraw-Hill.

Schlichting, H. 1979. *Boundary Layer Theory,* 7th ed. New York: McGraw-Hill.

von Schmidt, D.V., and Tilmann, P.M. 1972. Über die Zirkulationsentwicklung in Nachläufen von Rundstäben. *Acustica.* **27**: 14-22.

Sherman, F.S. 1990. *Viscous Flow.* New York: McGraw-Hill.

Shetz, J.A. 1993. *Boundary Layer Analysis.* Englewood Cliffs, N.J.: Prentice Hall.

Shigemi, M. 1987. Application of Discrete Vortex Method to Analysis of Separated Flow Around Airfoils. *Transactions Japan Society for Aeronautical and Space Sciences.* **29**: 107-19.

Shirahata, H., and Daiguji, H. 1982. An Analysis of Unsteady Diagonal Cascade Flow Using a Discrete Vortex Method. *Bulletin of Japan Society of Mechanical Engineers.* **25** (201): 334-41.

Shoaff, R.L., and Franks, C.B. 1981. A Discrete Vortex Analysis of Flow About Noncircular Cylinders. *Proceedings Third International Conference on Numerical Ship Hydrodynamics.* Paris: Bassin d' Essais des Carènes: 319-33.

Smith, P.A. 1986. Computation of Viscous Flows by the Vortex Method. Ph.D. Dissertation, University of Manchester.

Smith, P.A., and Stansby, P.K. 1987. Generalized Discrete Vortex Method for Cylinders Without Sharp Edges. *AIAA Journal.* **25** (2): 199-200.

Smith, P.A., and Stansby, P.K. 1988. Impulsively Started Flow Around a Circular Cylinder by the Vortex Method. *Journal of Fluid Mechanics.* **194**: 45-77.

Sokolnikoff, I.S., and Redheffer, R.M. 1958. *Mathematics of Physics and Modern Engineering.* New York: McGraw-Hill.

Sommerfeld, A. 1950. *Mechanics of Deformable Bodies.* New York: Academic Press: 129-67.

Squire, H.B. 1955. *The Growth of a Vortex in Turbulent Flow.* Great Britain Aeronautical Research Council, Paper No. 16666. (see also: 1965. *The Aeronautical Quarterly.* **XVI** (3): 302-06.)

Srinivasan, G.R. 1985. Computations of Two-Dimensional Airfoil-Vortex Interactions. NASA Contractor Report 3885.

Srinivasan, G.R., McCroskey, W.J., and Baeder, J.D. 1986. Aerodynamics of Two-Dimensional Blade-Vortex Interaction. *AIAA Journal.* **24** (10): 1569-76.

Srinivasan, G.R. and McCroskey, W.J. 1993. Euler Calculations of Unsteady Interaction of Advancing Rotor with a Line Vortex. *AIAA Journal.* **31** (9): 1659-66.

Stansby, P.K. 1977. An Inviscid Model of Vortex Shedding from a Circular Cylinder in Steady and Oscillatory Far Flows. *Proceedings of the Institution of Civil Engineers.* **63** (2): 865-80.

Stansby, P.K. 1979. Mathematical Modelling of Vortex Shedding from Circular Cylinders in Planar Oscillatory Flows, Including Effects of Harmonics. *Mechanics of Wave-Induced Forces on Cylinders* (ed. T.L. Shaw). Marshfield, Ma.: Pitman: 450-60.

Stansby, P.K. 1981. The Force on a Cylinder in Sinusoidal Flow. American Society of Mechanical Engineers Paper 81-WA/FE27.

Stansby, P.K., and Dixon, A.G. 1982. The Importance of Secondary Shedding in Two-Dimensional Wake Formation at Very High Reynolds Numbers. *The Aeronautical Quarterly.* **XXXIII** (2): 105-23.

Stansby, P.K., and Dixon, A.G. 1983. Simulation of Flows Around Cylinders by a Lagrangian Vortex Scheme. *Applied Ocean Research.* **5** (3): 167-78.

Stokes, Sir G.G. 1851. On the Effect of the Internal Friction of Fluids on the Motion of Pendulums. *Cambridge Philosophical Transactions.* **IX** (2): 8-106.

Stratford, B.S. 1954. *Flow in the Laminar Boundary Layer Near Separation.* Great Britain Aeronautical Research Council R&M 3002.

Stratford, B.S. 1959. The Prediction of Separation of the Turbulent Boundary Layer. *Journal of Fluid Mechanics.* **5** (1): 1-16.

Stremel, P.M. 1985. Aerodynamic Interaction Between Vortical Wakes and the Viscous Flow About a Circular Cylinder. Paper AIAA-85-4063.

Stremel, P.M. 1987. Aerodynamic Interation Between Vortical Wakes and Lifting Two-Dimensional Bodies. Paper 43rd Annual Forum of the American Helicopter Society. St. Louis, Mo. May.

Stremel, P.M. 1990. The Calculation of Rotor/Fuselage Interaction for Two-Dimensional Bodies. NASA Technical Memorandum 102855.

Swirydczuk, J., Wilder, M.C., and Telionis, D.P. 1993. The Interaction of Coherent Vortices with Short Flat Plates. *Transactions of the ASME.* **115**: 590-6.

Takada, H. 1975. An Extension to the Critical Flow of Stratford's Theory for Predicting the Turbulent Separation Position. *Journal of the Physical Society of Japan.* **39** (4): 1106-12.

Tang, W. and Sankar, L.N. 1987. Strong Blade-Vortex Interactions Including Collision. *Forum on Unsteady Flow Separation* (ed. K.N. Ghia): 45-54.

Tang, X.-P., and Rockwell, D. 1983. Instantaneous Pressure Fields at a Corner Associated with Vortex Impingement. *Journal of Fluid Mechanics.* **126**: 187-204.

Telste, J.G., and Lugt, H.J. 1980. *Vortex Shedding from Finned Circular Cylinders.* Report DTNSRDC-80/124, David W. Taylor Naval Ship Research and Development Center, Bethesda, Md.

Thwaites, B. 1949. Approximate Calculation of the Laminar Boundary Layer. *The Aeronautical Quarterly.* **I** (III): 245-80.

Tiemroth, E.C. 1986a. Simulation of the Viscous Flow Around a Cylinder by the Random Vortex Method. Ph.D. Dissertation, University of California, Berkeley.

Tiemroth, E.C. 1986b. The Simulation of the Viscous Flow Over a Cylinder in a Wave Field. *Proceedings 16th Symposium on Naval Hydrodynamics.* University of California, Berkeley (ed. W.C. Webster), National Academy Press: 490-513.

Van der Vegt, J.J.W. 1988. A Variationally Optimized Vortex Tracing Algorithm for 3-Dimensional Flows Around Solid Bodies. Ph.D. Dissertation, Maritime Research Institute, The Netherlands.

Van der Vegt, J.J.W., and Huijsman, R.H.M. 1984. Numerical Simulation of Flow Around Bluff Bodies at High Reynolds Numbers. *Proceedings 15th Symposium on Naval Hydrodynamics.* Hamburg: 569-85.

Van der Vegt, J.J.W. 1985. Numerical Simulation of Flow Around Circular Cylinders at High Reynolds Numbers. *Proceedings BOSS '85*. Elsevier Science Publishers, Amsterdam: 227-38.

Walker, J.D.A. 1978. The Boundary Layer Due to Rectilinear Vortex. *Proceedings of the Royal Society A*. **359**: 167-188.

Walker, J.D.A., Smith, C.R., Doligalski, T.L., and Cerra, A.W. 1987. Impact of a Vortex Ring on a Wall. *Journal of Fluid Mechanics*. **181**: 99-140.

Wang, X. 1989. A Numerical Study of Unsteady Flows Past a Circular Cylinder. Ph.D. Dissertation, University of Houston.

Wang, X., and Dalton, C. 1991. Oscillating Flow Past a Rigid Circular Cylinder: A Finite-Difference Calculation. *ASME Journal of Fluids Engineering*. **113**: 377-383.

Ward, E.G., and Dalton, C. 1969. Strictly Sinusoidal Flow Around a Stationary Cylinder. *ASME Journal of Basic Engineering*. **91**: 707-13.

White, F.M. 1986. *Fluid Mechanics*, 2nd ed. New York: McGraw-Hill.

Wilder, M.C., Pesle, M.M., Telionis, D.P., Poling, D.R., and Dadone, L. 1990 Blade-Vortex Interaction Experiments--Velocity and Vorticity Fields. Paper AIAA-90-0030.

Williamson, C.H.K. 1985. Sinusoidal Flow Relative to Circular Cylinders. *Journal of Fluid Mechanics*. **155**: 141-74.

Wilson, J.R. 1983. Pressure Measurements About Cylinders in Oscillatory Flow. Master's Thesis, Naval Postgraduate School, Monterey, Ca.

Yuen, N.Q.S. 1985. Oscillating Flow About Circular Cylinders at Low Keulegan-Carpenter Numbers. Master's Thesis, Naval Postgraduate School, Monterey, Ca.

Ziada, S. and Rockwell, D. 1982. Vortex-Leading-Edge Iteraction. *Journal of Fluid Mechanics*. **118**: 79-107.

# INITIAL DISTRIBUTION LIST

| | | No. Copies |
|---|---|---|
| 1. | Defense Technical Information Center<br>Cameron Station<br>Alexandria VA 22304-6145 | 2 |
| 2. | Library, Code 52<br>Naval Postgraduate School<br>R00m 104<br>411 Dyer RD<br>Monterey CA 93943-5101 | 2 |
| 3. | Professor T. Sarpkaya<br>Department of Mechanical Engineering, Code ME-SL<br>Naval Postgraduate School<br>Room M2<br>699 Dyer RD<br>Monterey CA 93943-5108 | 10 |
| 4. | Chairman, Department of Mechanical Engineering<br>Department of Mechanical Engineering, Code ME<br>Naval Postgraduate School<br>Room M3<br>699 Dyer RD<br>Monterey CA 93943-5108 | 1 |
| 5. | Professor G. Hobson<br>Department of Aeronautics and Astronautics, Code AA-Hg<br>Naval Postgraduate School<br>Room 137<br>699 Dyer RD<br>Monterey CA 93943-5106 | 1 |
| 6. | Naval Engineering Curricular Office<br>Code 34<br>Naval Postgraduate School<br>Room 220<br>699 Dyer RD<br>Monterey CA 93943-5109 | 1 |
| 7. | CAPT M.R. Maixner<br>PRESINSURV<br>Suite 250<br>2600 Tarawa CT<br>Norfolk VA 23521-3234 | 5 |

| | | |
|---|---|---|
| 8. | Commander<br>Naval Sea Systems Command<br>ATTN: Code 03 (RADM M.S. Firebaugh)<br>2531 Jefferson Davis HWY<br>Arlington VA 22242-5160 | 1 |
| 9. | Doctor Frederick S. Sherman<br>261 Grizzly Peak BLVD<br>Kensington CA 94700 | 1 |
| 10. | RADM P.R. Olson<br>PRESINSURV<br>Suite 250<br>2600 Tarawa CT<br>Norfolk VA 23521-3234 | 1 |
| 11. | Doctor David R. Poling<br>Boeing Helicopters<br>P.O. Box 16858, MS P32-74<br>Philadelphia PA 19142-0858 | 1 |

N
SCHOOL
MONTEREY CA 93943-5101

GAYLORD S

DUDLEY KNOX LIBRARY
3 2768 00312570 9